The Effect of Light Intensity and Reactor Configuration on *Rhodopseudomonas palustris* Growth and Hydrogen Production

by
Brandon Sean Ross

Thesis presented in partial fulfilment of the requirements for the degree of Master of Engineering (Chemical Engineering) in the Faculty of Engineering at Stellenbosch University

Supervisor: Professor RWM Pott

March 2024

Declaration

By submitting this thesis electronically, I declare that the entirety of the work contained therein is my own, original work, that I am the sole author thereof (save to the extent explicitly otherwise stated), that reproduction and publication thereof by Stellenbosch University will not infringe any third party rights and that I have not previously in its entirety or in part submitted it for obtaining any qualification.

Graduation March 2024

PLAGIARISM DECLARATION

1. Plagiarism is the use of ideas, material and other intellectual property of another's work and to present is as my own.

2. I agree that plagiarism is a punishable offence because it constitutes theft.

3. I also understand that direct translations are plagiarism.

4. Accordingly all quotations and contributions from any source whatsoever (including the internet) have been cited fully. I understand that the reproduction of text without quotation marks (even when the source is cited) is plagiarism.

5. I declare that the work contained in this assignment, except where otherwise stated, is my original work and that I have not previously (in its entirety or in part) submitted it for grading in this module/assignment or another module/assignment.

Student number: ……..

Initials and surname: BS Ross

Signature: ……..

Date: 01 March 2024

ABSTRACT

Biological hydrogen production is a promising replacement for the current modes of hydrogen production seen in industry today. However, key issues with the process still need to be solved, such as its economic viability and whether environmentally sustainable production is possible. The use of photosynthetic bacteria such as the purple non sulphur bacterium *Rhodopseudomonas palustris* to produce hydrogen *via* photofermentation has shown to have a low environmental impact but the required energy input is greater than the energy derived from the hydrogen produced. To increase the efficiency of the hydrogen production process the ratio of energy consumed to energy produced must be improved. One method of enhancement is the design and development of photobioreactor (PBR) systems to improve the hydrogen production of the process. The majority of PBRs have been designed for microalgae systems, with very few reactors designed for photosynthetic bacteria. PBR designs are therefore required to improve the hydrogen production of bacterial systems. Outdoor operation has also been earmarked as a means to improve the economic viability of the process as the required light energy will be provided by sunlight, which is a free source of light energy. However, the effect of light intensity on the growth of *R. palustris* is fairly poorly understood. The aim of this study was to determine the effect of light intensity on the growth of *R. palustris,* and to design and construct a multipurpose PBR that can be used for the cultivation of planktonic and immobilised *R. palustris* to produce biological hydrogen.

The first objective was to compare the effect of changing light intensity on the growth kinetics of *R. palustris.* The results of this comparison showed that *R. palustris* grows readily over the range of light intensity investigated (70 to 600 W/m^2), with photo-limitation occurring at low intensities (30 and 70 W/m^2), photosaturation occurring between 200 and 400 W/m^2, and photo-limitation occurring when the light intensity increased to 600 W/m^2. The highest maximum specific growth rate of 0.0420±0.014 h^{-1} was achieved at a light intensity of 400 W/m^2. A predictive model for the cell growth and substrate utilisation of *R. palustris* over the range of light intensity investigated (70 to 600 W/m^2) was successfully developed with the model showing good fit to the experimental data.

A PBR that facilitated hydrogen production by *R. palustris* either as a growing planktonic cell culture or immobilised in a PVA cryogel matrix was successfully designed and constructed. The performance of the PBR operating with planktonic cells was compared to immobilised cells operating as a fluidised bed PBR (FBPBR) and a packed bed PBR (PBPBR). The FBPBR achieved the highest maximum specific hydrogen production rate of 15.74±2.2 mL/g/h. The planktonic culture and PBPBR achieved lower production rates of 12.6±8.0 mL/g/h and 4.53±0.8 mL/g/h respectively. In terms of the substrate conversion efficiency, the FBPBR achieved a conversion of 43% which outperformed the PBPBR which only achieved a conversion

of 26.7%. The conversion efficiency of the planktonic cell culture was between the two immobilised cell configurations with an efficiency of 32%.

TABLE OF CONTENTS

1 INTRODUCTION 1

1.1 BACKGROUND 1

1.2 RESEARCH MOTIVATION 2

1.3 OBJECTIVES 2

1.4 THESIS OVERVIEW 3

2 LITERATURE REVIEW 5

2.1 STATUS OF ENERGY PRODUCTION AND ENVIRONMENTAL RAMIFICATIONS 5

2.2 HYDROGEN PRODUCTION 6

2.2.1 Non-renewable methods of hydrogen production 6

2.2.2 Renewable methods of hydrogen production – a focus on biological production 7

2.3 RHODOPSEUDOMONAS PALUSTRIS 11

2.3.1 Taxonomy and reproduction of R. palustris 11

2.3.2 Metabolic pathways of R. palustris 13

2.3.3 R. palustris metabolism with regards to hydrogen production 14

2.3.4 Photosystem 17

2.3.5 Current industrial usage of R. palustris 18

2.4 MODELLING OF BIOLOGICAL PROCESSES 19

2.4.1 Modelling of biological growth 19

2.4.2 Modelling of light through biological culture 21

2.5 SUBSTRATES FOR HYDROGEN PRODUCTION BY *R. PALUSTRIS* 22

2.6 IMMOBILISATION OF *R. PALUSTRIS* 24

2.6.1 Hydrogel immobilisation matrices 25

2.7 BIOREACTOR ENGINEERING 27

2.7.1 Packed bed reactor 28

2.7.2 Fluidised bed reactor 30

2.8 PRODUCTION CONDITIONS 32

2.8.1 Feedstock 32

2.8.2 Operating conditions 32

2.9 PERFORMANCE PARAMETERS 37
2.9.1 Maximum specific growth rate 37
2.9.2 Biomass yield 37
2.9.3 Substrate conversion efficiency 37
2.9.4 Specific hydrogen production rate 38
3 RESEARCH SCOPE 39
3.1 AIM 39
3.2 OBJECTIVES 39
3.3 KEY QUESTIONS 40
4 MATERIALS AND METHODOLOGY 43
4.1 MATERIALS 43
4.2 MICROBIAL MAINTENANCE 44
4.2.1 Culture revival from lyophilised cells 44
4.2.2 Culture long term storage in glycerol 44
4.2.3 Periodic revival of culture from glycerol 44
4.3 CULTURE MEDIUM 44
4.3.1 Solid medium 44
4.3.2 Liquid medium 46
4.3.3 Immobilisation medium 48
4.4 EXPERIMENTAL PROCEDURE 48
4.4.1 Bacterial culturing 48
4.4.2 Immobilisation of R. palustris 53
4.4.3 Fluidised bed photobioreactor 55
4.4.4 Packed bed photobioreactor 56
4.5 ANALYTICAL TECHNIQUES 57
4.5.1 Cell concentration 57
4.5.2 Hydrogen concentration 60
4.5.3 Glycerol concentration 61
4.5.4 Glutamate concentration 62

4.5.5 Pigment extraction 63
4.5.6 Statistical analysis 64
5 RESULTS AND DISCUSSION 67
5.1 EFFECT OF LIGHT INTENSITY ON THE GROWTH OF *R. PALUSTRIS* 67
5.1.1 Growth curves 69
5.1.2 Maximum specific growth rates 73
5.1.3 Substrate utilisation 81
5.1.4 Pigment extractions 83
5.1.5 Modelling the effect of light intensity 88
5.2 HYDROGEN PRODUCTION BY *R. PALUSTRIS* IN FREE CELL CULTURES 100
5.2.1 Growth kinetics 100
5.2.2 Hydrogen production kinetics 103
5.2.3 Estimation of average light intensity in the column and Schott bottle PBR 107
5.3 HYDROGEN PRODUCTION BY *R. PALUSTRIS* IN IMMOBILISED MATRIX 110
5.3.1 Hydrogen production performance: immobilisation vs planktonic cells 110
5.3.2 FBPBR versus PBPBR 114
5.3.3 Summary of results 118
6 CONCLUSIONS 121
7 RECOMMENDATIONS 125
7.1 PROPOSAL FOR PHD 125
7.1.1 Introduction 125
7.1.2 Research scope 126
7.1.3 Methodology 127
7.1.4 Intended contribution 130
8 REFERENCES 133
APPENDICES 143
A PHOTOBIOREACTOR DESIGN SHEETS 143
B PERISTALTIC PUMP CALIBRATION CURVE 145

C GROWTH AND SUBSTRATE COMPARISON FOR EACH LIGHT INTENSITY 146

D GLUTAMATE CONCENTRATION CURVE..... 150

E GAS COMPOSITION ANALYSIS..... 151

F PREDICTED GROWTH CURVE IN SCHOTT BOTTLE PBR..... 152

G PREDICTIVE MODEL TEST EXPERIMENT 153

List of Figures

Figure 2.1: World total primary energy supply of 13 647 Mtoe by fuels in 2015. 5
Figure 2.2: Breakdown of the current renewable hydrogen production methods. Figure adapted from Kumar and Himabindu (2019). 7
Figure 2.3: Representation of the budding cell cycle of Rhodopseudomonas palustris. Diagram reproduced from Westmacott and Primrose (1976). 12
Figure 2.4: Electron micrograph image of R. palustris strain TIE-1 (American Society for Microbiology, 2009)..... 13
Figure 2.5: Schematic diagram of the biological hydrogen production metabolism of R. palustris which occurs during photoheterotrophic, anaerobic and nitrogen fixing conditions adapted from Pott (2013). The outer most grey line indicates the outer membrane of the cell. The thick grey line indicates the inner cell membrane. The yellow lightning symbols indicates light excitation. Straight black arrows indicate the flow of electrons. The blue arrows indicate the flow of CO_2 or fixed CO_2. The red arrows indicate proton (H^+) flow. The curved black arrows indicate a reaction occurring. The curved purple arrows indicate the cyclic electron transport system that forms part of the photosynthetic apparatus. 15
Figure 2.6: A representation of the major membrane proteins involved in the light reaction of purple photosynthetic bacteria, adapted from Roszak et al. (2003). Photon energy is represented yellow arrows. The LH2 antenna is the purple complex with the labels B800 and B850 representing the wavelength of maximal absorption. The LH1 antenna is the red complex with the B880 label, again referring to the wavelength corresponding to maximal absorption. The reaction centre is labelled RC. Red arrows represent electron flow. The cytochrome bc_1 complex is represented by the blue block. The ATP synthase which sees ATP synthesised is represented by the orange figure. 18
Figure 2.7: Comparison of the emission spectrums of common light sources encountered in indoor environments. Reproduced from Virtuani et al. (2006). 35
Figure 4.1: R. palustris 11774 streaked on the fast-growing solid nutrient agar 45
Figure 4.2: Schematic diagram of the Schott bottle PBR system used for inoculum culturing and Schott bottle PBR experiments. The above diagram is the side view of the entire setup. The Schott bottle is in a temperature-controlled water bath that is not depicted in the diagram. 49
Figure 4.3: Schematic diagram of the tubular PBR system used for all experiments pertaining to the effect of light intensity. The above diagram is the front view of the entire setup. The entire tubular PBR system was in a temperature-controlled water bath that is not depicted in the diagram. Total illuminated length and volume is 2.86 m and 500 mL respectively. 50

Figure 4.4: Schematic diagram of the column PBR system operating with a free-cell culture. The above diagram is the side view of the entire setup. The culture was recirculated using a peristaltic pump and the reactor was illuminated by six 60W Eurolux incandescent light bulbs. 52
Figure 4.5: Schematic diagram of bead making procedure. The PVA/bacteria solution is kept at a constant temperature of 45°C using a heated water bath. A peristaltic pump is used to transfer the solution from the Schott bottle to the multi-dripper head. The beads form as they are dripped into the liquid nitrogen. 54
Figure 4.6: Schematic diagram of the FBPBR system operating with R. palustris immobilised in PVA cryogel. The above diagram is the side view of the entire setup..... 56
Figure 4.7: Schematic diagram of the PBPBR system operating with R. palustris immobilised in PVA cryogel. The above diagram is the side view of the entire setup..... 57
Figure 4.8: Cell concentration standard curve for bacterial cultures grown in Van Niels medium. Data points represent the mean of triplicate repeats. The error bars show the uncertainty associated with both the CDW measurements and the optical density measurements. 59
Figure 4.9: Cell concentration standard curve for bacterial cultures grown in minimal medium. Data points represent the mean of triplicate repeats. The error bars show the uncertainty associated with both the CDW measurements and the optical density measurements..... 60
Figure 4.10: Glycerol concentration standard curve developed from HPLC analysis for conversion from area under the absorbance peaks. 62
Figure 4.11: Glutamate concentration curve 63
Figure 5.1: Change in average light intensity through the width of a cylindrical bioreactor with an incident light intensity of 100 W/m^2 and a biomass concentration of 4 g/L. 67
Figure 5.2: Transmittance (UV/Vis spectrophotometer, Varian at 875nm) of light through varying concentrations of R. palustris cultures in 1 cm cuvettes, with Van Niels medium as the blank. The culture used for these measurements was grown in a 500mL Schott bottle with bioreactor fittings in modified Van Niels medium at a temperature of 35°C and light intensity of 200 W/m^2 with illumination provided by incandescent light bulbs (100W Eurolux bulbs). Data points represent the mean of triplicate repeats and the error bars show the uncertainty associated with the CDW measurements and the transmittance measurements..... 68
Figure 5.3: Growth curves (CDW vs time) of R. palustris with illumination provided by incandescent light bulbs (60W or 100W Eurolux bulbs depending on the light intensity required) for varying light intensities, i.e. 30, 70, 200, 400 and 600 W/m^2. R. palustris was cultivated using modified Van Niels medium and sparged with filter sterilised argon to promote anaerobic conditions. The CDW of the varying light intensities over times is provided in this figure. All experiments were completed at a constant

temperature of 35°C and a volumetric flow rate of 0.651 L/min. Data points represent the mean of quadruple repeats and the error bars show the uncertainty associated with the CDW measurements. 71
Figure 5.4: Maximum CDW of R. palustris achieved with illumination provided by incandescent light bulbs (60W or 100W bulbs depending on the light intensity required) for varying light intensities, i.e. 30, 70, 200, 400 and 600 W/m^2. R. palustris was cultivated using modified Van Niels medium and sparged with filter sterilised argon to promote anaerobic conditions. All experiments were completed at a constant temperature of 35°C and a volumetric flow rate of 0.651 L/min. Data points represent the mean of quadruple repeats and the error bars show the uncertainty associated with the CDW measurements. 73
Figure 5.5: Natural logarithm of R. palustris CDW within the exponential phase with illumination provided by incandescent light bulbs (60 W or 100 W bulbs depending on the light intensity required) for varying light intensities, i.e. a) 30, b) 70, c) 200, d) 400 and e) 600 W/m^2. R. palustris was cultivated using modified Van Niels medium and sparged with filter sterilised argon to promote anaerobic conditions. All experiments were completed at a constant temperature of 35°C and a volumetric flow rate of 0.651 L/min. Data points represent the mean of quadruple repeats. 75
Figure 5.6: Maximum specific growth rate of R. palustris achieved with illumination provided by incandescent light bulbs (60 W or 100 W bulbs depending on the light intensity required) for varying light intensities, i.e. 30, 70, 200, 400 and 600 W/m^2. R. palustris was cultivated using modified Van Niels medium and sparged with filter sterilised argon to promote anaerobic conditions. All experiments were completed at a constant temperature of 35°C and a volumetric flow rate of 0.651 L/min. Data points represent the mean of quadruple repeats and the error bars show the propagated uncertainty originally associated with the CDW measurements. 77
Figure 5.7: Light spectrum of the sun for full days (measurement every 10 minutes): a) light intensity over time during the month of May (autumn) and b) light intensity over time during the month of July (winter). A pyranometer (Campbell Scientific CR300 Series Compact Datalogger) was placed on the roof of a four-story building at the Department of Process Engineering in Stellenbosch. 80
Figure 5.8: Light spectrum of the sun for full days (measurement every 10 minutes): a) light intensity over time during the month of May (autumn) and b) light intensity over time during the month of July (winter). A pyranometer (Campbell Scientific CR300 Series Compact Datalogger) was placed on the roof of a four-story building at the Department of Process engineering in Stellenbosch. 81
Figure 5.9: Glycerol utilization of R. palustris with illumination provided by incandescent light bulbs (60W or 100W bulbs depending on the light intensity required) for varying light intensities, i.e. 30, 70, 200, 400 and 600 W/m^2. R. palustris was cultivated using modified Van Niels medium with glycerol as the carbon source (40mM) and sparged with filter sterilised argon to promote anaerobic conditions. The glycerol concentration of the varying light intensities over times is provided in this figure. All experiments were

completed at a constant temperature of 35°C and a volumetric flow rate of 0.651 L/min. Data points represent the mean of quadruple repeats. The error bars show the uncertainty associated with the glycerol concentration measurements that were obtained from HPLC analysis using the methods described in section 4.5.3. 82

Figure 5.10: The growth curve (●) and glycerol utilization (Δ) of R. palustris 11774 with illumination provided by incandescent light bulbs (100W bulbs) at a light intensity of 200 W/m2 is provided in this figure. R. palustris 11774 was cultivated using modified Van Niels medium and sparged with filter sterilised argon to promote anaerobic conditions. All experiments were completed at a constant temperature of 35°C and a volumetric flow rate of 0.651 L/min. Data points represent the mean of quadruple repeats. The error bars show the uncertainty associated with the CDW and glycerol measurements. Biomass concentration corresponds to the left-hand ordinate and the glycerol concentration to the right-hand ordinate. 83

Figure 5.11: Absorption spectra of pigments in R. palustris 11774 cultivated under anaerobic conditions with illumination provided by incandescent light bulbs (100W bulbs) at an incident light intensity of 200 W/m^2. The experiment was run at a constant temperature of 35°C and a volumetric flow rate of 0.651 L/min with the sample taken in the exponential growth phase. (••) refer to carotenoids; (•) refers to BChl-α peaks. 84

Figure 5.12: Bchl-α/carotenoid ratio of pigments of R. palustris 11774 during the exponential growth phase of bacterial culturing with illumination provided by incandescent light bulbs (60W or 100W bulbs depending on the light intensity required) for varying light intensities, i.e. 30, 70, 200, 400 and 600 W/m^2. R. palustris 11774 was cultivated using modified Van Niels medium and sparged with filter sterilised argon to promote anaerobic conditions. All experiments were completed at a constant temperature of 35°C and a volumetric flow rate of 0.651 L/min. Data points represent the mean of either triplicate or quadruple repeats and the error bars show the uncertainty between the calculated ratios from each experimental run. 85

Figure 5.13: Bonferroni test for statistical comparison of each light intensity investigated. 86

Figure 5.14: The emission spectra of incandescent light bulb (60W or 100W bulbs depending on the light intensity) for the various light intensities investigated, i.e. 30, 70, 100, 200, 400 and 600 W/m^2. The emission spectra were measured at different light intensities by an imaging spectrograph (RGB photonics Q-mini) as a function of wavelength. 87

Figure 5.15: The emission spectra of incandescent light bulb (100 W bulb) and sunlight over a wavelength range of 500 to 1000 nm with both corresponding to an incident light intensity of 600 W/m^2. The emission spectra were measured using an imaging spectrograph as a function of wavelength. 88

Figure 5.16: Transmittance (spectrophotometer – 875nm) of light through R. palustris cultures of varying cell concentrations with Van Niels medium as the blank. The culture used for these measurements was grown in a 500mL Schott bottle with bioreactor fittings in modified Van Niels medium at a temperature of 35°C and light intensity of 200 W/m^2 with illumination provided by incandescent light bulbs (100W bulbs). Data points represent the mean of triplicate experimental runs (o) and the trendline represents the two-flux model fitted to the data using lsqnonlin. The error bars show the uncertainty associated with the CDW measurements and the transmittance measurements. 89
Figure 5.17: Light intensity profile through the tubular PBR with an incident light intensity of 30 W/m^2 and a biomass concentration of 4 g/L. 91
Figure 5.18: Algorithm flow diagram illustrating the nested loop function for nonlinear regression. 93
Figure 5.19: Non-linear regression of best fit parameters of biomass and substrate concentrations for each light intensity investigated versus the actual experimental values. a) 30, b) 70, c) 200, d) 400 and e) 600 W/m^2. 95
Figure 5.20: Estimation of average light intensity in the tubular PBR over time. a) 30, b) 70, c) 200, d) 400 and e) 600 W/m^2 97
Figure 5.21: Estimation of the response of average light intensity as the biomass concentration increases. a) 30, b) 70, c) 200, d) 400 and e) 600 W/m^2 99
Figure 5.22: Comparison of growth curves of R. palustris cultured in a Schott bottle PBR (○) and the custom designed PBR (Δ). Illumination for both reactor configurations provided by incandescent light bulbs (60 W bulbs) at an incident light intensity of 100 W/m^2. R. palustris was cultivated using modified minimal medium with glycerol (50mM) as the carbon source and glutamate (10 mM) as the nitrogen source. Schott bottle experiments were completed at a mixing rate of 300rpm and the custom reactor at a recirculation volumetric flow rate of 0.651 L/min. Data points for the column PBR are the mean of triplicate repeats and data points for the Schott bottle PBR are the mean of quadruple repeats. The error bars show the uncertainty associated with the CDW measurements. 102
Figure 5.23: Glycerol utilization of R. palustris cultured in a Schott bottle PBR (○) and the custom designed PBR (Δ). Illumination for both reactor configurations provided by incandescent light bulbs (60 W) at an incident light intensity of 100 W/m^2. R. palustris was cultivated using modified minimal medium with glycerol (50mM) as the carbon source and glutamate (10 mM) as the nitrogen source. Schott bottle experiments were completed at a mixing rate of 300 rpm and the custom reactor at a recirculation volumetric flow rate of 0.651 L/min. Data points for the column PBR are the mean of triplicate repeats and data points for the Schott bottle PBR are the mean of quadruple repeats. The error bars show the uncertainty associated with the glycerol concentrations obtained through HPLC analysis. 103

Figure 5.24: Comparison of cumulative hydrogen production by R. palustris cultured in a Schott bottle PBR (○) and the custom designed PBR (Δ). Illumination for both reactor configurations provided by incandescent light bulbs (60 W bulbs) at an incident light intensity of 100 W/m^2. R. palustris was cultivated using modified minimal medium with glycerol (50mM) as the carbon source and glutamate (10 mM) as the nitrogen source. Schott bottle experiments were completed at a mixing rate of 300 rpm and the custom reactor at a recirculation volumetric flow rate of 0. L/min. Data points for the column PBR are the mean of triplicate repeats and data points for the Schott bottle PBR are the mean of quadruple repeats. The error bars show the uncertainty associated with the hydrogen collected. 105
Figure 5.25: Comparison of specific hydrogen production rate by R. palustris cultured in a Schott bottle PBR (○) and the custom designed PBR (Δ). Illumination for both reactor configurations provided by incandescent light bulbs (60 W bulbs) at an incident light intensity of 100 W/m^2. R. palustris was cultivated using modified minimal medium with glycerol (50mM) as the carbon source and glutamate (10 mM) as the nitrogen source. Schott bottle experiments were completed at a mixing rate of 300 rpm and the custom reactor at a recirculation volumetric flow rate of 0.651 L/min. Data points for the column PBR are the mean of triplicate repeats and data points for the Schott bottle PBR are the mean of quadruple repeats. The error bars show the propagated uncertainty associated with the CDW and hydrogen production. 106
Figure 5.26: Experimental data and modelled data of the biomass concentration cultured in the Scott bottle PBR. Experimental data represent the mean of quadruple repeats and the error bars show the uncertainty associated with the measured CDW. 108
Figure 5.27: Experimental data and modelled data of the biomass concentration cultured in the column PBR. Experimental data represent the mean of triplicate repeats and the error bars show the uncertainty associated with the measured CDW. 108
Figure 5.28: Predicted average light intensity in the column and Schott bottle PBR with the change in biomass concentration. 109
Figure 5.29: Comparison of specific hydrogen production rate by free-cell R. palustris cultured in a column PBR (○) and immobilised R. palustris in the FBPBR (Δ). Illumination for both reactor configurations provided by incandescent light bulbs (60 W bulbs) at an incident light intensity of 100 W/m^2. R. palustris was cultivated using modified minimal medium with glycerol (50mM) as the carbon source and glutamate (10 mM) as the nitrogen source (only for the planktonic cell culture). FBPBR experiments were completed at a volumetric flow rate 1.06 L/min and planktonic cell culture at a recirculation volumetric flow rate of 0.651 L/min. Data points for the column PBR are the mean of triplicate repeats and data points for the FBPBR are the mean of quadruple repeats. The error bars show the propagated uncertainty associated with the CDW and hydrogen production. 112

Figure 5.30: Glycerol utilization by free-cell R. palustris cultured in a column PBR (○) and immobilised R. palustris in the FBPBR (Δ). Illumination for both reactor configurations provided by incandescent light bulbs (60 W bulbs) at an incident light intensity of 100 W/m^2. R. palustris was cultivated using modified minimal medium with glycerol (50mM) as the carbon source and glutamate (10 mM) as the nitrogen source (only for planktonic culture). FBPBR experiments were completed at a volumetric flow rate 1.06 L/min and planktonic cell culture at a recirculation volumetric flow rate of 0.651 L/min. Data points for the planktonic cell column PBR are the mean of triplicate repeats and data points for the FBPBR are the mean of quadruple repeats. The error bars show the uncertainty associated with the glycerol concentrations obtained through HPLC analysis. 113
Figure 5.31: Comparison of cumulative hydrogen production by immobilised R. palustris in the column PBR. Illumination for both reactor configurations provided by incandescent light bulbs (60 W bulbs) at an incident light intensity of 100 W/m^2. R. palustris was cultivated using modified minimal medium with glycerol (50mM) as the carbon source. FBPBR experiments were completed at a volumetric flow rate 1.06 L/min and PBPBR experiments at a recirculation volumetric flow rate of 0.347 L/min. Data points are the mean of quadruple repeats and the error bars show the uncertainty associated with the cumulative hydrogen produced. 115
Figure 5.32: Comparison of specific hydrogen production rate by immobilised R. palustris in the column PBR. Illumination for both reactor configurations provided by incandescent light bulbs (60 W bulbs) at an incident light intensity of 100 W/m^2. R. palustris was cultivated using modified minimal medium with glycerol (50mM). FBPBR experiments were completed at a volumetric flow rate 1.06 L/min and PBPBR experiments at a recirculation volumetric flow rate of 0.347 L/min. Data points are the mean of quadruple repeats. The error bars show the uncertainty associated with the cumulative hydrogen produced. ... 117
Figure 5.33: Glycerol utilization of immobilised R. palustris in the column PBR. Illumination for both reactor configurations provided by incandescent light bulbs (60 W bulbs) at an incident light intensity of 100 W/m^2. R. palustris 11774 was cultivated using modified minimal medium with glycerol (50mM). FBPBR experiments were completed at a volumetric flow rate 1.06 L/min and PBPBR experiments at a recirculation volumetric flow rate of 0.347 L/min. Data points are the mean of quadruple repeats. The error bars show the uncertainty associated with the glycerol concentrations obtained through HPLC analysis. 118
Figure 5.34: Comparison between all the bioreactor configurations used in the column PBR in terms of maximum specific hydrogen production rate and substrate conversion efficiency. 119
Figure 7.1: Schematic diagram of the MBPBR system operating with a free-cell culture. The above diagram is the side view of the entire setup. The culture was recirculated using a peristaltic pump and the reactor was illuminated by six 60W Eurolux incandescent light bulbs. 129

List of Tables

Table 2.1: Renewable hydrogen production methods with some of their major advantages and disadvantages (Acar and Dincer, 2014; Dincer and Joshi, 2013; Hallenbeck and Ghosh, 2009; Shiva Kumar and Himabindu, 2019). 8

Table 2.2: Summary of the modes of growth of R. palustris: photoautotrophic, photoheterotrophic, chemoautotrophic and chemoheterotrophic and some of their key traits (Pott, 2013). 13

Table 2.3: Hydrogen production rates (mL/g_{dw}/h) by R. palustris from different carbon sources 23

Table 2.4: Operating temperatures of photofermentation systems using R. palustris. 34

Table 2.5: Operating pH of photofermentation systems using R. palustris 36

Table 4.1: List of all chemicals used during experimentation along with purities and suppliers. TG – technical grade. 43

Table 4.2: Adjusted Van Niels Yeast Broth components and concentrations. *Sterile addition to Van Niels Yeast Broth after autoclaving. 46

Table 4.3: Bulk nutrients and buffers components and concentrations stock solutions. 47

Table 4.4: Trace element and vitamin solution components and concentration (Pott et al., 2013) 47

Table 4.5: PBS solution components and concentrations 54

Table 4.6: Summary of HPLC specifications for analysis of glycerol concentrations that are to be determined 61

Table 5.1: Summary of Single Factor ANOVA on maximum specific growth rate at various light intensities 78

Table 5.2: Summary of the ad hoc t-test on maximum specific growth rate at 200 and 400 W/m^2 79

Table 5.3: Summary of Single Factor ANOVA on Bchl-α/carotenoid ratio at various light intensities 85

Table 7.1: Proposed articles for submission for peer review in the listed journals. 131

NOMENCLATURE

Δ	Uncertainty	-
μ	Specific growth rate	h^{-1}
μ	Death rate	h^{-1}
μmax	Maximum specific growth rate	h^{-1}
Ar	Archimedes number	-
ATP	Adenosine triphosphate	-
ATPase	ATP synthase	-
ATR	Autothermal reforming	-
BChl-α	Bacteriochlorophyll alpha	-
CBB	Calvin-Benson-Bassham	-
CDW	Cell dry weight	-
CG	Crude glycerol	-
Cyt c	Cytochrome c	-
$Cytbc_1$	Cytochrome b/c_1	-
d	Distance	m
DMSO	Dimethyl sulfoxide	-
DSMZ	Deutsche Sammlung von Mikroorganismen und Zellkulturen	-
e^-	Reducing equivalents	-
E. coli	Escherichia coli	-
Ea	Mass absorption coefficient	m^2/g
Es	Scattering coefficient	m^{-1}
FBPBR	Fluidised bed photobioreactor	-
Fd	Ferredoxin	-
g	Gravitational acceleration	m^2/s
GC	Gas chromotography	-
H	Height of bed	m
HPLC	High-performance liquid chromatograph	-
Hup	Hydrogenase	-
I	Light intensity	W/m^2
I0	Incident light intensity	W/m^2
ID	Inner diameter	m or mm
IEA	International Energy Agency	-
KI	Light saturation coefficient	W/m^2

Ki	Photoinhibition coefficient	W/m^2
Ks	Half-saturation coefficient	-
LH	Light harvesting complexe	-
MBPBR	Membrane photobioreactor	-
Mtoe	Mega tonnes of oil equivalent	Tonnes
N_2ase	Nitrogenase	-
$NADP^+$	Nicotinamide adenine dinucleotide phosphate	-
NRMS	Normalised root mean squared	-
ODE	Ordinary differential equation	-
P	Pressure	kPa
PBPBR	Packed bed photobioreactor	-
PBR	Photobioreactor	-
PBS	Phosphate buffered saline	-
PEMFC	Proton exchange membrane fuel cells	-
PHB	Poly(hydroxybutrate)	-
PI	Prediction intervals	-
PLM	Path length multiplication	-
PNSB	Purple non-sulphur bacteria	-
POX	Partial oxidation	-
PVA	Polyvinyl alcohol	-
Q	Ubiquinone	-
R	Radius	m
R. palustris	*Rhodopseudomonas palustris*	-
R. sphaeroides	*Rhodobacter sphaeroides*	-
RC	Reaction centre	-
Re	Reynolds number	-
RMS	Root mean squared	-
s	Substrate concentration	g/L
SR	Steam reforming	-
t	Time	hours
T	Temperature	°C
TCA	Tricarboxylic acid cycle	-
TCD	Thermal conductivity detector	-
TCG	Treated crude glycerol	-

U	Velocity	m/s
UF	Ultrafiltration	-
VFA	Volatile fatty acid	-
X	Biomass concentration	g/L
x	Diameter	m
Yx/s	Biomass yield coefficient	-
α	Extinction coefficicent	-
ε	Voidage	-
κ	Kappa	-
ρ	Density	kg/m^3
σ	Stefan Boltzmann constant	$W/m/K^4$
λ	Wavelength	nm

1 INTRODUCTION

1.1 Background

Anthropogenic greenhouse gas emissions are ever increasing due to mankind's need to produce energy and have been identified as one of the main causes of climate change (IPCC, 2007). Fossil fuel consumption is seen as the key factor in the release of greenhouse gases, specifically carbon dioxide (CO_2), due to the fact that approximately 70% of anthropogenic greenhouse gas emissions originate from the energy sector (Höök and Tang, 2013). Thus, dual challenges have arisen: the need for development of possible alternatives for the depleting fossil fuel reserves and reducing the greenhouse gas emissions within the energy sector.

Hydrogen (H_2) is seen as a potential answer to the above stated problems due to it being a clean and renewable fuel source (Crabtree et al., 2004; Crabtree and Dresselhaus, 2008). Hydrogen has an energy content of 141.8 MJ/kg which is comparatively larger than methane and diesel which have an energy content of 55.5 MJ/kg and 47.3 MJ/kg respectively (Çengel and Boles, 2006). In fact, hydrogen has one of the highest known energy contents. Higher energy content on a unit mass basis than current fuels used in the energy sector combined with the fact that combustion of hydrogen only produces water and no harmful greenhouse gases emphasises why hydrogen has been identified as a suitable replacement for fossil fuels. However, it should be noted that there are significant limitations which make it difficult to use hydrogen as a fuel. Production of hydrogen often occurs at atmospheric pressure where it is in the gaseous phase. Compression is required for use in fuel cells (Blomen and Mugerwa, 2013) and as fuel in the transportation sector (Balat, 2008). Storage also requires expensive materials due to the low molecular weight of hydrogen.

The majority of hydrogen (48%) is produced using natural gas, with petroleum (30%), coal (18%) and water electrolysis (4%) used to produce the balance (Konieczny et al., 2008). This illustrates that 96% of hydrogen is produced using fossil fuels. Production of hydrogen from fossil fuels still results in the formation of greenhouse gases which means that the production of these harmful gases is merely shifted upstream within the energy production process. Renewable hydrogen production methods have seen an increased focus due to its lower greenhouse gas emissions. These renewable methods are divided into three main categories, namely biological, thermochemical and water splitting methods for hydrogen production. Of these three methods, biological hydrogen production has been identified as an attractive option due to the possibility of waste reformation and its lower capital cost in comparison to the other two methods.

There are three major categories of biological hydrogen production: biophotolysis, dark fermentation and photofermentation (Hallenbeck and Ghosh, 2009; Hay et al., 2013; Shiva Kumar and Himabindu,

2019). The theoretically high conversion of organic substrates to hydrogen during photofermentation makes this category an attractive option as a renewable hydrogen production method. Photofermentation of organic waste could possibly reduce an environmental burden with the added advantage of producing a clean source of energy. Glycerol has been selected as the organic waste test example as it considered a financial and environmental burden, because it is no longer financially viable to refine the crude glycerol for use in the food and pharmaceutical industries and is therefore disposed of as a waste product (Pott, 2013).

1.2 Research motivation

Although biological hydrogen production is promising, key issues with the process still need to be solved, such as its economic viability and whether environmentally sustainable production is possible. According to Adessi and De Philippis (2014) the use of photosynthetic bacteria to produce hydrogen has a low environmental impact. However, the required energy input is higher than the energy derived from the hydrogen produced. Therefore, to increase the efficiency of the biohydrogen production process the ratio of energy consumed to energy produced must be improved. One method of improvement is the design and development of an optimal photobioreactor (PBR) (Adessi and De Philippis, 2014). Comparison between multiple PBR systems has been identified as a potential strategy to enhance the efficiency of the process.

Microbial hydrogen production provides the added benefit of potential waste degradation. This increases the economic viability of the process as unwanted waste material can be used as the feed to the PBR systems.

1.3 Objectives

The aim of this research is to produce biological hydrogen from a synthetic waste stream (glycerol) by the selected photosynthetic bacteria *Rhodopsuedomonas palustris* (*R. palustris*). This could lead to a renewable and clean source of energy as well as the biodegradation of a waste stream that would be an environmental burden if not used as the feedstock. Specific focus has been placed on investigating the effect of light intensity on the growth of *R. palustris* as well as the design and development of a PBR that can be used for production of hydrogen by planktonic and immobilised *R. palusrtris*.

In order to achieve the project aim and answer the key questions that arose from an in-depth literature review, the experimental research is divided into five objectives. Firstly, to examine the effect of light intensity on the *R. palustris* cells in terms of growth, substrate utilisation and pigment production when cultivated in a tubular PBR. This experimentation leads to the next objective which is to then model the response of cell growth and average light intensity in the tubular PBR at various light intensities. The third

objective is to design and construct a PBR system that could be a viable option in the culturing of *R. palustris* in both free-cell and immobilised form, performing at a similar or enhanced level in terms of hydrogen production and substrate conversion efficiency when compared to current lab-scale bioreactor systems. The developed PBR can then be used to determine whether the hydrogen production of the immobilised bacterium is comparable to that of the free cell bacterial cultures. The last objective is to compare the performance of the fluidised bed PBR versus the packed bed PBR based on their biological hydrogen production and substrate conversion efficiency.

1.4 Thesis overview

Chapter 2, Literature Review, is a review of previous literature to develop an understanding on the metabolism of the photosynthetic bacteria, *R. palustris*, and to identify gaps in the research field that require further investigation and experimentation.

Chapter 3, Research Scope, outlines the main aim of the project, the objectives along with a discussion on the reason for each objective and the identified gap in literature, and the development of key questions whose answers will help to meet the stipulated objectives.

Chapter 4, Materials and Methodology, provides a description of the experimental methods and materials used in this investigation that are required to answer the key questions developed in Chapter 3.

Chapter 5, Results and Discussion, provides a discussion into the experimental results obtained for the effect of light intensity on *R. palustris* growth, modelling of this growth and the design and testing of the novel PBR in terms of the hydrogen production and substrate utilisation performance of planktonic and immobilised cells by *R. palustris*.

Chapter 6 is a general conclusion to the work done in the thesis with specific conclusions for each objective of this project.

Chapter 7 outlines some recommendations for future work in this research field and provides a research scope and intended contributions for this thesis to be considered for upgrade from a master's project to a PhD due to the contribution of this work to the research field.

2 LITERATURE REVIEW

2.1 Status of energy production and environmental ramifications

Energy is an indispensable commodity that we require for everyday life. The demand for global energy is ever increasing and is expected to increase by more than 50% by the year 2025 (Khanal et al., 2008). The International Energy Agency (IEA) reports the total primary energy supply by fuel in 2015. As can be seen in Figure 2.1 below, majority of energy is supplied from oil, coal and natural gas making up approximately 81.4% of energy supplied. Thus, 81.4% of fuel supplied is a fossil fuel which when combusted to produce energy releases an unwanted by-product: carbon dioxide. The major problem with carbon dioxide is that it is a greenhouse gas which have been identified as one of the main causes of climate change.

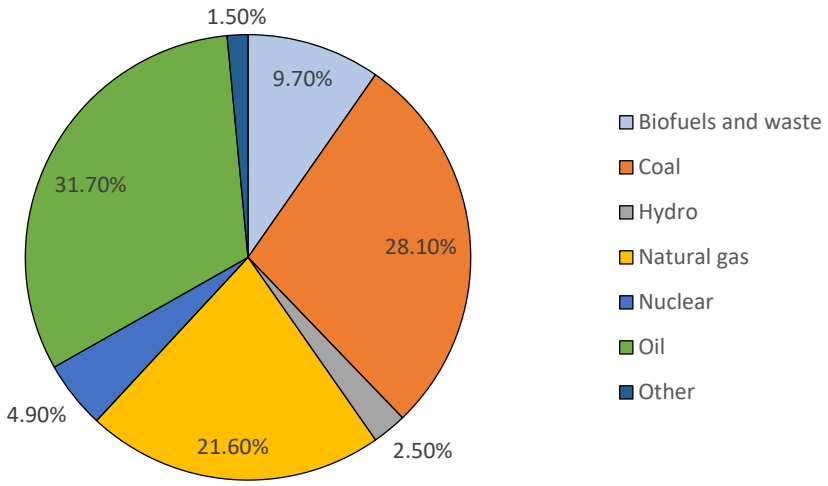

Figure 2.1: World total primary energy supply of 13 647 Mtoe by fuels in 2015.

According to McMichael (2013) global climate change is part of the proposed epoch known as the Anthropocene syndrome. This forms a large part of the human-induced global environmental changes which also include ocean acidification, disruptions and depletions of the ozone concentration, etc. McMichael (2013) also describes how greenhouse gas emissions through generation of energy using fossil fuels as well as emissions from the agriculture and transport sectors are leading to global warming due to increase heat retention in the lower atmosphere. In fact, it is estimated that the surface temperature of the earth has increased by approximately 0.74°C over the past 100 years by recent estimates (IPCC, 2007).

With global carbon dioxide emissions not set to decrease in the near future, prompt and considerable international action to lower these emissions is required. Without any actions it is estimated that by 2050 surface temperature is likely to have increased by 1 to 2°C and by 3 to 4°C by 2100 (McMichael, 2013).

Depleted fossil fuel reserves, rapidly increasing consumption rates, the environmental ramifications of energy production and the energy insecurity with regards to regional instability means that the demand for an energy source that is both clean and renewable is ever increasing (Khanal et al., 2008). Hydrogen is seen as a potential answer to these problems as it is a clean fuel source with one of the highest known energy contents.

2.2 Hydrogen production

Hydrogen has been identified as a potential replacement for fossil fuels in the energy production sector as doing so will lead to reduced carbon emissions which will aid in slowing down the estimated increase in the earth's surface temperature. As mentioned above, hydrogen is also an attractive alternative source of energy due to its high energy density and its increased efficiency with regards to conversion to usable power (Hallenbeck and Ghosh, 2009). The production of the hydrogen itself plays an important role in whether it will be a suitable source of renewable energy that is both environmentally benign and sustainable (Dincer and Joshi, 2013). This is due to the majority of current hydrogen production methods being non-renewable and the greenhouse gases, such as carbon dioxide, merely being shifted upstream to the production of the hydrogen. This upstream shift of carbon emissions is discussed in more detail in section 2.2.1.

Hydrogen can be produced using both renewable and non-renewable sources of energy. Hydrogen produced using renewable sources currently has the advantage of being environmentally friendly (Dincer and Joshi, 2013) whereas energy produced using non-renewable resources is currently the most economical method of hydrogen production.

2.2.1 Non-renewable methods of hydrogen production

Approximately 96% of hydrogen is produced using fossil fuel processing technologies which convert hydrogen containing fossil fuels, such as natural gas, coal, hydrocarbons and methanol or ethanol into a gas stream that is rich in hydrogen (Kalamaras and Efstathiou, 2013; Konieczny et al., 2008).

There are a number of technologies for converting hydrocarbons into synthesis gas (a mixture of carbon monoxide and hydrogen). Currently the most common options are steam reforming (SR), partial oxidation (POX) and autothermal reforming (ATR). Plasma reforming is a recently developed technology that is a very promising facilitator of the SR, POX and ATR processes (Kalamaras and Efstathiou, 2013).

These three main technologies all require significant downstream processing. Fossil fuels contain sulphur which must be removed from the production gas using desulphurisation techniques (Kalamaras and Efstathiou, 2013). This is due to hydrogen and sulphur possibly reacting to form hydrogen sulphide, which is a poisonous and corrosive gas. Due to the nature of the hydrogen production technologies, large

quantities of carbon monoxide are also produced alongside the hydrogen gas. Therefore, subsequent steps are required to convert carbon monoxide (poisonous) to carbon dioxide (inert) via the water-gas shift reaction (Kalamaras and Efstathiou, 2013). This illustrates how we are left with a fuel that is environmentally benign, based on zero carbon emissions, but the release of greenhouse gases (carbon dioxide) have merely been shifted upstream to the formation of hydrogen.

2.2.2 Renewable methods of hydrogen production – a focus on biological production

Methane, coal and oil are currently the main sources for the production of hydrogen, with major research going into the minimisation of environmental damage due to the resulting greenhouse gas emissions (Dincer and Joshi, 2013). It is therefore necessary to move towards renewable methods of hydrogen production to obtain a clean source of energy in a sustainable manner. Figure 2.2 provides a breakdown of the current methods of renewable hydrogen production with Table 2.1 providing some of the major advantages and disadvantages associated with each discussed method.

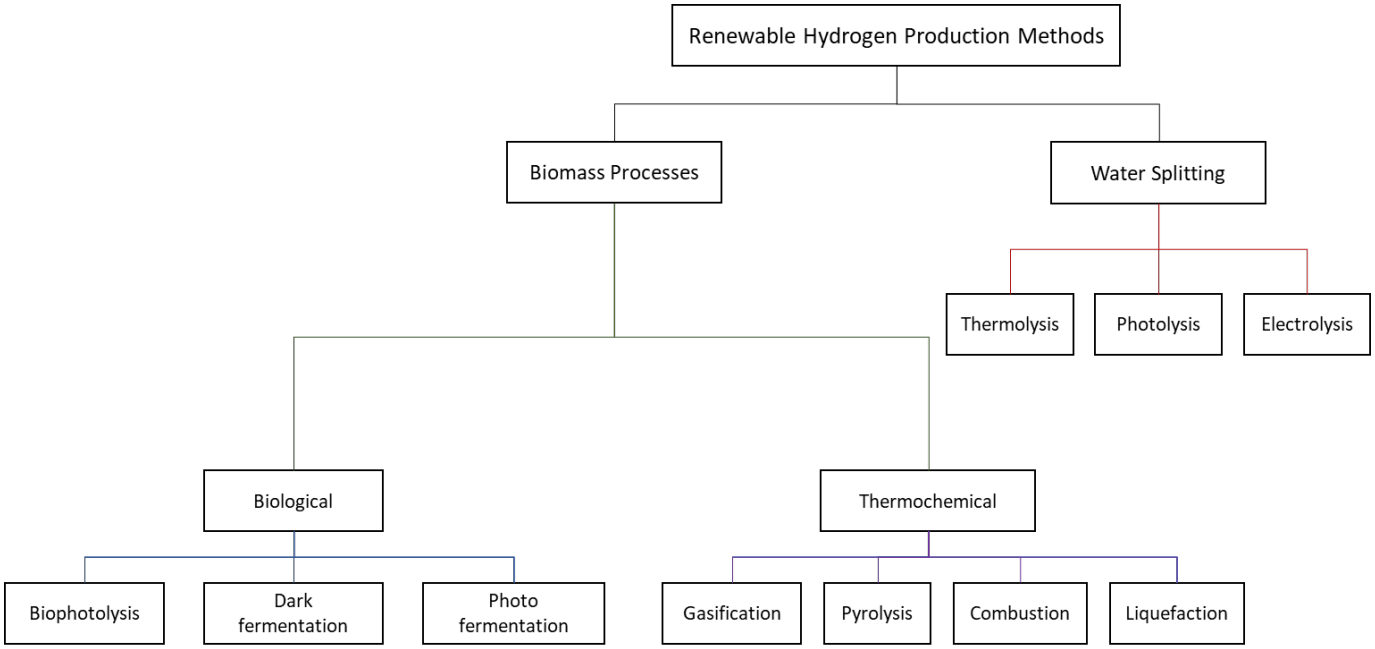

Figure 2.2: Breakdown of the current renewable hydrogen production methods. Figure adapted from Kumar and Himabindu (2019).

Table 2.1: Renewable hydrogen production methods with some of their major advantages and disadvantages (Acar and Dincer, 2014; Dincer and Joshi, 2013; Hallenbeck and Ghosh, 2009; Shiva Kumar and Himabindu, 2019).

Renewable hydrogen production method	**Advantages**	**Disadvantages**
Biophotolysis	Byproduct is O_2, carbon negative process and uses sunlight as energy source.	Low light conversion efficiencies and hydrogenase sensitivity to O_2.
Dark fermentation	H_2 production with no light source required, not limited by O_2, carbon neutral and uses a waste stream.	Low conversion efficiency and volatile fatty acid (VFA) production common.
Photofermentation	Uses organic compounds in waste streams and has very high substrate conversion efficiencies.	Low hydrogen yields and production rates.
Biomass gasification	Feedstock is plentiful and is generally a waste stream such as municipal or animal waste.	Still sees the release of CO_2 when the biomass is oxidised and fluctuating H_2 production.
Pyrolysis	Abundant and cheap feedstock.	H_2 yield fluctuations due to feedstock impurities and tar formation.
Thermolysis	Clean H_2 and O_2 as products with abundant feed stream.	High capital costs as well as corrosion problems.
Photolysis	Clean H_2 with O_2 as a byproduct, carbon free and only requires light energy from the sun.	Low efficiency and high cost.
Electrolysis	Clean H_2 with no CO_2 or sulphur emissions.	Very high capital costs ~25 times more than current fossil fuel-based methods.

The majority of thermochemical and electrochemical hydrogen production methods provided in Figure 2.2 and Table 2.1 are energy-intensive and in some cases not entirely environmentally friendly compared to the biological hydrogen production methods. Hydrogen production from the biological methods also allow for utilisation of substrates associated with waste streams which leads to renewable energy from a waste stream that is possibly inexhaustible (Das and Veziroğlu, 2001). Based on this, biological hydrogen production methods will be investigated further.

There are three major categories of biological hydrogen production: biophotolysis, dark fermentation and photofermentation (Hallenbeck and Ghosh, 2009; Hay et al., 2013; Shiva Kumar and Himabindu, 2019). All three technologies rely either on hydrogenase or nitrogenase enzymes which catalyses the reduction of certain compounds leading to hydrogen evolution. The enzymes derive energy via two methods, either directly from light or indirectly from carbon compounds (Hallenbeck and Ghosh, 2009). The mechanism of these enzymes is discussed in more detail in section 2.3.3.2. These three categories of biological hydrogen production are discussed in the sub sections below.

2.2.2.1 Direct biophotolysis

Direct biophotolysis occurs in certain organisms such as cyanobacterium and photosynthetic microalgae, both of which obtain their energy through photosynthesis. Due to this nature the organisms use solar energy to split water molecules (H_2O) to produce oxygen and electrons are used for reduction of redox carriers, such as ferrodoxin and nicotinamide adenine dinucleotide phosphate ($NADP^+$) (Hallenbeck and Ghosh, 2009; Lee et al., 2010). It is the reduction of the redox carriers that can be used for the production of hydrogen which is catalysed by hydrogenase enzymes present in certain cyanobacteria and microalgae (Lee et al., 2010).

Biophotolysis is a very attractive technology, as the process sees water converted to hydrogen and oxygen which results in a carbon free process that is powered by solar energy, the ultimate renewable energy source (Hallenbeck and Ghosh, 2009; Lee et al., 2010). However, low light conversion efficiencies and the hydrogenase enzymes sensitivity to oxygen has limited the process (Hallenbeck and Ghosh, 2009). The hydrogenase is inhibited by the presence of oxygen, as it irreversibly inactivates the enzyme (Kim and Kim, 2011).

2.2.2.2 Dark fermentation

In the dark fermentation process microbes are used anaerobically to breakdown substrates that are rich in carbohydrates to produce hydrogen along with some acids and alcohols (Hallenbeck and Ghosh, 2009). A diverse group of bacteria can be used in the dark fermentation process. During dark fermentation the bacteria utilizes pyruvate-ferrodoxin-hydrogenase or pyruvate-formate lyase with the electron donor being an organic compound (Lee et al., 2010).

The consortium of bacteria (usually mixed-cultures) used in dark fermentation are robust and can consume a variety of organic substrates, ranging from cellulose to municipal waste (Lee et al., 2010). The fact that no light energy is required for the process means that the only energy input required is that of mixing, therefore decreasing the energy input to the system (Hallenbeck and Ghosh, 2009; Lee et al., 2010). The formation of the undesired products (acids and alcohols) is a known disadvantage (Hallenbeck and Ghosh, 2009) as this leads to the creation of a waste stream that will either need to be processed further to obtain a useful product or to be disposed of in an environmentally safe manner. The gas stream produced (product stream) is usually an equal parts mixture of hydrogen and carbon dioxide and therefore will also require downstream processing to purify to mixture in terms of the hydrogen content if it is to be used in a fuel cell (Levin et al., 2004). Purification is required due to fuel cells such as the proton exchange membrane fuel cells (PEMFC) requiring streams of gas with more than 99% hydrogen purity.

Hallenbeck (2009) states that dark fermentation can only have a maximum conversion efficiency of 33%, i.e. only 33% of potential electrons available go to the production of hydrogen, with the remainder going to the production of the before mentioned waste products. This is illustrated in Equation 1 and 2 below, where Equation 1 is the Thauer limit for glycerol and Equation 2 is the reaction in theory.

Thauer limit: $$C_6H_{12}O_6 + 2H_2O \rightarrow 2CH_3COOH\ (acetic\ acid) + 2CO_2 + 4H_2 \quad [1]$$

Theory: $$C_6H_{12}O_6 + 6H_2O \rightarrow 6CO_2 + 12H_2 \quad [2]$$

Therefore, in practice only 4 moles of hydrogen can be produced in comparison to the theoretical amount of 12 moles, with the remainder of the hydrogen going to the formation of the acid by-product which in this case is acetic acid. Thus, the limiting factor for the commercial application of dark fermentation is its low conversion efficiency.

2.2.2.3 Photofermentation

Photofermentation is the conversion of organic substrates to hydrogen and is displayed by a variety of photosynthetic bacteria. As the name suggests it differs from the afore-mentioned dark fermentation process as photofermentation requires light to proceed. One class of photosynthetic bacteria are purple non-sulphur bacteria (PNSB), which carry out anaerobic photosynthesis to produce adenosine triphosphate (ATP) and high energy electrons that reduce ferredoxin (Hallenbeck and Ghosh, 2009). The reduced ferredoxin and ATP then drive proton reduction to hydrogen via the nitrogenase enzyme. The PNSB derive electrons from organic compounds which means that photofermentation has potential for waste treatment due to the conversion of organic compounds (waste) to hydrogen and carbon dioxide (Hallenbeck and Ghosh, 2009).

McKinlay et al., (2014) provides the reaction network for the theoretical maximum amount of hydrogen that can be produced via photofermentation when acetate (organic substrate) is fully oxidized. This was used to develop a general reaction network for any organic substrate fed to the process and is provided in Equations 3 to 5. Equation 5 can now be used to determine the theoretical moles of hydrogen that can be produced per mole of organic substrate used.

$$C_mH_nO_o + (2m - o)H_2O \rightarrow mCO_2 + (4m + n - 2o)H^+ + (4m + n - 2o)e^- \quad [3]$$

$$(4m + n - 2o)H^+ + (4m + n - 2o)e^- \rightarrow \left(2m + \frac{n}{2} - o\right)H_2 \quad [4]$$

$$C_mH_nO_o + (2m - o)H_2O \rightarrow mCO_2 + \left(2m + \frac{n}{2} - o\right)H_2 \quad [5]$$

The PNSB family has been the most studied photosynthetic bacteria for its use in photofermentative processes to produce biological hydrogen. This is likely due to its high conversion efficiency that will be discussed in section 2.5.

Equation 6 and 7 below provide the stoichiometric reaction for the production of hydrogen when the same substrate (in this case glycerol) is either used in photofermentation or dark fermentation. Equation 6 shows that 7 moles of hydrogen can theoretically be produced per mole of glycerol fermented, whereas during dark fermentation a theoretical maximum of 3 moles of hydrogen per mole of glycerol is possible with acetic acid as the by-product.

Photofermentation: $$C_3H_8O_3 + 3H_2O \rightarrow 3CO_2 + 7H_2 \quad [6]$$

Dark fermentation: $$C_3H_8O_3 + H_2O \rightarrow CH_3COOH\ (acetic\ acid) + CO_2 + 3H_2 \quad [7]$$

Thus, photofermentation can theoretically produce 4 extra moles of hydrogen per mole of glycerol when compared to dark fermentation. The theoretically high conversion of an organic substrate to hydrogen during photofermentation makes it an attractive option as a renewable hydrogen production method.

2.3 Rhodopseudomonas palustris

Rhodopseudomonas palustris (*R. palustris*) has been identified as a PNSB that has been used in the photofermentation of multiple organic substrates to produce hydrogen. This photosynthetic bacterium has consequently been selected for this study.

2.3.1 Taxonomy and reproduction of R. palustris

R. palustris is a PNSB that belongs to the proteobacterium phylum and the alphaproteobacterium class (Larimer et al., 2004). The robustness and versatility of *R. palustris* is illustrated by the wide range of environments that *R. palustris* can be found: from earthworm droppings to pond water and swine waste lagoons (Larimer et al., 2004).

According to Whittenbury and McLee (1967) one of the most prominent features of the *R. palustris* bacterium was the variation in the size, shape and opacity of the cells. This variety in size and shape suggested that these organisms possess a 'life cycle'. This life cycle is known as the budding cell cycle which produces two morphologically distinct phases, i.e. the 'mother cell' that is immotile and the 'swarmer' that is smaller and motile.

The budding cell cycle is presented in Figure 2.3, reproduced from Westmacott and Primrose (1976).

The cycle has been described by Whittenbury and McLee (1967) and Pott (2013) as follows: the small 'swarmer' cell (a) begins to extrude a short phase contrast-translucent tube, which is narrower than the

original cell (b through c). At the end of this tube a bud develops (d) which swells to give the whole structure a dumbbell shape (e). Division then occurs between what is now distinctly the 'mother cell' and the smaller, motile 'swarmer cell' (f). The 'swarmer cell' has a single polar or sub-polar flagellum whereas the 'mother cell' remains immotile. The tip of the 'mother cell' (on the pole opposite to the tube) is known as the 'holdfast' and is sticky. This allows the 'mother cells' to join one another by their 'holdfast' which creates a rosette like structure.

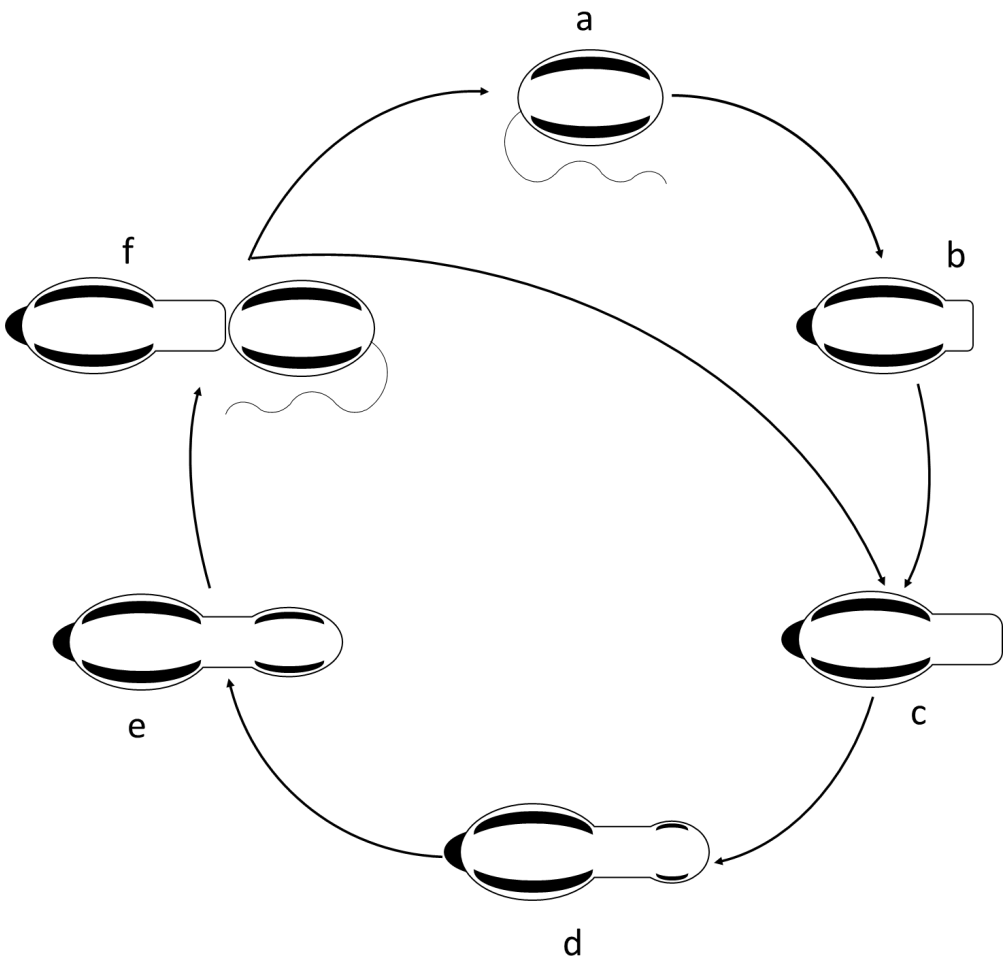

Figure 2.3: Representation of the budding cell cycle of Rhodopseudomonas palustris. Diagram reproduced from Westmacott and Primrose (1976).

Individual *R. palustris* cells are rod-shaped to ovoid in shape and are occasionally curved (Brenner et al., 2005). The size of individual cells can vary significantly but are usually in the range of $0.6 - 0.9 \times 1.2\text{-}2.0\ \mu m$ (Brenner et al., 2005). *R. palustris* cell cultures are a red to brownish-red colour (Brenner et al., 2005) due to the individual cell colour being a red/pink colour as can be seen in Figure 2.4 (a digitally-colourised image of *R. palustris* strain TIE-1 that was obtained via electron microscopy).

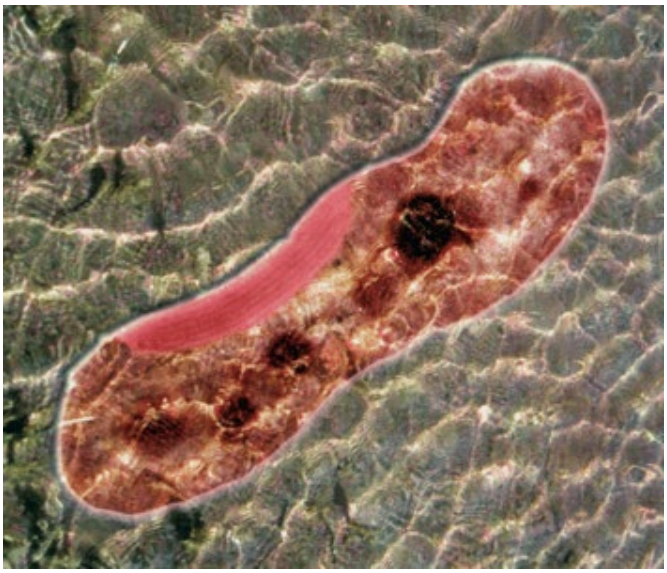

Figure 2.4: Electron micrograph image of R. palustris strain TIE-1 (American Society for Microbiology, 2009)

2.3.2 Metabolic pathways of R. palustris

R. palustris can grow via all four main modes of metabolism that support life, which are as follows: photoautotrophic (energy from light and carbon from carbon dioxide), photoheterotrophic (energy from light and carbon from organic compounds), chemoautotrophic (energy from inorganic compounds and carbon from carbon dioxide) and chemoheterotrophic (carbon and energy from organic compounds) (Larimer et al., 2004), these growth modes are summarised in Table 2.2. This characteristic lends to it being one of the most metabolically versatile bacteria.

Table 2.2: Summary of the modes of growth of R. palustris: photoautotrophic, photoheterotrophic, chemoautotrophic and chemoheterotrophic and some of their key traits (Pott, 2013).

Growth mode	**Aerobic/ anaerobic**	**Light/ no Light**	**Carbon source**	**Electron source/ energy source**	**Hydrogen production?**
Photoautotrophic	Anaerobic	Light	Carbon dioxide	Hydrogen, thiosulphate and other inorganic electron donors/light	Hydrogen consumption
Photoheterotrophic	Anaerobic	Light	Organic carbon	Organic carbon/ light	Significant hydrogen production in the absence of ammonia
Chemoautotrophic	Aerobic	No Light	Carbon dioxide	Hydrogen, thiosulphate and other inorganic electron donors	Hydrogen consumption
Chemoheterotrophic	Aerobic	No Light	Organic carbon	Organic carbon	None

2.3.3 R. palustris metabolism with regards to hydrogen production

This investigation focuses on the production of hydrogen. The metabolic pathway of *R. palustris* facilitates this, which motivates the selection of *R. palustris* for this study. Table 2.2 indicates that *R. palustris* produce hydrogen only under photoheterotrophic growth and in the absence of ammonia. Further investigation into the hydrogen production metabolism under these conditions is required. Brenner et al. (2005) suggests that *R. palustris* preferred mode of growth is photoheterotrophic growth under anoxic conditions which bodes well for the production of hydrogen gas.

2.3.3.1 Hydrogen production metabolism

As stated above hydrogen production by *R. palustris* occurs under photoheterotrophic growth, and thus occurs when the culture is subjected to an anaerobic atmosphere, under illumination and with an organic substrate available for utilisation. According to Koku et al. (2002) ammonium, which is commonly used as a nitrogen source in the culturing of PNS bacteria, inhibits hydrogen production as it suppresses the synthesis of nitrogenase and also inhibits the nitrogenase enzyme activity. The inhibition of the nitrogenase is reversible which means that when the ammonium is fully consumed the nitrogenase enzyme activity will fully recover. This is also the case for other non-ammonium containing nitrogen sources, which means that the culture should be under nitrogen limitation to ensure hydrogen production. According to Koku et al. (2002) and Pott (2013) hydrogen production with glutamate as the sole nitrogen source is also possible as it is able to stimulate the synthesis and activity of the nitrogenase enzyme. The hydrogen production metabolism under these conditions is made up of several key components, i.e. the nitrogenase and hydrogenase enzyme, the photosystem, the Calvin-Benson-Bassham (CBB) cycle and the storage compounds (Pott, 2013). Figure 2.5 illustrates the biological hydrogen production metabolism in the conditions mentioned.

In Figure 2.5 light photons are absorbed by the light harvesting complexes (LH1 and LH2) which then rapidly transfer the energy to the photosynthetic reaction centre (RC). This energy is used to initiate the cyclic electron transport (curved purple arrows) between the RC and the cytochrome b/c_1 ($Cytbc_1$). Here the reducing equivalents are transported by ubiquinone (Q). Figure 2.5 indicates that a proton gradient is produced that is utilised by the ATP synthase (ATPase) to produce the required ATP. A flux of reducing equivalents (e^-) leaves the ubiquinone pool and are transported by ferredoxin (Fd), which mediates electron transfer, to the nitrogenase (N_2ase) enzyme to fix nitrogen to ammonia with the concomitant obligate of hydrogen produced. As discussed previously the hydrogenase enzyme present in the cyanobacterium and photosynthetic microalgae used in direct biophotolysis is used in the production of hydrogen. However, generally in PNS bacteria the hydrogenase (Hup) (if there is an active hydrogenase enzyme), converts hydrogen to electrons and protons used for ATPase. The reducing equivalents are also

used in the Calvin cycle (CBB pathway) to fix carbon dioxide and to store the carbon as poly(hydroxybutrate) (PHB) and glycogen. The tricarboxylic acid (TCA) cycle, also known as the Krebs cycle, metabolises organic substrates to produce protons and electrons. Protons are used in the formation of hydrogen and electrons are used as reducing equivalents in the photosystem. (Pott, 2013; Roszak et al., 2003)

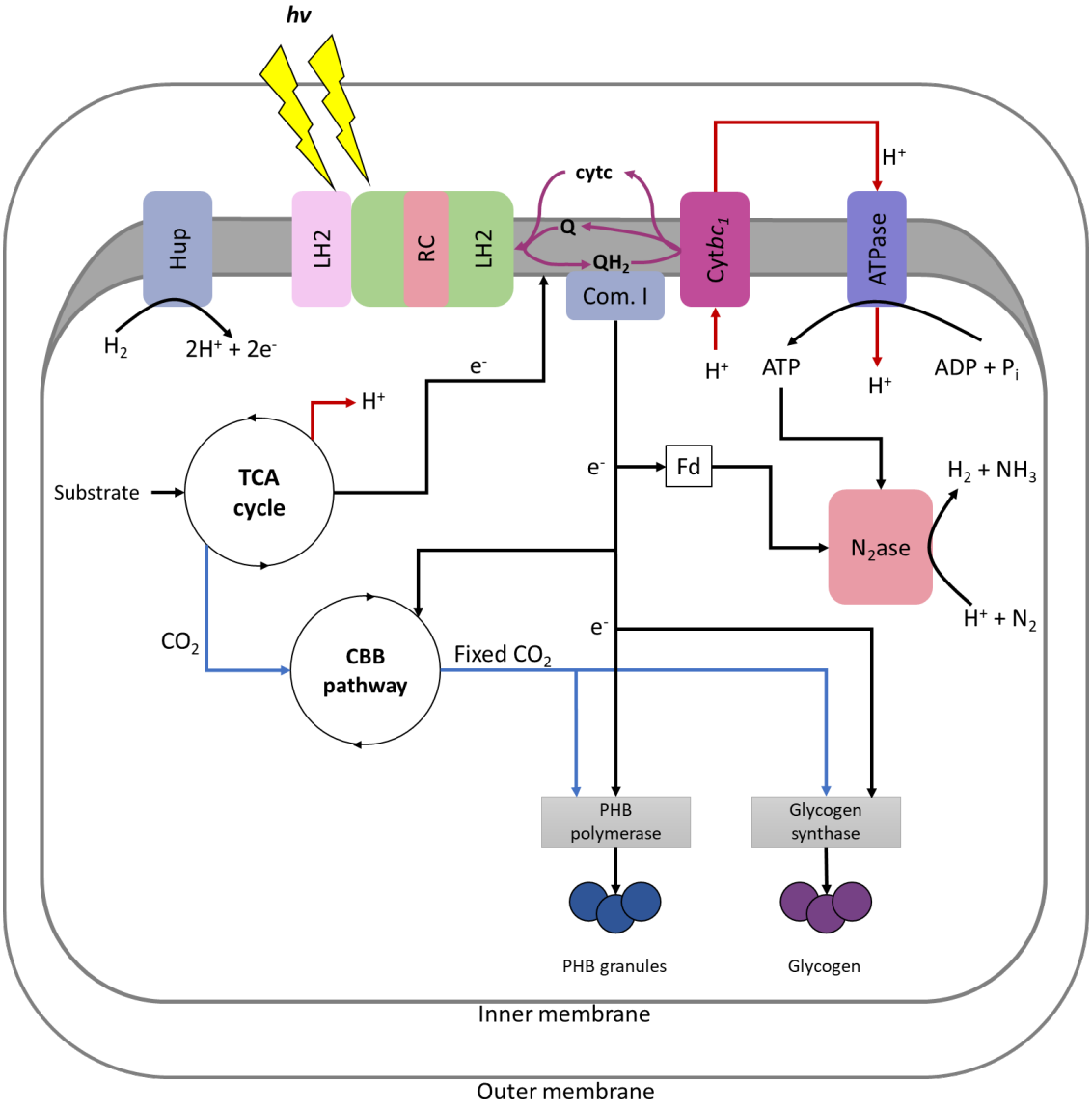

Figure 2.5: Schematic diagram of the biological hydrogen production metabolism of R. palustris which occurs during photoheterotrophic, anaerobic and nitrogen fixing conditions adapted from Pott (2013). The outer most grey line indicates the outer membrane of the cell. The thick grey line indicates the inner cell membrane. The yellow lightning symbols indicates light excitation. Straight black arrows indicate the flow of electrons. The blue arrows indicate the flow of CO_2 or fixed CO_2. The red arrows indicate proton (H^+) flow. The curved black arrows indicate a reaction occurring. The curved purple arrows indicate the cyclic electron transport system that forms part of the photosynthetic apparatus.

2.3.3.2 Major enzymes

As discussed in the section above, two major enzymes are involved in the evolution of hydrogen by *R. palsutris,* i.e. the hydrogenase and nitrogenase enzyme. The total hydrogen produced is the balance of the two enzymes. According to Koku et al. (2002) the primary inhibitor/repressor of these enzymes is the presence of oxygen. The presence of oxygen irreversibly deactivates the enzymes (Kim and Kim, 2011) and is therefore the major reason why *R. palsutris* must be cultivated in anaerobic conditions if hydrogen production is required. The mechanism of each major enzyme is discussed in detail below.

a) Nitrogenase

R. palustris produces hydrogen via the nitrogenase enzyme (McKinlay et al., 2014). The nitrogenase enzyme catalyses the energy intensive process of reducing dinitrogen to ammonia which is driven by ATP hydrolysis (Burris, 1991). According to Wall (2004) the action of the nitrogenase enzyme can be described by the following reactions, where the stoichiometry is dependent on the metal cofactor (either molybdenum (Mo), vanadium (V) and iron (Fe)):

Mo: $$N_2 + 8H^+ + 8e^- + 16\text{ATP} \rightarrow 2NH_3 + H_2 + 16ADP \quad [8]$$

V: $$N_2 + 8H^+ + 8e^- + 24\text{ATP} \rightarrow 2NH_3 + 3H_2 + 24ADP \quad [9]$$

Fe: $$N_2 + 8H^+ + 8e^- + 42\text{ATP} \rightarrow 2NH_3 + 7.5H_2 + 42ADP \quad [10]$$

In PNS bacteria the Mo-cofactor is the most frequently occurring isozyme as it has the lowest energy requirement to catalyse the reaction. However, this isozyme also has the lowest conversion efficiency and therefore large enzyme concentrations are required to ensure a high rate of hydrogen production (Pott, 2013).

However, when PNS bacteria such as *R. palustris* is cultured in a nitrogen free atmosphere, a different reaction path is followed, because the absence of dinitrogen means the reducing equivalents are redirected entirely to hydrogen production (Burris, 1991). In these conditions the hydrogen production is stoichiometrically four-fold higher as illustrated in Equation 11 provided by (Burris, 1991).

$$8H^+ + 8e^- 16\text{ATP} \rightarrow 4H_2 + 16ADP \quad [11]$$

Thus, theoretical maximum hydrogen production will be obtained when *R. palustris* is grown via the photoheterotrophic metabolism, where light and organic carbon is supplied, in an oxygen and nitrogen free atmosphere. An inert gas such as argon can be used to sparge the culturing system to remove nitrogen and oxygen from the systems atmosphere.

b) Hydrogenase

The hydrogen uptake of the hydrogenase enzyme is defined by the reversible reaction provided in Equation 12.

$$2H^+ + 2e^- \leftrightarrow H_2 \qquad [12]$$

The direction of the hydrogenase enzyme reaction is dependent on the culturing condition. In general, the conditions utilised during photofermentation favour the reverse reaction and thus the hydrogenase enzyme consumes hydrogen. Therefore, the hydrogen produced by the nitrogenase subtracted by the hydrogen consumed by the hydrogenase is equal to the total hydrogen that can theoretically be produced. It should be noted that there are certain strains of *R. palustris*, such as *R. palustris* CGA009, that have an inactive hydrogenase and therefore do not consume any hydrogen.

2.3.4 Photosystem

Photosynthesis is the process by which solar energy is converted into chemical energy through the synthesis of complex organic molecules (Blankenship et al., 2006; Hu et al., 2002).The process can be carried out by a variety of organisms such as photosynthetic bacteria, algae and plants (Hu et al., 2002). Purple photosynthetic bacteria, such as *R. palustris,* have been studied extensively due to their relatively simple photosystems (Roszak et al., 2003) that is similar to the photosystem II found in higher order plants. However, there is a significant difference between photosynthesis of PNSB and the photosynthesis carried out by plants and algae and that is that PNSB does not contain photosystem I, which means it does not have the ability to split water to evolve oxygen (Pott, 2013). Thus, photosynthesis in PNS bacteria can only take place in anoxic conditions as the low oxygen presence triggers formation of photosynthetic pigments (Mcewan, 1994).

A diagrammatic representation of the major membrane proteins involved in the light reaction of purple photosynthetic bacteria is provided in Figure 2.6. The photosynthetic reactions begin with photons (yellow arrows) absorbed by the LH2 antenna at wavelength bands of 800 and 850 nm (labelled B800 and B850in the LH2 complex) which correspond to absorption maxima of bacteriochlorophyll-α (BChl-α) pigments (Roszak et al., 2003). The LH2 BChl-α then passes the absorbed energy to the BChl-α (denoted by B880) in the second antenna complex (LH1) (Roszak et al., 2003). The BChl-α in the LH1 complexes usually have one adsorption band in the wavelength range of 870 to 890 nm. Charge separation in the RC reduces the lipid soluble electron carrier (ubiquinone), then the aqueous phase cytochrome *c* re-reduces the RC. After adsorption of a second photon a twice reduced ubiquinone diffuses into the cytochrome bc_1 complex, which passes the electrons from the ubiquinone to reduce the water phase in the cytochrome c (Cyt c) (Pott, 2013). Thus, the cyclic electron transport chain is closed with the

generated chemical potential preserved as a proton (H+) gradient, which can then be used by the ATP synthase to produce ATP from ADP.

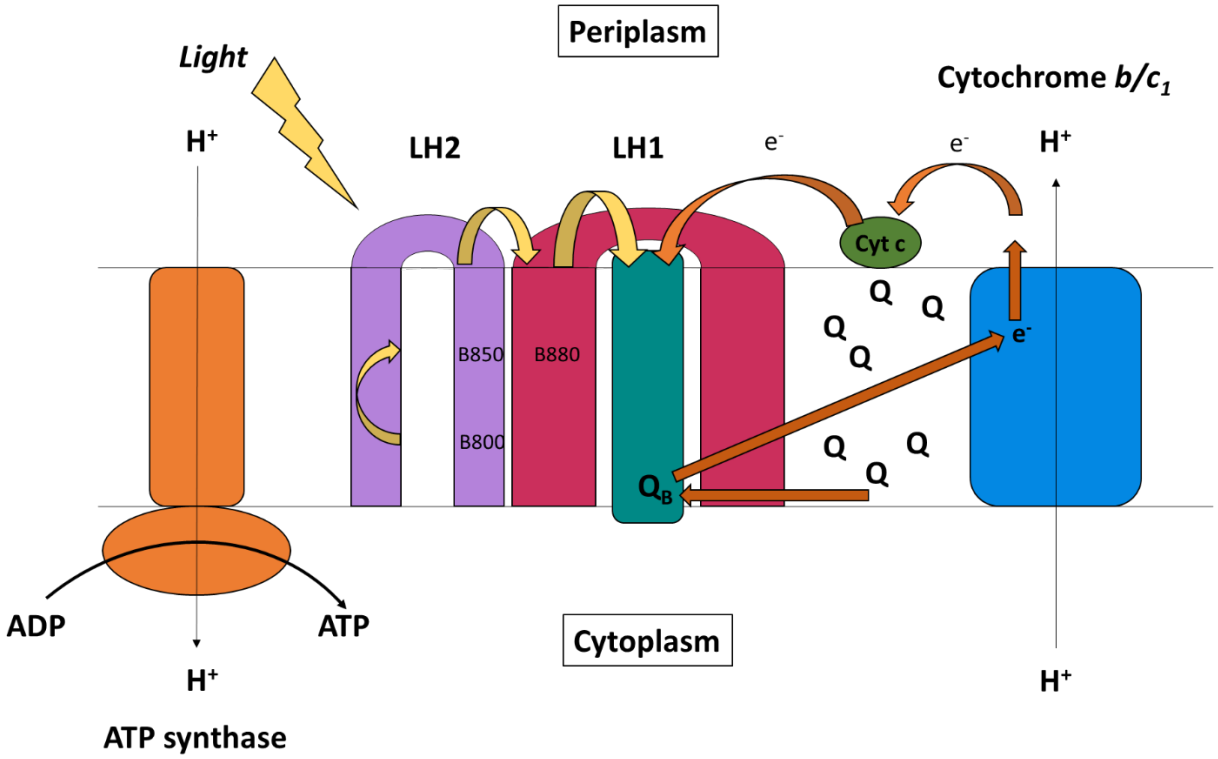

Figure 2.6: A representation of the major membrane proteins involved in the light reaction of purple photosynthetic bacteria, adapted from Roszak et al. *(2003). Photon energy is represented yellow arrows. The LH2 antenna is the purple complex with the labels B800 and B850 representing the wavelength of maximal absorption. The LH1 antenna is the red complex with the B880 label, again referring to the wavelength corresponding to maximal absorption. The reaction centre is labelled RC. Red arrows represent electron flow. The cytochrome bc_1 complex is represented by the blue block. The ATP synthase which sees ATP synthesised is represented by the orange figure.*

There are various pigments present in the LH complexes such as carotenoids, bacteriochlorophylls (BChl's) and bilin pigments (Blankenship et al., 2006; Damjanović et al., 1999). With specific focus on *R. palustris* the two major pigments present in their LH complexes are carotenoids and BChl-α (Brenner et al., 2005). BChl α pigments' major function is light harvesting whereas carotenoids perform three major roles: (i) light harvesting at lower wavelengths (blue-green wavelength range), (ii) photoprotection and (iii) stabilising LHs as structural components (Damjanović et al., 1999; Paulsen et al., 1999).

2.3.5 Current industrial usage of R. palustris

Wastewater treatment facilities use a combination of microbial populations in the digestion section of the process, PNSB being one of the major components (Larimer et al., 2004). According to Larimer et al.

(2004) *R. palustris* thrives in the environments that are common in wastewater treatment facilities and has the ability to metabolise lignin monomers, fatty acids and dicarboxylic acids, animal fats, seed oils and multiple other organic compounds. *R. palustris* also has the ability to degrade nitrogen-containing compounds such as amino acids and some aromatic compounds. Some common chlorinated compounds found in industrial wastes can also be dehalogenated and degraded using the *R. palustris* bacteria (Larimer et al., 2004).

The ability of *R. palustris* to degrade organic waste streams to produce high purity hydrogen makes it highly attractive in the context of this investigation.

2.4 Modelling of biological processes

Combining experimental work with mathematical modelling allows for meaningful and quantitative interpretation of the results obtained from the experimental results and can possibly reveal new aspects of microbial physiology (Mahanta et al., 2014).

2.4.1 Modelling of biological growth

Blackman gave one of the earliest models for describing biotechnological processes in 1905 (Kovarova-Kovar and Egli, 1998; Mahanta et al., 2014). In the Blackman model it is assumed that the specific growth rate (μ) is proportional to substrate concentration (s) when the substrate concentration is low. When the substrate concentration is high the growth rate is independent of the substrate concentration. This relationship is described in Equation 13 (Mahanta et al., 2014). From Equation 13 it can also be seen that the function is not smooth, due to the transition from first order to zero order when the substrate concentration is larger than half-saturation coefficient (K_s) (Mahanta et al., 2014).

$$\begin{aligned} \mu(s) &= \frac{\mu_{max} \cdot s}{K_s} \qquad if\ s < K_s \\ \mu &= \mu_{max} \qquad if\ s \geq K_s \end{aligned} \qquad [\ 13\ ]$$

For the past 70 years, most of the modelling of microbial growth has seen the Monod equation employed (Liu, 2007). The Monod model provides a relationship between the specific growth rate and the substrate concentration in the form provided in Equation 14. The Monod model is often mistakenly thought of as a theoretical model when in fact it is empirical based on curve fitting to experimental data.

$$\mu(s) = \frac{\mu_{max} \cdot s}{K_s + s} \qquad [\ 14\ ]$$

The Monod model describing the specific growth rate can be used to quantify cell growth using Equation 15, which is known as Monod growth kinetics (Clarke, 2013).

$$\frac{dX}{dt} = \mu X \qquad [\ 15\ ]$$

The Monod model and the various variations thereof are used to model the growth and substrate utilisation of many different bacteria, but are not considered to be applicable to photosynthetic bacteria due to the models not taking into account the effects of light on these parameters. The Aiba model, shown in Equation 16, has often been employed to simulate the effect of light intensity on the growth rate of photosynthetic bacteria (Palamae et al., 2018; Zhang et al., 2015b, 2015a). According to Zhang et al. (2015a) the Aiba model is capable of modelling the photolimitation regime that can occur at low light intensities, the photosaturation regime under optimal light intensities, and the photoinhibition regime under very high light intensities.

$$\mu(I) = \mu_{max} \cdot \frac{I}{I + K_I + \frac{I^2}{K_i}} \quad [16]$$

In Equation 16, I is the light intensity, K_I is the light saturation coefficient and K_i, the photoinhibition coefficient. The Aiba model assumes the growth rate is only dependent on light, however substrate utilisation should also be taken into account if it has a limiting effect on the growth. The model can then be adjusted into the form provided in Equation 17.

$$\mu(I, s) = \frac{\mu_{max} \cdot s}{K_s + s} \cdot \frac{I}{I + K_I + \frac{I^2}{K_i}} \quad [17]$$

With a suitable equation to describe the specific growth rate of photosynthetic bacteria (either Equation 16 or 17) the growth rate $\left({}^{dX}/_{dt}\right)$ can be determined using an equation such as the one supplied in Equation 15. This equation can be modified to take into account the death rate (μ_d) of cells that occurs in the death phase (Palamae et al., 2018). Equation 18 provides a modified form of Equation 15 that includes the death rate.

$$\frac{dX}{dt} = \mu X - \mu_d X \quad [18]$$

In cases where the specific growth rate is a function of light and substrate concentration (Equation 17), Equation 18 cannot be explicitly solved on its own, hence an equation describing the substrate concentration and light intensity is required. Robinson and Tiedje (1983) provide an equation (Equation 19) describing the rate of change of substrate consumption by a bacterium growing in a batch culture that can be used in conjunction with Equation 18 to simultaneously solve for both the biomass and substrate concentration.

$$\frac{ds}{dt} = -Y_s \mu_{max} \left(\frac{s}{K_s + s}\right) X \quad [19]$$

2.4.2 Modelling of light through biological culture

According to Molina Grima et al. (1999) the growth rate is a function of the light intensity and the light profile which the cells are subject within a homogenous culture. Denser cultures cause light penetration to be impeded due to self-shading and light absorption by the cells, thus zones of different levels of illumination exist in the culture (Molina Grima et al., 1999). This means that cells nearer to the light incident surface experience higher intensities in comparison to cells in other regions of the cell culture, therefore the cell growth varies according to their position in the culture. Based on the effects of cell concentration and cell shading a mean value of irradiance is used to define the light intensity that each cell is experiencing with in a homogenously distributed culture. This mean value, which will be referred to as the average light intensity, is dependent on the following factors: (i) the incident light intensity (I_0) on the surface of the reactor, (ii) the geometry of the reactor which the bacteria is being cultured in, (iii) the concentration of the cells in the culture, (iv) the absorption of the cell pigments (Molina Grima et al., 1999) and (v) the direction(s) of light on the culture. A method for quantifying the light intensity through the reactor that accounts for the above factors is therefore required.

One of the most well-known equations used in the assessment of radiant light energy profiles is the Beer-Lambert law (Equation 20), however due to the aggregation of the effects of cell adsorption and light scattering by cells into a single extinction coefficient it has been stated to have poor accuracy with regards to modelling light attenuation in PBRs (Cornet et al., 1995).

$$I(X,z) = I_0 e^{-\alpha \cdot X \cdot z} \qquad [20]$$

Where α is the aggregated extinction coefficient and z is the light path length.

Modified versions of Equation 20 have been developed to improve the accuracy of the model by including an additional extinction coefficient that takes into account scattering by bubbles (Palamae et al., 2018; Zhang et al., 2015a) or by increasing the measured light path length using an optical path length multiplication (PLM) factor in order to take into account light scattering (Wágner et al., 2018).

On the other end of the spectrum the general theory of radiative transfer, which is far more complex (see Equation 21), has been applied to model radiant light energy transfer in PBRs.(Cornet et al., 1995). This is, however, no easy task and comes at a great computational cost (Cornet et al., 1995).

$$\frac{dI_\lambda(\vec{r},\vec{s})}{ds} + \left(a_\lambda + \sigma_{\lambda,s}\right) I_\lambda(\vec{r},\vec{s}) = \frac{a_\lambda n^2 \sigma T^4}{\pi} + \frac{\sigma_{\lambda,s}}{4\pi} \times \int_0^{4\pi} I_\lambda(\vec{r},\vec{s_i}) \Phi_\lambda(\vec{s_i},\vec{s}) d\Omega_i \qquad [21]$$

Where $I_\lambda(\vec{r},\vec{s})$is the wavelength ($\lambda$) radiation intensity at a specific light path direction ($\vec{s}$) and position vector ($\vec{r}$) ; a_λ is a wavelength dependent absorption coefficient; $\sigma_{\lambda,s}$ is a wavelength dependent scattering coefficient; s is the light path length, $\vec{s_i}$ is the scattering direction; n the refractive index; σ is the Stefan Boltzmann constant, T is the local temperature and $d\Omega_i$ solid angle.

Due to the complexity of the radiant light transfer equation and the simplicity of the Beer-Lambert law, a compromise was proposed by Cornet et al. (1995): a simple two-flux model which was derived based on assumptions made by Schuster (1905), that takes into account absorption and scattering of light by cells and that provides an analytical solution. The two-flux approximation is provided in Equations 22 to 24 below (Huang et al., 2015).

$$\frac{I_z}{I_0} = \frac{4\alpha_1}{(1+\alpha_1)^2 \cdot e^{\alpha_2} - (1-\alpha_1)^2 \cdot e^{-\alpha_2}} \quad [22]$$

$$\alpha_1 = \sqrt{\frac{E_a}{E_a + E_s}} \quad [23]$$

$$\alpha_2 = (E_a + E_s) \cdot \alpha_1 \cdot X \cdot z \quad [24]$$

From the equations above, E_a is the mass absorption coefficient and E_s is the scattering coefficient. It should be noted that the two-flux approximation simplifies to the Beer-Lambert law (Equation 20) if the effects of scattering are ignored ($E_s = 0$). The effects of scattering can be ignored at low biomass concentrations (Krujatz et al., 2015); however, when the biomass concentration increases the Beer-Lambert law cannot be applied to predict the light intensity profile inside the PBR (Berberoglu et al., 2007).

2.5 Substrates for hydrogen production by *R. palustris*

As previously stated, *R. palsutris* has the ability to metabolise a wide variety of compounds due to its metabolic diversity. Therefore, a copious number of substrates have been investigated in literature. Table 2.3 below provides a short list of some of the carbon sources that have been used to culture *R. palustris* to produce hydrogen. The reported specific hydrogen production rates are also provided to illustrate their ability to produce hydrogen through photofermentation.

Table 2.3: Hydrogen production rates (mL/g_{dw}/h) by R. palustris from different carbon sources

Carbon source	Hydrogen production rate (mL/g_{dw}/h)	Reference
Acetate	~23	(Pott et al., 2013)
	~38	(Barbosa et al., 2001)
Butryate	~20	(Pott et al., 2013)
	~22	(Wu et al., 2010)
Crude glycerol	~24	(Pott et al., 2013)
	~12	(Ghosh et al., 2012)
Glucose	~28	(Pott et al., 2013)
	~37	(Tian et al., 2010)
Glycerol	~31	(Pott et al., 2013)
	~32	(Sabourin-Provost and Hallenbeck, 2009)
Lactate	~24	(Pott et al., 2013)
	~39	(Vincenzini et al., 1982)
Malate	~15	(Pott et al., 2013)
	~40	(Fiβler et al., 1995)

Equation 6 in section 2.2.2.3 provided the reaction network for the theoretical maximum amount of hydrogen that can be produced via photofermentation of glycerol. This Equation is provided once more below for easy reference.

Equation 6: $$C_3H_8O_3 + 3H_2O \rightarrow 3CO_2 + 7H_2$$

According to Hallenbeck and Liu (2016) with glycerol as the carbon source a yield of 6.9 mol of H_2 per mol of crude glycerol has been achieved which is 96% of the theoretical maximum of 7 mol of H_2. Pott et al. (2013) also reported high yields of H_2 compared to the theoretical maximum (80-85%) when glycerol was used as the carbon source. The ability to achieve near stoichiometric conversion of glycerol to hydrogen makes it an extremely attractive substrate for photofermentation.

Glycerol is a polyol compound that is an obligate concomitant produced during transesterification in the biodiesel production process. Due to glycerol being a useful commodity chemical that was used in a multitude of industries, it was initially considered as a bonus in the biodiesel industry as it was a by-product that could improve the economics of the entire process (Pott, 2013). There has been a significant increase in the production of biodiesel which has seen the value of glycerol decreasing due to the inverse relationship between price and supply when the demand remains the same. Glycerol is now considered a financial and environmental burden because it no longer financially viable to refine the crude glycerol

for use in the food and pharmaceutical industries and is therefore disposed of as a waste product which is costly and has possible negative effects on the environment.

Photofermentation could therefore be used as a sink for this waste stream for the production of hydrogen.

2.6 Immobilisation of *R. palustris*

The immobilisation of microorganisms in solid supports has frequently been used in laboratory scale experiments as well as in industry. Cell immobilisation has been a highly discussed aspect of biotechnology for the past four decades because of i) its ability to improve performance and economics of fermentation processes (Zhu, 2007), due to improved thermal and mechanical stability, and ii) higher production rates due to the possibility of increased biomass loading when compared to free-cell cultures (Coiffier et al., 2001). Therefore, immobilisation of *R. palustris* has been considered as a promising avenue in the attempt to improve biohydrogen production (Wang et al., 2010). Pott (2013) provides a few key characteristics that an immobilisation matrix should display if it is to be used in the production of biohydrogen by *R. palustris*: i) the matrix should be non-toxic to the cells as well as biocompatible, ii) it should be translucent as the *R. palustris* hydrogen production metabolism is light driven, and iii) the material should be chemically and mechanically stable at the intended operating conditions.

Zhu (2007) cites several studies that attempted to utilise immobilised cells in fermentation processes. Vincenzini et al. (1982) immobilised *R. palustris* in an agar matrix and reported that immobilised cells retained their hydrogen producing activity for longer than free cell cultures that were operated at the same conditions. Fiβler et al. (1995) immobilised *R. palustris* in multiple matrices, namely agar, carrageenan and sodium alginate, and reported high hydrogen yields when compared to the theoretical maximum for all matrices. They also reported that hydrogen production by *R. palustris* doubled when immobilised in alginate compared to free-cell cultures, and was also able to produce hydrogen for extended periods (55 days) with slow decrease in efficiency.

Another method of bacterial immobilisation is the immobilisation on glass beads. Investigations into hydrogen production using porous glass plates and non-porous glass beads were done by Zagrodnik et al. (2013) and Zagrodnik et al. (2015) with *Rhodobacter sphaeroides* (*R. sphaeroides*) as the PNS bacteria of choice. The main drawback with this method of immobilisation is the low concentration of bacteria within the volume of the glass bead as the bacteria is only immobilised on the surface of the glass. This would result in ineffective use of reactor volume as most of the reactor will be filled with non-reactive glass beads with only the surface, where the bacteria are attached, able to metabolise the substrate within the reactor. This method of immobilisation is also extremely difficult in comparison to other immobilisation techniques. Immobilisation on porous glass also only lends itself to bioreactors with very

high surface to volume ratios such as flat panel bioreactors in order for the photosynthetic bacteria to receive the required light.

Wang et al. (2010) developed a hybrid matrix of polyvinyl alcohol (PVA)/sodium alginate/carrageenan which was immobilised with *R. palustris* and showed good hydrogen production. Pott (2013) developed novel PVA cryogel with glycerol as the co-solvent that was immobilised with *R. palsutris*. This matrix was reported to have similar hydrogen production to free-cell cultures.

From the above short literature survey, it is clear that PNS bacteria (in particular *R. palustris*) has been extensively investigated in the field of immobilisation. This is due to the fact that immobilisation of the bacteria in a hydrogel has been identified as covering several key areas relating to optimisation of process parameters that need to be improved to scaleup processes using PNS bacteria to produce biohydrogen. These areas include but are not limited to i) protection from physio-chemical challenges, ii) cryptic growth, iii) higher biomass concentration than in planktonic systems, and iv) reduced number of cell divisions resulting in metabolic energy being focused on product formation (Dervakos and Webb, 1991). Several hydrogel types have been developed and used in the immobilisation of bacteria. They are discussed next.

2.6.1 Hydrogel immobilisation matrices

Hydrogels can be defined as a network of cross-linked polymer chains that are often found as colloidal gels with water as the dispersion medium (Ahmed, 2015). These hydrogels can retain a significant fraction of water due to the hydrophilic functional groups present on the polymeric backbone with the cross-linked polymer chains preventing dissolution in water (Ahmed, 2015). These materials are used in various biomedical applications (Pott, 2013), due to their tissue-like degree of flexibility (Ahmed, 2015) and macroporous structure which allows for quick diffusion of substrates and products through the matrix. Several types of hydrogels are examined below with specific focus on the key characteristics that an immobilisation matrix should display if it is to be used in the production of biohydrogen by *R. palustris*.

2.6.1.1 Chitosan hydrogel

Chitosan is a biopolymer that is produced by N-deacetylation of chitin and cellulose (Dambies et al., 2001). Chitin is extracted from cuticles of anthropods and fungal biomass and is considered the most abundant natural polymer (Dambies et al., 2001). Chitosan gel beads are produced by dissolving the chitosan powder in acetic acid before dropwise addition to a molybdate solution or a sodium hydroxide solution coagulating bath (Dambies et al., 2001; Zhao et al., 2007). Zhao et al. (2007) state that after the chitosan gel beads solidify during preparation they became opaque. Thus, chitosan gel beads present stumbling blocks, as the required light will not reach the immobilised photosynthetic bacteria.

2.6.1.2 Carrageenan hydrogels

Kappa-carrageenan (κ-carrageenan) is a natural sulphated polysaccharide extracted from red seaweed (Yang et al., 2018). It is often used in the food industry as a thickener, stabiliser or texturing agent as well as in the cosmetic and pharmaceutical industries due to its distinguished biocompatibility and biodegradability (Yang et al., 2018). κ-carrageenan forms a thermo-reversible hydrogel when cooled in an aqueous solution containing either mono or double positive ions (K^+, Na^+ or Ca^{2+}) (Yang et al., 2018). During this gelation process the κ-carrageenan powder is dissolved in the aqueous solution at approximately 80°C, which means it would be unviable as an immobilisation matrix if a temperature-labile bacterium is used.

2.6.1.3 PVA cryogels

Polyvinyl alcohol (PVA) is a readily available non-expensive synthetic polymer that is used in a wide range of industries (Paţachia et al., 2009). PVA is manufactured via hydrolysis of polyvinyl acetate that has been synthesised from free radical polymerisation of vinyl acetate. It also consists of a secondary alcohol group that is attached to a linear carbon chain (Wan et al., 2014). The alcohol group plays an important role in the production of a hydrogel that has a high-water content when the PVA is dissolved in an aqueous solution, as it leads to the formation of hydrogen bonds (Wan et al., 2014). PVA cryogels are produced by freeze-thaw cycling of cells suspended in an aqueous PVA solution (Lozinsky and Plieva, 1998). Firstly, the PVA is dissolved in an aqueous solution that is then brought down to temperatures of -20°C to freeze the water phase present in the solution. The freezing of the water phase creates two regions, namely a high polymer concentration region where crystallites are formed and a low polymer concentration region, where pores are formed. Subsequently, the cryogel is thawed down to room temperature which leads to the formation of a solid gel (Lozinsky and Plieva, 1998; Paţachia et al., 2009; Wan et al., 2014).

PVA has sought-after properties such as biodegradability, biocompatibility, water solubility and non-toxicity (Paţachia et al., 2009). These exceptional properties are then passed on to the PVA cryogel. Wan et al. (2014) investigated the mechanical properties of PVA cryogel in terms of its compressibility, tensile strength and its stress relaxation characteristics. These tests illustrated that the PVA crygol is very durable, is non-brittle and it has a high modulus of elasticity (Hyon et al., 1989).

a) Opaque PVA cryogel

Currently PVA cryogels performance has not been investigated with photosynthetic bacteria as the immobilised cell. This is likely due to the PVA cryogels' opaque and translucent characteristics (Hyon et al., 1989). This opacity means that light may not be able to penetrate the solid PVA cryogel and reach the bacteria (in this case *R. palustris*). This may be detrimental to the hydrogen production as it was

concluded in section 2.3.1 that to produce hydrogen *R. palustris* would need to operate photoheterotrophically.

b) Transparent PVA cryogel

Many applications may require a transparent PVA cryogel, such as photofermentation processes and the biomedical field where they can be used for ocular medical devices or sensor design (Paţachia et al., 2009). Hyon et al. (1989) also stated the need for a PVA cryogel that has excellent transparency. Hyon et al. (1989) achieved a PVA cryogel with 99% light transmittance (at 570nm) when the aqueous solution used with the PVA had a dimethyl sulfoxide (DMSO) co-solvent with a concentration of 80% in water (w/w%). This level of transmittance would be ideal for photosynthetic bacteria. The problem with DMSO, however, is that it is cytotoxic at these high concentrations, and will therefore cause irreparable damage to cells during immobilisation (Pott, 2013).

Pott (2013) developed an alternative novel transparent PVA cryogel that could be used as an immobilisation matrix for photosynthetic bacteria. This was done by substituting DSMO with glycerol as a non-cytotoxic co-solvent has the additional advantage of cryoprotection during the before mentioned freeze-thaw cycle. Pott (2013) investigated the effect of glycerol concentrations on the percentage light transmission through the hydrogel matrix. During these experiments PVA concentration was kept constant at 10% (w/v). From this investigation it was concluded that a glycerol concentration of 50% in water was optimal with high light transmittance (>89%). As mentioned previously it was concluded that this matrix had similar hydrogen production levels when immobilised with *R. palustirs* compared to free-cell cultures of *R. palustris.*

Due to the novelty of the PVA cryogel immobilisation matrix there has been no work done with regards to the design of a bioreactor system or configuration that can utilise the immobilised *R. palustris* to produce hydrogen.

2.7 Bioreactor engineering

A bioreactor is defined as a vessel in which a biological reaction takes place, with these reactions executed through the metabolic activity of enzymes, microorganisms or tissues (Wang and Zhong, 2007). The purpose of the reactor vessel is, for example, to provide a microorganism with the optimum external environment to facilitate the biological reactions to produce the desired product (Wang and Zhong, 2007). In this investigation the desired product is hydrogen and the biological activity is the nitrogenase activity carried out by the *R. palustris* bacteria.

Not all bioreactors require illumination by light, however this is critical when designing a bioreactor for the culturing of *R. palustris* to produce hydrogen. This is due to the requirement of photon energy in the

hydrogen production metabolism of *R. palustris* (see section 2.3.3). Therefore, any proposed bioreactor systems must be able to accommodate light within the system, which means a PBR is to be designed. Currently the majority of PBRs used for the production of hydrogen have been designed and developed for the cultivation of green algae with the most noteworthy designs being column reactors, tubular reactors and flat panel reactors (Xu, 2007). The photosystem and hydrogen metabolism of green algae is substantially different to that of *R. palustris*, and therefore many of these common reactor systems are not interchangeable in terms of culturing algal and bacterial cultures. This has led to many novel reactor designs for the culturing of *R. palustris* for photofermentative hydrogen production, such as novel optical fibre-illuminating PBRs (Chen et al., 2006) and anaerobic fluidised bed with carbon fibre as a bacterial carrier (Ren et al., 2012). Following the novelty of the PVA cryogel immobilisation matrix developed by Pott (2013) there has been little work done with regards to the design of a viable bioreactor system or configuration that can utilise the immobilised *R. palustris* to produce hydrogen.

According to Wang and Zhong (2007) biological reaction systems can be divided into two main groups, namely suspension systems and immobilisation systems. Within the free cell category some common bioreactors are stirred-tank reactors', membrane bioreactors and bubble columns and with the immobilised category packed bed reactors, fluidised bed reactors and stirred-tank reactors (Wang and Zhong, 2007). Stirred-tank reactors mixing regime often results in low homogeneity with regards to incoming light, which means it is often not ideal for PBR systems without modifications, such as the insertion of optical fibres (Chen et al., 2006) into the stirred-tank. This is not the case with packed bed and fluidised bed reactors. Due to the photosynthetic requirements of *R. palustris* these reactor systems stand out as viable options for the production of hydrogen using *R. palustris* immobilised in the PVA cryogel matrix.

The subsections below delve into the possibilities of both a packed bed PBR (PBPBR) and a fluidised bed PBR (FBPBR).

2.7.1 Packed bed reactor

Packed bed systems have been studied for more than a century with initial investigations into the flow of water through a packed bed of sand in 1856 by Henry Darcy (Rhodes, 2008). The viability of packed bed reactors in bioreactor processes was only realised when immobilisation of bacteria became possible. Packed bed reactors operating as bioreactors with immobilised cells are discussed next.

When cells are immobilised in the selected matrix, they are packed into the reactor which results in high solid-liquid specific interfacial contact areas. Film resistance to mass transfer is also lessened due to the low velocities of liquid over the stationary solid particles (Wang and Zhong, 2007). Other advantages of a packed bed reactor is the fact that it is simple to operate and its ability to achieve high reaction rates.

However, a major disadvantage of the packed bed reactor is the achievable mass and heat transfer rates which are relatively poor due to the low liquid velocities (Wang and Zhong, 2007). Low liquid velocities are expected due to the similarity in densities between the feedstock and the immobilised matrix as fluidisation of the bed is not desired.

According to Wang and Zhong (2007), packed bed reactors are the most frequently used bioreactor for immobilisation systems, this is likely due to them being used in wastewater and waste gas treatment facilities. This illustrates their applicability to biodegradation processes, which is an integral part of this investigation. Wang et al. (2013) studied hydrogen production using immobilised *R. palustris* in a flat panel packed bed reactor. Flat panel reactors are often used in PBR systems due to their high surface to volume ratio, however a major disadvantage with this configuration is that it has limited scalability. As stated previously the PVA cryogel has high light transmittance which could allow for a column reactor to be used instead, which would have a lower surface to volume ratio, but could be scaled-up with more ease.

An equation that describes the flow of fluid through a randomly packed bed of spherical particles was developed by Sabri Ergun in 1952 through extensive experimentation (Rhodes, 2008). The developed equation is known as the Ergun equation and is provided in Equation 25 below. The Ergun equation can be used to calculate the pressure drop over the packed bed reactor when the particle diameter, fluid velocity and voidage is known.

$$\frac{(-\Delta p)}{H} = 150\frac{vU}{x^2}\frac{(1-\varepsilon)^2}{\varepsilon^2} + 1.75\frac{\rho_f U^2}{x}\frac{(1-\varepsilon)}{\varepsilon^3} \qquad [25]$$

$$\begin{pmatrix}\text{laminer}\\ \text{component}\end{pmatrix} \quad \begin{pmatrix}\text{turbulent}\\ \text{component}\end{pmatrix}$$

$Where,$

$\Delta p = pressure\ drop$

$H = height\ of\ the\ bed$

$v = visocity\ of\ the\ fluid$

$U = velocity\ of\ the\ liquid$

$x = diameter\ of\ the\ immobilised\ gel\ beads$

$\varepsilon = voidage\ of\ the\ bed$

$\rho_f = density\ of\ the\ fluid$

The pressure drop across the bed of a packed bed reactor is one of the most important parameters when designing these reactor systems. This is due to the pressure drop being related to the flow distribution

and pumping power required, as illustrated in Equation 25. The higher the pressure drop is, the bigger the effect will be on the operational cost of the reactor.

2.7.2 Fluidised bed reactor

When a fluid passes upwards through a packed bed a point is reached where the drag force exerted by the fluid on the particles is equal to the apparent weight of the particles. When this occurs the particles are lifted upwards by the fluid, causing bed expansion and fluidisation (Rhodes, 2008). This is the fundamental principles of the fluidised bed reactor.

The fluidised bed reactor is commonly used as a bioreactor system when immobilised bacteria are employed. Wang and Zhong (2007) provide a list of advantages that fluidised bed reactors present over packed bed reactors:

1. The system is closer to homogeneity, meaning it is easier to control the operating conditions, i.e. temperature and pH.
2. The reactor system has good mixing brought about by upward movement of fluid.
3. Higher mass and heat transfer rates occur in comparison to packed bed reactors, due to the mixing movement of the particles (immobilised beads).
4. Easy particle sampling can.
5. The fluidised bed reactor can be scaled-up without increasing the concentration gradient.

One major advantage that FBPBR present over PBPBR that is not mentioned by Wang and Zhong (2007), due to it being specific to PBRs, is the fact that the fluidization of the immobilised bacteria allows each individual particle a higher light ‘residence time’. This is due to the homogenous mixing that will occur when fluidised, compared to when the bed is packed, and the solid phase is static. There has been no work done on fluidised photosynthetic organisms immobilised in hydrogel matrices.

A disadvantage of fluidised bed reactors is that scale-up is hampered by the unpredictability of fluidization, back mixing as well as the narrow range of optimum operating conditions (Wang and Zhong, 2007).

A force balance over a fluidized bed results in an equation that can be used to determine the pressure drop over the bed at any point during expansion. This is shown below in Equation 26. This pressure drop equation is only valid at the point of fluidisation, before then Equation 25 is used to calculate pressure drop over the bed.

$$\Delta p = H(1-\varepsilon)(\rho_p - \rho_f)g \quad [26]$$

$Where,$

$\Delta p = pressure\ drop$

$H = height\ of\ the\ bed$

$\varepsilon = voidage\ of\ the\ bed$

$\rho_p = density\ of\ the\ particle$

$\rho_f = density\ of\ the\ fluid$

$g = gravitational\ acceleration\ constant$

The velocity of the fluid at the point where the upward drag force is equal to the apparent weight of the particles is known as the minimum fluidisation velocity (U_{mf}). At the minimum fluidisation velocity Equation 25 also applies as the bed is still on the verge of fluidisation. Thus, Equation 26 can be substituted into Equation 25. This substitution results in three Equations shown below:

$$Ar = 150\frac{(1-\varepsilon)}{\varepsilon^3}Re_{mf} + 1{,}75\frac{1}{\varepsilon^3}Re_{mf}^2 \quad [27]$$

$$Re_{mf} = \frac{U_{mf}x_{sv}p_f}{v} \quad [28]$$

$$Ar = \frac{p_f(p_p - p_f)gx_{sv}^3}{v^2} \quad [29]$$

$Where,$

$Ar = Archimedes\ \ number$

$\varepsilon = voidage\ of\ the\ bed$

$Re = Reynolds\ number$

$U = velocity\ of\ the\ liquid$

$x = diameter\ of\ the\ immobilised\ gel\ beads$

$\rho_f = density\ of\ the\ fluid$

$v = visocity\ of\ the\ fluid$

$\rho_p = density\ of\ the\ particle$

$g = gravitational\ acceleration\ constant$

With the physical properties of the fluid and particles all defined, the minimum fluidisation velocity can easily be determined using the above equations, this makes it easy to determine the minimum velocity that the feedstock must be fed at in order to fluidise the bed.

2.8 Production conditions

Production conditions refer to the feedstock and the operating conditions of the PBRs. These are critical to the operation of the bioreactors as the function of the system is to provide an optimal environment to the bacteria (Wang and Zhong, 2007).

2.8.1 Feedstock

Based on *R. palustris'* versatile metabolic ability it can use both organic and inorganic compounds as sources of energy. Possible inorganic compounds include thiosulphate and hydrogen gas (Larimer et al., 2004). However, based on propensity of *R. palustris* to operate photoheterotrophically, organic compounds must be used as the substrate available in the feedstock for the reactor to produce the desired product, namely hydrogen. *R. palustris* can consume a wide range of organic compounds, such as organic acids (acetic, lactic, succinic butyric and malic acids), animal fats and seed oils (Larimer et al., 2004; Pott et al., 2013). However, Ghosh et al. (2012), Sabourin-Provost and Hallenbeck (2009) and Pott et al. (2013) have all shown that the photofermentation of glycerol is possible and that near stoichiometric reforming to hydrogen and high yields of hydrogen is possible when glycerol is used as the substrate.

Pott et al. (2013) provides a comparison of maximum growth rates (h^{-1}) and hydrogen production rates ($mL/g_{dw}/h$) for *R. palustris* on a variety of carbon sources, namely glycerol, treated crude glycerol (TCG), acetate, butynate, sucrose, glucose, malate, lactate and untreated crude glycerol. All sources contained 10 mM carbon and 5 mM glutamate. It was concluded that glycerol had the highest maximum growth rate and hydrogen production over the other carbon sources investigated, with TCG only slightly less in both cases.

2.8.2 Operating conditions

As discussed above photofermentation is influenced by nutritional factors such as the choice of carbon and nitrogen source, as well as the initial carbon to nitrogen ratio in the substrate. Photofermentation is also influenced by environmental factors such as temperature, light intensity and the pH of the substrate (Eroglu and Melis, 2011). These factors all contribute to the operating conditions of PBRs and have some influence on the production of hydrogen. Therefore, it is necessary to determine the recommended ranges for these operating conditions to ensure that hydrogen production in the PBRs will not be hindered by factors that are not being investigated.

The operating conditions discussed in the subsections below are temperature, light intensity and pH.

2.8.2.1 Temperature

According to Basak et al. (2016) hydrogen production can be reduced significantly if temperatures vary during photofermentation processes. This may be due to the bacteria expending energy on the adaptation to changes to high or low temperatures. It is therefore crucial to keep the temperature as stable as possible around a set value. The question remains at what temperature the photofermentation process should operate at. The operating temperature will be dependent on the photobacteria that is used in the photofermentation process, as bacteria can be divided into five groups with respect to the temperature ranges they can survive in. Bacteria are either psychrophiles, psychrotrophs, mesophiles, thermophiles or hyperthermophiles. The majority of *R. palustris* strains can only grow in the mesophilic temperature range (20 to 45°C) with optimum temperature ranges between 25 and 35°C. Table 2.4 below indicates the operating temperatures of photofermentation systems using *R. palustris,* either immobilised or in a free cell system.

Table 2.4: Operating temperatures of photofermentation systems using R. palustris.

Bacteria	Immobilised/Free	Reactor system	Temperature	Reference
R. palustris R1	Free	Cylindrical bottle (0.15L)	30°C	(Barbosa et al., 2001)
R. palustris DSM 123	Free	Angular triple jacket photobioreactor (1L)	33±1°C	(Basak et al., 2016)
R. palustris 42OL	Free	Tubular photobioreactor (53L)	30±1°C	(Carlozzi and Sacchi, 2001)
R. palustris CGA009	Free	Serum bottles (0.125L)	30°C	(Ghosh et al., 2012)
R. palustris CQW01	Immobilised	Biofilm photobioreactor (0,125L)	30°C (tested optimum)	(Guo et al., 2011))
R. palustris CQW01	Immobilised	Flat panel photobioreactor (0,8L)	30°C	(Liao et al., 2010)
R. palustris NCIMB 11774	Free	Conical flask (0.1L) or Schott bottle (0.5L)	30°C	(Pott et al., 2013)
R. palustris CGA009	Free	Serum bottles (0.125L)	30°C	(Sabourin-Provost and Hallenbeck, 2009)
R. palustris CQW01	Immobilised	Biofilm photobioreactor (1,2L)	25°C (tested optimum)	(Tian et al., 2010)
R. palustris CQW01	Immobilised	Packed bed reactor (0.8L)	30°C	(Wang et al., 2010)
R. palustris CQW01	Immobilised	Packed bed reactor (0,8L)	30°C	(Wang et al., 2013)
R. palustris W004	Free	Photobioreactor (0.35L)	32°C	(Wu et al., 2010)
R. palustris CQW01	Immobilised	Groove-type photobioreactor (0,1L)	30°C	(Zhang et al., 2010)

2.8.2.2 Light source and intensity

As discussed in section 2.3.3 and 2.3.4, light absorption of the photosystem in the PNS bacteria such as *R. palustris* is essential for hydrogen production. Thus, illumination of the reactor system is a critical operating condition, as hydrogen production may be affected if the correct aspects of illumination are not considered. There are two main aspects of illumination that must be considered: the light source and light intensity.

With regards to the available light sources, solar light energy is the most abundant natural light source available on earth and is considered advantageous due to its abundance, the fact that it is a free in terms of the available light energy and that it contains the full spectrum of light (Chen et al., 2008). Therefore, sunlight has commonly been used as the light source for PBRs that are culturing algae or photosynthetic bacteria (Chen et al., 2008). For lab-scale experiments it is therefore necessary to use an artificial light source that can closely mimic the emission spectrum of sunlight so that any trends observed with regards to the effect of light intensity on the lab-scale can be applied to outdoor conditions. Figure 2.7 below provides a comparison of the emission spectrums of common light sources encountered in indoor environments. From Figure 2.7, incandescent light bulbs provide the closest representation in terms of spectral light emission when compared to sunlight over the wavelength range of 550 to 1000 nm. This wavelength range was selected, as it includes all wavelengths of interest to the organism. Incandescent light bulbs have been used for culturing of *R. palustris* in previous investigations (Pott, 2013; Xiao, 2017).

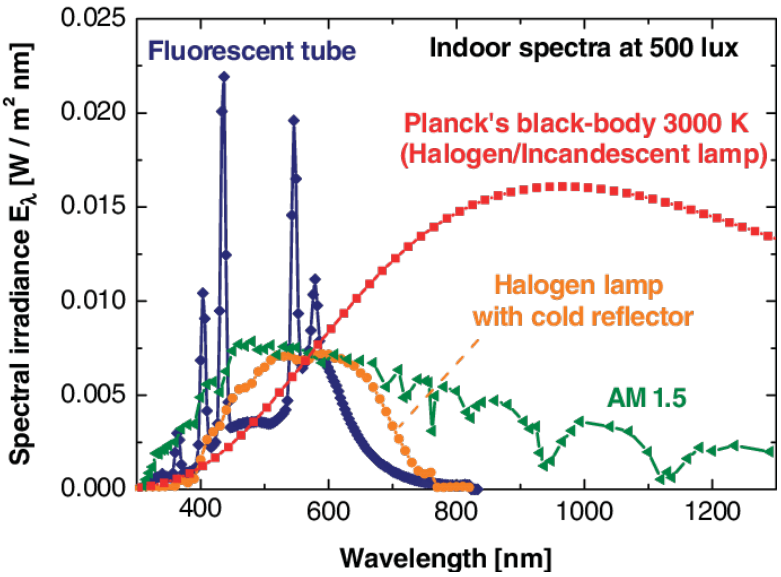

Figure 2.7: Comparison of the emission spectrums of common light sources encountered in indoor environments. Reproduced from Virtuani et al. (2006).

The light intensity can affect the growth (Carlozzi, 2009) and hydrogen production of *R. palustris* (Wang et al., 2013; Xiao, 2017). Specifically, at too low a light intensity photo-limitation can occur and at too high a light intensity photoinhibition can occur. Photoinhibition is a common term used to define the damaging effects of light on the photosystem in oxygen-evolving organisms, where damage to PSII electron transport and the D1 reaction centre subunits are initiated by oxidative damage by singlet oxygen (Tandori et al., 2001). Tandori et al. (2001) reported that photoinhibition in anaerobic organisms is also possible and is likely brought upon by visible light with inhibition of the electron transport and/or possible damage to protein subunits occurring. Xiao (2017) reported reduced hydrogen production rates within the light intensity range of 26 to 65 W/m^2 due to photo-limitation of *R. palustris* and that hydrogen

production saturates over a light intensity range of 65 to 285 W/m^2. Carlozzi (2009) reported that hydrogen production decreased when the light intensity was higher than 500 W/m^2. This is likely due to the afore mentioned photoinhibition.

2.8.2.3 pH

Bacteria can be classified as either an acidophile, neutrophile or alkaphile with regards to the pH they can grow in. Most bacteria are considered neutrophiles as they grow optimally at a pH of 7±1. According to Pott et al. (2013) *R. palustris* was tolerant to pH values of 5 and 9 but showed very limited growth below a pH of 5 and above a pH of 9. This points to *R. palustris* being a neutrophilic bacterium, with optimum growth and hydrogen production being around a pH of 7.

Table 2.5 below provides the pH values of the media used during the production of hydrogen using *R. palustris*. From this it is clear that the recommended pH of the media (feedstock) is approximately 7.0. Pott et al. (2013), Tian et al. (2010) and Zhang et al. (2010) all investigated the optimum pH of the media to achieve the maximum hydrogen production rate. All found that a pH of 7 was optimum for hydrogen production where *R. palustris* is the photosynthetic bacteria.

Table 2.5: Operating pH of photofermentation systems using R. palustris

Bacteria	**pH**	**Reference**
R. palustris R1	7,0	Barbosa et al. (2001)
R. palustris DSM 123	6,7±0,1	Basak et al. (2016)
R. palustris 42OL	7,0±0,05	Carlozzi and Sacchi (2001)
R. palustris CQW01	7,0	Guo et al. (2011)
R. palustris CQW01	7,0	Liao et al. (2010)
R. palustris NCIMB 11774	7,0 (tested optimum)	Pott et al. (2013)
R. palustris CQW01	7,0 (tested optimum)	Tian et al. (2010)
R. palustris CQW01	7,0	Wang et al. (2010)
R. palustris CQW01	7,0	Wang et al. (2013)
R. palustris W004	6,8	Wu et al. (2010)
R. palustris CQW01	7,0 (tested optimum)	Zhang et al. (2010)

2.9 Performance parameters

2.9.1 Maximum specific growth rate

The maximum specific growth rate is when the rate of cell division is at a maximum and corresponds to the exponential growth phase on the bacterial growth curve. The maximum specific growth rate can be determined using a graphical method, by plotting $\ln(n)\ versus\ t$, where *n* is the biomass concentration at time *t* during an experimental run (Clarke, 2013). The linear slope of the plot is equal to the maximum specific growth rate, provided that the bacteria are in the exponential growth phase. Microsoft Excel's built in linear regression function was used to plot a linear regression line through the necessary data points to obtain an equation where the gradient is the maximum specific growth rate.

2.9.2 Biomass yield

The biomass yield coefficient ($Y_{X/s}$) relates the cell growth directly to the substrate utilisation for cell production and is described by Equation 30 (Clarke, 2013).

$$Y_{X/s} = \frac{dX/dt}{ds/dt} \qquad [30]$$

Where x refers to the biomass, s to the substrate and t to time. Integration of Equation 30 allows for easy calculation of $Y_{X/s}$ via Equation 31 below (Clarke, 2013). In this Equation, x_0 and $s_0$refer to the initial experimental conditions.

$$Y_{X/s} = \frac{X - X_0}{s_0 - s} \qquad [31]$$

2.9.3 Substrate conversion efficiency

Conversion efficiency is defined as the number of moles of hydrogen produced in comparison to the theoretical stoichiometric quantity possible (Hallenbeck, 2009; Pott, 2013). The stoichiometric moles of hydrogen is governed by the substrate used and the corresponding reaction equation (see Equation 5 in section 2.2.2.3). The conversion efficiency of carbon substrate to H_2 is provided in Equation 32 below (Adessi and De Philippis, 2014):

$$conversion\ efficiency(\%) = \frac{mol\ H_2\ obtained}{mol\ H_2\ theoretical} \times 100 \qquad [32]$$

The conversion efficiency is considered to be one of the most relevant parameters to be considered for design and optimisation of PBRs for the production of hydrogen via photofermentation (Adessi and De Philippis, 2014).

2.9.4 Specific hydrogen production rate

The specific hydrogen production rate describes the hydrogen produced per gram of CDW per hour and was calculated using Equation 33.

$$Specific\ H_2\ rate\ (mL/g_{CDW}/h) = \frac{\left(\frac{H_{2,t_2} - H_{2,t_1}}{\left(CDW_{t_2} + CDW_{t_1}\right)/_2}\right)}{t_2 - t_1} \quad [33]$$

3 RESEARCH SCOPE

3.1 Aim

The aim of this work is to produce biological hydrogen from a synthetic waste stream (glycerol) by the photosynthetic bacteria *R. palustris*. This leads to a renewable and clean source of energy as well as the biodegradation of a waste stream that would be an environmental burden if not used as the feedstock. Specific focus has been placed on the effect of light intensity on the growth of *R. palustris* as well as the design and development of a PBR that can be used for the production of hydrogen by immobilised *R. palusrtris*.

3.2 Objectives

1. *Examine the effect of light intensity on the cells and cell growth of R. palustris in a tubular PBR operating with a planktonic cell culture in batch configuration.*

There is not sufficient literature on the effect of light intensity on the growth and substrate utilisation of *R. palustris*. The work that has been done used bioreactors with relatively large diameters: 70 mm (Xiao, 2017) and 96 mm (Carlozzi, 2009). This has been identified as a possible shortcoming in these investigations results, as the effects of light attenuation and cell mutual shading would have a significant impact and therefore these relatively large diameters would not provide an accurate measure of the effect of light intensity on the growth of *R. palustris*.

2. *Model the response of cell growth and average light intensity in the tubular PBR to changing light intensity.*

A vast amount of work has been done in the past fifty years on the modelling of biological processes. However, there has been less focus on the modelling of photosynthetic bacteria. There has been no work done on the modelling of the effect of light intensity on the growth of *R. palustris* and limited work on the modelling of average light intensity in cylindrical PBRs geometries (commonly approximated as square geometry). This gap in the literature has promoted an investigation into modelling the attenuation of light through cylindrical reactors which allows for modelling the effect of light intensity on growth and the determination of the average light intensity in a reactor based on biomass concentration.

3. *Design a PBR that could be a viable option in the culturing of R. palustris in both free-cell and immobilised form, and that performs at a similar or enhanced level in terms of hydrogen production and substrate conversion efficiency when compared to current lab-scale bioreactor systems.*

Currently no major work has been done on possible bioreactor configurations for photosynthetic bacteria immobilised in a hydrogel matrix. As a first step a bioreactor will be designed to grow planktonic cell cultures as this can be compared to the hydrogen production performance of current laboratory bioreactors. This comparison will indicate the viability of the reactor design for hydrogen production by *R. palustris*. The reactor will be designed to allow for minor changes to the configuration to be able to house cells immobilised in a PVA cryogel.

4. *Determine whether the hydrogen production of the immobilised bacterium is comparable to that of the free cell bacterial cultures.*

With a PBR system designed and constructed for hydrogen production by *R. palustris*, either as a growing planktonic cell culture or immobilised in a hydrogel matrix, the performance of the two possible bioreactor systems could be investigated. With regards to hydrogen production and substrate conversion efficiency the performance of the immobilised reactor system in comparison to the planktonic cell culture is required, in order to determine if the immobilisation of the cells is warranted.

5. *Compare the performance of the fluidised bed PBR versus the packed bed PBR based on their biological hydrogen production.*

As discussed in section 2.7 two possible reactor configurations stand out as promising options for the production of hydrogen from immobilised cells, namely PBPBR and FBPBR. It is necessary to determine which reactor configuration proves to be the more viable option for operation in the designed PBR in terms of the substrate utilisation and hydrogen production kinetics.

3.3 Key questions

I. How are the growth and associated growth parameters of *R. palustris* affected by changing the light intensity?
II. Is the bacteriochlorophyll alpha to carotenoid ratio influenced by an increase in the incident light intensity of the bacterial culture?
III. Does the effect of light intensity on the growth of *R. palustris* influence possible outdoor culturing?

IV. Do planktonic cells cultured in the designed and constructed column PBR show improved performance with respect to growth, substrate utilisation, hydrogen production and conversion efficiencies compared to current common lab-scale bioreactors?

V. Do immobilised systems outperform free cell systems based on hydrogen production performance parameters when cultured in the column PBR?

VI. Does the operating configuration of the column PBR loaded with immobilised *R. palustris* affect the hydrogen production kinetics (specifically, the hydrogen production rate, substrate conversion efficiency and light conversion efficiency)?

4 MATERIALS AND METHODOLOGY

4.1 Materials

The major chemical reagents used in the experimental methods which are described in the subsequent sections are provided in Table 4.1 below. The chemical names along with their respective formulas, purity and the supplier of the reagents are provided.

Table 4.1: List of all chemicals used during experimentation along with purities and suppliers. TG – technical grade.

Chemical	Formula	Purity (%)	Supplier
Acetone	$(CH_3)_2CO$	≥99,5	Sigma-Aldrich
Bacteriological agar	-	-	Biolab Diagnostics Laboratory Inc.
Boric acid	H_3BO_3	99	UniLab
Calcium chloride	$CaCl_2$ $2H_2O$	99	MERCK
Cobalt (II) chloride	$CoCl_2$ $6H_2O$	97	MERCK
Copper (II) chloride	$CuCl_2$ $2H_2O$	97	MERCK
Cyanocobalamin	$C_{63}H_{88}CoN_{14}O_{14}P$	≥98	Sigma-Aldrich
Dipotassium phosphate	K_2HPO_4	98-101	MERCK
Ethanol	C_2H_6O	99,9	MERCK
Ferric citrate	$C_6H_5FeO_7$	TG	Sigma-Aldrich
L-Glutamatic acid monosodium	$C_5H_8NNaO_4$	≥98,0	Sigma-Aldrich
Glycerol	$C_3H_8O_3$	99	Science World
Hydrochloric acid	HCl	32	Kimix
Magnesium sulphate	$MgSO_4$ $7H_2O$	≥99	Kimix
Manganese (II) chloride	$MnCl_2$ $4H_2O$	≥99	Sigma-Aldrich
Methanol	CH_4	≥99,5	MERCK
Monopotassium phosphate	KH_2PO_4	≥99	Sigma-Aldrich
Nickel (II) chloride	$NiCl_2$ $6H_2O$	≥97	Sigma-Aldrich
Ninhydrin	$C_9H_6O_4$	-	MERCK
Para-aminobenzoic acid	$C_7H_7NO_2$	≥99	Sigma-Aldrich
Poly(vinyl) alcohol	$(C_2H_4O)x$	≥98	Scientific Polymer Products Inc.
Potassium chloride	KCl	≥99	Sigma-Aldrich
Sodium chloride	NaCl	99,0-100,5	MERCK
Sodium hydroxide	NaOH	98	MERCK
Sodium molybdate	Na_2MoO_4 $2H_2O$	≥99,5	UnivAR
Sodium thiosulphate	$Na_2S_2O_3$ $5H_2O$	99	Science World
Thiamine hydrochloride	$C_{12}H_{18}Cl_2N_4OS$	AG	Sigma-Aldrich
Yeast extract	-	-	Biolab Diagnostics Laboratory Inc.
Zinc chloride	$ZnCl_2$	≥97	MERCK

4.2 Microbial maintenance

4.2.1 Culture revival from lyophilised cells

In this investigation hydrogen was produced using *R. palustris* NCIMB 11774. This strain of *R. palustris* was obtained from the Deutsche Sammlung von Mikroorganismen und Zellkulturen (DSMZ). The microorganism was delivered in a freeze-dried format and was revived using the methods provided by DSMZ. This involved aseptically breaking the glass vile containing the freeze-dried cell pellet and adding 0.5 mL of liquid minimal medium (see section 4.3.2.2) to rehydrate the pellet. After rehydration an inoculum loop was used to inoculate a test tube containing the liquid medium (see section 4.3.2.2) and a nutrient agar plate (see section 4.3.1.1).

4.2.2 Culture long term storage in glycerol

Cultures were preserved in a solution of glycerol and water. The solution was made up of 30% glycerol (v/v) in water and was used for the long-term storage of the microorganism. These stocks were made by aseptically transferring 5 mL of the before mentioned sterile glycerol/water solution onto an agar plate that had been streaked with *R. palustris*. The bacteria-rich solution was then pipetted into a sterile Nalgene cryogenic vial (Thermo Fischer Scientific) and dropped into liquid nitrogen to instantly freeze before being stored at a temperature of -20°C.

4.2.3 Periodic revival of culture from glycerol

These preserved cultures were restored from frozen stocks by aseptically transferring one loop (0.01 mL) of the culture with an inoculating loop to 25mL of nutrient medium. The culture was then incubated in an orbital shaker incubator (Labcon) at 30°C for 24 hours. Nutrient agar plates were inoculated with the bacterium by aseptically streaking one loop of the incubated nutrient medium on the plate. The streaked plates were further incubated at 30°C for 72 hours after which they could be stored at 4°C. These plates were then used to streak subsequent agar plates on a biweekly basis and to inoculate media used for the inoculation of experimental runs. Agar plates were made using the method described in section 4.3.1.1.

4.3 Culture medium

4.3.1 Solid medium

4.3.1.1 Long term storage solid medium

The solid nutrient agar used for the long term storage of streaked bacteria was produced by dissolving 15 g of bacteriological agar in 1 L minimal media (see 4.3.2.2) with no additions. The dissolving of the agar in the minimal media was facilitated by mixing the solution with a magnetic stirrer at a slightly elevated

temperature. The liquid agar was then sterilised to ensure that no microorganisms were present in the nutrient agar solution. This was done by autoclaving (Speedy autoclave) the media at a temperature and pressure of 121°C and 101 kPa for 30 minutes. The high temperature of the autoclave assisted in dissolving any undissolved agar left in the solution. Once autoclaved the sterilised liquid agar was allowed to cool to approximately 60°C before 10 mL of 5 M glycerol was added to the solution aseptically. Approximately 25 mL of liquid agar was then aseptically transferred to each agar plate and allowed to solidify.

4.3.1.2 Fast growing solid medium for checking contamination

The solid nutrient agar used to check for the contamination of experimental runs was produced by dissolving 20 g of bacteriological agar in 1 L of Van Niels media (see 4.3.2.1) with no additions. This agar promotes extremely fast growth which would allow contamination to be identified after 24 hours in the incubator at 30°C. The nutrient agar was further prepared in the same manner described above. Once autoclaved the sterilised liquid agar was allowed to cool to approximately 60°C before 10 mL of 5 M glycerol was added to the solution aseptically. Approximately 25 mL of liquid agar was then aseptically transferred to each agar plate and allowed to solidify. Figure 4.1 below provides an image of R. *palustris* 11774 streaked on the fast-growing solid nutrient agar.

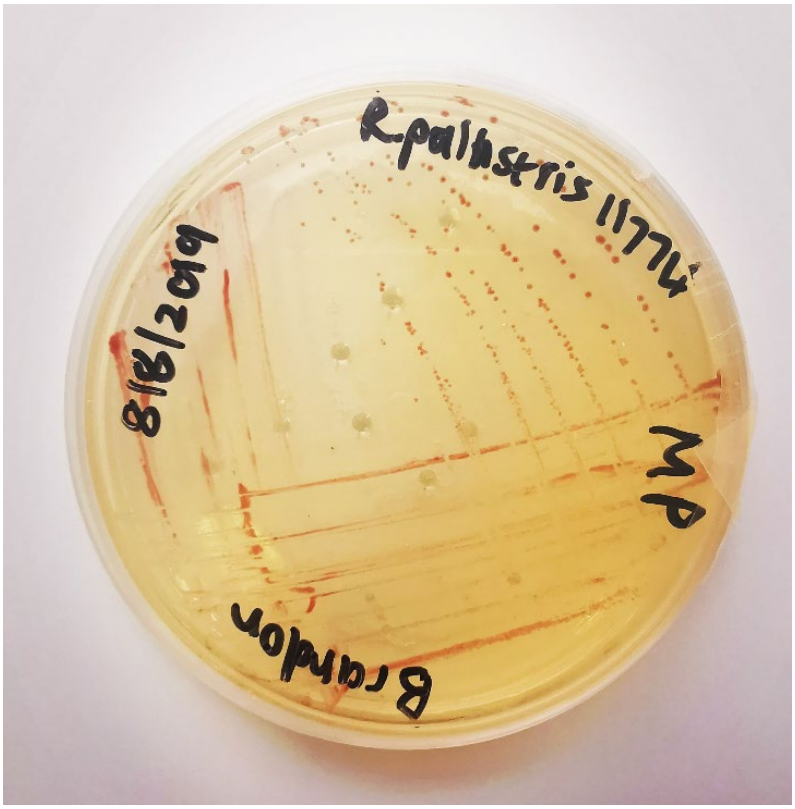

Figure 4.1: R. palustris 11774 streaked on the fast-growing solid nutrient agar

4.3.2 Liquid medium

4.3.2.1 Van Niels medium

Van Niels medium was used in all experiments pertaining to the investigation of the effect of light intensity on the growth of *R. palustris*. This medium was developed through the adjustment of the Van Niels Yeast Broth (ATCC Medium 12) through the addition of glycerol as the main carbon source. Table 4.2 provides a summary of the adjusted Van Niels medium along with the concentrations of each component.

*Table 4.2: Adjusted Van Niels Yeast Broth components and concentrations. *Sterile addition to Van Niels Yeast Broth after autoclaving.*

Component	Concentration (g/L)	Concentration (mM)
*Glycerol	3.684	40
K_2HPO_4	1.000	7.348
$MgSO_4.7H_2O$	0.500	2.029
Yeast extract	10.000	-

The Van Niels medium was prepared by dissolving the monopotassium phosphate, magnesium sulphate heptahydrate and yeast extract in deionised water using a magnetic stirrer plate. The final pH of the growth medium was then adjusted to a pH of 7.0±0.1 using 0.1 M NaOH if necessary before it was sterilised by autoclaving (Speedy autoclave) for 40 minutes at a temperature of 121°C and pressure of 101 kPa. A 4 M stock solution of glycerol was prepared and autoclaved separately, before 10 mL/L was added to the above solution to obtain a final glycerol concentration of 40 mM in the growth medium.

4.3.2.2 Minimal medium

The concentration of the nutrient components within the minimal liquid growth medium were obtained from Pott et al. (2013). The liquid medium can be broken down into three main components, i.e. the bulk nutrients, the buffers and the sterile additions. The components and corresponding concentrations of the bulk nutrients and the buffers are found in Table 4.3. The concentrations in Table 4.3 refer to the stock solutions of each respective solution. When making up a litre of the minimal media 100mL of bulk nutrients and 4 mL of each buffer stock solution were added.

Table 4.3: Bulk nutrients and buffers components and concentrations stock solutions.

Solution	Component	Concentration (g/L)	Concentration (mM)
Bulk Nutrients	NaCl	4	68.446
	$Na_2S_2O_3.5H_2O$	2.51	10.113
	$MgSO_4.7H_2O$	0.2	0.811
	$CaCl_2.2H_2O$	0.05	0.340
	Yeast extract	0,2	-
	Ferric citrate	0.005	0.020
	Para-aminobenzoic acid	0.002	0.015
Buffers	K_2HPO_4	142.9	820.321
	KH_2PO_4	466	3424.305

There are three sterile additions added to the above minimal media, namely trace element solution, vitamin solutions, the carbon source and the nitrogen source. Table 4.4 provides the components of all the sterile solutions with their concentrations as stock solutions. 1 mL of the trace elements and vitamin solutions were added per 1 L of the minimal medium. 10 mL of the glycerol stock solution was added per 1 L of medium to obtain a final concentration of 50 mM of glycerol. 4 mL of glutamate stock solution was added per 1 L of medium to obtain a final concentration of 10 mM of glutamate.

Table 4.4: Trace element and vitamin solution components and concentration (Pott et al., 2013)

Solution	Component	Concentration (g/L)	Concentration (mM)
Trace elements	$ZnCl_2$	0,070	0,514
	$MnCl_2.4H_2O$	0,100	0,505
	H_3BO_3	0,06	0,970
	$CoCl_2.6H_2O$	0,2	0,841
	$CuCl_2.2H_2O$	0,02	0,117
	$NiCl_2.6H_2O$	0,02	0,084
	$Na_2MoO_4.2H_2O$	0,04	0,165
Vitamin solution	Thiamine HCl	1,2	3,558
	Cyanocobalamin	0,01	0,007
Carbon source	Glycerol	460.47	5000
Nitrogen source	Glutamate	422.775	2500

During preparation of the growth medium the bulk nutrients and buffers were sterilised together with the deionised water by autoclaving (Speedy autoclave) for 40 minutes at a temperature of 121°C and pressure of 101 kPa after which the sterile additions were added aseptically.

4.3.3 Immobilisation medium

The immobilisation medium for the transparent PVA cryogel beads was an 11% (w/v) solution of PVA. PVA (88 kDa, Scientific Polymer Products, Inc.) was weighed out using a lab scale (Sartorius AG BP 61S 5 decimal lab scale) and added to a 50% (v/v) glycerol-deionized water solution. The PVA solution was then dissolved via vigorous stirring at approximately 95°C (to avoid boiling) over-night to ensure all the PVA was dissolved. The PVA solution was then autoclaved (Speedy autoclave) for 40 minutes at 121°C and 101 kPa to sterilise the medium. The PVA solution would solidify in the Schott bottle once it cooled to ambient temperatures and could then be melted by microwaving for 5 minutes to obtain a liquid PVA solution when needed.

4.4 Experimental procedure

4.4.1 Bacterial culturing

4.4.1.1 Inoculum

Bacterial cultures used for the inoculation of non-stationary experimental runs were grown using 500 mL glass reagent bottles and were fitted with airtight lids containing gas and liquid sampling ports, see Figure 4.2. The liquid medium (either Van Niels medium or minimal medium) was added to the bioreactors aseptically before being inoculated with a loop of *R. palustris* streaked from a fresh agar plate. The airtight reagent bottles were then sparged with argon through a 0.22 µm PTFE filter for 10 minutes to induce anaerobic and dinitrogen-free conditions. Mixing within the bioreactor was facilitated by a magnetic stir plate (300 rpm) with the temperature controlled by placement of the reactors into a temperature-controlled water bath. Illumination was provided by 100 W tungsten-filament incandescent light bulbs with the illumination intensity set at 200 W/m^2 in the wavelength range of 500-1100 nm as this corresponds to the photosynthetic range utilised by *R. palustris*. Low hydrogen-permeability tubing (Tygon Laboratory tubing S3-E3603) was connected to the gas sampling port to collect any gas that was produced during operation. The gas was collected by displacement of water in an inverted 1 L measuring cylinder.

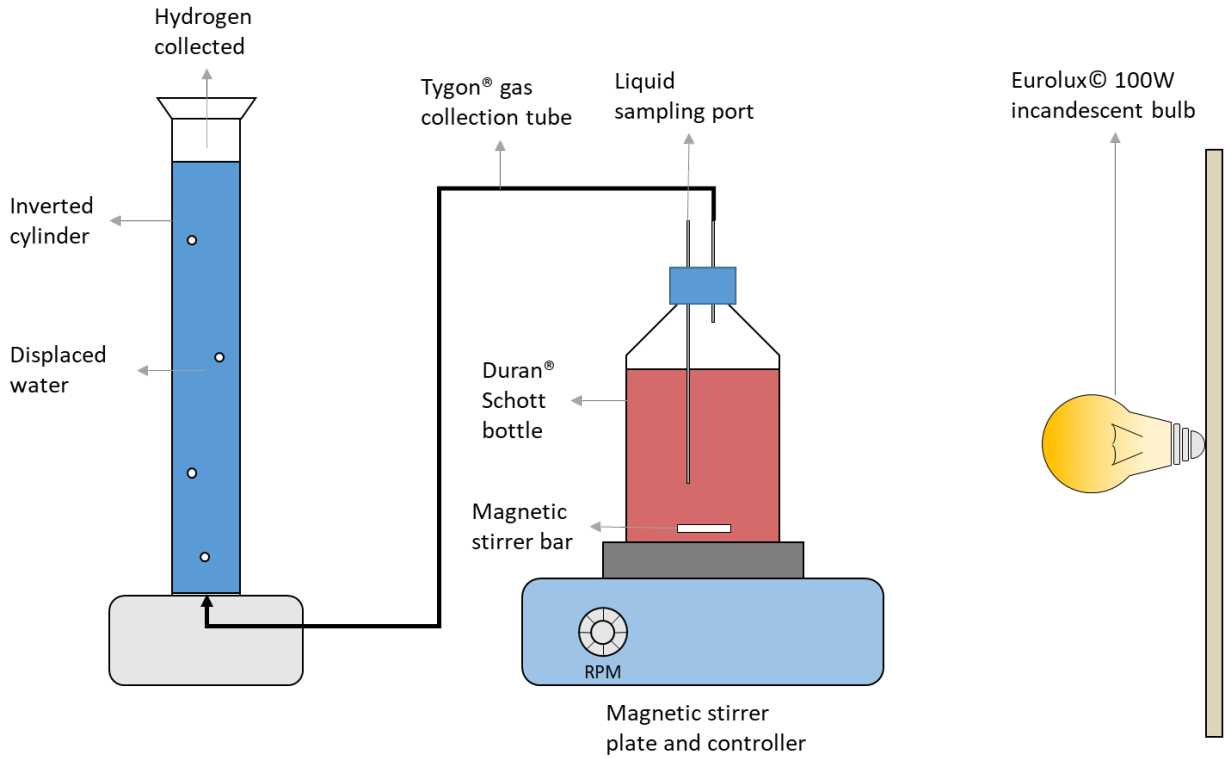

Figure 4.2: Schematic diagram of the Schott bottle PBR system used for inoculum culturing and Schott bottle PBR experiments. The above diagram is the side view of the entire setup. The Schott bottle is in a temperature-controlled water bath that is not depicted in the diagram.

4.4.1.2 Schott bottle bioreactors

Schott bottle bioreactors for non-stationary phase experiments were performed using the rig shown in Figure 4.2. The Schott bottle bioreactors were setup using the procedure described in 4.4.1.1 with a few minor adjustments. The reactors in the experimental run were inoculated using the inoculum described previously not via a streak from an agar plate. The volume of inoculum added was based on the required starting concentration and was determined by first measuring the concentration of the bacterium in the inoculum (see 4.5.1). This was done to ensure that the staring concentration was above a certain threshold to reduce the chance of any stochastic effects.

4.4.1.3 Tubular photobioreactor setup and procedure

Borosilicate glass tubing was used to make the tubular PBR system used in this investigation. The reactor had a total active volume of 500 mL with the following dimensions: 2.83 m long with an internal diameter of 0.015 m and a wall thickness of 1.8×10^{-3} m (full design sheet provided in Figure A.1 in Appendix A). Figure 4.3 provides a schematic of the experimental setup used for the tubular PBR system. The system consisted of a clear glass water bath with a heat circulator (Julabo Corio heat immersion circulator) used to control the temperature of the experiment at 35°C. The system was set up to operate as a batch type

system with a 1L Schott bottle as the reservoir for the returning outlet stream and the exiting inlet stream. The Schott bottle lid also housed a liquid sampling port which was used to sparge the system with argon through a 0.22 µm PTFE filter for 10 minutes to induce anaerobic and dinitrogen-free conditions as well as a gas outlet port. Norprene Industrial Grade Tygon Tubing A-60-G was used for transportation of the culture medium in and out of the reservoir. Tygon A-60-G has a low gas permeability, was purpose-fit for peristaltic pumps and could also withstand the high temperatures experienced during autoclaving. An added benefit of the Tygon A-60-G tubing was that it was opaque, so the bacterial culture only absorbed light when it was in the active section of the tubular PBR. A peristaltic pump (Runze Fluid YZ1515X) was used to transport the bacterial culture from the reservoir to the tubular reactor with the outlet of the reactor returning to the reservoir. The peristaltic pump was used due to its non-invasive nature, which limits the possibility of contamination of the system. Circulation through the reactor was kept constant throughout all experiments done using this setup at a flow rate of 0.651 L/min.

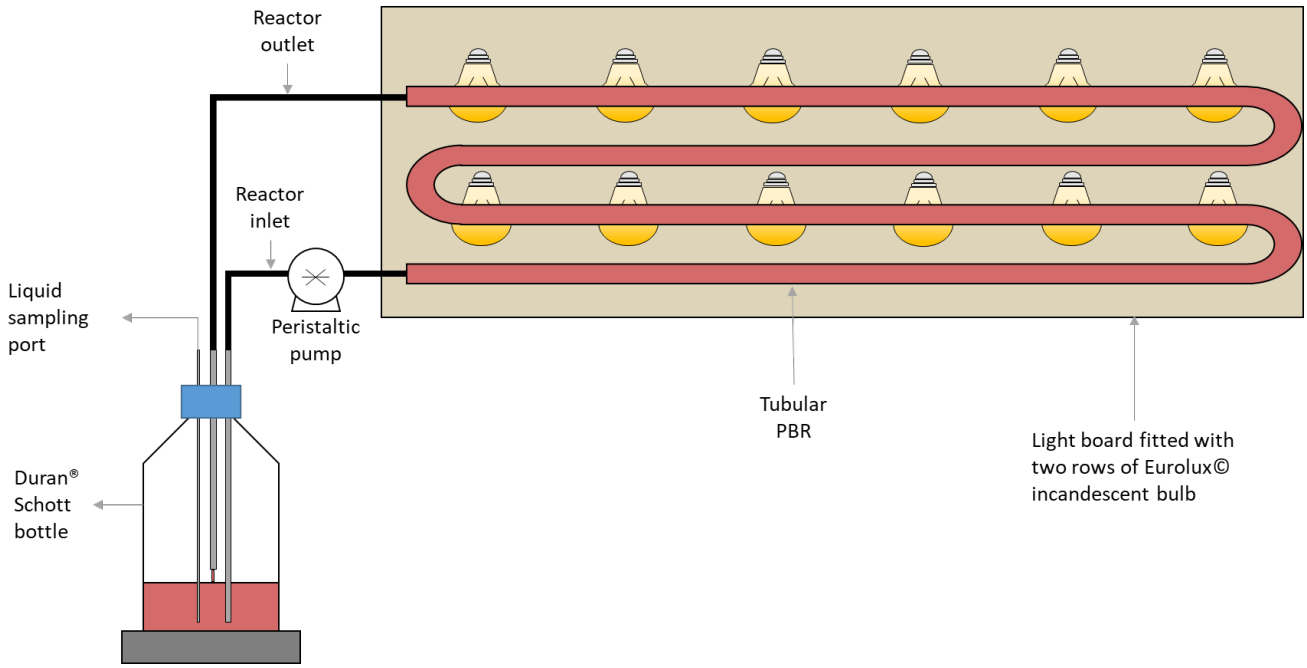

Figure 4.3: Schematic diagram of the tubular PBR system used for all experiments pertaining to the effect of light intensity. The above diagram is the front view of the entire setup. The entire tubular PBR system was in a temperature-controlled water bath that is not depicted in the diagram. Total illuminated length and volume is 2.86 m and 500 mL respectively.

Illumination of the PBR system was done using 60 W or 100 W tungsten-filament incandescent light bulbs. As can be seen in Figure 4.3, two rows of bulbs were used to illuminate the external surface of one side of each tubular bioreactor. Light was provided for the entire experimental run, with checks done at the end of the experimental run to ensure no major decrease in light intensity due to aging bulbs. Light bulbs were replaced after every experimental run to ensure consistency in the light intensity for each new

experiment. The light intensity was an investigated parameter and therefore was adjusted as required by either shifting the light board closer or further from the surface of the bioreactor. The illuminated surface area of the tubular PBR was approximated as half of the total surface area of the tubular reactor as it was assumed that exactly half of the reactor would receive direct illumination with the light coming from one side only.

During the experimental setup procedure, the entire PBR system was assembled and autoclaved (Speedy autoclave) for 50 minutes at a temperature of 121°C and pressure of 101 kPa. Once autoclaved the reactor system was sparged with argon before being loaded with inoculated Van Niels medium that had already been sparged with argon.

4.4.1.4 Column photobioreactor design, setup and procedure

The column PBR was a custom designed reactor and was purpose-designed to operate with various culture types and configurations, namely i) a simple planktonic culture, ii) a packed bed PBR and iii) a fluidised bed PBR.

The bioreactor was made of borosilicate glass which meant that the reactor was autoclavable - a necessity as the system needed to be sterile. The main body of the reactor was a 0.68 m tall glass column with an external diameter of 0.0536 m and an internal diameter of 0.05 m (wall thickness of 1.8×10^{-3} m). The base of this glass column was sealed with a rubber stopper that had a hose connector fitted inside of it for the liquid medium to enter at the base of the reactor. The top of the glass column was fitted with a glass Schott bottle thread. This was done so that the lid of a Schott bottle with bioreactor fittings could be used to seal the top of the reactor, which would then allow for easy loading of the reactor with the immobilised bacteria as well as to collect the hydrogen gas from the headspace of the reactor.

All experiments performed using this reactor were operated as a batch system. This was achieved through the recirculation of the liquid medium which exited the top of the reactor through an overflow port (located near the top of the reactor) and returned to the base of the column. Tygon A-60-G was used as the tubing to recirculate the liquid medium with the use of a peristaltic pump (Runze Fluid YZ1515X). The benefits of this combination used to transport the medium was discussed previously. Circulation flow rate through the reactor was dependent on the configuration of the reactor. However, when it was operated with planktonic cells the flow rate was set to 0.651 L/min. A liquid sampling port was located in line with the Tygon A-60-G tubing.

A simple stainless-steel mesh was used as a distributor plate and was installed at the base of the reactor above the rubber stopper to allow for more even distribution of the liquid entering the reactor. When operating with immobilised bacteria this plate also stopped the PVA cryogel beads from collecting in the

tubing that enters at the base of the reactor. The active section of the column was from the distributor plate to the overflow port which measured at 0.62 m and meant that the active volume of the reactor was 1 L. The design sheet of the column PBR is provided in Appendix A. The entire reactor system could be autoclaved to ensure a sterile environment.

During the setup for bacterial culturing in the column PBR the entire PBR system as shown in Figure 4.4 was assembled and autoclaved (Speedy autoclave) for 50 minutes at a temperature of 121°C and pressure of 101 kPa. Once autoclaved the reactor system was sparged with argon before being loaded with inoculated minimal medium. Illumination of the PBR system was done using 60 W tungsten-filament incandescent light bulbs. The light intensity at the surface of the bacterial culture was set at 100 W/m^2. The illuminated surface area of the column PBR was approximated as half of the total surface area of the column PBR as it was assumed that exactly half of the reactor would receive direct illumination with the light coming from one side only.

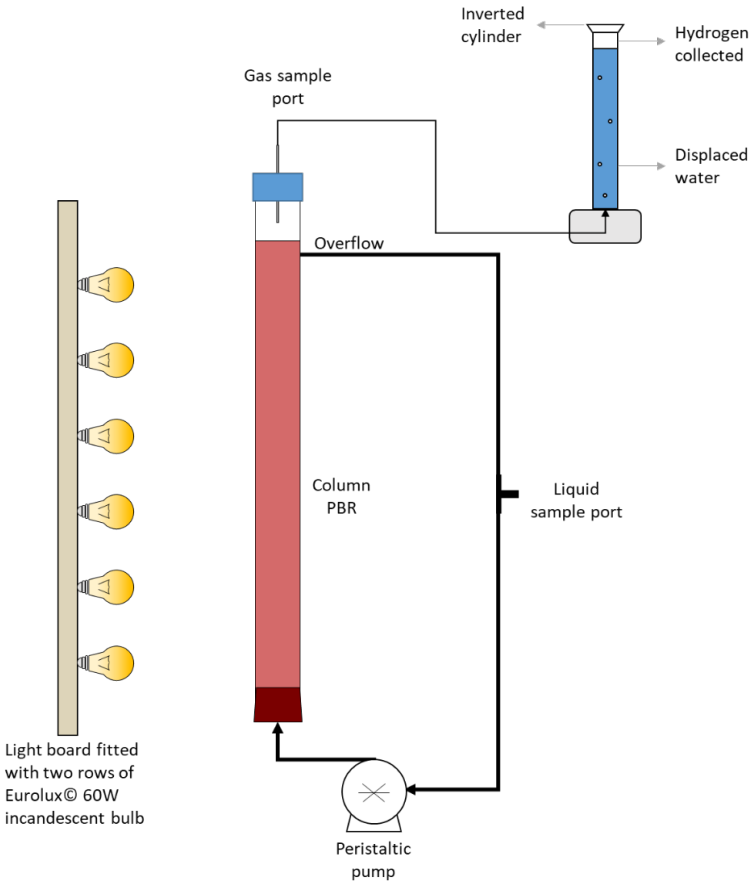

Figure 4.4: Schematic diagram of the column PBR system operating with a free-cell culture. The above diagram is the side view of the entire setup. The culture was recirculated using a peristaltic pump and the reactor was illuminated by six 60W Eurolux incandescent light bulbs.

Every 24 hours of the experimental run a 2 mL liquid sample was taken through the sample port. The sample was then centrifuged for 5 minutes at $13900 \times g$ to form a cell pellet. The supernatant was then removed and placed in a storage vile and frozen at -20°C until the sample was required for glycerol and glutamate analysis. The cell pellet was used to determine the cell concentration (see Section 4.5.1). The hydrogen produced during experimental runs was collected in an inverted 1 L measuring cylinder filled with water. The raw volume of hydrogen produced was equal to the volume of water displaced.

4.4.2 Immobilisation of R. palustris

The bacteria used for immobilisation was grown as described in Section 4.4.1.1 for 4 days in Van Niels medium to ensure that the culture was in the exponential growth phase and the amount of dead bacteria present in the culture are minimised. The bacterial culture was then centrifuged at $4000 \times g$ (Hermle Z306 Universal Centrifuge) for 20 minutes in 250mL Nalgene™ centrifuge bottles (Thermo Scientific™ Nalgene™ Products). The supernatant was then discarded, leaving only the cell pellet. The cell pellet was then resuspended in minimal medium with no additions before being centrifuged at $4000 \times g$ for 5 minutes. This was done to wash off excess yeast extract that may have been entrained with the bacteria ensuring that when the bacterium was immobilised in the PVA it would remain in the stationary phase. The resuspension and centrifugation were repeated once more. After the last cell pellet washing the cell pellet was resuspended using a 50% (v/v) sterile glycerol solution, with biomass loading calculated on a 1.5% wet cell pellet to PVA on a volume to mass ratio.

8.25mL of the bacterial suspension was dispersed per 100 g of the PVA (liquid at 45°C) that was developed using the method described in Section 4.3.3. The addition of the bacterial solution meant that the 11% (w/v) PVA solution became a 10% (w/v) PVA solution as it is assumed that the bacterial suspension is merely a 50% (v/v) glycerol solution. Dispersion was aided by a magnetic stirrer plate with the temperature of the mixture held constant at 45°C using a water bath. The solution was then dripped into liquid nitrogen through sterile tubing and a custom-made multi-head dripper with the aid of a peristaltic pump. The frozen beads were then placed in sterile storage vessels which were stored at -86°C until they were required for an experimental run. The experimental setup used to make the immobilised bacteria is provided in Figure 4.5.

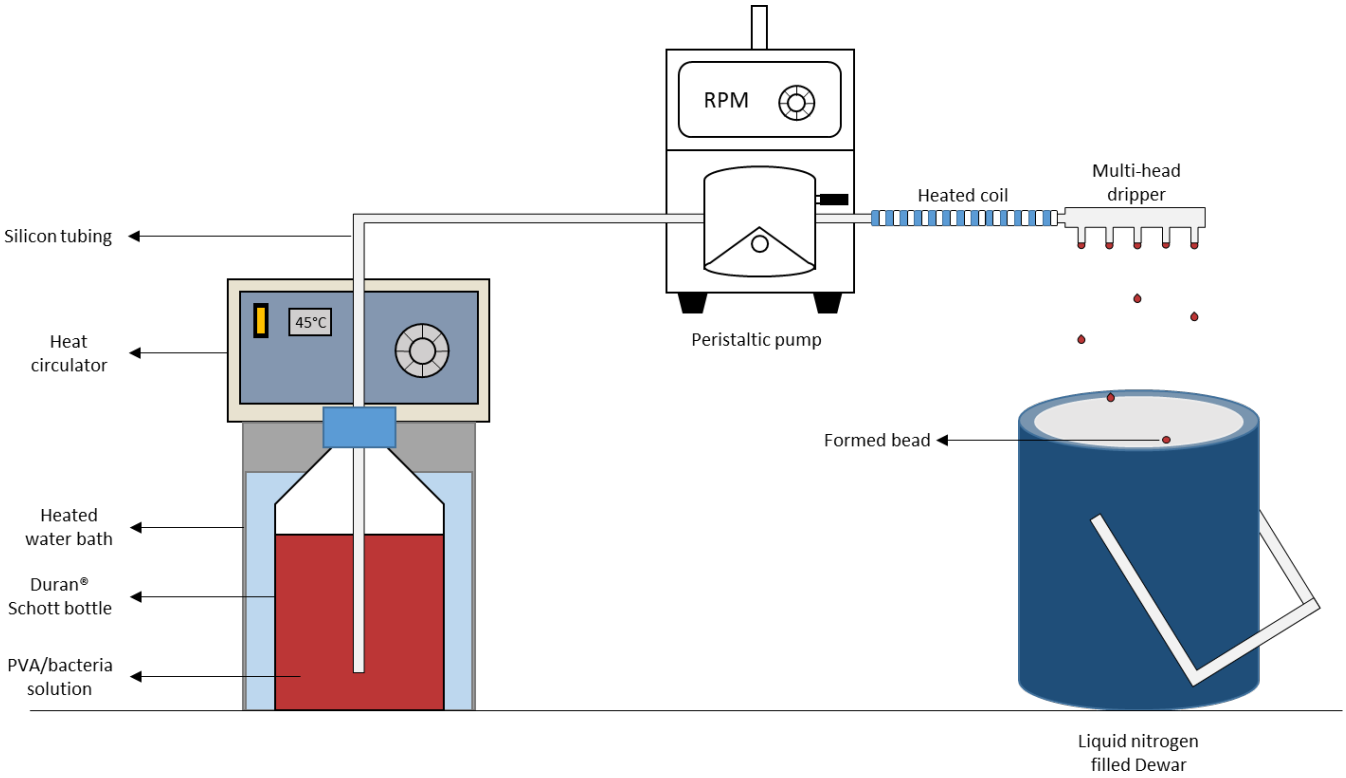

Figure 4.5: Schematic diagram of bead making procedure. The PVA/bacteria solution is kept at a constant temperature of 45°C using a heated water bath. A peristaltic pump is used to transfer the solution from the Schott bottle to the multi-dripper head. The beads form as they are dripped into the liquid nitrogen.

When the immobilised bacteria were required, they were left to thaw fully to room temperature. The beads then underwent a three-stage washing procedure using sterile phosphate buffered saline (PBS) with a pH of 7.1 to remove bacteria on the surface of the beads that were unbound. See Table 4.5 for PBS components and corresponding concentrations. The three-stage washing procedure was done in a glass beaker with mixing facilitated by a magnetic stirrer bar. The first stage was a PBS wash for 30 minutes with the second and third wash being an hour each.

Table 4.5: PBS solution components and concentrations

Component	Concentration (g/L)	Concentration (mM)
NaCl	8	137
KCl	0.2	2.7
Na_2HPO_4	1.44	10
KH_2PO_4	0.24	1.8

The bacterial loaded PVA cryogel beads were then incubated for 72 hours in a 1L Schott bottle reactor with nitrogen free and addition free minimal media. The reactor configuration described in 4.4.1.2 was used during this washing period which was operated at a temperature of 35°C and at a light intensity of

200 W/m^2. This long washing period was done to remove the glycerol co-solvent to ensure that the bacterial metabolic state and nitrogenase activity is not adversely affected.

4.4.3 Fluidised bed photobioreactor

The fluidised bed PBR was investigated using the column PBR discussed in 4.4.1.4. During the setup for the fluidised bed the column PBR system shown in Figure 4.4 was assembled and autoclaved (Speedy autoclave) for 50 minutes at a temperature of 121°C and pressure of 101 kPa. Once autoclaved the reactor system was sparged with argon before being loaded with 250g of PVA immobilised bacterium which was produced using the procedure above. Argon sparged minimal medium with sterile additions was then loaded into the column through the liquid sampling port with the aid of a peristaltic pump. The fluidisation of the bed was facilitated by the peristaltic pump recirculating the medium from the overflow to the base of the reactor. Figure 4.6 illustrates the setup when fluidisation was implemented, the volumetric flow rate of the fluid was constant at 1.06 L/min when the bed was fluidised. The peristaltic pump calibration curve relating the pump RPM setting to the volumetric flow rate is provided in Figure B.1 in Appendix B.

Illumination of the PBR system was done using 60 W tungsten-filament incandescent light bulbs. The light intensity at the surface of the one side of the reactor was set at 100 W/m^2.

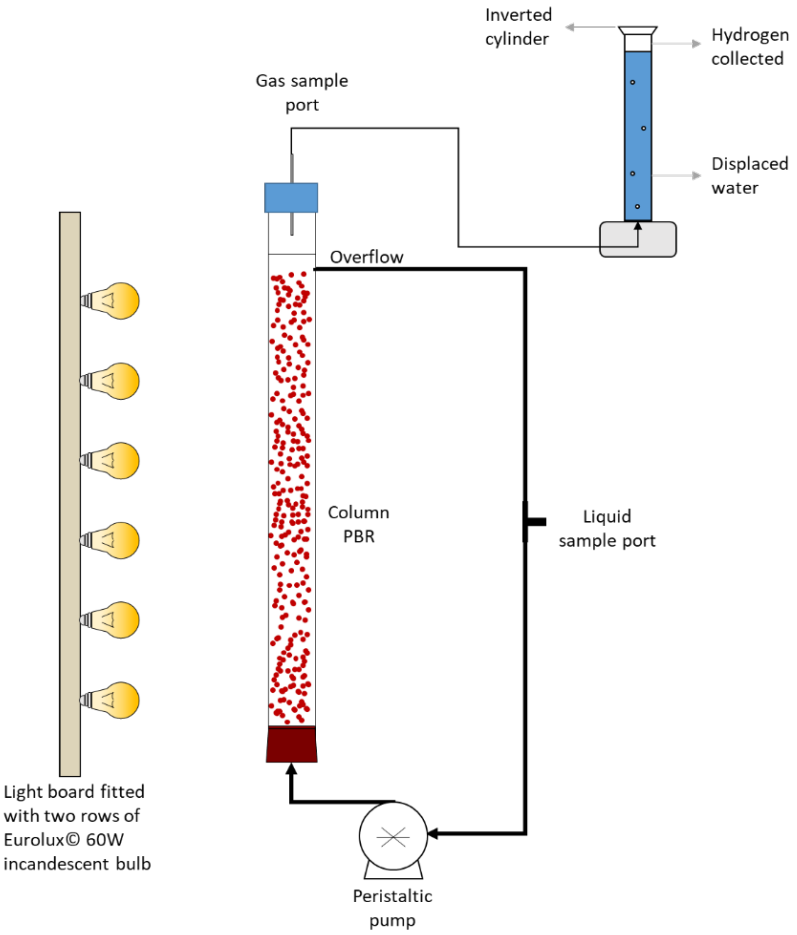

Figure 4.6: Schematic diagram of the FBPBR system operating with R. palustris immobilised in PVA cryogel. The above diagram is the side view of the entire setup.

Every 24 hours of the experimental run a 2 mL liquid sample was taken through the sample port. Before a sample was taken the dead volume present in the sample port was removed to ensure that the sample taken correctly represented the experimental run time. After centrifugation the sample was placed in a storage vile and frozen at -20°C until the sample was required for glycerol analysis. The hydrogen produced during experimental runs was collected in an inverted 1 L measuring cylinder filled with water. The raw volume of hydrogen produced was equal to the volume of water displaced.

4.4.4 Packed bed photobioreactor

The packed bed PBR was investigated using the column PBR discussed in 4.4.1.4. The packed bed PBR was setup in the exact manner described in section 4.4.3. However, the flow rate was reduced to below the minimum fluidisation flow rate. This flow rate was determined experimentally to be 0.347 L/min. Figure 4.7 illustrates the setup when the packed bed configuration was implemented.

Illumination of the PBR system was done using 60 W tungsten-filament incandescent light bulbs. The light intensity at the surface of the one side of the reactor was set at 100 W/m^2.

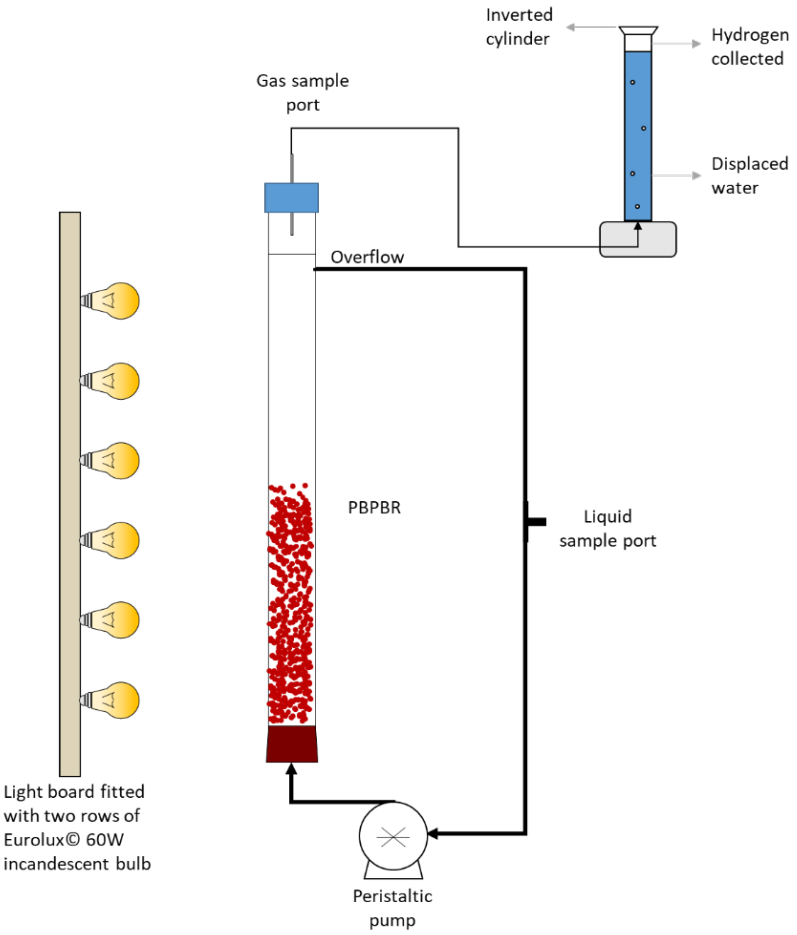

Figure 4.7: Schematic diagram of the PBPBR system operating with R. palustris immobilised in PVA cryogel. The above diagram is the side view of the entire setup

Every 24 hours of the experimental run a 2 mL liquid sample was taken through the sample port. Before a sample was taken the dead volume present in the sample port was removed to ensure that the sample taken correctly represented the experimental run time. After centrifugation the sample was placed in a storage vile and frozen at -20°C until the sample was required for glycerol analysis. The hydrogen produced during experimental runs was collected in an inverted 1 L measuring cylinder filled with water. The raw volume of hydrogen produced was equal to the volume of water displaced.

4.5 Analytical techniques

4.5.1 Cell concentration

The characteristic microbial growth phases and the growth kinetics are reliant on the change in cell concentration over time. The cell concentration can be quantified as either the cell dry weight (CDW) or by the number of cells. In this study the cell concentration will be defined as the CDW.

Determination of CDW for each sample would be time consuming, therefore a standard curve which relates optical density to the CDW was developed due to the relative ease in obtaining the optical density of samples, on the assumption that cell size and optical properties are constant throughout the experiments. The optical density is an indirect measurement of cell concentration meaning that there is a relationship between the optical density and the CDW. The techniques employed for the measurement of CDW and optical density are discussed in detail below.

4.5.1.1 Cell dry weight

A Buchner vacuum filter fitted with a 0.22 µm nylon filter paper (FilterBio Sterile Nylon Membrane Filter – 47 mm diameter) was used when determining the CDW. Firstly, the filter paper was dried in an oven for 24 hours at 60°C and cooled in a desiccator. This was done to remove all moisture that may be present in the filter paper. With the drying complete, the weight of the filter paper was measured to four decimal places using a lab scale (Sartorius AG BP 61S 5 decimal lab scale). A bacterial culture in the exponential growth phase was used when measuring the CDW for the standard curve and was grown using the methods described in 4.4.1.1. The bacterial culture was used to make a series of dilutions, each with a total volume of 10 mL. Each dilution was then passed through their own respective filter papers in the Buchner vacuum filter and rinsed with deionised water to remove salts and media off the cells. The filter paper loaded with the wet cells were then dried as before and weighed to five decimal places using the lab scale (Sartorius AG BP 61S 5 decimal lab scale). The CDW was then calculated as the difference between the two weights, divided by the volume of the sample. CDW measurements were only done for samples used to set up the standard curve.

4.5.1.2 Optical density

The optical density of a sample was measured using a spectrophotometer (Varian) at a wavelength of 660 nm. Before measurement the culture sample required the necessary preparation. This involved taking a 1 mL sample from the bioreactor through the liquid sampling point using a syringe and placing the sample into a micro-centrifuge tube. The culture samples were then centrifuged (Eppendorf Minispin Plus) at $13900 \times g$ for 5 minutes. This was done to form two phases, namely a solid cell pellet and the liquid supernatant. The supernatant was then removed from the micro-centrifuge tube and replaced by 1 mL of deionized water. The cell pellet was then re-suspended in the deionised water via vortexing.

Deionised water was used as the blank when doing measurements with the spectrophotometer. Samples with an optical density above 1.5 were diluted for it to lie within the linear region of the CDW standard curve.

4.5.1.3 Cell concentration standard curve

The cell concentration standard curve relates the optical density to the CDW. The optical density was measured for all samples where cell dry weight analysis was performed. The optical densities were then plotted against their respective CDW to obtain the cell concentration standard curve. For all future cell concentration measurements, the optical density was measured, and the standard curve was used to obtain the corresponding CDW.

Figure 4.8 below shows the plot of CDW versus optical density for *R. palustris* grown in Van Niels medium. From the plot it is clear that CDW and optical density only have a linear relationship up to an optical density of 1.5 After this point the CDW begins to increase exponentially as the optical density increases. Linear regression was then used to determine the equation of the line of best fit through the data points up to and include the data point at and optical density of 1.5. The regression equation is provided in Equation 34 and was used when determining the CDW of cultures grown in Van Niels medium. The regression line for this data showed a very good R^2 value (0.9934), indicating a very good linear fit for the data.

$$OD = 2{,}0154(CDW) + 0{,}1409 \quad [34]$$

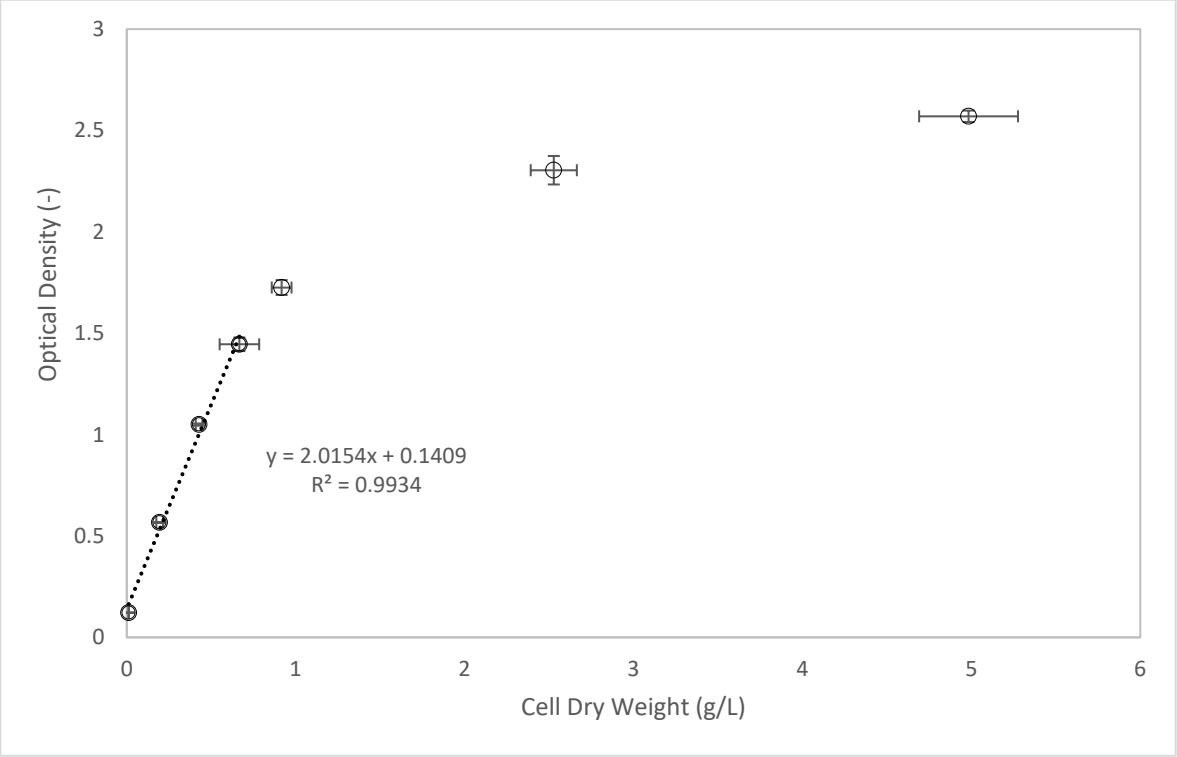

Figure 4.8: Cell concentration standard curve for bacterial cultures grown in Van Niels medium. Data points represent the mean of triplicate repeats. The error bars show the uncertainty associated with both the CDW measurements and the optical density measurements.

Figure 4.9 shows the CDW standard curve which was setup for *R. palustris* grown in minimal medium with sterile additions. Linear regression was then used to determine the equation of the line of best fit through the data points. The regression equation is provided in Equation 35 and was used when determining the CDW of cultures grown in minimal medium. The linear regression used for the standard curve also provides the R^2 value which is used to determine the goodness-of-fit of the data points to the regression line. The regression line for this data showed a very good R^2 value (0.9983), indicating a very good linear fit for the data.

$$OD = 1{,}5654(CDW) + 0{,}1048 \quad [35]$$

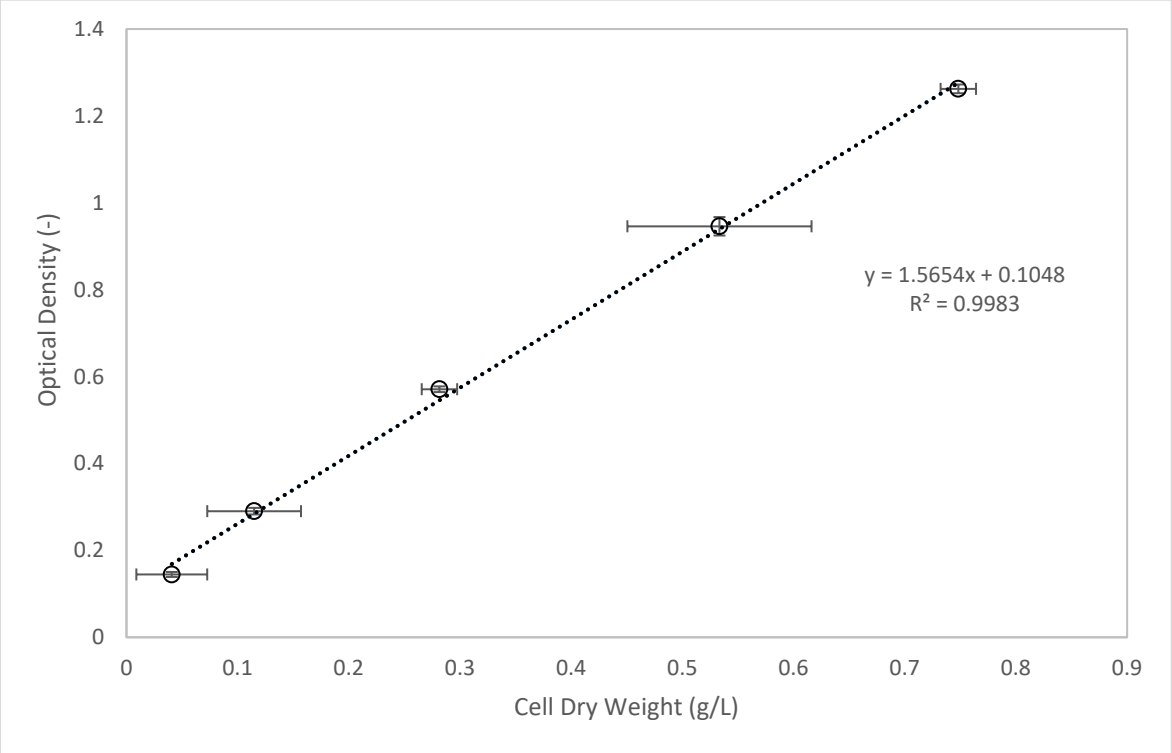

Figure 4.9: Cell concentration standard curve for bacterial cultures grown in minimal medium. Data points represent the mean of triplicate repeats. The error bars show the uncertainty associated with both the CDW measurements and the optical density measurements.

4.5.2 Hydrogen concentration

Hydrogen concentration and overall composition of the gas produced during experimentation was determined using a Global Analyser Solutions CompactGC with argon carrier stream and thermal conductivity detector (TCD). Hydrogen and carbon dioxide were reported as relative percentages.

4.5.3 Glycerol concentration

The concentration of glycerol in the stored supernatant samples from experimental runs was determined using high-performance liquid chromatography (HPLC). The summary of the HPLC specifications are provided in Table 4.6 below.

Table 4.6: Summary of HPLC specifications for analysis of glycerol concentrations that are to be determined

Instrument	Components	Description
TSP (Thermo Separations Product) HPLC	Column	Biorad HPX-87H column, 250 x 7.8mm with guard cartridge
	Mobile phase and flow rate	0.005M H2SO4 @ 0.6ml/min
	Sample volume	30ul
	Column temperature	65°C
	Detector	Shodex 101 RI detector (for glycerol)
Dionex UltiMate 3000 HPLC	Column	Biorad HPX-87H column, 250 x 7.8mm with guard cartridge
	Mobile phase and flow rate	0.005M H2SO4 @ 0.6ml/min
	Sample volume	20ul
	Column temperature	65°C
	Detector	ERC Refracto Max520 RI detector (for glycerol)

A 1mL sample was prepared for HPLC analysis by passing the sample through a 0.22 µm syringe filter to remove any solids that could possibly clog the HPLC column. After filtration the samples were injected into the HPLC for analysis.

Prior to injection of samples into the HPLC column a standard curve relating glycerol concentration to the area under the absorption peaks obtained from the HPLC results was developed and is supplied in Figure 4.10.

The standard curve was developed by injecting a series of dilutions of known glycerol concentrations into the HPLC column. The area under the absorption peaks obtained from the HPLC analysis was then plotted with the corresponding glycerol concentrations. The regression line for this data showed a very good R^2 value (1), indicating a perfect linear fit for the data. Equation 36 provides the equation of the line of best fit which was used to calculate the glycerol concentrations using the area under the absorption peak of each sample analysed.

$$Glycerol\ concentration\ =\ 0{,}2255 \times (Area) \qquad [\ 36\ ]$$

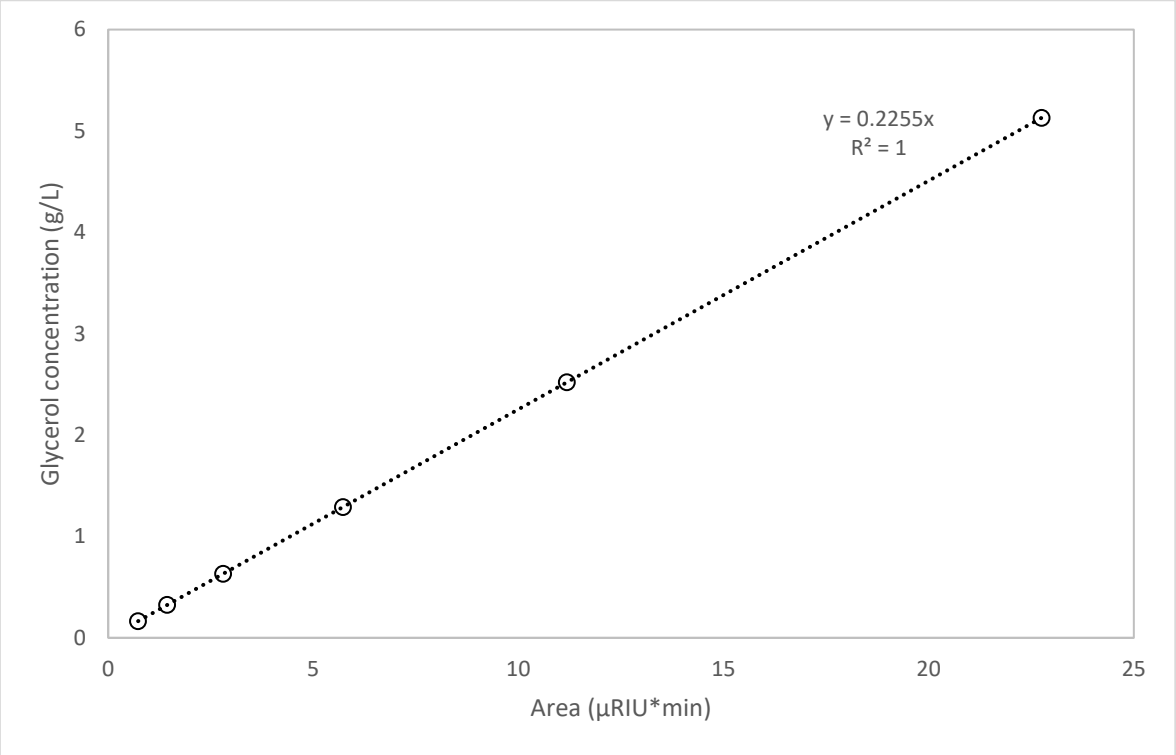

Figure 4.10: Glycerol concentration standard curve developed from HPLC analysis for conversion from area under the absorbance peaks.

4.5.4 Glutamate concentration

Glutamate concentration was determined using a modified ninhydrin assay. This was done by adding 800 µL of a 4 mM stock solution made up of ninhydrin in absolute ethanol to 200 µL of cell free supernatant (removal of cells described in Section 4.5.3) in a centrifuge tube. The centrifuge tube was then incubated for 15 minutes at 80°C before 200 µL of the content was pipetted into a well of a standard 96 well plate with absorbance read at 590 nm in a microplate reader. The measured absorbance was used along with the standard curve provided in Figure 4.11 to calculate the glutamate concentration present in the sample.

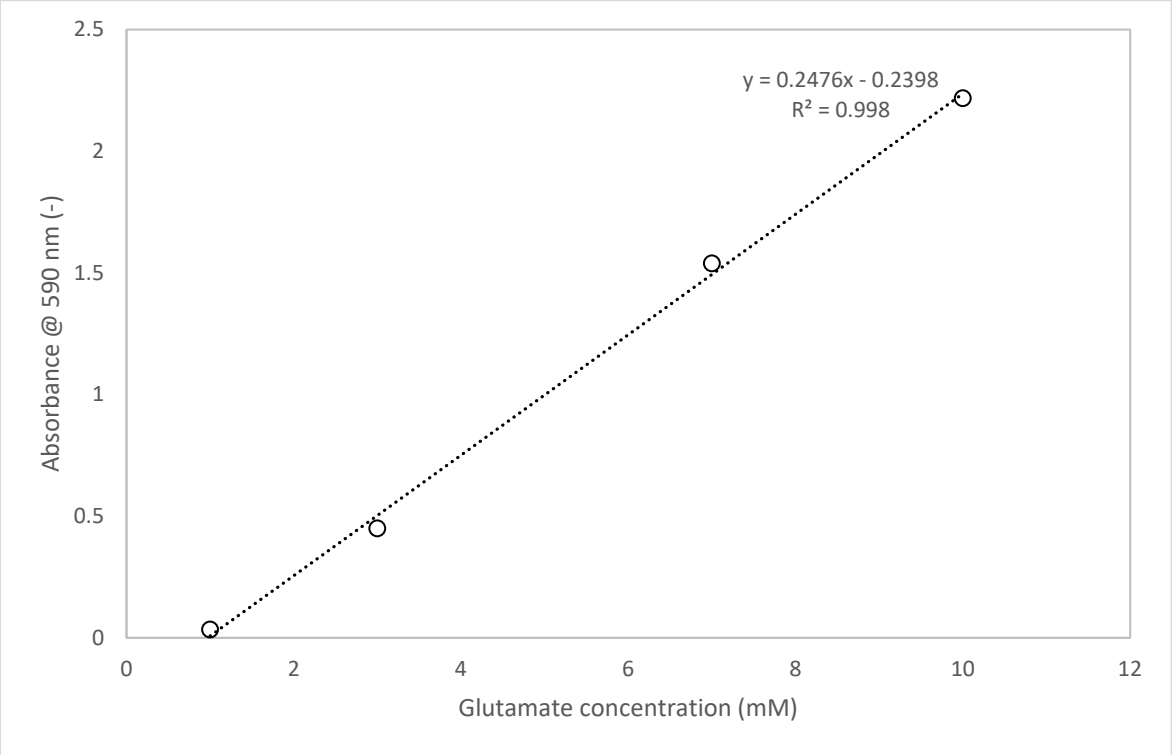

Figure 4.11: Glutamate concentration curve

4.5.5 Pigment extraction

All pigment extractions were carried out on fresh samples taken when the bacterial culture was in the exponential growth phase. Two 1mL samples were taken at the same time, one used to measure the CDW of the culture and the other used to perform the pigment extraction on.

Firstly, the sample was centrifuged for 5 minutes at $13900 \times g$ to form a cell pellet and supernatant (see section 4.5.1.2). The supernatant was carefully removed, and the cell pellet resuspended in a 7:2 (v/v) acetone/methanol solution through vortexing for 10 minutes to ensure full contact between the cells and solution. The solution was then centrifuged for 5 minutes at $13900 \times g$. The supernatant containing the extracted pigments was then transferred to a sample vile and the remaining cell pellet was re-extracted using the above method until the unit cells were completely colourless. For all pigment extraction experiments only two re-extractions were required. During these extractions care was taken to keep the samples out of light due to the pigments' sensitivity to light, this meant making sure all sample viles were covered with tin foil to avoid exposure to light.

The absorption spectrum of the supernatant containing the pigments were analysed using a Varian CARY 1E UV/Vis Spectrophotometer in the range of 400-900nm with the before mentioned acetone/methanol mixture used as the blank.

The BChl-α absorbance was measured at 772 nm. The absorbance was then used to calculate the BChl-α and the concentration was calculated using Equation #.

(Evans et al., 1990): $$\mathrm{BChl-\alpha\ (mg)} = \frac{Absorbance@772\ nm}{0.076} \times \frac{1}{MW_{BChl-\alpha}} \quad [37]$$

The carotenoid absorbance was measured at 480 nm and the concentration was calculated using Equation #.

(Soon et al., 2014) $$Carotenoid\ (mg) = \frac{Absorbance@480\ nm \times sample\ volume}{4} \quad [38]$$

4.5.6 Statistical analysis

4.5.6.1 Statistics on experimental data

Uncertainty (Δ) parameter was used as the statistical analysis on repeated experimental data points. This analysis was used for all experimental data. Calculation of the uncertainty parameter is described Equation 39 shown below.

$$\Delta = \pm t(\alpha, n-1)s_n \quad [39]$$

$Where,$

$\alpha = significance\ level\ (0.05\ selected)$

$n = sample\ size$

$t(\alpha, n-1) = students\ t\ distribution\ inverse\ (two-tailed)$

$s_n = standard\ error; s_n = \frac{s}{\sqrt{n}}$

$s = standard\ deviation; s = \sqrt{\frac{1}{n-1}\sum_{j-1}^{n}\left(x_{i,j} - \bar{x_i}\right)^2}$

4.5.6.2 Statistics on predicted data

When using regression to predict the average y value associated with a given x value, it is necessary to determine the measure of the spread of the y values around the average y value. To do this, the root mean squared (RMS) error can be employed in order to assess the predictive accuracy of a model. The RMS error can was determined using Equation 40:

$$RMSError = \sqrt{\frac{\sum_{i=1}^{n}\left(z_{p,i}-z_{o,i}\right)^2}{n}} \quad [40]$$

$Where,$

$z_{p,i} = predicted\ value\ of\ z\ for\ the\ ith\ observation$

$z_{o,i} = observed\ value\ of\ z\ for\ the\ ith\ observation$

$n = sample\ size$

From inspection of Equation 40, it can be seen that the RMS error aggregates the magnitudes of the errors, between the predicted and the observed values into a single measure of predictive power. This provided a measure of precision for the model. The RMS error was normalised against the mean of the response variable (y) measurements for easy interpretation of model performance. The normalised RMS (NRMS) error can have a value between 0 and 1, a value of 0 means that there is no spread of the y values which means that all the experimental points lie on the regression line.

For regression analysis 95% prediction intervals (PIs) were calculated for response variables. A PI is an estimate of the range that is likely to contain the response value of future observations, given what has already been observed. The 95% PI was calculated using the built in MATLAB functions and *nlpredci*.

5 RESULTS AND DISCUSSION

5.1 Effect of light intensity on the growth of *R. palustris*

To investigate the effect of the incident light intensity on the cell growth of *R. palustris* 11774 the reactor system described in section 4.4.1.3 was employed. The tubular PBR system operated with the Van Niels medium and therefore contained high nitrogen levels (yeast extract consists of ±10% total nitrogen). The nitrogen present in the culture inhibits hydrogen production as it suppresses the synthesis of nitrogenase and inhibits the nitrogenase enzyme activity. A tubular reactor with a very small inner diameter (ID) relative to common laboratory bioreactor systems (Schott bottle-based bioreactors) was designed to reduce the effect of light attenuation through the reactor as the cell concentration of the culture increased. As discussed in section 2.4 , the equations that describes light attenuation through a reactor is dependent on the concentration of the biomass and the reactor width. Therefore, a reactor with a smaller diameter is going to experience lower attenuation of light in comparison to a larger reactor if the biomass concentration remains constant .This is illustrated below in Figure 5.1, where the light intensity decreases by approximately 40% through a bioreactor with a diameter of 0.015 m (corresponding to the tubular reactor) compared to an 80% reduction seen in the Schott bottle reactor (diameter of 0.086) at a biomass concentration of 4 g/L, thus illustrating the reduced effects of light attenuation when using a smaller ID reactor.

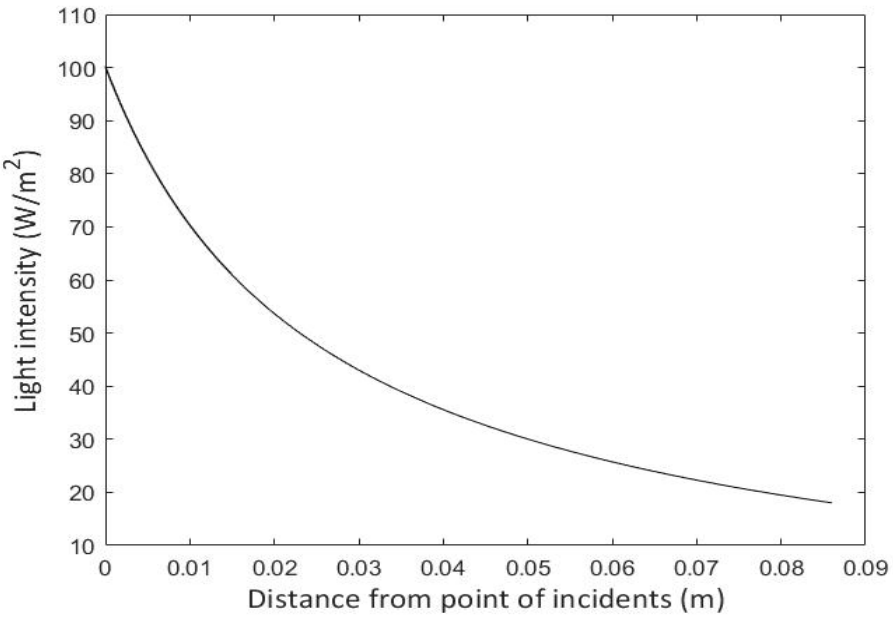

Figure 5.1: Change in average light intensity through the width of a cylindrical bioreactor with an incident light intensity of 100 W/m^2 and a biomass concentration of 4 g/L.

The effect of *R. palustris* biomass concentration on light attenuation was investigated through the light transmittance of the culture and is discussed in more detail below. Figure 5.2 below provides a graphical

representation of how transmittance (%) of light through an *R. palustris* culture changes as the concentration of cells in the culture increase. The transmittance was measured using a spectrophotometer (UV/Vis spectrophotometer, Varian) at a wavelength of 875nm corresponding to the bacteriochlorophyll α adsorption peak. All measurements were done in a standard cuvette with a width of 1cm. At cell concentrations as low as 0.01 g/L approximately 20% of the light is absorbed by the culture and at 0.92 g/L 97.53% of the light is already absorbed by the culture. This illustrates how much light is absorbed over a linear distance of 1 cm (standard cuvette) even when the culture density is less than 1 g/L. Therefore, the larger the diameter of the reactor, the greater the effect of mutual shading. Mutual shading is when the efficiency of light absorption energy by cells is higher in cells near the illuminated reactor surface, but lower in the cells deep within the culture, i.e. furthur from the illuminated surface (Yen and Chiang, 2012). High biomass concentrations can also cause mutual shading to hinder the light path entering the reactor and further inhibit the light absorption of the bacterial cells in the PBR (Yen and Chiang, 2012).

This is not ideal if the effect of light intensity on *R. palustris* is being tested, as there would be large variability in the average light intensity throught the reactor's cross-sectional area if the diameter of the reactor is significantly large.

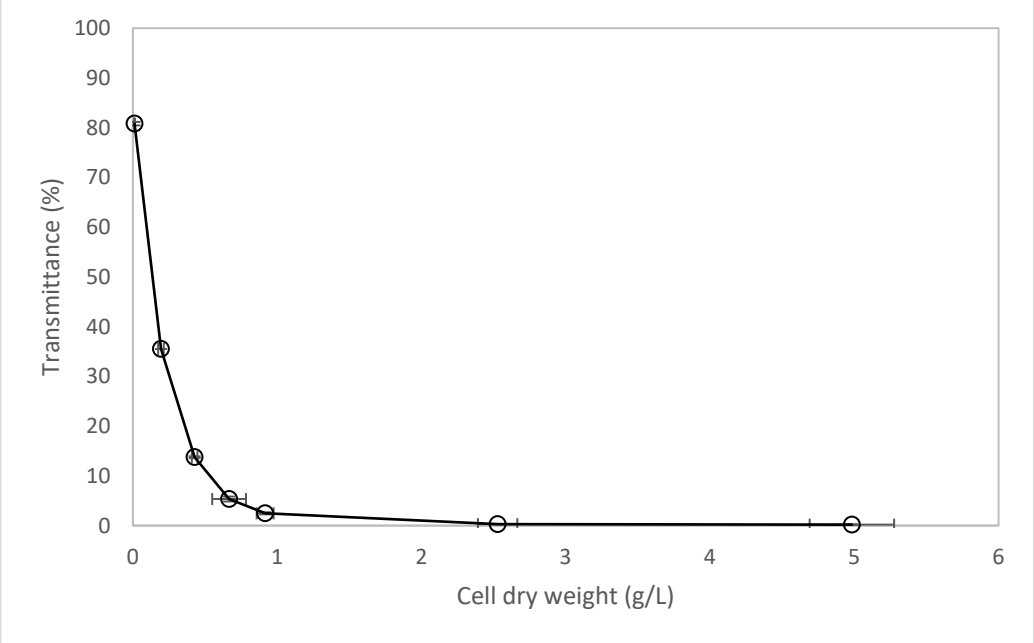

Figure 5.2: Transmittance (UV/Vis spectrophotometer, Varian at 875nm) of light through varying concentrations of R. palustris cultures in 1 cm cuvettes, with Van Niels medium as the blank. The culture used for these measurements was grown in a 500mL Schott bottle with bioreactor fittings in modified Van Niels medium at a temperature of 35°C and light intensity of 200 W/m^2 with illumination provided by incandescent light bulbs (100W Eurolux bulbs). Data points represent the mean of triplicate repeats and the error bars show the uncertainty associated with the CDW measurements and the transmittance measurements.

The experimental rig discussed in 4.4.1.3 was used for all experiments pertaining to the investigation into the effect of light intensity on *R. palustris* growth. The incident light intensity was measured using a spectrometer (RGB Photonics Q-mini) over the wavelength range of 500 to 1000 nm. The selection of the wavelength range was due in part to the limitation of the light meter (high level of noise below 500 nm), but was mainly based on the wavelength range where *R. palustris* can absorb light. The illumination was provided by incandescent light bulbs (Eurolux) with the light intensity being altered by adjusting the distance between the incident surface and the light bulbs. For high light intensities (200, 400 and 600 W/m^2) 100 W incandescent light bulbs were used and for the lower light intensities (30 and 70 W/m^2) 60 W incandescent light bulbs were used. Incandescent light bulbs were used as they provide the closest representation in terms of spectral light emission to sunlight over the wavelength range of 550 to 1000 nm when compared to other common indoor light sources such as florescent and LED lights (see discussion in section 2.8.2.2).

Five light intensities were investigated namely 30, 70, 200, 400 and 600 W/m^2. The minimum and maximum values in this range, i.e. 30 and 600 W/m^2, correspond to the limits of the experimental setup. The effect of light intensity on the *R. palustris* 11774 growth metabolism will be investigated through the comparison of the general growth behaviour, substrate utilisation, maximum specific growth rate and pigment formation at the varying light intensities selected.

5.1.1 Growth curves

The growth curves of *R. palustris* 11774 grown in modified Van Niels medium at varying light intensities using the tubular PBR system depicted in 4.4.1.3 can be seen in Figure 5.3 below. For each light intensity it can be noted that the typical trend of batch bacterial growth cultures is followed. There are distinct growth phases, namely the acceleration phase, exponential phase, deceleration phase, stationary phase and in some instances a death phase.

Batch cultures often have a period of stasis at the start of culturing where no cell division occurs Here cells are merely adapting to the culture conditions and synthesising required enzymes for growth. This period is known as the lag phase. In most cases steps are taken during culturing to minimise or remove this lag phase entirely to reduce the time it takes for the culture to enter the exponential growth phase. This was done in the experiment by culturing the *R. palustris* inoculum in the same medium and at the same temperature as the actual experimental environment, as well as inoculating when the inoculum was in the exponential phase of growth, so that cells could begin to divide almost immediately after inoculation. It can be seen in Figure 5.3 that the lag phase was successfully minimised. An in-detail discussion of the growth curve of each light intensity investigated follows:

i. 30 W/m^2

The acceleration phase starts from time zero and has a duration of 48 hours, after which the exponential phase is reached. The exponential phase is where the maximum growth rate is achieved. The exponential phase then ends at the 72-hour mark, corresponding to a 24-hour exponential phase. The growth of the cells begins to decrease as it enters the deceleration phase, which continues for 48 hours. Corresponding to a total incubation period of 120 hours. A short 9 hour long stationary phase then follows, which is where the rate of cell division is equal to the rate of cell death. This is succeeded by the death phase, which is where the rate of cell death is higher than the rate of cell division, often resulting in a linear decrease. The maximum CDW achieved at a light intensity of 30 W/m^2 was 4.182±0.157 g/L after 120 hours of culturing.

ii. 70 W/m^2

The acceleration phase starts from time zero and has a duration of 48 hours after which the start of exponential phase is reached. The exponential phase then ends at the 72-hour mark corresponding to a 24-hour exponential phase. The growth of the cells then begins to decrease as it enters the deceleration phase which continues for 31 hours, corresponding to a total incubation period of 103 hours. The deceleration has almost plateaued to the stationary phase at this point. No data was collected in the death phase. The maximum CDW achieved at a light intensity of 70 W/m^2 was 4.319±0.311 g/L and was achieved at the end of the experimental run, which was after 103 hours.

iii. 200 W/m^2

The acceleration phase starts from time zero and has a duration of 48 hours, after which the start of exponential phase is reached. The exponential phase then ends at the 72-hour mark, corresponding to a 24-hour exponential phase. The growth of the cells begins to decrease very gradually as it enters the deceleration phase, which continues for only 24 hours. At this point in the culture growth (96 hours) a very abrupt stationary phase is reached, which plateaus for 9 hours before gradually decreasing as it enters the death phase after a total incubation time of 103 hours. After 96 hours of biomass culturing the maximum CDW achieved at a light intensity of 200 W/m^2 was 4.923±0.338 g/L.

iv. 400 W/m^2

The acceleration phase starts from time zero and has a duration of 48 hours, after which the start of exponential phase is reached. The exponential phase then ends at the 72-hour mark, corresponding to a 24-hour exponential phase. The growth of the cells then begins to decrease gradually as it enters the deceleration phase which continues for only 24 hours. After 96 hours of biomass culturing the maximum

CDW was reached: 5.015±0.061 g/L. No stationary phase was observed as the culture immediately enters the death phase.

v. 600 W/m^2

The acceleration phase starts from time zero and has a duration of 48 hours after which the start of exponential phase is reached. The exponential phase then ends at the 72-hour mark corresponding to a 24-hour exponential phase. The growth of the cells then begins to decrease as it enters the deceleration phase, which continues for 50 hours, corresponding to a total incubation period of 122 hours. The deceleration almost plateaued to the stationary phase at this point. No data was collected in the death phase. The maximum CDW achieved at a light intensity of 600 W/m^2 was 4.172± g/L and was achieved at the end of the experimental run which was after 122 hours.

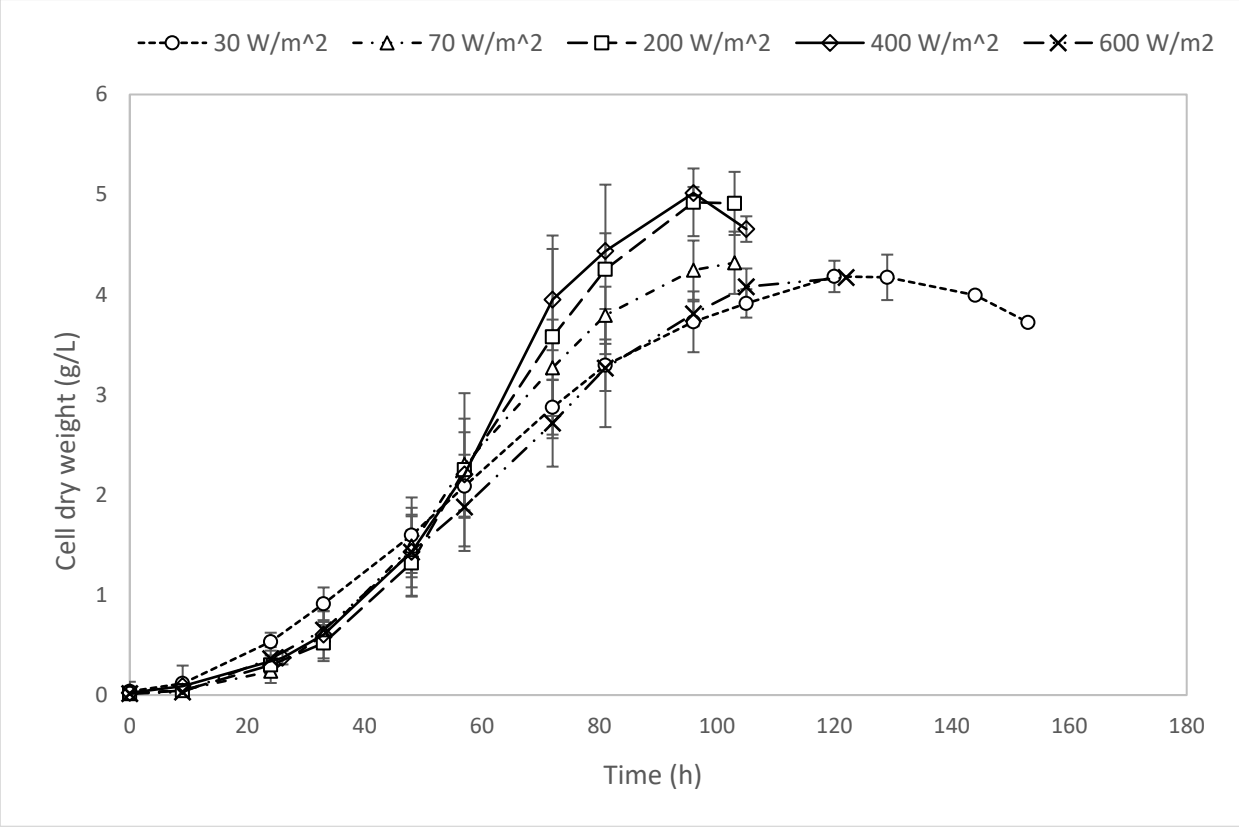

Figure 5.3: Growth curves (CDW vs time) of R. palustris with illumination provided by incandescent light bulbs (60W or 100W Eurolux bulbs depending on the light intensity required) for varying light intensities, i.e. 30, 70, 200, 400 and 600 W/m^2. R. palustris was cultivated using modified Van Niels medium and sparged with filter sterilised argon to promote anaerobic conditions. The CDW of the varying light intensities over times is provided in this figure. All experiments were completed at a constant temperature of 35°C and a volumetric flow rate of 0.651 L/min. Data points represent the mean of quadruple repeats and the error bars show the uncertainty associated with the CDW measurements.

From the detailed discussion on each individual growth curve it can be noted that there are clear similarities between all the light intensities investigated with regards to the timespan of the acceleration phase and the exponential phase. This implies that the period of these phases is not affected by the incident light intensity even though the rate of growth is. More sample points within these phases could possibly illustrate that the period is affected by light although these influences would likely be miniscule.

Almost identical growth curves were achieved for the 200 W/m^2 and 400 W/m^2 experimental runs, which indicates that the growth rate likely saturates when the light intensity increases to beyond a certain level. This will be discussed later in more detail in section 5.1.2 which divulges into the maximum specific growth rates achieved at each light intensity investigated.

Figure 5.4 below provides a graphical representation of how the maximum CDW (g/L) achieved changes as the incident light intensity increases. As the light intensity increases the maximum CDW that can be achieved increases until saturation occurs at 200 W/m^2. Saturation then continues until 400 W/m^2, after which photoinhibition occurs, which causes the maximum achievable CDW to decrease. There is an upward trend in the maximum CDW from 30 W/m^2 to 200 W/m^2, which corresponds to a CDW increase of 15.04% from 4.182±0.157 g/L to 4.923±0.338 g/L. The maximum CDW achieved then plateaus between 200 W/m^2 to 400 W/m^2 where there is a difference of only 1.84% between the two light intensities. The maximum CDW then decreases by 16.82% from 5.015±0.061 g/L to 4.172± g/L when the light intensity increases to 600 W/m^2.

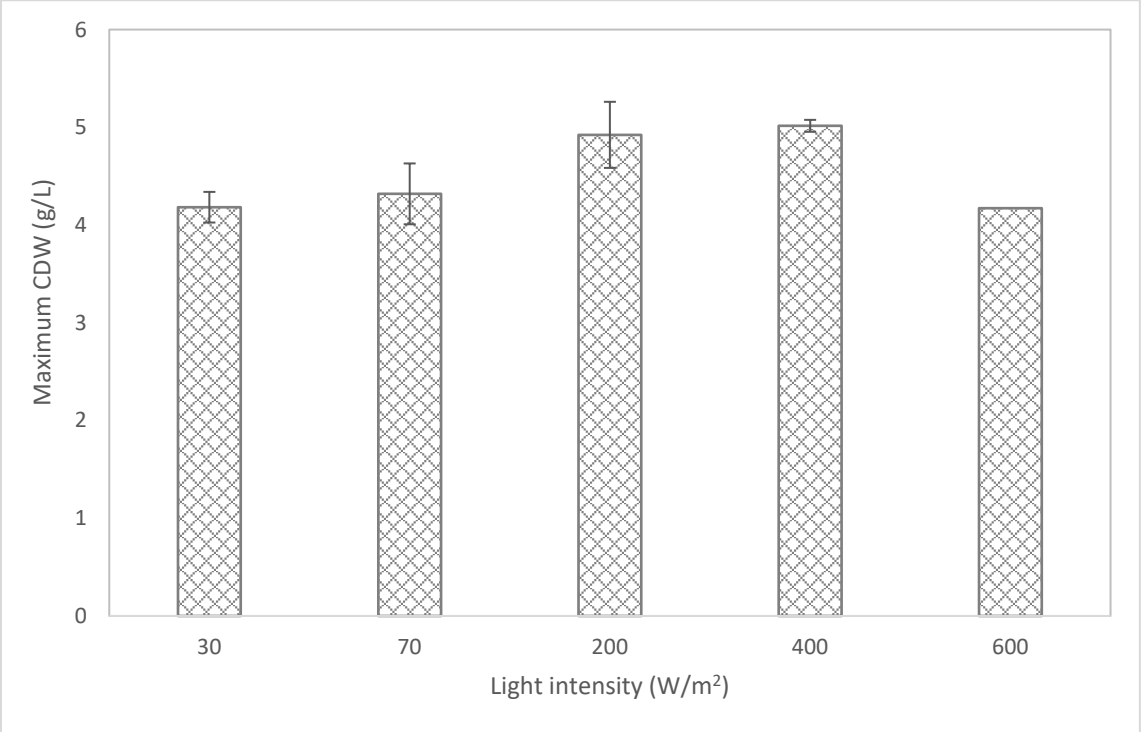

Figure 5.4: Maximum CDW of R. palustris achieved with illumination provided by incandescent light bulbs (60W or 100W bulbs depending on the light intensity required) for varying light intensities, i.e. 30, 70, 200, 400 and 600 W/m². R. palustris was cultivated using modified Van Niels medium and sparged with filter sterilised argon to promote anaerobic conditions. All experiments were completed at a constant temperature of 35°C and a volumetric flow rate of 0.651 L/min. Data points represent the mean of quadruple repeats and the error bars show the uncertainty associated with the CDW measurements.

The ability of *R. palustris* 11774 to have relatively similar growth curves and maximum CDW with only a ±15% difference between a large range of light intensities is extremely positive. This would mean that if *R. palustris* was cultured in outdoor PBR that the large variation in the intensity of direct sunlight may not have a significant effect on the growth of the bacterium. This is of course if it is below a possible light intensity that limits growth altogether. The reason that this is so attractive is the fact that solar light energy is the most abundant natural light source available on earth and is considered advantageous due to this abundance as well as the fact that it is a free light source and that it contains the full spectrum of light required for bacterial growth.

5.1.2 Maximum specific growth rates

As discussed previously, the maximum specific growth rate is when the rate of cell division is at a maximum and corresponds to the exponential growth phase on the growth curve. The maximum specific growth rate of each light intensity investigated was determined using the graphical method discussed in section 2.9.1.

Figure 5.5 shown below demonstrates how this graphical method was employed for determination of the maximum specific growth rates for each of the light intensities investigated. The natural logarithm of the CDW values in the exponential phase were plotted versus the corresponding times. Microsoft Excel's built-in linear regression function was used to plot a linear regression line through the necessary data points to obtain an equation where the gradient is the maximum specific growth rate.

Figure 5.5 contains five subplots that are labelled a, b, c, d and e. Each subplot represents the graphical method used for determining the maximum specific growth rate of each individual light intensity investigated. These plots have been separated for ease of viewing. As discussed in the preceding section, the exponential growth stages of all the light intensities fell within the 48 hour and 72-hour experimental time points, therefore the graphical method for determining the maximum specific growth rate was employed over this timespan for all growth curves. This can be seen in Figure 5.5a-e, with a linear regression line passing through the natural logarithm of biomass concentrations at the three experimental time points that correspond to the exponential phase. The maximum specific growth rate is then equal to the gradient of the linear regression line. The coefficient of determination (R^2) for each linear regression line is provided on each subplot in Figure 5.5. The R^2 values for each light intensity's regression line is greater than 0.95, which indicates good fit to the data set.

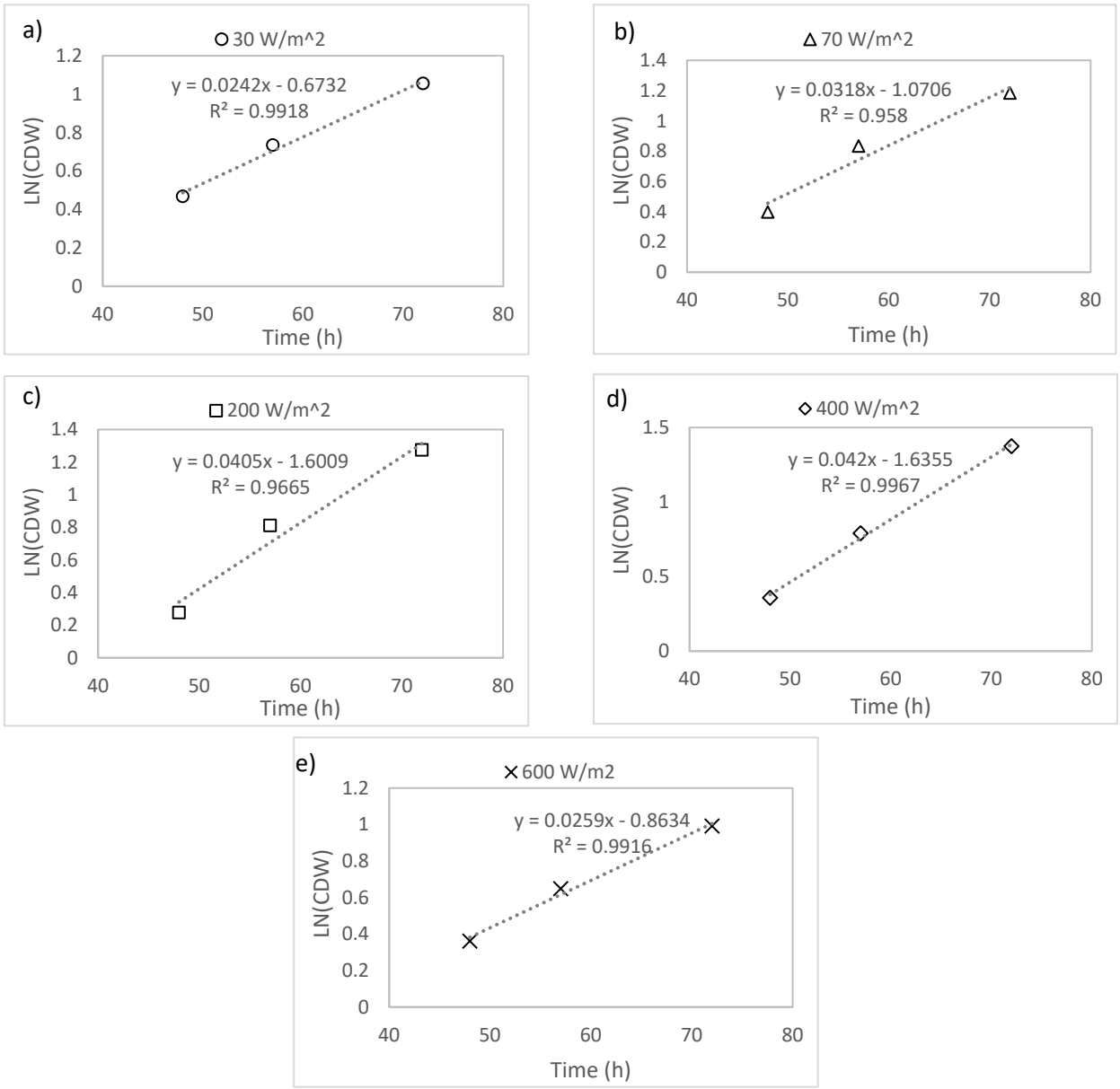

Figure 5.5: Natural logarithm of R. palustris CDW within the exponential phase with illumination provided by incandescent light bulbs (60 W or 100 W bulbs depending on the light intensity required) for varying light intensities, i.e. a) 30, b) 70, c) 200, d) 400 and e) 600 W/m^2. R. palustris was cultivated using modified Van Niels medium and sparged with filter sterilised argon to promote anaerobic conditions. All experiments were completed at a constant temperature of 35°C and a volumetric flow rate of 0.651 L/min. Data points represent the mean of quadruple repeats.

Figure 5.6 provides the maximum specific growth rates achieved during the culturing of *R. palustris* at the five light intensities investigated. The general trend in Figure 5.6 is that the maximum specific growth rate increases from the minimum light intensity investigated (30 W/m^2) through 70 W/m^2 and 200 W/m^2 before reaching a maximum at 400 W/m^2. After this, the maximum specific growth rate decreases when the incident light intensity increases to 600 W/m^2.

From Figure 5.6 onwards a steep increase can be seen in the specific growth rate (+23.99%), when the incident light intensity more than doubles in intensity from 30 to 70 W/m^2. The increase in maximum specific growth rate from 0.0242±0.0077 h^{-1} at 30 W/m^2 to 0.0318±0.0034 h^{-1} at 70 W/m^2 indicates that at these low light intensities *R. palustris* is photo-limited and therefore any increase in light intensity from 30 W/m^2 sees an increase in energy available for growth and division of the cell, leading to an increase in the specific growth rate.

An increase in incident light intensity from 70 W/m^2 to 200 W/m^2, which corresponds to a 185% increase in intensity, sees the maximum specific growth rate increase by 21.12% from 0.0318±0.0034 h^{-1} to 0.0405±0.0095 h^{-1}. This indicates that an increase in the light intensity is beginning to have a reduced effect on the specific growth rate however the effect is still significant.

The next increase in incident light intensity sees a doubling in the light intensity (100% increase) from 200 W/m^2 to 400 W/m^2. This change in light intensity causes a very slight increase in the maximum specific growth rate from 0.0405±0.009 h^{-1} to 0.0420±0.014 h^{-1}, which corresponds to a mere 6.36% increase. The sudden reduction in the effect of increasing light intensity on the maximum specific growth rate indicates that *R. palustris* 11774 becomes photo-saturated in this reactor system at these incident light intensities. Photo-saturation of *R. palustris* means that the bacterium is converting the maximum possible amount of light to energy for growth and enzymatic activity. These maximum specific growth rates are low in comparison to workhorse microorganisms such as *Escherichia coli* (*E. coli*) which are in the range of 0.4 to 0.9 h^{-1} (Godwin and Slater, 1979). However, they do compare well to the growth rates achieved by another strain of *R. palustris* (420 L) of approximately 0.026 h^{-1} (Carlozzi, 2009).

The final increase in incident light intensity is from 400 W/m^2 to the maximum light intensity investigated, namely 600 W/m^2. This is only a 50% increase in light intensity and was the maximum possible with this experimental setup. This change in light intensity causes a sudden decrease in the maximum specific growth rate from 0.0420±0.014 h^{-1} to 0.0226± 0,0051 h^{-1} which corresponds to a 37.88% decrease. The significant reduction in the maximum specific growth rate indicates that *R. palustris* 11774 becomes photoinhibited in this reactor system at this incident light intensity. Photoinhibition is likely brought upon by visible light, which can cause the inhibition of the electron transport and/or possible damage to protein subunits (Tandori et al., 2001).

The response of the growth metabolism of *R. palsutris* to changing incident light intensity is similar to the response of the hydrogen production metabolism. As discussed in section 2.8.2.2, Xiao (2017) reported that the hydrogen production rate increased as light intensity increased from 26 W/m^2 to 65 W/m^2, after which the hydrogen production rate saturated with increasing light intensity up to 285 W/m^2. Thus, the results with regards to the effect of changing incident light intensity on the maximum specific growth

rate align well with the reported response of hydrogen production rate. Saturation of the hydrogen metabolism was reported to be from 65 W/m^2, which is lower than the light intensity at which photo-saturation of the growth metabolism (200 W/m^2) occurred in this study. This is possibly due to the difference in bioreactor geometry between the two studies. In the previous study a bioreactor with significantly larger diameter (70 mm) was used compared to this study (15 mm), thus mutual shading would likely cause saturation to occur at lower light intensities, as the average light intensity in the larger diameter reactor would be considerably lower. Photoinhibition has been reported by Carlozzi (2009) to be at 500 W/m^2 with regards to the hydrogen production rate. This once again aligns well with the findings in this investigation that saw the maximum specific growth rate as well as the maximum CDW drastically decrease two between 400 W/m^2 and 600 W/m^2.

The impact of these results on the eventual culturing of *R. palustris* in outdoor PBR with sunlight as the light source is discussed in more detail later in this section with reference to specific light intensities experienced in Stellenbosch, South Africa.

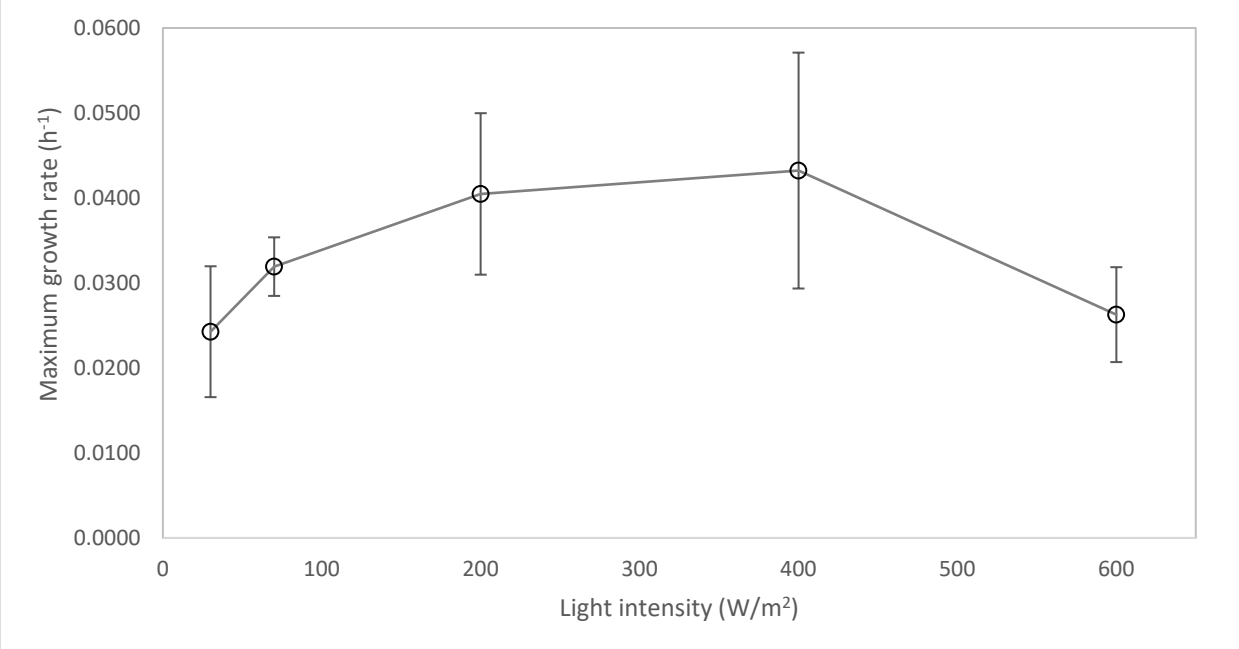

Figure 5.6: Maximum specific growth rate of R. palustris achieved with illumination provided by incandescent light bulbs (60 W or 100 W bulbs depending on the light intensity required) for varying light intensities, i.e. 30, 70, 200, 400 and 600 W/m^2. R. palustris was cultivated using modified Van Niels medium and sparged with filter sterilised argon to promote anaerobic conditions. All experiments were completed at a constant temperature of 35°C and a volumetric flow rate of 0.651 L/min. Data points represent the mean of quadruple repeats and the error bars show the propagated uncertainty originally associated with the CDW measurements.

A single-factor ANOVA (with $\alpha = 0.05$) was used to determine if there was a statistically significant difference between the maximum specific growth rates at each light intensity. A summary of results

obtained from the single-factor ANOVA are provided in Table 5.1. The p-value of 0.00109 is less than the stated significance of 0.05 which indicates strong evidence against the null hypothesis that the maximum specific growth rates are equal over the light intensity range investigated. The F-value (8.461) is also larger than the F-crit (3.112). Thus, the null hypothesis can be rejected and the alternative hypothesis that states that not all growth rates are the same can be accepted.

Table 5.1: Summary of Single Factor ANOVA on maximum specific growth rate at various light intensities

ANOVA

Source of Variation	*SS*	*df*	*MS*	*F*	*P-value*	*F crit*
Between Groups	0,00105	4	0,000262	8,461	0,00109	3,112
Within Groups	0,000433	14	3,09E-05			
Total	0,00148	18				

The results of the maximum specific growth rates provided in Figure 5.6, suggested that saturation occurred at a light intensity of between 200 and 400 W/m2, based on the marginal difference in their maximum specific growth rates. To determine if these values were significantly different or in fact statistically equal an ad hoc analysis was employed. The T-test as an ad hoc analysis indicated that there was no significant difference (with $\alpha = 0.05$) in the maximum specific growth rates at light intensities of 200 and 400 W/m^2, as the P(T<=) two-tail value (0.621) provided in Table 5.2 is larger than the selected significance. Therefore, it can be stated that there is a 95% chance that these maximum specific growth rates are equal.

Table 5.2: Summary of the ad hoc t-test on maximum specific growth rate at 200 and 400 W/m²

	200 W/m²	*400 W/m²*
Mean	0,040475	0,043225
Variance	3,56E-05	7,6E-05
Observations	4	4
Pooled Variance	5,58E-05	
Hypothesized Mean Difference	0	
df	6	
t Stat	-0,5204	
P(T<=t) one-tail	0,31071	
t Critical one-tail	1,94318	
P(T<=t) two-tail	0,62142	
t Critical two-tail	2,446912	

Figure 5.7 below provides data obtained from a pyranometer that measures the intensity of direct sunlight over a full 24-hour period. The meter was placed on the roof of a four-story building located in Stellenbosch, South Africa, in order to obtain intensities over the entire period with no possible interruptions from shading. Figure 5.7a provides the direct sunlight intensities in the wavelength range of 500 to 1000 nm over a 7-day period in the month of May (falling in autumn). In this seasonal period the average maximum light intensity is approximately 550 W/m^2. In this seasonal period good growth of *R. palustris* is likely to occur as the culture will only experience light intensities that may cause photoinhibition for a brief period with all other sun exposure times being within the range of 30 to 500 W/m^2.

Figure 5.7b provides the direct sunlight intensities in the wavelength range of 500 to 1000 nm over a 26-day period in the month of July (falling in winter). In this seasonal period the average maximum light intensity is approximately 86 W/m^2. This indicates that in this seasonal period, usually associated with overcast weather with limited direct sunlight, relatively good growth of *R. palustris* would still be possible, although there would be photo-limitation such as that seen in the range of 30 to 70 W/m^2 in the above experiments. This is extremely positive, as it would mean that outdoor culturing would most probably not be significantly limited by outdoor light intensity and culturing could possibly be done all year round. This still needs to and should be verified in outdoor experiments where sunlight is the sole light source.

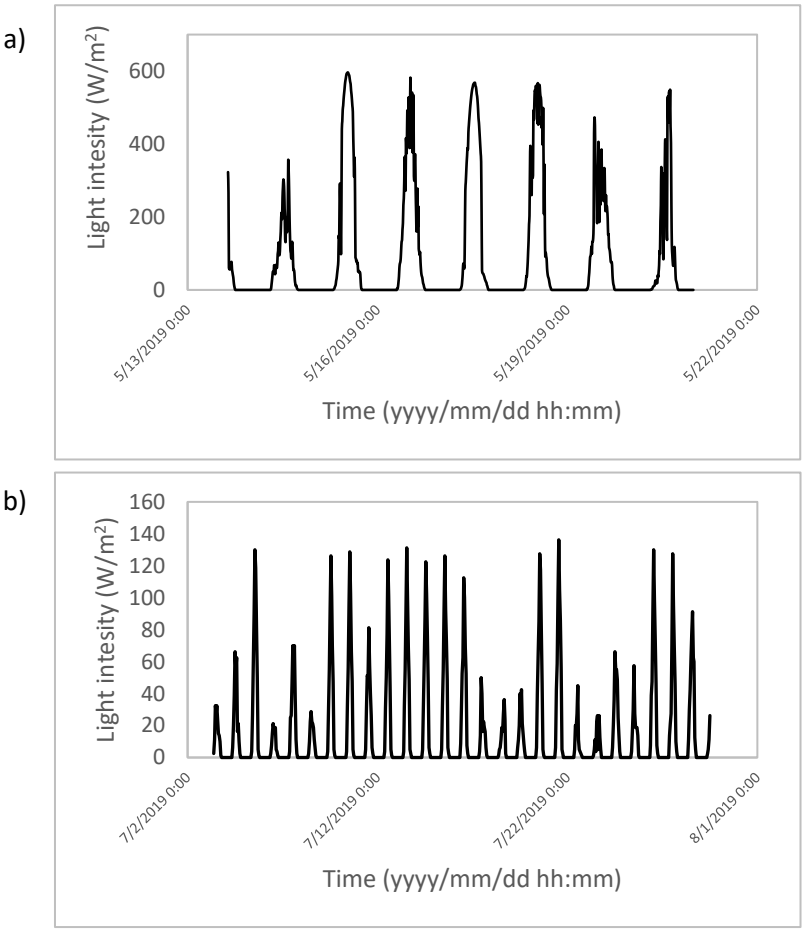

Figure 5.7: Light spectrum of the sun for full days (measurement every 10 minutes): a) light intensity over time during the month of May (autumn) and b) light intensity over time during the month of July (winter). A pyranometer (Campbell Scientific CR300 Series Compact Datalogger) was placed on the roof of a four-story building at the Department of Process Engineering in Stellenbosch.

Continuing from the above discussion a more detailed look into the profile of incident sunlight intensity over a single day was examined. Figure 5.8 provides the change in light intensity over a 24-hour time period for a day in May (•) and in July (▲). Superimposing these two graphs illustrates the drastic difference in the amplitude of the light intensity over the course of a day with direct sunlight throughout, compared to a day with overcast conditions. The decrease in the duration of daylight between a day in May and July is also noticeable with a 3-hour reduction. This results in a reduction in the amount of photo-fermentation that is possible within a single day. With regards to the light intensity profile from the month of May, approximately four hours in the day sees incident sunlight above 500 W/m^2. Thus, outdoor PBRs would experience photoinhibition during this period. This is however dependent on reactor size and whether the sinusoidal trend of sunlight intensity will have the same effect as continuous high light intensity exposure. The sinusoidal trend can be seen in Figure 5.8 where light intensity increases from when the sun rises, until the maximum peak is reached during mid-day and then decreases gradually

until zero when the sun sets. Before outdoor culturing the effect of sunlight intensity exposure over a full day on biomass growth should be investigated in a controlled lab setup.

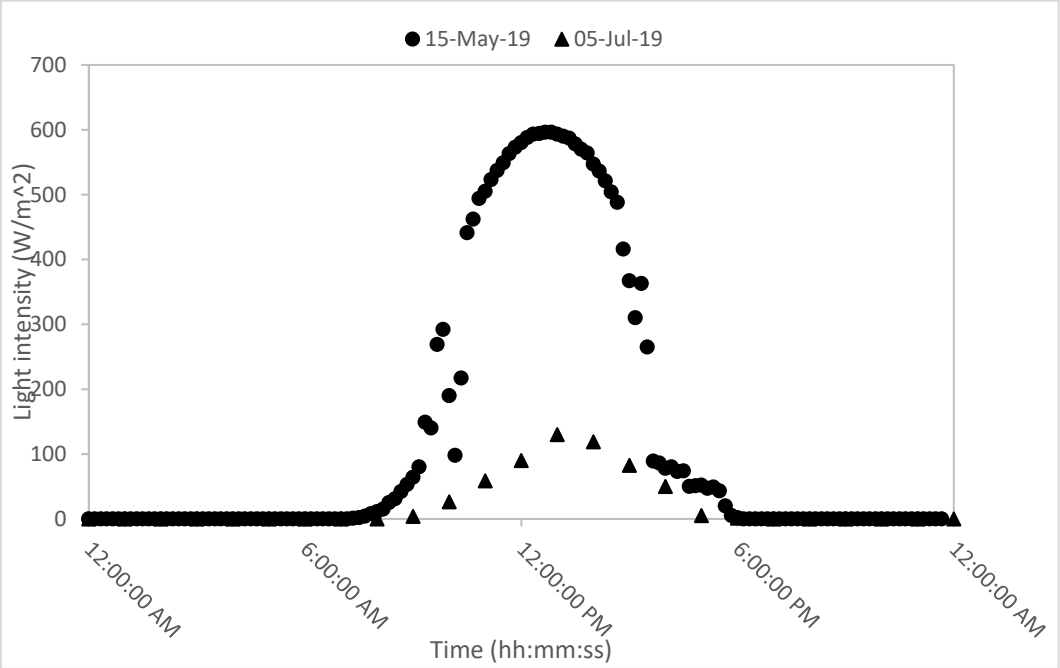

Figure 5.8: Light spectrum of the sun for full days (measurement every 10 minutes): a) light intensity over time during the month of May (autumn) and b) light intensity over time during the month of July (winter). A pyranometer (Campbell Scientific CR300 Series Compact Datalogger) was placed on the roof of a four-story building at the Department of Process engineering in Stellenbosch.

5.1.3 Substrate utilisation

R. palustris 11774 glycerol utilisation in the modified Van Niels medium at varying light intensities using the tubular PBR system depicted in 4.4.1.3 can be seen in Figure 5.9 below. The starting glycerol concentration was set at 40mM as stated in Table 4.2. It can be seen in Figure 5.9 that concentrations at the start of the experimental run (t=0) are consistent and located around a glycerol concentration of 40 mM. Slight variation and error are due to slight difference in inoculum volume as well as error associated with HPLC analysis. The form of each light intensity change in glycerol concentration over time are congruent with one another.

With reference to the growth of *R. palustris* shown in the growth curves above, the change in glycerol concentration follows an inverse path. Minimal utilisation of glycerol in the beginning stages of culturing (0 to 48 hours) corresponds to a reduced lag phase and the acceleration growth phase. Glycerol utilisation then reaches a maximum rate after the first 48 hours, which is in line with the initiation of the exponential growth phase. The rate of utilisation then slows down, before all the glycerol is consumed and reaches a

concentration of 0 mM. This correlates with the deceleration phase and the entering of the stationary and/or death stage seen in the growth curves.

The change in the rate of substrate utilisation with changing light intensity corresponds with the effect of changing light intensity on both the maximum CDW achieved and the maximum specific growth rate. There is an unexpected variation in the change in glycerol concentration over time between the 200 W/m^2 and 400 W/m^2 experimental run as these two light intensities were almost identical in terms of their growth curve. The variation is minor and with error bar cross-over it is likely just due to variation in analysis of the glycerol concentration.

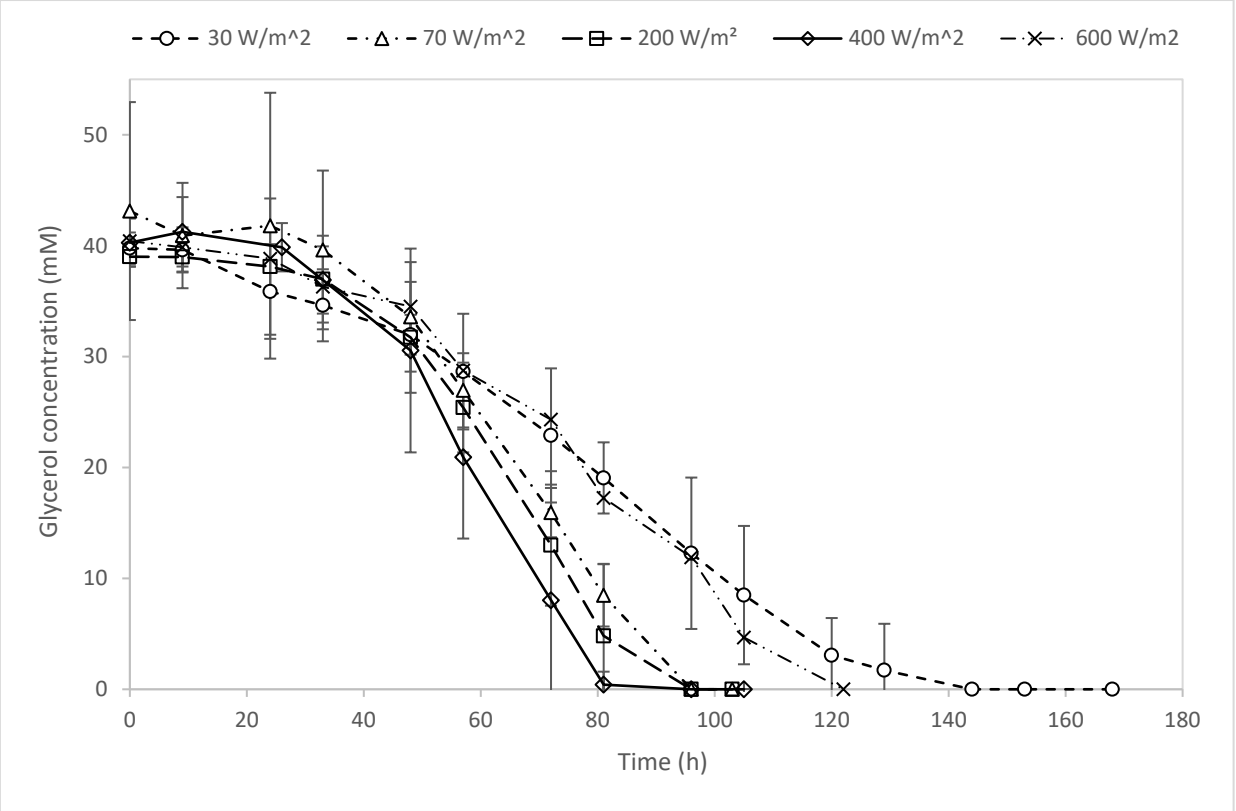

Figure 5.9: Glycerol utilization of R. palustris with illumination provided by incandescent light bulbs (60W or 100W bulbs depending on the light intensity required) for varying light intensities, i.e. 30, 70, 200, 400 and 600 W/m^2. R. palustris was cultivated using modified Van Niels medium with glycerol as the carbon source (40mM) and sparged with filter sterilised argon to promote anaerobic conditions. The glycerol concentration of the varying light intensities over times is provided in this figure. All experiments were completed at a constant temperature of 35°C and a volumetric flow rate of 0.651 L/min. Data points represent the mean of quadruple repeats. The error bars show the uncertainty associated with the glycerol concentration measurements that were obtained from HPLC analysis using the methods described in section 4.5.3.

In order to validate that it is glycerol limitation which brings about the transition from deceleration phase into stationary phase, the glycerol concentrations were monitored and compared to the growth cycle of the culture grown at an incident light intensity of 200 W/m^2. Figure 5.10 below illustrates this, showing

how the biomass concentration reaches the stationary phase after 96 hours, with no increase in biomass. This corresponds to the depletion of glycerol, which reached a concentration of zero after 96 hours. This illustrates that glycerol is the limiting nutrient during the culturing of *R. palustris* in this system. This was also the case for all other light intensities investigated and the comparison for the remaining light intensities is provided Figure C.1 to C.4 in Appendix C.

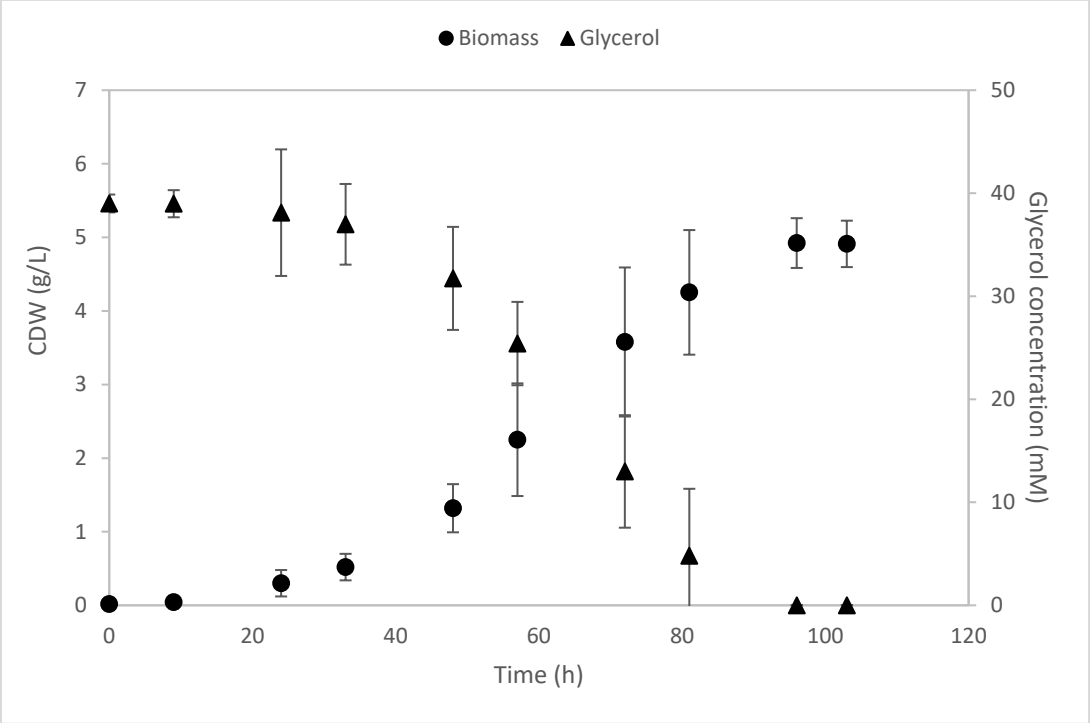

Figure 5.10: The growth curve (●) and glycerol utilization (Δ) of R. palustris 11774 with illumination provided by incandescent light bulbs (100W bulbs) at a light intensity of 200 W/m2 is provided in this figure. R. palustris 11774 was cultivated using modified Van Niels medium and sparged with filter sterilised argon to promote anaerobic conditions. All experiments were completed at a constant temperature of 35°C and a volumetric flow rate of 0.651 L/min. Data points represent the mean of quadruple repeats. The error bars show the uncertainty associated with the CDW and glycerol measurements. Biomass concentration corresponds to the left-hand ordinate and the glycerol concentration to the right-hand ordinate.

5.1.4 Pigment extractions

Pigments were extracted using the methods described in section 4.5.5. The extraction of pigments aimed at determining the effect of changing incident light intensity on Bchl-α to carotenoid ratio. As discussed previously, carotenoids main function is protection, whereas the Bchl-α absorbs light that is converted to energy for growth. It was hypothesised that an increase in incident light intensity would likely result in the ratio of Bchl-α to carotenoid pigments to decrease due to an increase in carotenoid production for protection against high light intensities.

The absorption spectra (400–900 nm) of extracted pigments for *R. palustris* 11774 cultivated under anaerobic conditions at an incident light intensity of 200 W/m^2 is depicted in Figure 5.11 provided below. This figure is from a single run at 200 W/m^2 and is provided here to aid the discussion of the peaks at which Bchl-α and carotenoid pigments are found when this extraction method was employed. This curve was developed for each run of every light intensity investigated. Over the spectral range of 400 to 900 nm three peaks can be seen in Figure 5.11: the first (••) at a wavelength of 480nm with the second and third (•) at wavelengths of 600 and 772 nm respectively. The first peak corresponds to the carotenoid pigments whereas the second and third peaks correspond to the Bchl-α pigments. The form of Figure *5*.11 is perfectly congruent with results obtained in literature (Muzziotti et al., 2017) where this extraction methodology was implemented.

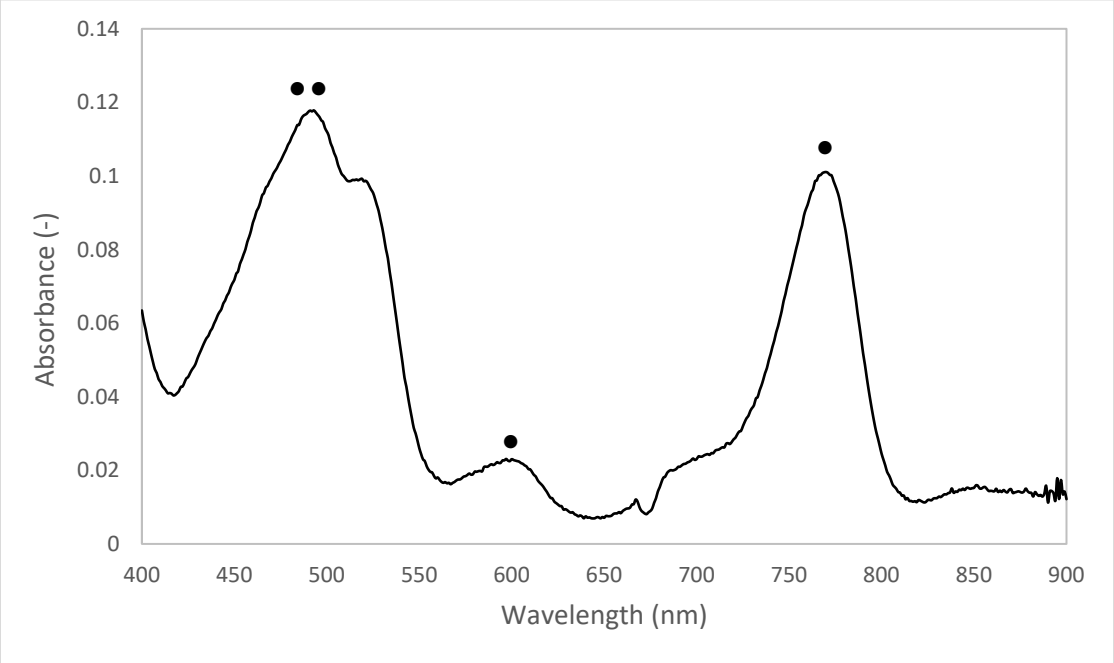

Figure 5.11: Absorption spectra of pigments in R. palustris 11774 cultivated under anaerobic conditions with illumination provided by incandescent light bulbs (100W bulbs) at an incident light intensity of 200 W/m^2. The experiment was run at a constant temperature of 35°C and a volumetric flow rate of 0.651 L/min with the sample taken in the exponential growth phase. (••) refer to carotenoids; (•) refers to BChl-α peaks.

Figure 5.12 below provides the ratio between the BChl-α and carotenoid pigments at each incident light intensity investigated. There is no clear trend with regards to how this ratio is affected by increase in light intensity. A decrease in BChl-α to carotenoid ratio was expected as the light intensity increased based on a predicted increase in the carotenoid production as a protection method against high light intensities. However, this was not the case as the ratio oscillated between of 3 and 4 as the selected incident light intensities increased. Based on this a single-factor ANOVA (with α = 0.05) followed by the Bonferroni confidence interval test as a post-hoc analysis was used to determine if there was significant difference

between the means of the ratios over all light intensities. A summary of results obtained from the single-factor ANOVA is provided in Table 5.3. Although the F-value is larger than F-crit and the p-value is less than 0.05, both values are so close to their respective cut-offs that it is considered to be marginal. Thus, the post-hoc analysis known as the Bonferroni test was employed to compare each ratio to see if the difference is statistically significant. This is discussed in more detail below with reference to Figure 5.13.

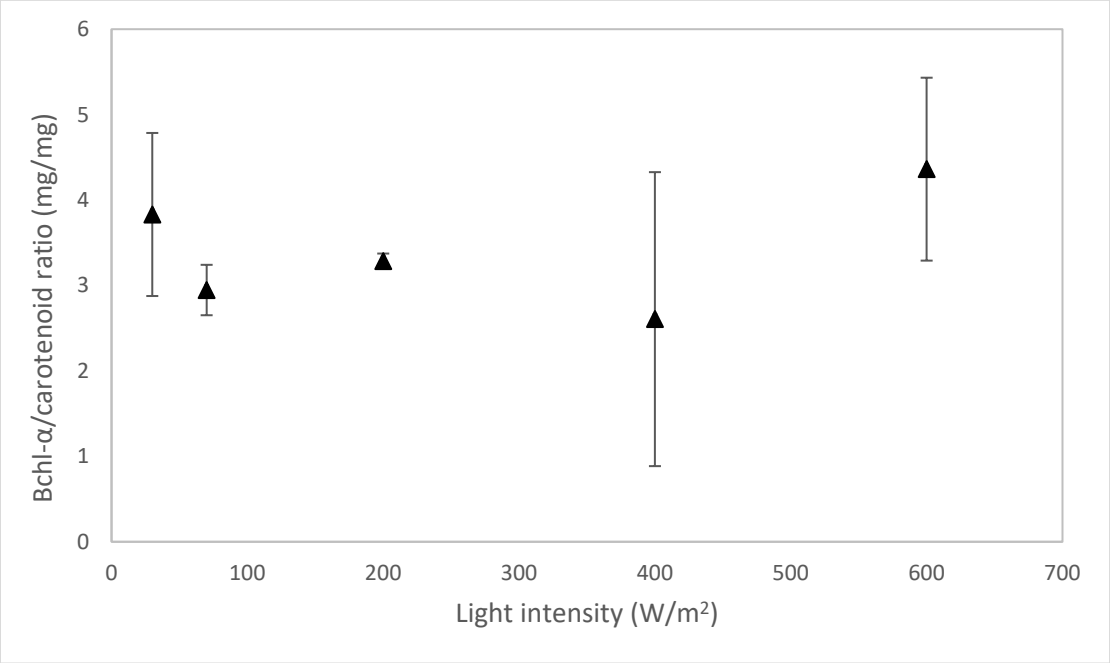

Figure 5.12: Bchl-α/carotenoid ratio of pigments of R. palustris 11774 during the exponential growth phase of bacterial culturing with illumination provided by incandescent light bulbs (60W or 100W bulbs depending on the light intensity required) for varying light intensities, i.e. 30, 70, 200, 400 and 600 W/m². R. palustris 11774 was cultivated using modified Van Niels medium and sparged with filter sterilised argon to promote anaerobic conditions. All experiments were completed at a constant temperature of 35°C and a volumetric flow rate of 0.651 L/min. Data points represent the mean of either triplicate or quadruple repeats and the error bars show the uncertainty between the calculated ratios from each experimental run.

Table 5.3: Summary of Single Factor ANOVA on Bchl-α/carotenoid ratio at various light intensities

ANOVA

Source of Variation	*SS*	*df*	*MS*	*F*	*P-value*	*F crit*
Between Groups	6,63308013	4	1,65827003	3,48194367	0,04527033	3,35669002
Within Groups	5,23873219	11	0,47624838			
Total	11,8718123	15				

Figure 5.13 provided below allows for simple visualisation of the numerical confidence intervals that were obtained through performing the Bonferroni test as the post-hoc analysis. In this figure the mean difference of each light intensity comparison is provided with the error bars corresponding to a positive and negative 95% confidence interval. If a confidence interval does not contain zero, the corresponding means are significantly different. Figure 5.13 illustrates that with a significance of α=0.05, seven out of the possible ten comparisons contain a zero in the confidence interval which means that there is no significant difference between there mean values. The three light intensity comparisons that, according to this post-hoc test is significantly different are 30 vs 400 W/m^2, 70 vs 600 W/m^2 and 400 vs 600 W/m^2. These statistically significant differences are marginal and do not point to any clear and obvious trends as the mean difference can be seen to be positive in one case and negative in the other two cases when comparing a low light intensity to a higher light intensity.

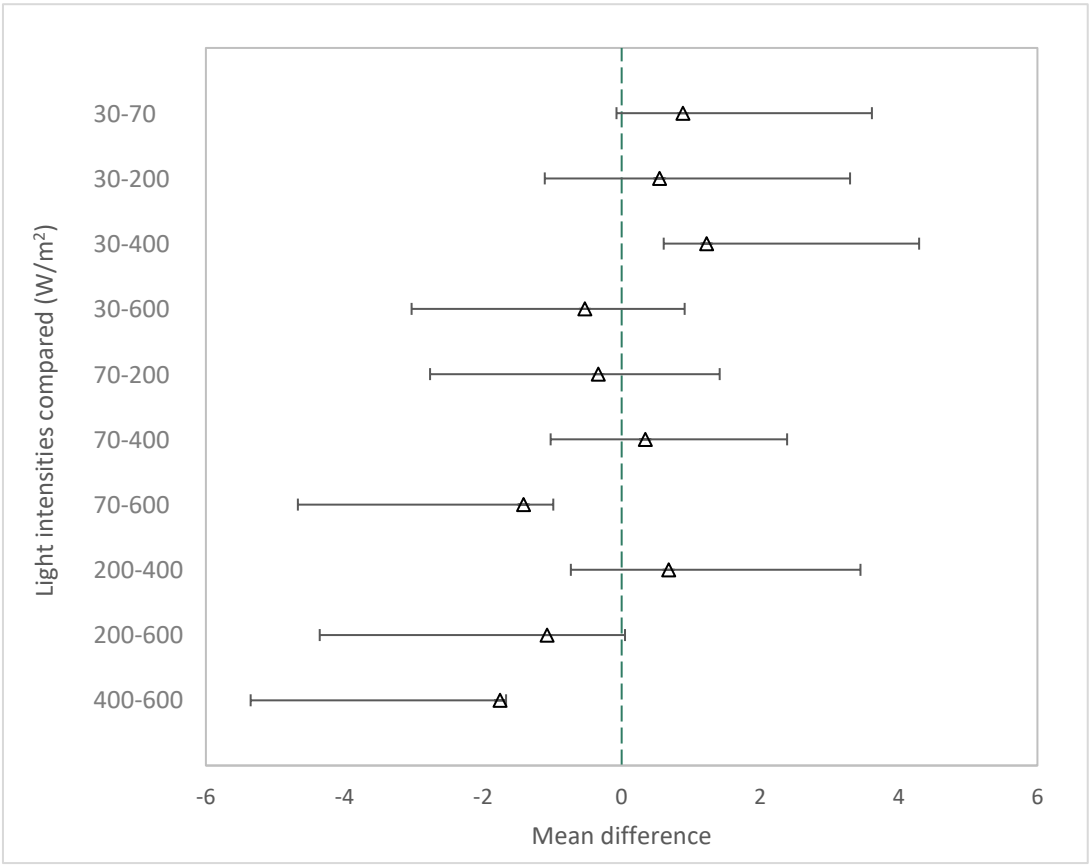

Figure 5.13: Bonferroni test for statistical comparison of each light intensity investigated.

The possible reason for the lack of change in the BChl-α to carotenoid ratio is due to the profile of the light spectrum of an incandescent light bulb. Figure 5.14 provides the emission spectrum of incandescent light bulbs at the incident light intensities investigated. The integral over the wavelength range (500-1000nm) is equal to the average incident light intensity (W/m^2). The wavelength of the carotenoid and BChl-α pigment in *R. palustris* has been marked by a vertical dotted line at 550nm and 875nm. The

profile of the emission spectrum is such that at the lower wavelengths where the carotenoid pigments absorb light the light, intensity is at its lowest. The opposite is true at a wavelength of 875nm where the BChl-α pigments absorb light. Here the light intensity is slightly less than the maximum intensity over the entire wavelength range. The low intensities at the carotenoid wavelength in comparison to the BChl-α wavelength possibly lead to little change in the ratio as the light intensity increases.

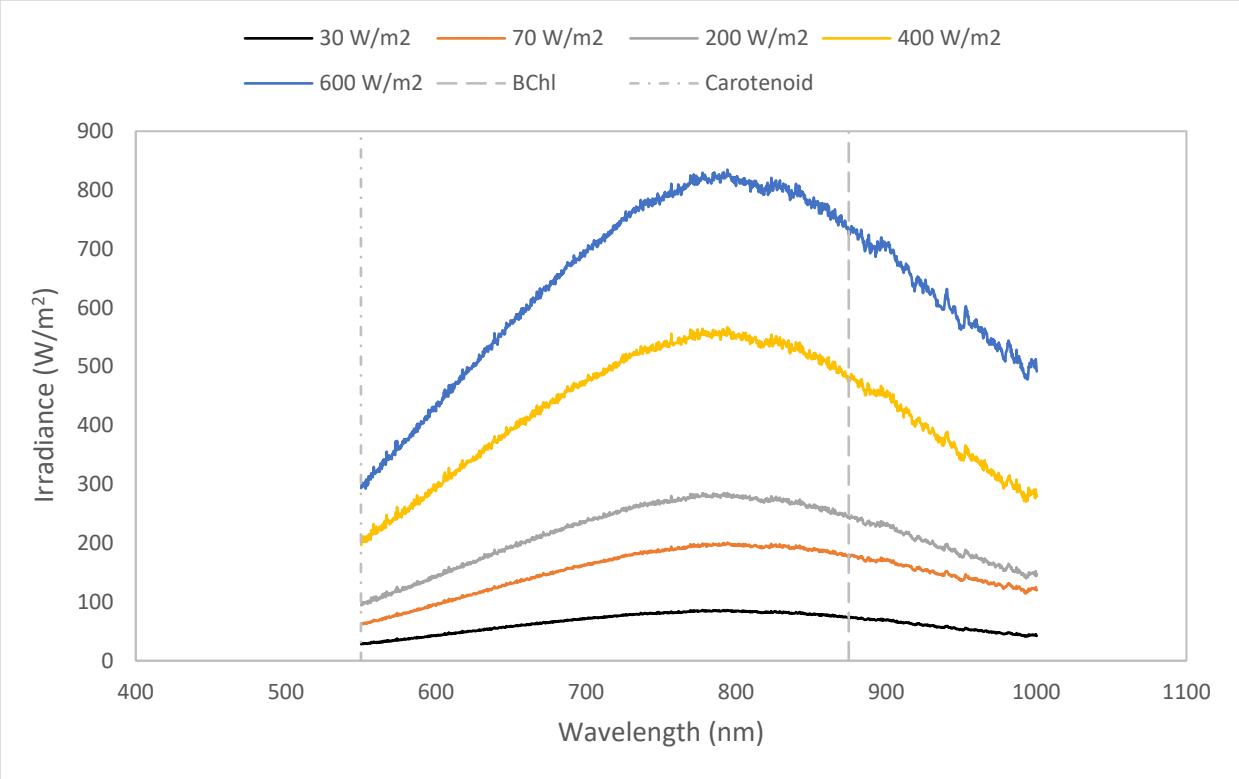

Figure 5.14: The emission spectra of incandescent light bulb (60W or 100W bulbs depending on the light intensity) for the various light intensities investigated, i.e. 30, 70, 100, 200, 400 and 600 W/m^2. The emission spectra were measured at different light intensities by an imaging spectrograph (RGB photonics Q-mini) as a function of wavelength.

The effect of changing incident light intensity on the BChl-α to carotenoid ratio may differ based on the light source used for culturing *R. palustris*. As stated previously, outdoor culturing with sunlight as the light source has been identified as the ideal culturing conditions to reduce the energy input into the PBR system. Therefore, the light spectrum of the incandescent light bulbs was compared to that of the sun at the same incident light intensity, 600 W/m^2, over a wavelength range of 550-1000 nm. This comparison is provided in Figure 5.15 below. Over this wavelength range the sunlight spectrum oscillates around 600 W/m^2, which means that the light intensity at the wavelengths corresponding to the BChl-α and carotenoid pigments are approximately equal. This will lead to differences in BChl-α to carotenoid ratios when *R. palsutris* is cultured in outdoor PBRs with sun as the light source, compared to incandescent light bulbs as the light source. A possible way of countering the difference in spectral light emission of

incandescent bulbs to the sun, is the inclusion of a blue/green LED strip that will boost the light intensity at the wavelength range corresponding to the carotenoid pigments to match that of sunlight. This would provide a more accurate response to what would occur in cultures grown in outdoor conditions.

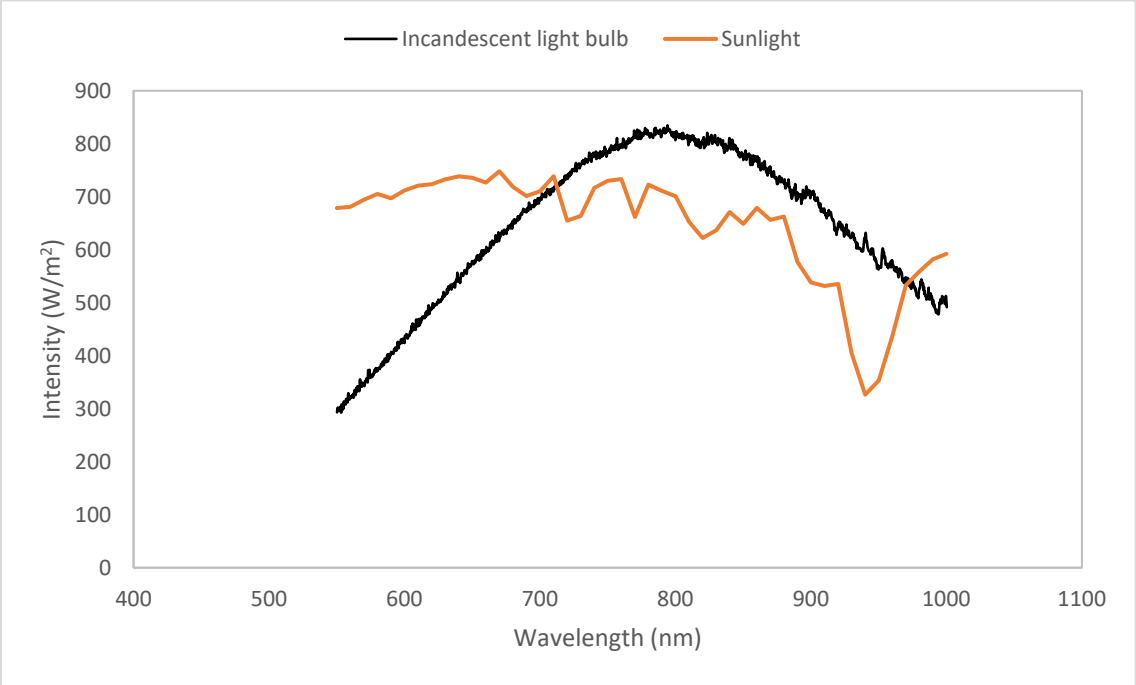

Figure 5.15: The emission spectra of incandescent light bulb (100 W bulb) and sunlight over a wavelength range of 500 to 1000 nm with both corresponding to an incident light intensity of 600 W/m². The emission spectra were measured using an imaging spectrograph as a function of wavelength.

5.1.5 Modelling the effect of light intensity

It has been explained in section 2.4 that when the biomass concentration is low, the microbial cell scattering is often assumed to be negligible allowing for the use of the Beer-Lambert law (Equation 20) for modelling of the light attenuation through the reactor. From the growth curves in Figure 5.3 it can be seen at each light intensity that the biomass concentration is high (in the order of 4 g/L), which means that the two-flux approximation (Equations 22 to 24) should be used for the modelling of light attenuation, as it takes into account the scattering of light by the microbial cells and the absorption of light by the cells. The two-flux approximation is provided once more below to aid the discussion:

$$\frac{I_z}{I_0} = \frac{4\alpha_1}{(1+\alpha_1)^2 \cdot e^{\alpha_2} - (1-\alpha_1)^2 \cdot e^{-\alpha_2}}$$

$$\alpha_1 = \sqrt{\frac{E_a}{E_a + E_s}}$$

$$\alpha_2 = (E_a + E_s) \cdot \alpha_1 \cdot X \cdot z$$

The two unknowns in the two-flux approximation equations is the mass absorption coefficient (E_a) and the scattering coefficient (E_s). Values of the mass absorption coefficient ($E_a = 20.2\, m^2/g$) and the scattering coefficient ($E_s = 0.341\, m^{-1}$) were estimated using the transmittance measurements provided in Figure 5.2. The built-in MATLAB function *lsqnonlin* can be used to solve nonlinear least-squares problems. This function could therefore be used to estimate the unknown parameters through the nonlinear data-fitting. Figure 5.16 below shows the two-flux approximation model with the estimated parameters fitted to the experimental data. This model shows a very good fit to the experimental data. It should be noted that the estimated parameters for the two-flux model were fitted at a wavelength of 875 nm, which corresponds to the BChl-α pigments where maximum absorption by the microbial cell occurs.

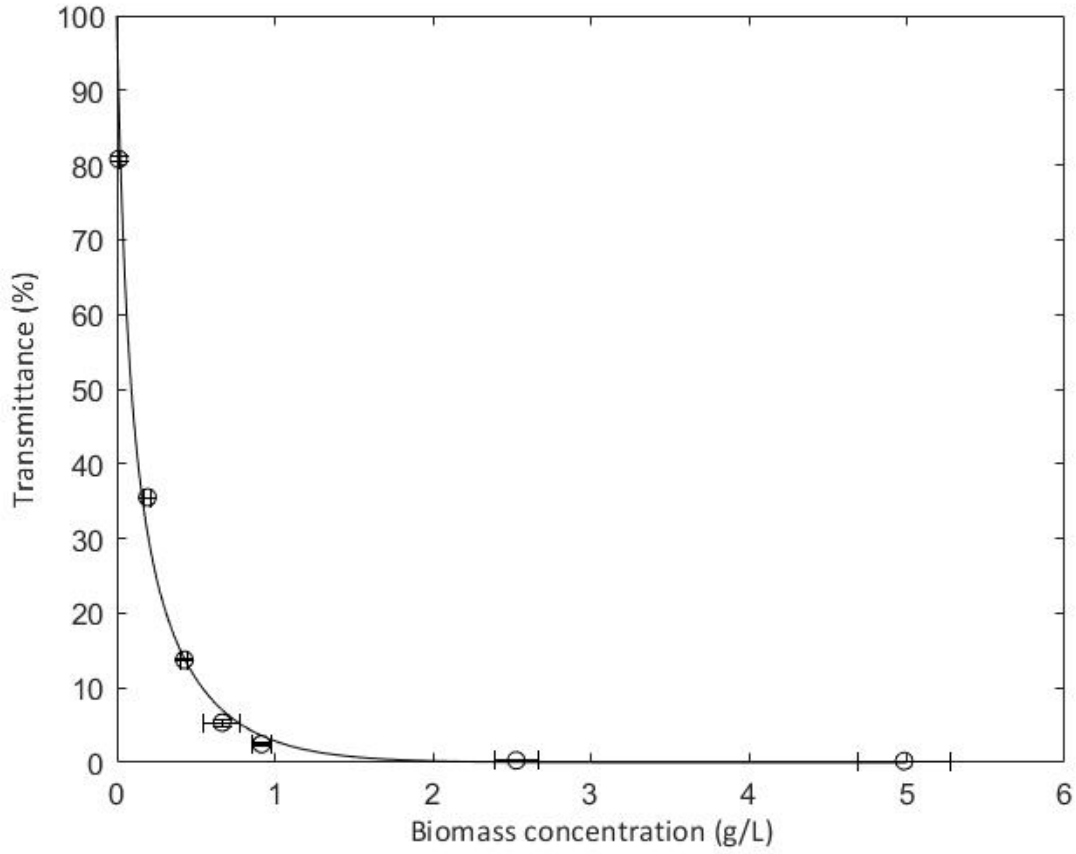

Figure 5.16: Transmittance (spectrophotometer – 875nm) of light through R. palustris cultures of varying cell concentrations with Van Niels medium as the blank. The culture used for these measurements was grown in a 500mL Schott bottle with bioreactor fittings in modified Van Niels medium at a temperature of 35°C and light intensity of 200 W/m^2 with illumination provided by incandescent light bulbs (100W bulbs). Data points represent the mean of triplicate experimental runs (o) and the trendline represents the two-flux model fitted to the data using lsqnonlin. The error bars show the uncertainty associated with the CDW measurements and the transmittance measurements.

A large portion of work in the modelling of light attenuation in PBRs has been done in reactors with rectangular geometries as this is a common reactor configuration for algae studies (Huang et al., 2015;

Obeid et al., 2009; Pruvost et al., 2016; Zhang et al., 2015a). Due to the vast work on light attenuation with this geometry some studies have made major assumptions to assess cylindrical reactors as if they had a rectangular geometry (Palamae et al., 2018). This is normally done by calculating the light capture surface area of the cylindrical geometry using the reactors diameter. The reactor is then assumed to have a square cross-sectional area that corresponds to a square face area that is the same as the area of the curved surface (Palamae et al., 2018). Such assumptions can lead to inaccurate estimations of the light attenuation profiles through the reactor and therefore lead to inaccurate predictions of the average light intensity experienced over the cross-sectional area of the reactor. Therefore, it was decided that this assumption should not be used further in the modelling of the effect of light intensity and to rather take on the difficulty of modelling light attenuation through the true geometry of the reactor used.

Figure 5.17 below, illustrates the light attenuation through the cross-section of the tubular PBR when the incident light intensity is set at 30 W/m^2 and has a biomass concentration of 4 g/L. Light is only provided from one side of the reactor and it was assumed that this side's entire surface area obtains the same light intensity which is equal to the incident light intensity. The decrease in light intensity as it moves through the reactor in the x-direction (left to right) is illustrated by the colour gradient change. To determine the light intensity profile as shown in Figure 5.17, it is necessary to know the exact distance any point in the cross-sectional area of the tubular PBR is from the incident light surface on the shared x-plane. The two-flux approximation can then be used to determine what the light intensity is at this point in the reactor, as the incident light intensity and biomass concentration are both known. A mesh grid of polar coordinates (radial and angular) was developed to create multiple nodal points over the reactor cross-sectional area. These polar coordinates were then converted to cartesian coordinates for easier calculation of the distance of each node to the surface of the incident light. This distance was calculated using Equation 41 provided below.

$$d = x + \sqrt{R^2 - y^2} \qquad [41]$$

$Where,$

$d = distance$

$x = to\ the\ x\ coordinate\ of\ the\ node$

$R = radius\ of\ the\ reactor$

$y = to\ the\ y\ coordinate\ of\ the\ node$

With the distance of each node known, the light intensity profile through the reactor can be calculated when the biomass concentration within the reactor is known. As stated previously the light intensity profile in Figure 5.17 is for an incident light intensity of 30 W/m^2 and a biomass concentration of 4 g/L,

which means that the 'dark side' of the reactor receives approximately half the intensity of the incident light intensity when the culture is in the later stage of growth.

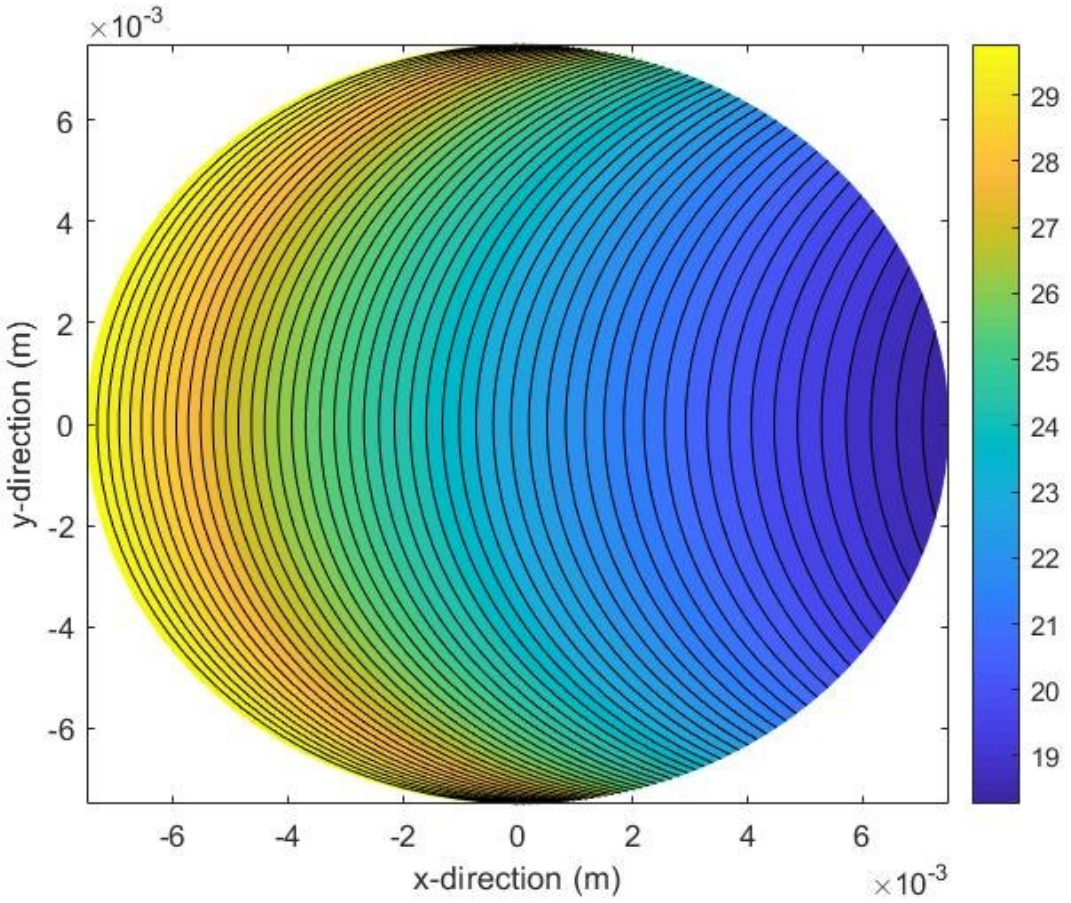

Figure 5.17: Light intensity profile through the tubular PBR with an incident light intensity of 30 W/m^2 and a biomass concentration of 4 g/L.

With the working model for light attenuation only the biomass concentration was required to determine the light intensity profile through the tubular PBR, that could then be integrated in the x and y direction to determine the average light intensity over the reactor's cross-sectional area. This integration was done using MATLAB's built in function *integral2* that can perform the double integration that is required. In order to determine the change in the average light intensity in the tubular PBR over the entire culturing period the biomass concentration was required. Therefore, a model for the prediction of the biomass growth, that is light intensity dependent, was established using the experimental data relating to the investigation into the effect of light intensity on biomass growth and substrate utilisation. This is discussed in more detail below.

5.1.5.1 Growth and substrate utilisation

As *R. palustris* is a photosynthetic bacterium the growth rate is likely to depend on the local light intensity (I). Based upon the results reported in the previous sections, this holds true as it was reported that there is a difference in the growth rates as the light intensity changes. Therefore, the Aiba model (Equation 42) could be employed to account for the effect of the light intensity on the biomass growth rate (dX/dt) (Aiba, 1982). The Aiba model consists of two unknown coefficients, i.e. K_I, the light saturation coefficient and K_i, the photoinhibition coefficient. As the carbon source (glycerol) was fully exhausted during most experimental runs the growth rate (dX/dt) of *R. palustris* is also assumed to depend on the glycerol concentration. This means the full growth rate model is dependent on the average light intensity, glycerol concentration and biomass concentration, as can be seen in Equation 43.

$$k(I) = \left(\frac{I}{K_I+I}\right)\left(\frac{K_i}{K_i+I}\right) \quad [42]$$

$$\frac{dX}{dt} = \mu_{max}\left(\frac{s}{K_s+s}\right)\left(\frac{I}{K_I+I}\right)\left(\frac{K_i}{K_i+I}\right)X - \mu_d X \quad [43]$$

In Equation 43, μ_d is the biomass decay rate.

The necessary inclusion of the effect of substrate on the growth rate meant that another unknown parameter (S) was introduced. Therefore, an equation that describes the rate of substrate utilisation needed to be included to solve for the substrate concentration.

$$\frac{ds}{dt} = -Y_s\mu_{max}\left(\frac{s}{K_s+s}\right)X \quad [44]$$

There are two ordinary differential equations (ODEs) that need to be solved to predict the biomass concentration and substrate utilisation (dX/dt and dS/dt). ODEs can be solved using the built in MATLAB function, *ode45*. However, there are multiple unknown parameters: K_I, K_i, μ_{max}, K_s, μ_d and Y_s. These unknowns can be estimated through nonlinear regression of the experimental data (growth curves and glycerol utilisation). Once more the nonlinear regression could be completed using the built in MATLAB function *lsqnonlin*, but the ODEs needed to be solved before regression could be done and *vice versa*. The ODEs and nonlinear regression therefore needed to be solved simultaneously, thus the two functions were nested. A flow chart illustrating the nested loop is provided in Figure *5.18* below. The *lsqnonlin* function requires an initial guess for all the unknown parameters, which is then used to solve the ODEs (Equations 43 and 44) using the two-flux approximation (Equation 20). The results of the ODE (biomass concentration and glycerol concentration over the experimental run) were then used to calculate the error between their predicted values and the actual experimental values at the corresponding time point. The error is then returned and if it is a large error a new initial guess is automatically used to recalculate the ODEs and then the errors. The regression ends when the error cannot be reduced further.

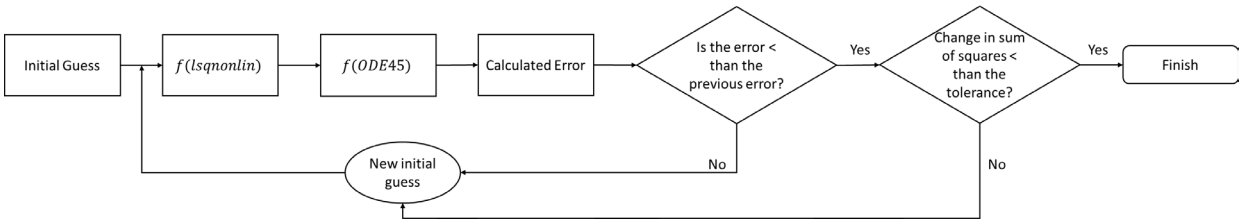

Figure 5.18: Algorithm flow diagram illustrating the nested loop function for nonlinear regression.

The above nested regression and ODE solver was run using all the experimental data from each light intensity to obtain values for the unknown parameters that could be used to fit growth curves and glycerol utilisations for a set light intensity (within the range investigated). Figure 5.19 below provides the plots of the non-linear regression of best fit parameters of biomass and substrate concentrations for each light intensity investigated versus the actual experimental values. Below is a detailed discussion on the predicted response of biomass and glycerol concentration for each light intensity versus their respective experimental results.

a) 30 W/m^2

The predicted growth and substrate utilisation response at an incident light intensity of 30 W/m^2 is provided in Figure 5.19a along with the experimental data that was discussed in sections 5.1.1 and 5.1.3. for this light intensity. The predicted response of the biomass and glycerol concentrations shows good fit to the experimental data, with an R^2 of 0.98 and 0.89 respectively. The 95% prediction intervals (PIs) were very tight and the normalised root mean squared errors (NRMSEs) were below 13% which indicates good precision. There is a slight over-prediction of the rate of substrate utilisation but is still within the experimental error.

b) 70 W/m^2

The predicted and experimental growth and substrate utilisation response at an incident light intensity of 70 W/m^2 is provided in Figure 5.19b. The predicted response of the biomass and glycerol concentrations shows good fit to the experimental data, both with very good R^2 values of 0.96 and 0.98 respectively. The 95% PIs were very tight and the NRMSE of biomass was 18% and substrate was 10%. There is a slight-over prediction of the acceleration stage which results in an over-prediction of the growth rate in the exponential phase.

c) 200 W/m^2

The predicted and experimental growth and substrate utilisation response at an incident light intensity of 200 W/m^2 is provided in Figure 5.19c. The predicted response of the biomass and glycerol concentrations shows good fit to the experimental data, both with very good R^2 values of 0.97 and 0.98

respectively. The 95% PIs were tight but were seen to be wider during the stationary phase of growth. This does correspond with an underprediction of the biomass concentration achieved during the stationary phase relative to the experimental data. The NRMSE of biomass was 15% and substrate was 9%.

d) 400 W/m^2

The predicted and experimental growth and substrate utilisation response at an incident light intensity of 400 W/m^2 is provided in Figure 5.19d. The predicted response of the biomass and glycerol concentrations shows good fit to the experimental data, both with very good R^2 values of 0.98 and 0.99 respectively. The 95% PIs had a similar response when compared to those at 200 W/m^2. The NRMSE of biomass was 11% and substrate was 9%.

e) 600 W/m^2

The predicted and experimental growth and substrate utilisation response at an incident light intensity of 600 W/m^2 is provided in Figure 5.19e. The predicted response of the biomass concentrations shows relatively good fit to the experimental data, with a good R^2 value of 0.94, however the predicted response of glycerol concentration did not show good fit to the experimental data (R^2=0.85) with an over prediction of the glycerol utilisation. The 95% PIs were very tight and the NRMSE of biomass and glycerol response were 21% and 17% respectively.

A single test experiment was done to check the ability of the model to predict the growth of an experimental run at conditions that were not used to train the model. The test conditions were conducted at light intensity of 100 W/m^2 in a PBR with an ID of 83 mm. The results of the single test experiment are shown in Figure G.1 in Appendix G. The model shows relatively good fit to the experimental data but overestimates the growth in the later stages of culturing. Therefore, the model possibly doesn't capture the full severity of cell mutual shading that occurs in the larger reactors when the culture has a high biomass concentration. However, this is only from a single repeat so more experimentation must be done to ensure the statistical significance of the prediction.

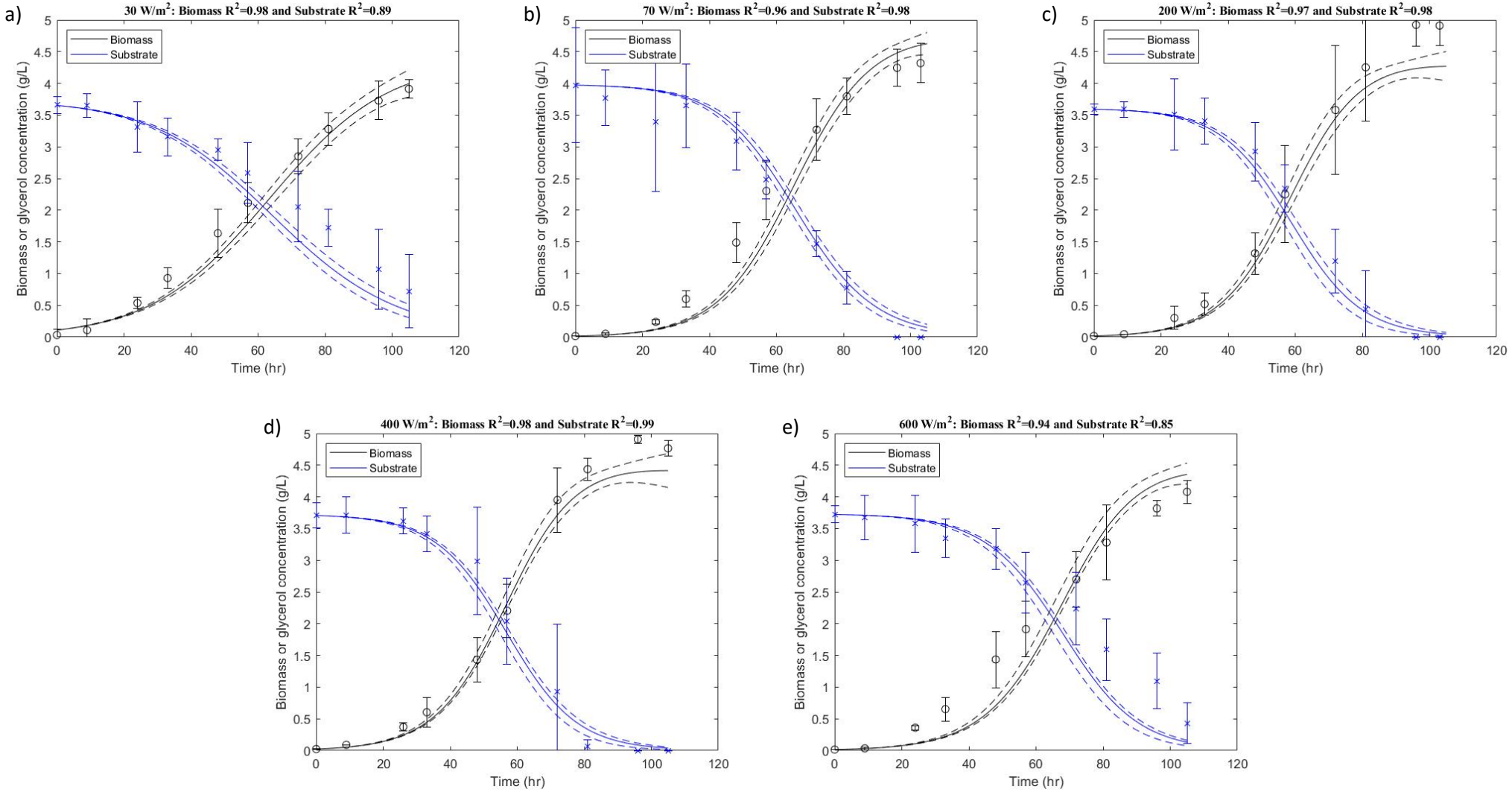

Figure 5.19: Non-linear regression of best fit parameters of biomass and substrate concentrations for each light intensity investigated versus the actual experimental values. a) 30, b) 70, c) 200, d) 400 and e) 600 W/m².

5.1.5.2 Light intensity modelling

With a working model for light attenuation and prediction of biomass concentration change over time for various light intensities, the average light intensity in the tubular PBR could be estimated. These predictions are provided in Figure 5.20. The average light intensity decreased over time with a trend inverse to each light intensity's corresponding growth curve. This profile aligned well with literature (Palamae et al., 2018) where a similar response was reported for average light intensity over time when culturing *R. sphaeroides* S10 in a tubular PBR system. The 95% PIs for average light intensity were propagated from the PIs calculated for biomass concentration.

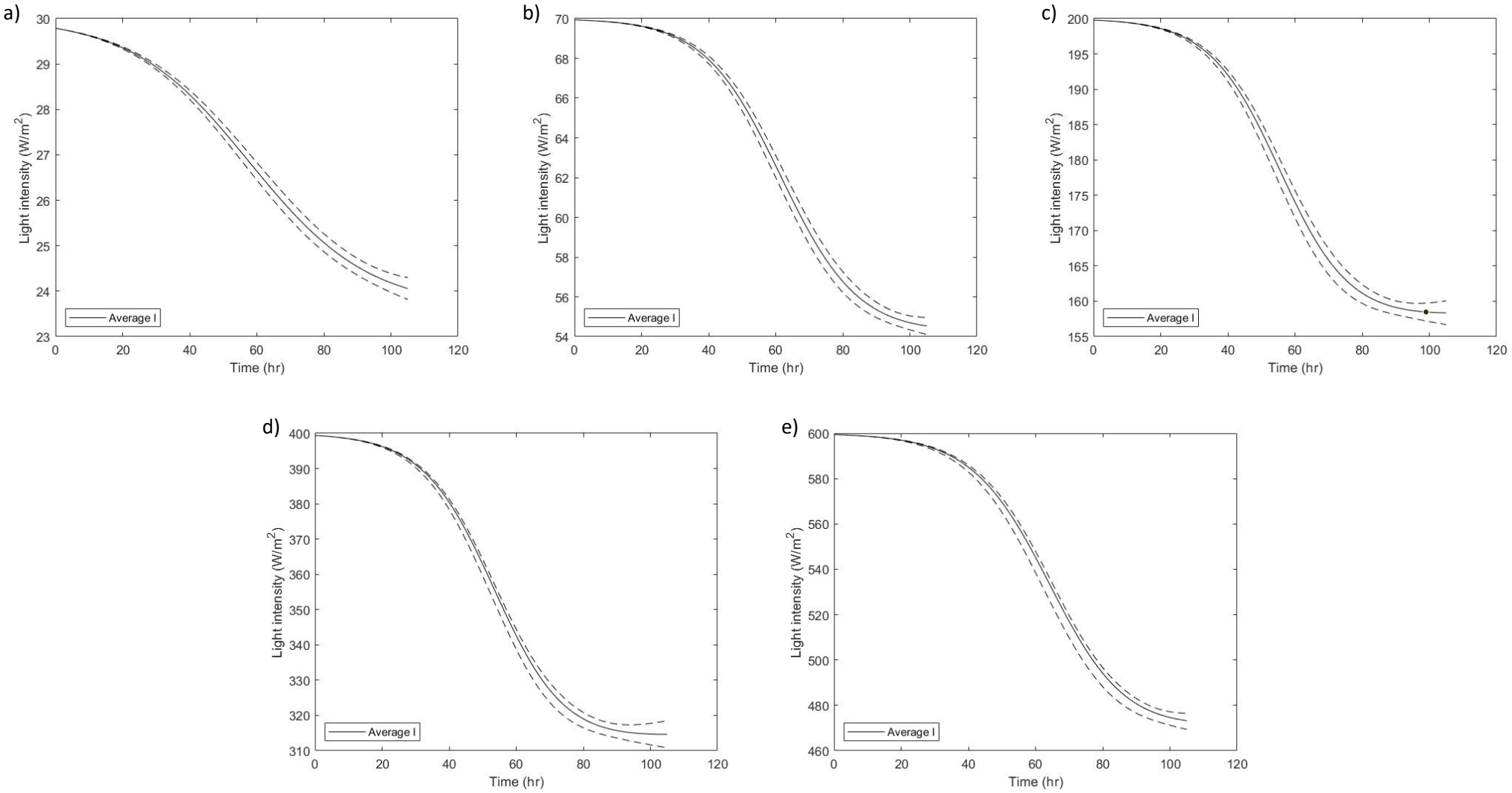

Figure 5.20: Estimation of average light intensity in the tubular PBR over time. a) 30, b) 70, c) 200, d) 400 and e) 600 W/m²

More of interest is the response of the average light intensity with changing concentration of biomass in the tubular PBR. Figure 5.21 provides this response for each incident light intensity investigated. As before, the general profile of each plot in Figure 5.21 was the same. The average light intensity decreased somewhat linearly as the biomass concentration increased. On average the light intensity in the tubular PBR decreased by ~20% from the starting incident light intensity until the maximum biomass concentration is achieved. This profile aligned well with literature (Palamae et al., 2018) where a similar response was reported for average light intensity versus biomass concentration, when culturing *R. sphaeroides* S10 in a tubular PBR system. A reduction of ~30% in average light intensity was reported at 4 g/L in the before mentioned investigation. This is also in line with what was achieved in this investigation and likely differs due to slightly different reactor diameters (Palamae *et al*. (2018) ID of 0.024 m). The 95% PIs were very tight which indicates good precision.

Considering that the reactor only has an internal diameter of 0.015 m, the average light intensity sees a significant decrease when the suspended solids (biomass) are at a concentration of only ~4.5 g/L. Upscaling of the culturing of *R. palustris* is made difficult, as an increasing diameter would lead to an increased amount of mutual shading by the bacterium in the bioreactor. This would lead to a decrease in energy available from the light source that is necessary for bacterial growth and/or product formation.

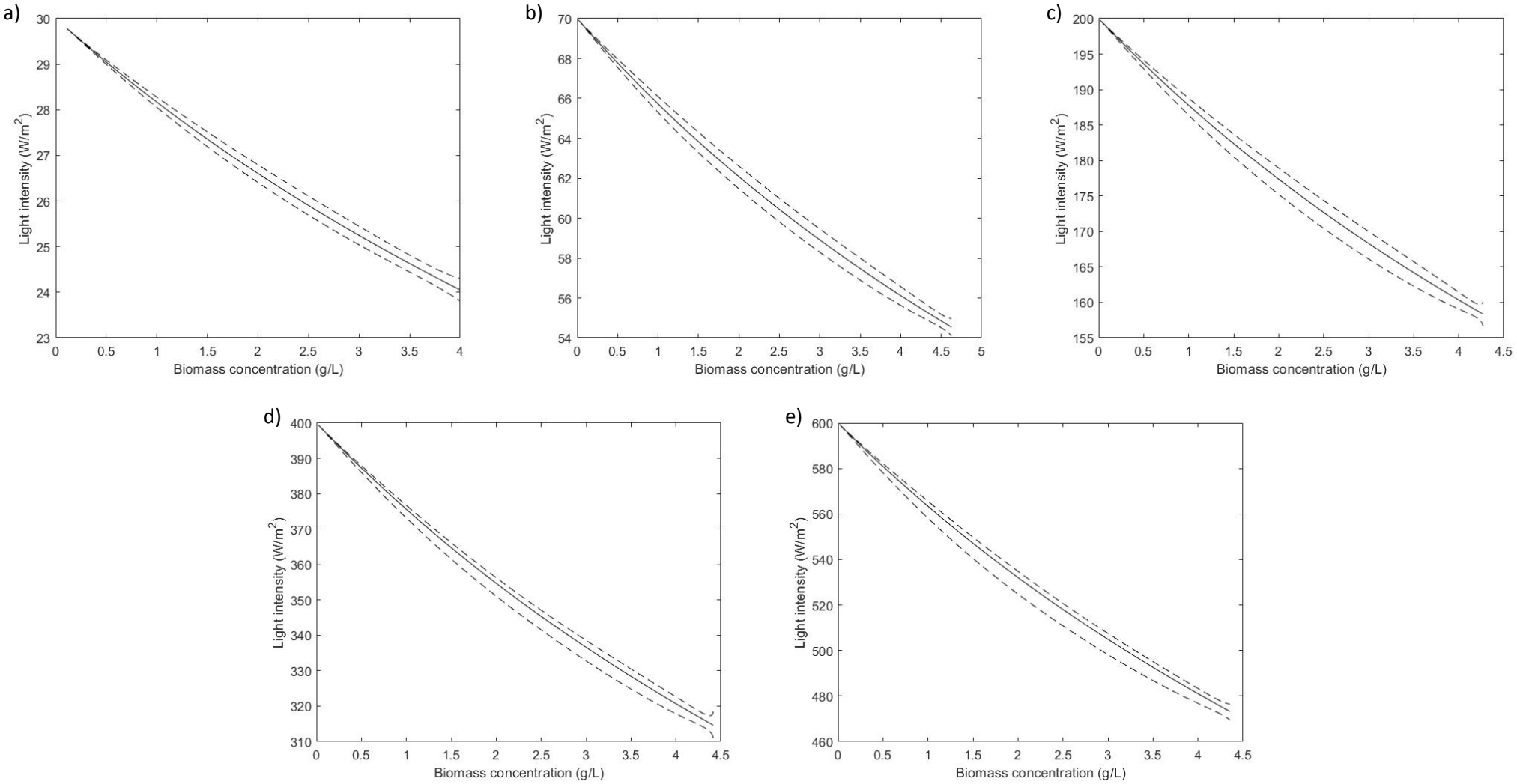

Figure 5.21: Estimation of the response of average light intensity as the biomass concentration increases. a) 30, b) 70, c) 200, d) 400 and e) 600 W/m²

5.2 Hydrogen production by *R. palustris* in free cell cultures

Investigations into the hydrogen production and photofermentation ability of *R. palustris* has mostly been done on a small scale, either in shake flask experiments or Schott bottle PBR setups, such as the one shown in section 4.4.1.2. These reactor types have small volumes (<0.5 L), are operated in a batch configuration and use either an orbital shaker or magnetic stirrer bar to agitate the culture. These setups offer little possibility for upscaling and are unlikely to be seen operating continuously. Thus, a reactor system that could be upscaled, operated continuously (and in batch) and mixed solely by fluid flow was designed. The design sheet of this PBR is provided in Figure A.2 in Appendix A and the system setup in Figure 4.4. This reactor has an active volume of 1 L and total volume of 1.13 L and relied on mixing through the recirculation of the culture via the peristaltic pump. The column PBR was designed with an overflow which means the reactor can be operated as a batch system (used in this experimentation) or a continuous system without any additional equipment. The simplicity of the design also means that the system could easily be upscaled for possible culturing in outdoor conditions.

To determine if this reactor design and setup would be a viable option in the culturing of *R. palustris* it was compared to the Schott bottle reactor in terms of growth, substrate utilisation and hydrogen production. In order to compare the results of each bioreactor type, the operating conditions in which *R. palustris* was cultured were kept constant. These conditions are : light source (incandescent), incident light intensity (100 W/m^2), starting OD (0.1), pH (7) and temperature (28 ± 1 °C). As the column reactor had no temperature control the temperature was monitored with a non-invasive infrared thermometer (Alla France IR Laser Pointer Thermometer) over the span of an experimental run (twice a day: early morning and late afternoon). The temperature remained relatively constant at 28 ± 1 °C over the entire run because the laboratory with the reactor was at all times being kept at a constant temperature via the thermostat. Based on this, the heat circulator (Julabo Corio heat immersion circulator used in the Schott bottle bioreactor rig was set to a temperature of 28°C. A comparison of the hydrogen production of each reactor type was to be investigated, therefore minimal medium with sterile additions was used. A comparison of the two reactor systems with regards to their growth, hydrogen production and substrate utilisation follows.

5.2.1 Growth kinetics

5.2.1.1 Growth curves and substrate utilisation

The growth curves of *R. palustris* 11774 cultured in minimal medium with glycerol (50 mM) as the carbon source and glutamate (10 mM) as the nitrogen source are provided in Figure 5.22. There is no lag phase present in the growth curve as the reactors were all inoculated with bacteria that was cultured in the same growth medium and were in the exponential growth phase. Both growth curves have linear trends

over the entire length of the experimental run indicating that the cultures growth rate remains relatively constant throughout culturing. There is no deceleration, stationary or death phase present in the growth curves, which indicates that there is no limiting substrate or inhibitory factor that effects the culture in the later stages of growth.

As mentioned previously the starting optical density of each reactor type was kept constant, hence the biomass concentration is also kept constant. This can be seen at the time zero sample point in Figure 5.22, as both cultures start at a biomass concentration of 0.064 g/L. A higher initial biomass loading was selected in an attempt to negate in possible stochastic effects as the growth rate is significantly lower when *R. palustris* is grown in the minimal medium compared to the modified Van Niels medium. A high rate of growth in the first 72 hours is present in both reactor systems. This was unexpected as it does not follow the growth trend that is typically seen with *R. palustris*. However, this high rate can be attributed to the fact that the inoculum used was cultured at a temperature of 35°C compared to 28°C. From temperature dependence studies done by a PhD candidate working with *R. palustris* 11774, it was determined that bacterium has a higher growth rate at 35°C when compared to 30°C. This is therefore the reason that the culture has a high growth rate in the first 72 hours of culturing which then decreases as the bacterium acclimatises to the lower temperature. The growth rate in the column PBR then decreases from 72 hours to 144 hours before reaching the exponential growth phase, which continues to the end of the experimental run after 190 hours. A similar trend can be seen for the bacterial growth in the Schott bottle PBR: the growth rate decreases after the first 72 hours and remains constant up to the 144-hour mark after which the growth rate increases as it enters the exponential growth phase until the end of the experimental run.

Parameters associated with the growth kinetics, i.e. the maximum specific growth rate and the yield of biomass on substrate are discussed in further detail later in this section. This is to review the performance of the column PBR in terms of growth and substrate utilisation when compared to the Schott bottle PBR in order to comment on the scalability of the proposed bioreactor design and configuration.

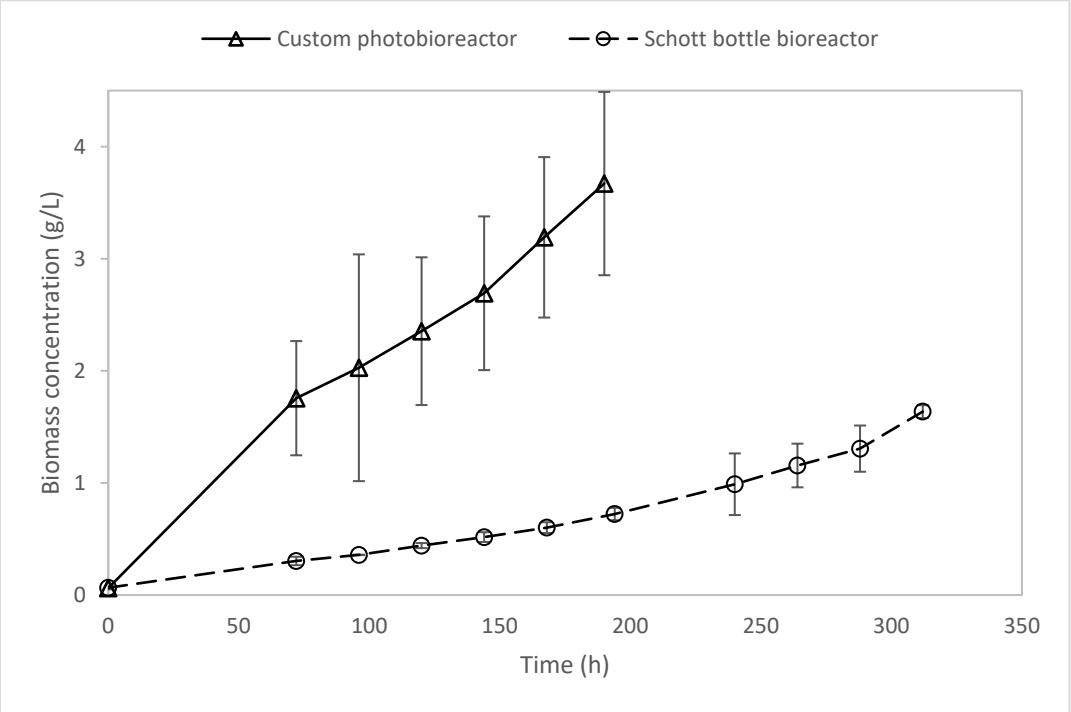

Figure 5.22: Comparison of growth curves of R. palustris cultured in a Schott bottle PBR (○) and the custom designed PBR (Δ). Illumination for both reactor configurations provided by incandescent light bulbs (60 W bulbs) at an incident light intensity of 100 W/m^2. R. palustris was cultivated using modified minimal medium with glycerol (50mM) as the carbon source and glutamate (10 mM) as the nitrogen source. Schott bottle experiments were completed at a mixing rate of 300rpm and the custom reactor at a recirculation volumetric flow rate of 0.651 L/min. Data points for the column PBR are the mean of triplicate repeats and data points for the Schott bottle PBR are the mean of quadruple repeats. The error bars show the uncertainty associated with the CDW measurements.

R. palustris glycerol utilisation in the minimal medium in the column and Schott bottle PBR is provided in Figure 5.23. The starting glycerol concentration was 50 mM for both reactor systems and this is illustrated in Figure 5.23 at time zero. The change in glycerol concentration of both reactors decreased in a linear fashion over the entirety of the experimental run. The trend of the decrease corresponds well with the increase in biomass of each reactor presented in Figure 5.22 above. In the column PBR *R. palustris* uses ~89% of the glycerol present in the liquid medium after 196 hours, this corresponds to decrease from 50 to 6 mM. If we review the glycerol consumption of *R. palustris* cultured in the Schott bottle PBR within the same time frame as the column reactor, only ~22% of the glycerol is consumed. This is a decrease from 50 mM to 40 mM. This was expected based on the difference in biomass concentration over time. In both reactor systems there is still glycerol present in the liquid medium which is why there is no stationary phase present in the growth curves in Figure 5.22 above.

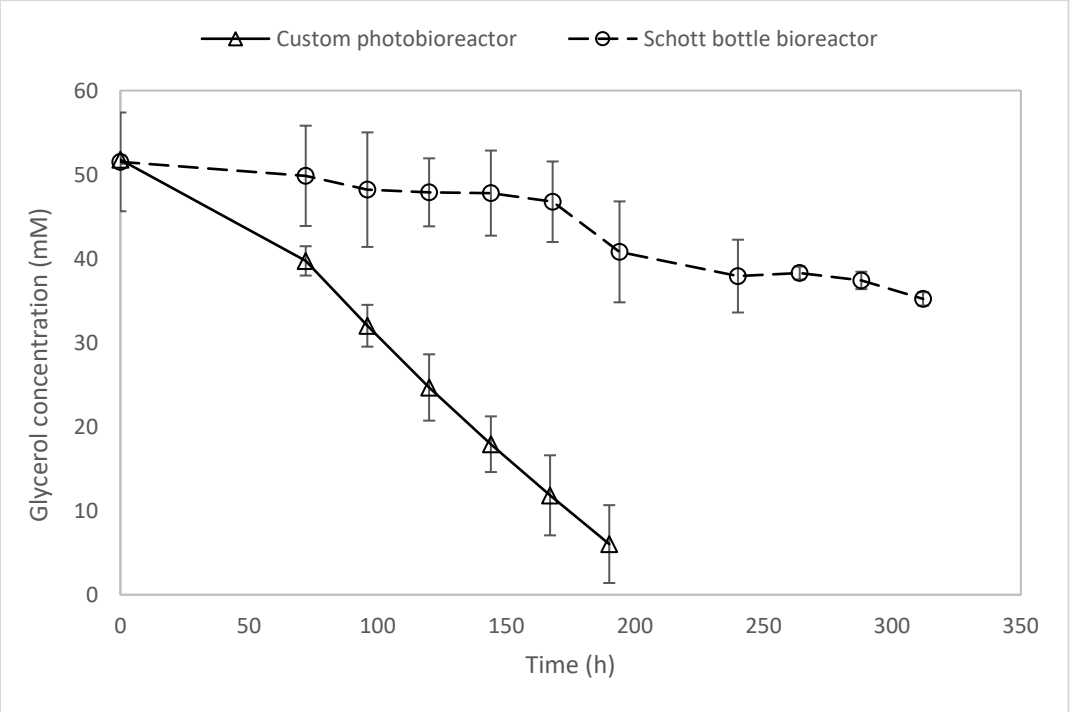

Figure 5.23: Glycerol utilization of R. palustris cultured in a Schott bottle PBR (○) and the custom designed PBR (Δ). Illumination for both reactor configurations provided by incandescent light bulbs (60 W) at an incident light intensity of 100 W/m^2. R. palustris was cultivated using modified minimal medium with glycerol (50mM) as the carbon source and glutamate (10 mM) as the nitrogen source. Schott bottle experiments were completed at a mixing rate of 300 rpm and the custom reactor at a recirculation volumetric flow rate of 0.651 L/min. Data points for the column PBR are the mean of triplicate repeats and data points for the Schott bottle PBR are the mean of quadruple repeats. The error bars show the uncertainty associated with the glycerol concentrations obtained through HPLC analysis.

5.2.2 Hydrogen production kinetics

In order to compare the hydrogen production of *R. palustris* cultured in the column and Schott bottle PBR the volume and composition of the gas stream collected from the head space of each reactor type was recorded. The composition of the gas stream was determined via GC analysis using the method described in section 4.5.2. The molar hydrogen concentration was ~97 mol% with the remainder being small traces of water vapour and carbon dioxide. See Appendix E for the full gas composition. The composition of hydrogen in the gas stream aligned well with values reported in literature (Pott, 2013). Due to carbon dioxides high solubility the gas, which is produced through respiration of *R. palustris*, is dissolved in the growth medium and thus not all released into the gas stream. Literature suggests that *R. palustris* utilises the Calvin cycle (section 2.3.3.1) to fix inorganic carbon, similarly to higher plants, as a mechanism for redox balance maintenance opposed to carbon acquisition for growth (McKinlay and Harwood, 2010). If the reaction described in Equation 6 occurred stoichiometrically the carbon dioxide composition in the gas stream would be 30% (v/v). However, Pott (2013) reported values for the composition of carbon

dioxide in the gas stream if it is assumed that *R. palustris* does no utilise any of the dissolved carbon dioxide to be 17% (v/v). This difference indicates that *R. palustris* is likely fixing a significant portion of the carbon dioxide that is produced metabolically, resulting in a gas stream that has a high purity with respect to hydrogen.

As discussed in section 2.2.2.2 dark fermentation results in a gas stream composition of equal volumes hydrogen and carbon dioxide. Thus, photofermentation would be advantageous on an industrial scale as it requires little to know downstream processing to increase the purity of the gas stream with regards to hydrogen content. These advantages would be in terms of capital and operating costs, as the separation of hydrogen and carbon dioxide is expensive because it requires either amine-CO_2 absorption or cryogenic cooling.

5.2.2.1 Cumulative hydrogen production

Figure 5.24 shows plots of the cumulative production of hydrogen as a function of time in the column and Schott bottle PBR from *R. palustris* grown in minimal medium with glycerol as the carbon source. For both the column and Schott bottle PBR the cumulative volume of hydrogen increases approximately linearly for the entire timespan of each reactors run. According to Pott (2013) product formation in biological systems is often growth associated product formation. However, it has been reported that the hydrogen production from *R. palustris* 11774 is not dependent on the growth and multiplication of the organism, but rather on the concentration of biomass present in the culture (Pott, 2013). Thus, the hydrogen production is non-growth associated. It was unlikely to see hydrogen production cease as the glycerol was not depleted when the experimental run finished, this is confirmed in Figure 5.24. The column PBR achieved a maximum cumulative hydrogen production of ~2600 mL after 194 hours of culturing, which is 10 times more than the cumulative hydrogen production in the Schott bottle PBR of ~260 mL. The Schott bottle PBR reached a maximum cumulative hydrogen production of 655 mL after 312 hours of culturing. Therefore, even with 118 hours of extra culturing the total hydrogen produced was still 4 times less.

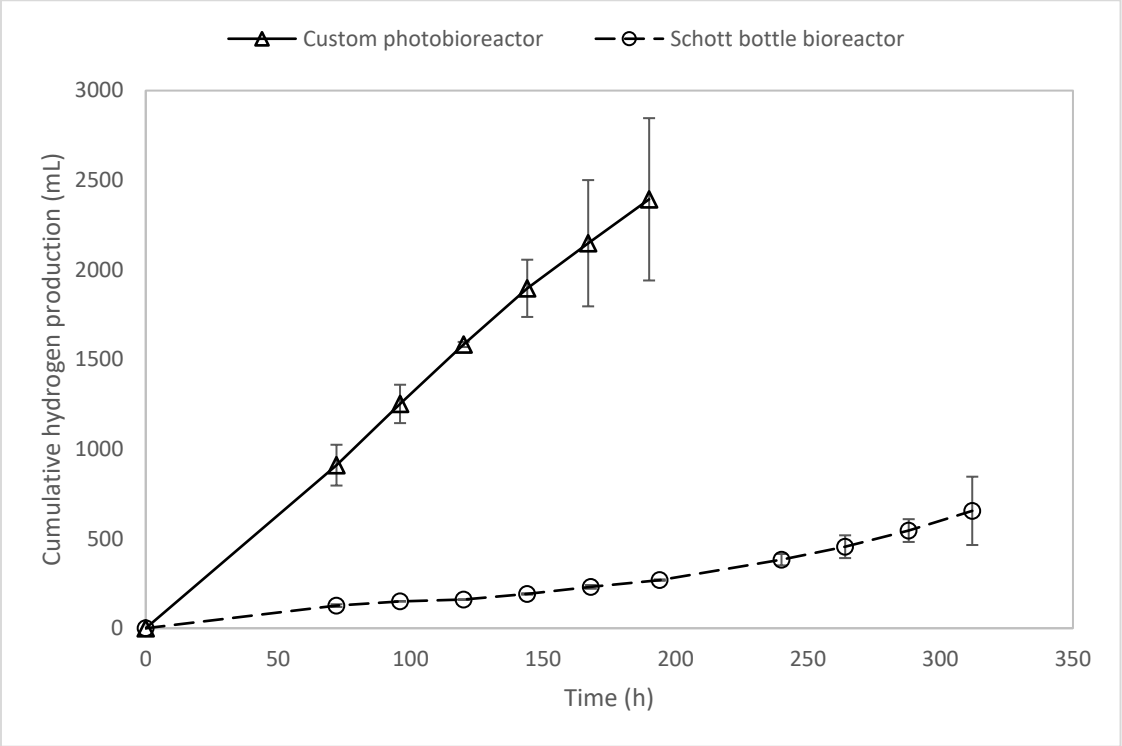

Figure 5.24: Comparison of cumulative hydrogen production by R. palustris cultured in a Schott bottle PBR (○) and the custom designed PBR (Δ). Illumination for both reactor configurations provided by incandescent light bulbs (60 W bulbs) at an incident light intensity of 100 W/m^2. R. palustris was cultivated using modified minimal medium with glycerol (50mM) as the carbon source and glutamate (10 mM) as the nitrogen source. Schott bottle experiments were completed at a mixing rate of 300 rpm and the custom reactor at a recirculation volumetric flow rate of 0. L/min. Data points for the column PBR are the mean of triplicate repeats and data points for the Schott bottle PBR are the mean of quadruple repeats. The error bars show the uncertainty associated with the hydrogen collected.

5.2.2.2 Specific hydrogen production rate

The specific hydrogen production rate was calculated with Equation 33 in section 2.9.4, using the change in biomass concentration and the cumulative hydrogen production over time. Figure 5.25 illustrates the change in the calculated specific hydrogen production rates over time for the column and Schott bottle PBR. Figure 5.25 indicates that both reactor systems have the same trend over each respective experimental period. With both systems maximum specific hydrogen production rate was achieved after the first 72 hours of culturing. After this the rate decreased exponentially for ~96 hours, after which the rate levelled out and continued at a relatively consistent production rate until the end of the experimental run. The column PBR had a maximum production rate of 12.6 ± 8.0 mL/g_{CDW}/h occurring after 72 hours of culturing, whereas the Schott bottle PBR had a maximum production rate of 19.0 ± 2.0 mL/g_{CDW}/h. After a total of 168 hours of culturing the hydrogen production rate in the Schott bottle bioreactor reaches a 'steady state' where the rate remains around 5.8 mL/g_{CDW}/h. After the same approximate culturing time the column bioreactor reaches a steady hydrogen production rate of ~3.8 mL/g_{CDW}/h. As

discussed previously the hydrogen production is non-growth associated, which means that the hydrogen production is dependent on the concentration of the biomass in the culture. The biomass concentration in the column reactor is significantly higher when compared to the Schott bottle reactor. This is likely due to the mutual shading that occurs in the reactor system at high biomass concentrations.

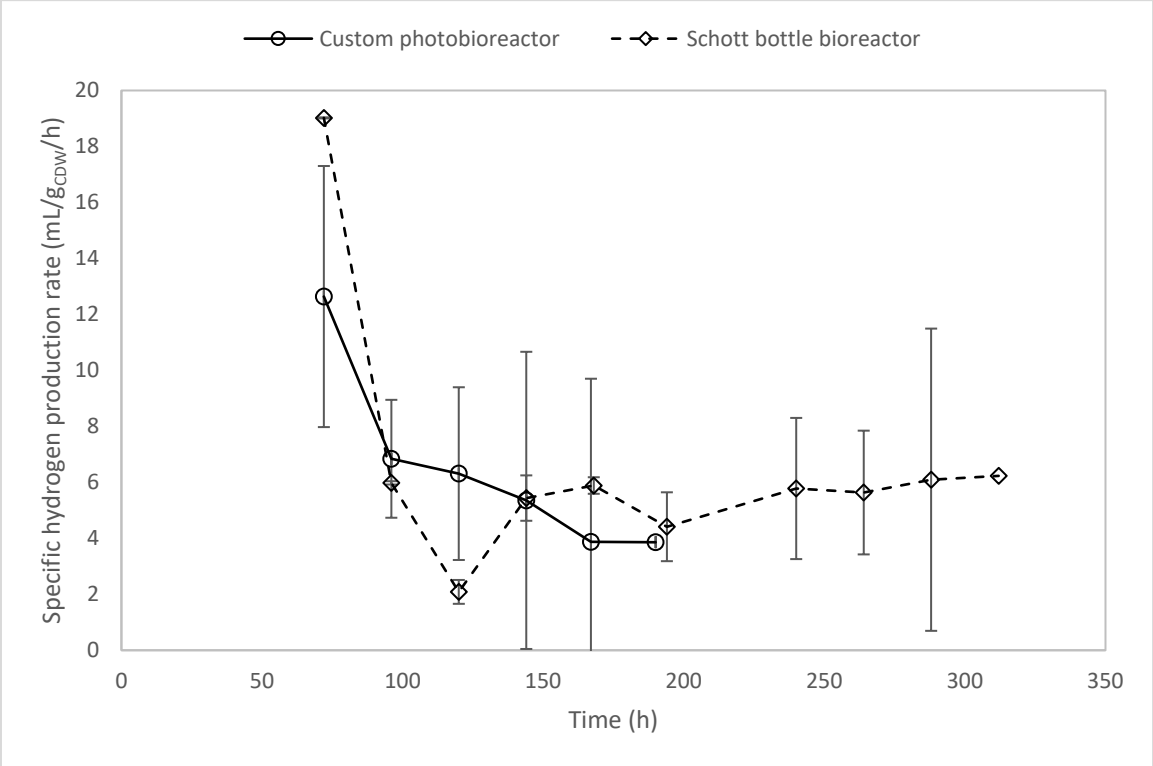

Figure 5.25: Comparison of specific hydrogen production rate by R. palustris cultured in a Schott bottle PBR (○) and the custom designed PBR (Δ). Illumination for both reactor configurations provided by incandescent light bulbs (60 W bulbs) at an incident light intensity of 100 W/m^2. R. palustris was cultivated using modified minimal medium with glycerol (50mM) as the carbon source and glutamate (10 mM) as the nitrogen source. Schott bottle experiments were completed at a mixing rate of 300 rpm and the custom reactor at a recirculation volumetric flow rate of 0.651 L/min. Data points for the column PBR are the mean of triplicate repeats and data points for the Schott bottle PBR are the mean of quadruple repeats. The error bars show the propagated uncertainty associated with the CDW and hydrogen production.

The conversion efficiency of the available electrons from the carbon substrate, glycerol, to hydrogen was determined using Equation 32 in section 2.9.3. The conversion efficiency in the Schott bottle PBR was calculated to be 32% over the first 192 hours of culturing. This means that for every mole of glycerol, only a third of the theoretical hydrogen was produced (2.2 moles). The conversion efficiency was identical in the column PBR and was calculated to be 32% over the experimental run (192 hour). The general low conversion efficiencies in both reactor systems in comparison to 96% achieved by *R. palsutris* as reported by Ghosh et al. (2011) is possibly due to the concentration of glycerol in the growth medium. Ghosh et al. (2011) achieved the 96% conversion efficiency at a glycerol concentration of 30 mM and

reported that at a glycerol concentration of 50 mM One mole of glycerol produced ~3 moles of hydrogen which is a conversion efficiency of 43%. Therefore the conversion efficiencies in this investigation align well with what has been reported in literature with the same glycerol concentration.

5.2.3 Estimation of average light intensity in the column and Schott bottle PBR

Differences in reactor geometry and size has a major effect on the light profiles that the cells in the culture experience. With regards to a cylindrical geometry, the diameter size impacts the light attenuation through the culture, as illustrated in Figure 5.1 and discussed in section 5.1. Therefore, there will be a significant difference in the light profile and average light intensity between the column (ID = 50 mm) and Schott bottle PBR (ID = 86 mm) as the two reactors' diameters differ. The models developed and discussed in section 5.1.5 for the prediction of the average light intensity in the bioreactor can be used here to compare how the average light intensity changes during culturing of *R. palustris* in the two different PBRs.

The change in biomass concentration over time was modelled using the methods described in section 2.4, that was used and discussed in section 5.1. The growth rate model (Equation 43) was adjusted slightly to that used in section 5.1.5 as the substrate was not completely utilised during the experimental run and therefore the growth rate is assumed to be only dependent on the light intensity and biomass concentration (Palamae et al., 2018). The adjusted equation is provided in Equation 45 below.

$$\frac{dX}{dt} = \mu_{max}\left(\frac{I}{K_I+I}\right)\left(\frac{K_i}{K_i+I}\right)X - \mu_d X \qquad [45]$$

The above growth rate equation along with the experimental growth data for the Schott bottle and column reactor could then be used with the model and algorithm flow chart (Figure 5.18) discussed in section 5.1.5. Figure 5.26 and Figure 5.27 below provide a plot of the modelled line of best fit to the experimental growth data observed when culturing *R. palustris* in the Schott bottle and column PBR respectively. Both models show good fit to the experimental data and could therefore be used for accurate prediction of the average light intensity during culturing of the cells in the different reactor systems.

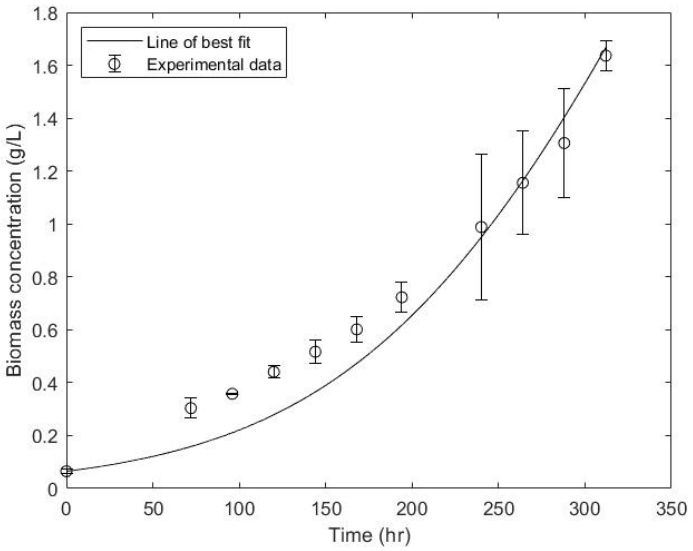

Figure 5.26: Experimental data and modelled data of the biomass concentration cultured in the Scott bottle PBR. Experimental data represent the mean of quadruple repeats and the error bars show the uncertainty associated with the measured CDW.

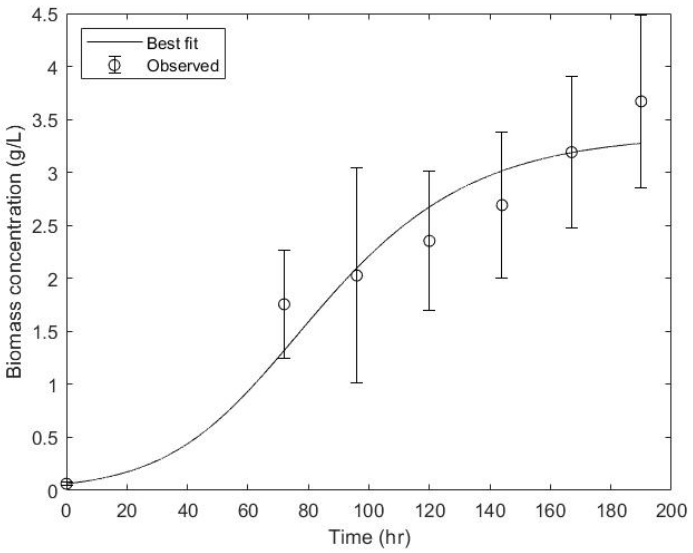

Figure 5.27: Experimental data and modelled data of the biomass concentration cultured in the column PBR. Experimental data represent the mean of triplicate repeats and the error bars show the uncertainty associated with the measured CDW.

The light intensity profile through the cross-section of each reactor was predicted using the two-flux approximation for light attenuation, provided in Equation 22, over the entire predicted growth curve. Integration of the light attenuation profile over the cross-sectional area of the reactor provided the average light intensity in the reactor over the entire predicted growth curve. The Schott bottle PBR growth was predicted up to the same maximum biomass concentration obtained in the column PBR for

comparison over the same biomass concentration range. This extended predicted growth curve, which assumes that growth can only be limited by light, is provided in Figure F.1 in Appendix F. The predicted average light intensity with changing biomass concentration for each reactor system is provided in Figure 5.28. From Figure 5.28, the average light intensity in the column PBR decreases in a near linear trend with increasing biomass concentration. However, the average light intensity in the Schott bottle PBR decreases exponentially in comparison to the column PBR. This leads to a 50% reduction in the average light intensity in the Schott bottle reactor compared to the 20% reduction predicted in the column reactor at the same biomass concentration of ~3.25 g/L. Increased reduction in average light intensity in the Schott bottle PBR compared to a PBR with a smaller diameter was reported by Palamae et al (2018), which align with the results obtained in Figure 5.28.

The significant reduction in average light intensity with an increase in reactor diameter of only 36 mm points out an eventual pitfall in the upscale of a PBR reactor for the culturing of *R. palustris* on an industrial scale. Measures are required to ensure the average light intensity remains elevated and the light attenuation through the reactor is minimal. Possible solutions include installing solar-energy-excited optical fibres in the PBR (Chen et al., 2008) to improve the light intensity profile within the reactor and genetic modification of the bacteria to reduce the pigments (Tandori et al., 2001) to reduce the light attenuation through the reactor.

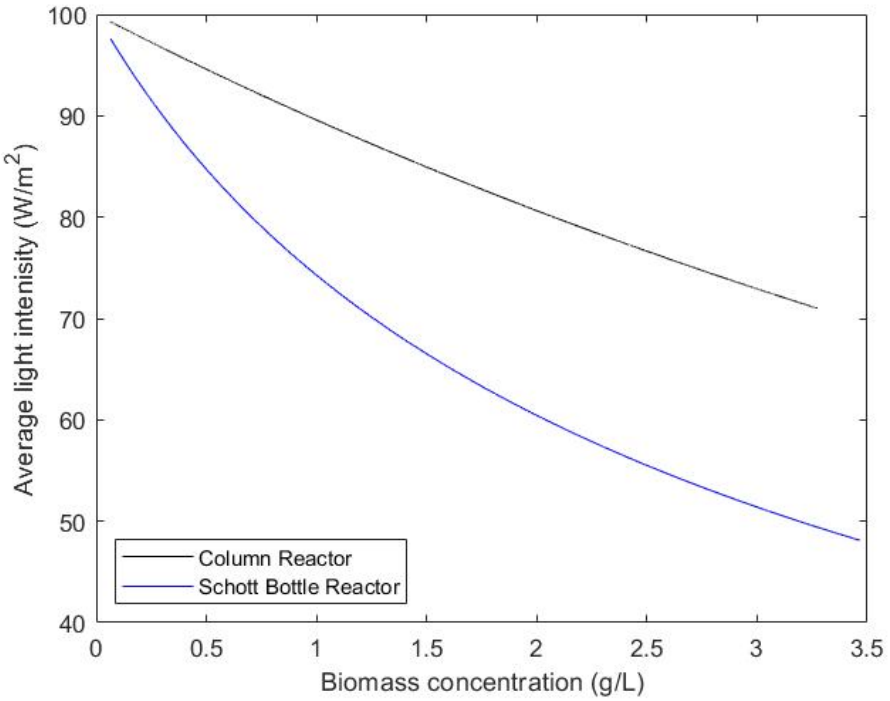

Figure 5.28: Predicted average light intensity in the column and Schott bottle PBR with the change in biomass concentration.

5.3 Hydrogen production by *R. palustris* in immobilised matrix

With the column PBR verified as a viable option for the culturing of *R. palustris* with regards to the biomass growth, substrate degradation and the production of hydrogen, the reactor system could be used to investigate different reactor configurations with *R. palustris* immobilised in a hydrogel matrix. As discussed previously, the scalability of processes using PNSB to produce biohydrogen relies on the optimisation of the process parameters, of which the immobilisation of the bacteria in a hydrogel has been identified as covering several of these key areas. These areas include but are not limited to: i) protection from physio-chemical challenges, ii) higher biomass concentration than in planktonic systems, and iii) reduced number of cell divisions resulting in metabolic energy being focused on product formation (Dervakos and Webb, 1991). In section 2.7, possible reactor configurations loaded with immobilised bacteria were proposed, i.e. a packed bed photobioreactor (PBPBR) and a fluidised bed photobioreactor (FBPBR). Therefore, testing of both reactor configurations was required in order to determine which configuration outperforms the other with regards to the hydrogen production kinetics. Before this, the performance of the column PBR with immobilised cells versus the growing planktonic cells were compared to ensure that a similar or greater level of performance with regards to hydrogen production is achieved and therefore warrant the need for immobilisation. These reactor configuration comparisons are provided in the remainder of this section.

5.3.1 Hydrogen production performance: immobilisation vs planktonic cells

In order to compare the difference in performance between immobilised cells and planktonic cells operating in the column PBR, the operating conditions of the reactor were kept constant. These conditions were the light source (incandescent), incident light intensity (100 W/m^2), pH (7) and temperature (28 ± 1 °C). As mentioned previously the column PBR had no temperature control. However, once again the environmental temperature was kept constant throughout the experimental runs. In cases where growing cultures were required glutamate was added as the nitrogen source in order to facilitate growth of the bacterium. In cases where no growth was required, and the medium was only to facilitate the production of hydrogen, no glutamate was added so that the bacterium would remain in the stationary phase. Thus, no glutamate was added to the medium used when the column PBR was operated with immobilised *R. palsutris*, as no growth was required in the PVA hydrogel beads. Yeast extract was also excluded from the minimal medium recipe to ensure that there was no nitrogen present in the medium. The bacteria loaded in the hydrogel beads should remain in the stationary phase during reactor operation due to the lack of a nitrogen source in the system. This could not be verified as the cell concentration in the hydrogel matrix is not currently measurable. It should be noted that this comparison

was done with the column PBR operating as a FBPBR when loaded with the PVA hydrogel loaded with *R. palsutris*.

Figure 5.29 below illustrates the change in the specific hydrogen production (mL/g_{CDW}) over time for immobilised cells and planktonic cells cultured in the column PBR. It can be seen in Figure 5.29 that the specific hydrogen production from the immobilised cells increases gradually over the first 192 hours, before a linear increase over the rest of the experimental run. The trend of the specific hydrogen production from the planktonic cells follows the form of an exponential decay (increasing form) curve as it increases over time, before saturating at a constant value. This indicates that the hydrogen production is negatively affected by too high a biomass concentration, likely due to the increased effects of mutual shading and the negative effects of increase light attenuation. This negative effect is avoided in the immobilised configuration as the biomass is assumed to not increase from the starting biomass loading and the FBPBR configuration meant that the light attenuation remained constant over the entire experiment.

As discussed previously, the column PBR with planktonic cells had a maximum hydrogen production rate of 12.6±8.0 mL/g_{CDW}/h, which corresponds to the linear region seen in Figure 5.29 over the first 72 hours of culturing. The maximum specific hydrogen production rate of the immobilised cells in the column PBR occurred after 192 hours and had a value of 14.7±2,5 mL/g_{CDW}/h. The linear increase from 192 to 264 hours corresponds to a constant specific hydrogen production rate, which is approximately 14 mL/g_{CDW}/h. This is approximately four times larger than the ‘steady state’ rate achieved by the planktonic culture, of ~3.8 mL/g_{CDW}/h. Thus, cells immobilised in PVA hydrogel outperform the planktonic cultures when operating as a FBPBR in the column reactor in terms of the specific hydrogen production rate.

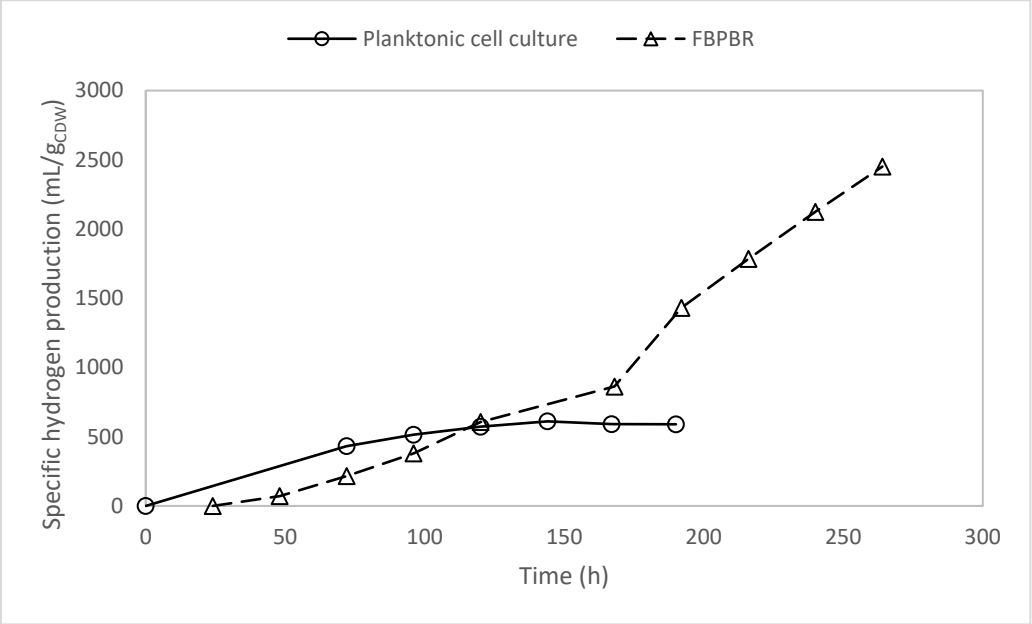

Figure 5.29: Comparison of specific hydrogen production rate by free-cell R. palustris cultured in a column PBR (○) and immobilised R. palustris in the FBPBR (Δ). Illumination for both reactor configurations provided by incandescent light bulbs (60 W bulbs) at an incident light intensity of 100 W/m^2. R. palustris was cultivated using modified minimal medium with glycerol (50mM) as the carbon source and glutamate (10 mM) as the nitrogen source (only for the planktonic cell culture). FBPBR experiments were completed at a volumetric flow rate 1.06 L/min and planktonic cell culture at a recirculation volumetric flow rate of 0.651 L/min. Data points for the column PBR are the mean of triplicate repeats and data points for the FBPBR are the mean of quadruple repeats. The error bars show the propagated uncertainty associated with the CDW and hydrogen production.

The conversion efficiency of the available electrons from the carbon substrate, glycerol, to hydrogen was determined using Equation 32 in section 2.9.3. As discussed previously, the conversion efficiency in the column PBR when cultured with planktonic cells was 32%. However, when operating the column PBR as a FBPBR loaded with immobilised cells, a conversion efficiency of 43% was achieved over the period where the hydrogen production rate was constant (192 to 264 hours). An increase should occur based on there being more electrons available for hydrogen production when the bacteria is non-growing, i.e. in the stationary phase.

It can be seen from Figure 5.30 that the starting glycerol concentration (~85mM) in the FBPBR is significantly higher than the 50mM concentration present in the medium used when operating the reactor in this configuration (Table 4.4). The higher concentration is due to the excess glycerol in the hydrogel beads that was not sufficiently removed when the beads were washed, following the process described in section 4.4.2. As discussed previously, high glycerol concentrations can negatively affect the conversion efficiency. This is a possible reason that only a slight increase in conversion efficiency is achieved by the FBPBR and PBPBR compared to the planktonic cells. The glycerol utilisation in the FBPBR

decreased linearly over time at a lower rate in comparison to the planktonic cells cultured in the column PBR. The large error in the glycerol concentration stems from the variation in the starting concentration due to varying amount of glycerol present in the beads after washing. The consistency in the error illustrates this, as the difference in glycerol concentration over the same time for each run shows only a negligible error.

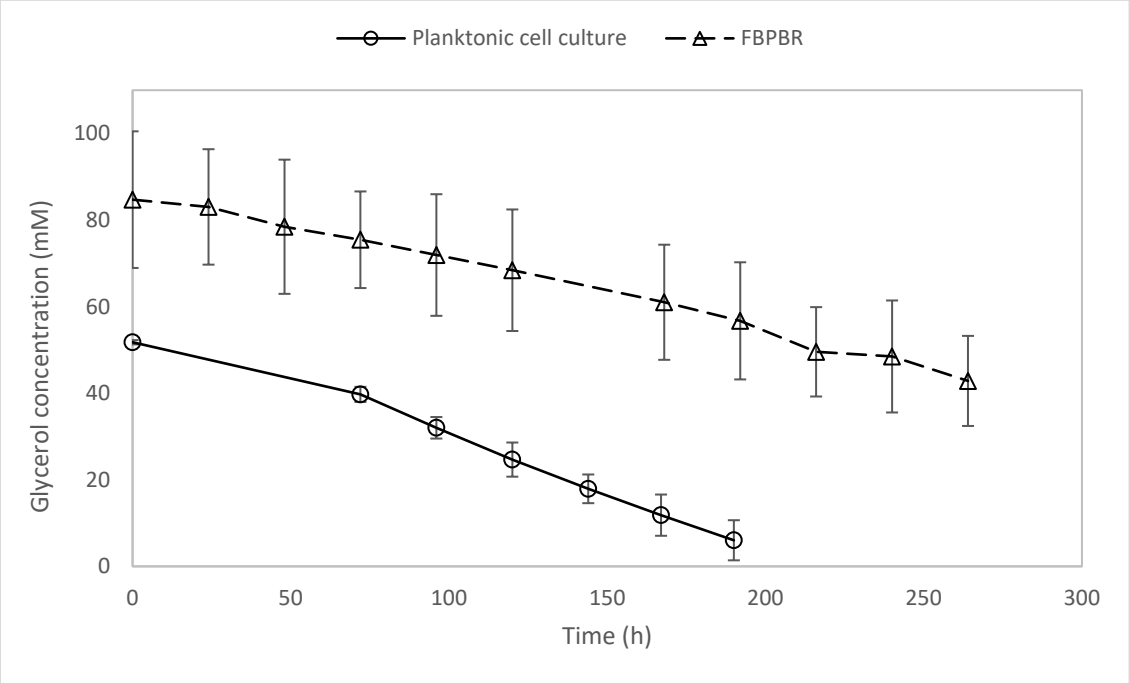

Figure 5.30: Glycerol utilization by free-cell R. palustris cultured in a column PBR (○) and immobilised R. palustris in the FBPBR (Δ). Illumination for both reactor configurations provided by incandescent light bulbs (60 W bulbs) at an incident light intensity of 100 W/m^2. R. palustris was cultivated using modified minimal medium with glycerol (50mM) as the carbon source and glutamate (10 mM) as the nitrogen source (only for planktonic culture). FBPBR experiments were completed at a volumetric flow rate 1.06 L/min and planktonic cell culture at a recirculation volumetric flow rate of 0.651 L/min. Data points for the planktonic cell column PBR are the mean of triplicate repeats and data points for the FBPBR are the mean of quadruple repeats. The error bars show the uncertainty associated with the glycerol concentrations obtained through HPLC analysis.

Operating the column reactor as FBPBR with *R. palsutris* immobilsed in a PVA hydrogel shows a clear advantage with regards to the specific hydrogen production rate and the conversion efficiency. Immobilisation therefore succeeds in optimising some of the before mentioned key process parameters and can be considered as a viable option to a achieve greater level of performance with regards to specific hydrogen production.

5.3.2 FBPBR versus PBPBR

With immobilised cells identified and proven to improve the performance of the column PBR with regards to the specific hydrogen production rate and conversion efficiency, the possible configurations with immobilised cells were investigated. The comparison of the FBPBR and PBPBR was done within the same experimental run to ensure consistency with regards to the immobilised hydrogel beads. All experimental runs started with the column PBR operating in the fluidised bed configuration, with fluidisation of the bed facilitated by the recirculation of the minimal medium from the overflow to the base of the reactor bed. The bed was characterised as fluidised when the liquid velocity through the reactor was higher than the minimum fluidisation velocity. When the column PBR configuration needed to be changed from a fluidised bed to a packed bed in order to test the performance of the PBPBR configuration, the flow velocity through the reactor was reduced below the minimum fluidisation velocity by reducing the flow rate of the peristaltic pump.

The minimum fluidisation velocity was determined experimentally. The flow rate through the reactor when the immobilised bacteria was a packed bed, was measured and then used with the diameter of the reactor to calculate the velocity. The minimum fluidisation was calculated to be 0.0029 m/s. The peristaltic pump was adjusted around this flow rate when the reactor configuration needed to be set or changed.

To determine which reactor configuration would be a viable option for the operation of the column PBR when loaded with *R. palustris* immobilised in PVA hydrogel, the substrate utilisation and hydrogen production kinetics were compared.

5.3.2.1 Cumulative hydrogen production

Figure 5.31 shows the plot of the cumulative hydrogen production as a function of time that was collected from the column PBR when operating with *R. palustris* immobilised in PVA hydrogel with minimal medium circulated through the bed of the reactor. The figure is divided into three sections which indicate what the configuration of the reactor was during those periods of operation: i) Fluidised bed from 0 to 264 hours, ii) Packed bed from 264 to 432 hours and iii) Fluidised bed from 432 to 504 hours. In section i) of Figure 5.31 it can be seen that the cumulative hydrogen production increases gradually over the first 192 hours, after which the increase is linear over time up to 264 hours of operation, where the cumulative hydrogen collected is ~2000 mL. At this stage the flow rate of the fluid in the reactor is reduced to below the rate corresponding to the minimum fluidisation velocity. The column PBR was now operating as a PBPBR in section ii) of Figure 5.31. During operation in this configuration the hydrogen production continues at a linear trend but at noticeably reduced rate for 168 hours (264 to 432) and only produces ~600mL of hydrogen. The flow rate was then increased to the starting flow rate to reintroduce

fluidisation. In section iii) of Figure 5.31 it can be seen that after the column PBR is changed from the PBPBR back to the FBPBR the linear trend continues but at a higher rate, similar to that seen in section i) between 192 and 264 hours of operation. The experimental run was then stopped after 504 hours and with a cumulative hydrogen production of ~3400 mL.

The change back to the FBPBR configuration was to confirm that any change in the hydrogen production and/or glycerol utilisation seen when the configuration was changed from fluidised to packed (section i to ii) was due solely to the configuration change and not based on the period of operation up to that point or the difference in concentration of substrates in the liquid medium. This will be discussed in more detail with respect to the specific hydrogen production rate achieved in the following section.

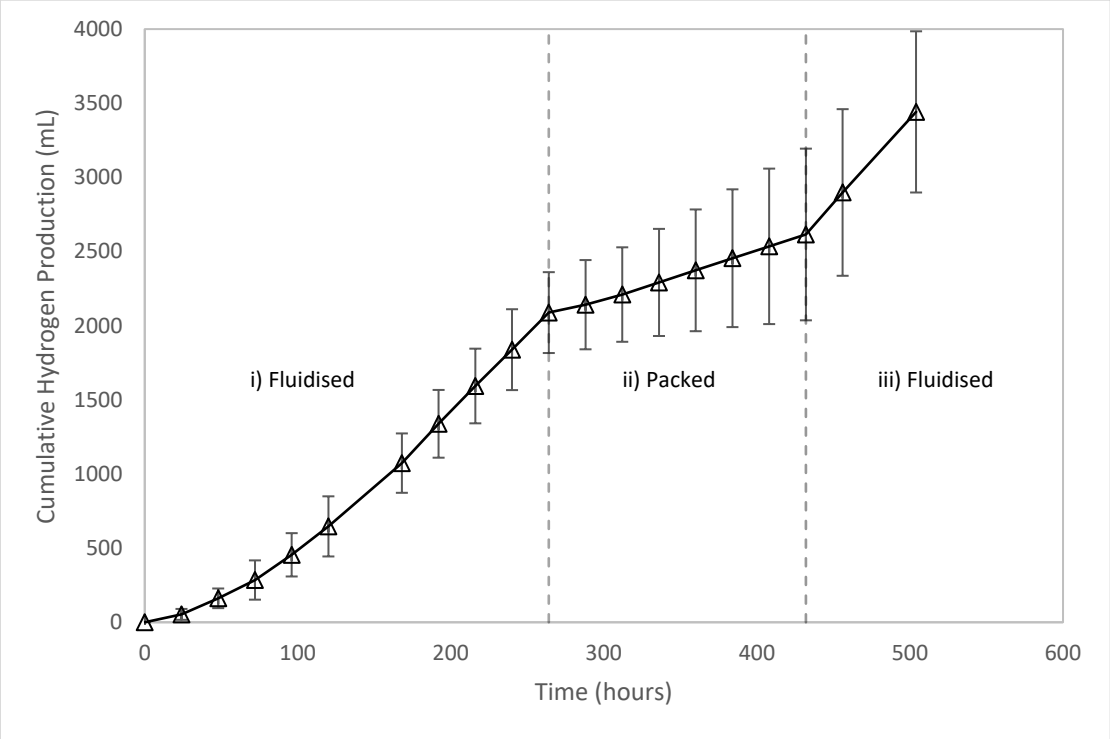

Figure 5.31: Comparison of cumulative hydrogen production by immobilised R. palustris in the column PBR. Illumination for both reactor configurations provided by incandescent light bulbs (60 W bulbs) at an incident light intensity of 100 W/m^2. R. palustris was cultivated using modified minimal medium with glycerol (50mM) as the carbon source. FBPBR experiments were completed at a volumetric flow rate 1.06 L/min and PBPBR experiments at a recirculation volumetric flow rate of 0.347 L/min. Data points are the mean of quadruple repeats and the error bars show the uncertainty associated with the cumulative hydrogen produced.

5.3.2.2 Hydrogen production kinetics

The specific hydrogen production rate was calculated using Equation 33 in section 2.9.4 using the change in cumulative hydrogen production over time and the biomass loaded into the hydrogel beads. The hydrogel-based beads had a biomass loading calculated on a 1.5 wt% wet cell pellet to hydrogel ratio.

Therefore, 250 g of PVA hydrogel contained 3.75 g of wet cells which corresponds to a CDW loading of 0.75 g. Figure 5.32 illustrates the change in the calculated specific hydrogen production rates over time for the column PBR with the FBPBR and PBPBR configurations. As before the figure is divided into three sections for the appropriate visualisation of which operating condition was being investigated, and over which time period. It can be seen in Figure 5.32 that the specific hydrogen production rate increases in a linear fashion right from the start of the experimental run up to 14.7 mL/g_{CW}/h after 192 hours of operation. During this period the immobilised cells are likely still adapting to the conditions of the bioreactor and are therefore not producing at the maximum specific hydrogen production rate right from the start of the experimental run. The production rate then steadies at approximately 14 mL/g_{CDW}/h for 72 hours, which corresponds to the linear region in section i) of Figure 5.31. At this point the configuration is changed form a FBPBR to a PBPBR by reducing the flow rate of the liquid medium being recirculated from the overflow to the base of the reactor.

After this change there is an immediate drop in the production rate from 13.89 mL/g_{CDW}/h to 2.96 mL/g_{CDW}/h within the first 24 hours of operation as a packed bed. The rate then increases gradually for 48 hours to a production rate of 4.53 mL/g_{CDW}/h at a total operation time of 336 hours. The specific hydrogen production rate then remains constant at ~4.5 mL/g_{CDW}/h for 96 hours, which corresponds with the linear region noted in section ii) of Figure 5.31. At this point the configuration is changed back to operate as a FBPBR by increasing the flow rate of the liquid medium back to the starting value.

The configuration change causes an increase in the specific hydrogen production rate all the way back to the constant production rate achieved during the first period of fluidisation. As stated previously, the reason for the change in configuration back to the FBPBR configuration was to validate that the drop in specific hydrogen production rate from the 264-hour mark to the 288-hour mark is solely due to the change in the operating configuration and not any other factor. Therefore, since the specific hydrogen production rate increased back to the constant hydrogen production rate achieved during the first period of fluidization, it is only the change in reactor configuration that causes the changes in the specific hydrogen production rate.

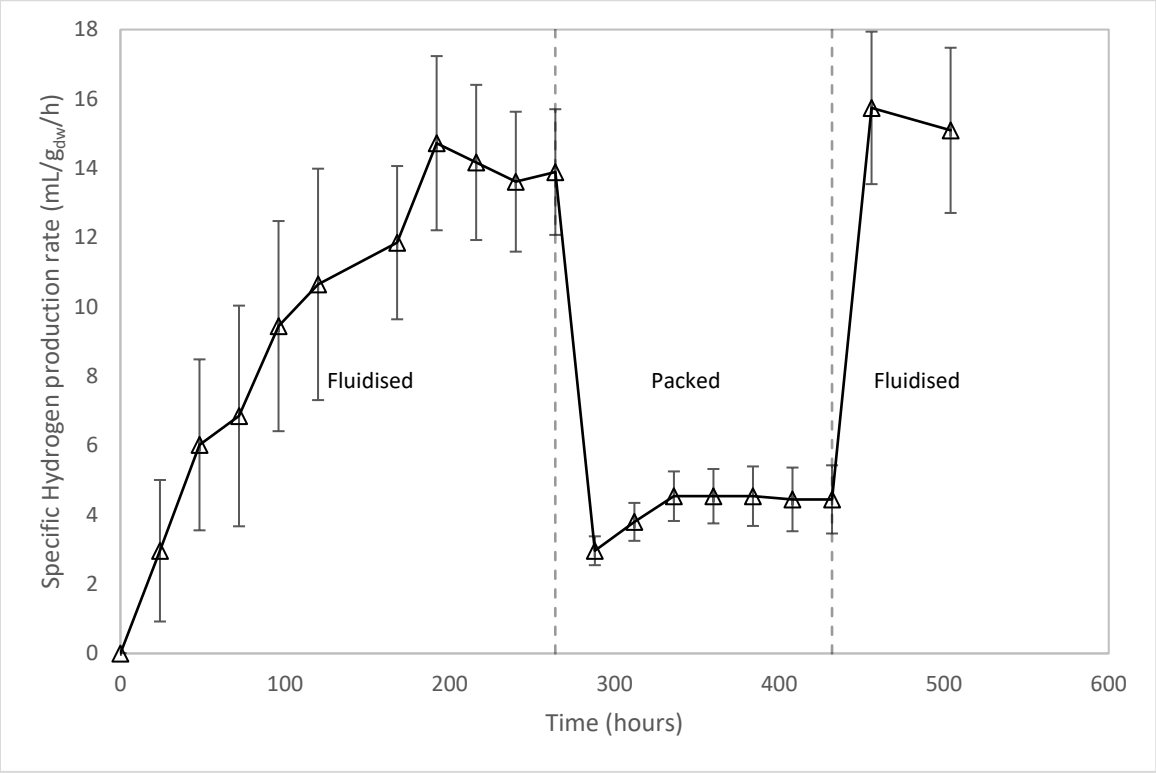

Figure 5.32: Comparison of specific hydrogen production rate by immobilised R. palustris in the column PBR. Illumination for both reactor configurations provided by incandescent light bulbs (60 W bulbs) at an incident light intensity of 100 W/m^2. R. palustris was cultivated using modified minimal medium with glycerol (50mM). FBPBR experiments were completed at a volumetric flow rate 1.06 L/min and PBPBR experiments at a recirculation volumetric flow rate of 0.347 L/min. Data points are the mean of quadruple repeats. The error bars show the uncertainty associated with the cumulative hydrogen produced.

The glycerol utilisation of immobilised *R. palustris* in the column PBR is provided in Figure 5.33 below. The starting glycerol concentration was higher (85 mM) than the concentration initially present in the liquid medium added to the reactor, due to the excess glycerol co-solvent in the PVA hydrogel that was not sufficiently removed during the pre-incubation of the hydrogel beads. It can be seen in Figure 5.33 that the trend of the reduction in glycerol concentration over the experimental run is the inverse of the cumulative hydrogen production curve provided in Figure 5.31. The glycerol concentration initially decreases slowly before being utilised at a constant rate from 48 hours to 264 hours of operation. After this the glycerol still decreases linearly over time but now at a much lower rate, which corresponds to a lower hydrogen production rate achieved by operating as PBPBR. When the configuration is reverted to a FBPBR the rate of substrate utilisation then increases back to the original rate when initially operated as a fluidised bed.

The conversion efficiency of the available electrons from glycerol to hydrogen was determined using Equation 32 in section 2.9.3. As discussed previously, the conversion efficiency in the column PBR when

cultured with planktonic cells was 32% and when operated as a FBPBR 43% was achieved over the period where the specific HPR was constant (192 to 264 hours). When the column reactors configuration was changed to the PBPBR a conversion efficiency of 26.7% was obtained over the period where the specific HPR was constant in section ii) of Figure 5.31 (336 to 432 hours).

The large error in the glycerol concentration stems from the variation in the starting concentration due to varying amount of glycerol present in the beads after washing. The consistency in the error illustrates this, as the difference in glycerol concentration over the same time for each run show negligible error.

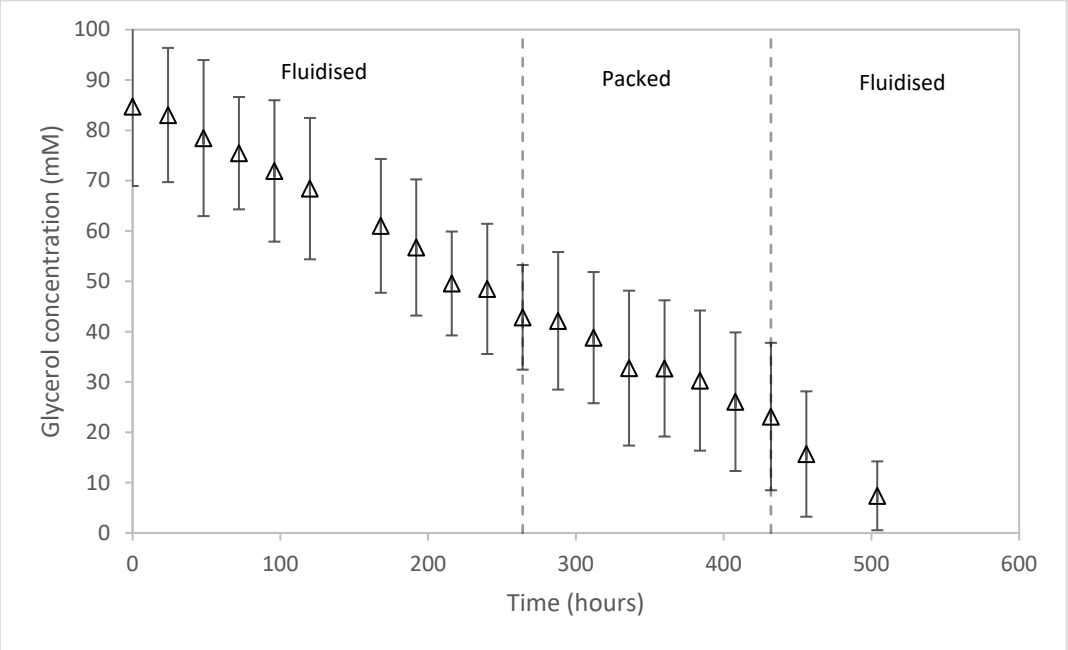

Figure 5.33: Glycerol utilization of immobilised R. palustris in the column PBR. Illumination for both reactor configurations provided by incandescent light bulbs (60 W bulbs) at an incident light intensity of 100 W/m^2. R. palustris 11774 was cultivated using modified minimal medium with glycerol (50mM). FBPBR experiments were completed at a volumetric flow rate 1.06 L/min and PBPBR experiments at a recirculation volumetric flow rate of 0.347 L/min. Data points are the mean of quadruple repeats. The error bars show the uncertainty associated with the glycerol concentrations obtained through HPLC analysis.

5.3.3 Summary of results

The maximum specific hydrogen production rate and percentage substrate conversion efficiencies of *R. palustris* obtained when operating in the column PBR with different reactor configurations are shown in Figure 5.34. It is apparent that the FBPBR is the superior configuration as it outperforms with regards to both hydrogen production and substrate conversion efficiency.

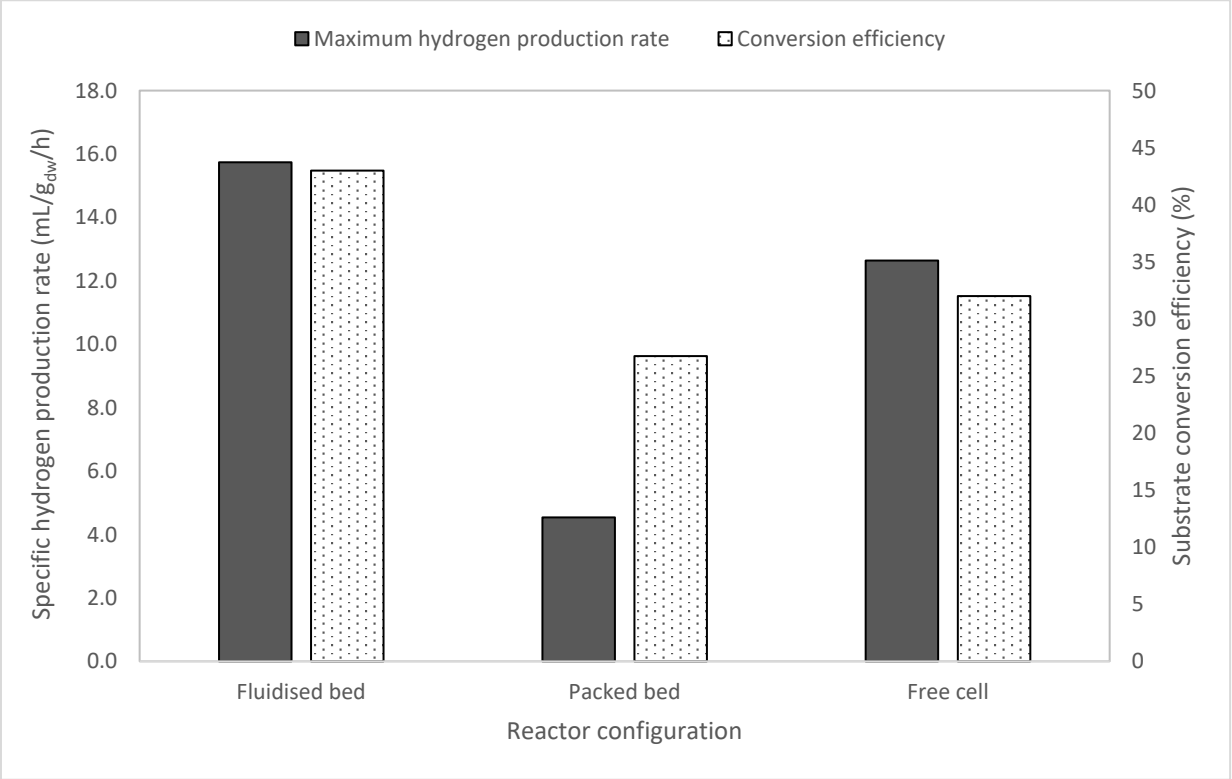

Figure 5.34: Comparison between all the bioreactor configurations used in the column PBR in terms of maximum specific hydrogen production rate and substrate conversion efficiency.

6 CONCLUSIONS

The aim of this work was to produce biological hydrogen from a synthetic waste stream (glycerol) by the photosynthetic bacteria *R. palustris*, thus leading to a renewable and clean source of energy as well as the biodegradation of a waste stream that would be an environmental burden if not used as the feedstock. The work described in this dissertation arose from the gaps identified in literature surrounding the effect of light intensity on *R. palustris* growth and the designing and developing of a new PBR system for culturing hydrogen producing *R. palustris* cells immobilised in PVA cryogel beads.

This study indicated that the upscale of photofermentation of glycerol and concomitant hydrogen production by *R. palustris* is promising due to the possibility of sustained growth over the full range of sunlight intensity experienced in a day and the overall improved performance of immobilised cells. Specific conclusions relating to the objectives proposed are detailed below.

1. **Examine the effect of light intensity on the cells and cell growth of *R. palustris* in a tubular PBR operating with a planktonic cell culture in batch configuration.**

From literature (Carlozzi, 2009; Xiao, 2017) it was identified that a possible shortcoming in the results obtained on the effect of light intensity on *R. palustris* growth and hydrogen production was the relatively large diameter reactors used. These large diameters introduce effects of light attenuation and cell mutual shading and therefore would not provide an accurate measure of the effect of light intensity on *R. palustris* kinetics. For this reason, a tubular reactor with a small inner diameter (0.015 m) was designed to minimise the effects of light attenuation during experiments on the effect of light intensity on growth kinetics of *R. palsutris*.

The main goal of this objective was to compare the effect of changing light intensity on the growth kinetics of *R. palustris.* The results of this comparison showed that *R. palustris* grows readily over the range of light intensity investigated (70 to 600 W/m^2), with photo-limitation occurring at low intensities (30 and 70 W/m^2), photosaturation between 200 and 400 W/m^2, and photo-limitation occurring when the light intensity increased to 600 W/m^2. The highest maximum specific growth rate of 0.0420±0.014 h^{-1} was achieved at a light intensity of 400 W/m^2, under the experimental conditions used. Although the maximum specific growth rate decreased by 38% when the light intensity increased from 400 to 600 W/m^2, it can still be concluded that *R. palustris* can tolerate continuous exposure to very high light intensities for over 100 hours. This is based on the good overall growth that is still achieved at the light intensity of 600 W/m^2. The growth rates obtained over the range of light intensities investigated along with observation of the daily sunlight intensity profiles indicated that outdoor culturing could be possible all year round with minimum photo-limitation and photoinhibition over the day.

The effect of changing light intensity on the bacteriochlorophyll alpha (BChl-α) to carotenoid ratio was also investigated. It was hypothesised that the BChl-α to carotenoid ratio would decrease as the light intensity increased, due to an increase in carotenoid content for protection against the high light intensities. This expected trend was not observed over the range of light intensities investigated. This is possibly due to the emission spectrum of incandescent light bulbs, which has a smaller percentage increase at the wavelength corresponding to the carotenoids compared to the increase at the wavelength corresponding to the BChl-α pigments.

2. Model the response of cell growth and average light intensity in the tubular PBR to changing light intensity.

There has been a significant amount of work done in the field of modelling of biological processes for more than 50 years. However, there has been less focus on the modelling of photosynthetic bacteria, compared to other microorganisms such as algae which have very different growth metabolisms. There has been no work on the modelling of the effect of light intensity on the growth of *R. palustris* and limited work on the modelling of average light intensity in cylindrical PBRs geometries. This gap in the literature promoted the work into modelling the attenuation of light through the tubular PBR which allowed for modelling the effect of light intensity on the growth of *R. palustris* and determination of the average light intensity in the reactor based on biomass concentration.

A method for determination of the light intensity profile based on the two flux-approximation for light attenuation was developed for the tubular reactor. This method could also be applied for column reactors with varying diameters (successfully done in section 5.2.3). A predictive model for the cell growth and substrate utilisation of *R. palustris* over the range of light intensity investigated (70 to 600 W/m^2) was successfully developed. The model showed good fit to the experimental data for each light intensity investigated, with high R^2 values and NRMSE values all below 20%. Prediction of the average light intensity in the PBR with changing biomass concentration was achieved with the trend and percentage reduction in light intensity aligning with the results reported for a similar PBR system in literature (Palamae et al., 2018).

3. **Design a PBR that could be a viable option in the culturing of *R. palustris* in both free-cell and immobilised form, and that performs at a similar or enhanced level in terms of hydrogen production and substrate conversion efficiency when compared to current lab-scale bioreactor systems.**

A column PBR that could facilitate hydrogen production by *R. palustris* cells operating in a planktonic culture or immobilised in a PVA cryogel was successfully designed and developed (see Figure A.2 in Appendix A for the detailed design). The performance of the column PBR was compared in terms of the hydrogen production and the substrate conversion efficiency to a Schott bottle bioreactor that is commonly used for culturing of *R. palustris* on laboratory scale. The results of this comparison showed that *R. palustris* cultured in the column PBR outperformed the Schott bottle reactor with regards to the cumulative hydrogen production, with the column PBR producing 2597±453 mL and the Schott bottle PBR only producing 268.75±3.98 mL. When examining the specific hydrogen production rate, the Schott bottle reactor outperformed the column PBR only slightly However, the relatively large difference in biomass concentration between the two reactors over the same culturing period does skew this comparison. Both reactor systems achieved the same substrate conversion efficiency of 32% when compared over the same timeframe.

From the above comparison the column PBR was verified as a viable option for the culturing of *R. palustris* with regards to the biomass growth, substrate degradation and the production of hydrogen. The PBR system was successfully utilised to investigate *R. palustris* immobilised in a PVA cryogel (achieved in objective 4 and 5), which meant that the designed reactor could be used for both planktonic cell culturing and as a FBPBR or PBPBR with the immobilised cells. The conclusions made with reference to the immobilised cells performance and comparison of different reactor configurations is discussed in more detail in the remaining conclusions.

The predicted average light intensity within the two reactor systems with the change in biomass concentration was determined using the model developed in section 5.1.5. From this it was determined that a 50% reduction in the average light intensity occurred in the Schott bottle reactor compared to the 20% reduction predicted in the column reactor at the same biomass concentration of ~3.25 g/L. From these results it can be concluded that the relatively small difference in the reactor diameter between the column PBR (50 mm) and the Schott bottle PBR (86 mm) causes a significant reduction in the average light intensity within the reactor. This is likely the reason for the overall improved performance in the column PBR, as the light distribution is improved within the smaller diameter and there is a reduced effect of mutual cell shading.

4. **Determine whether the hydrogen production of the immobilised bacterium is comparable to that of the free cell bacterial cultures.**

With a PBR designed and constructed that facilitated hydrogen production by *R. palustris* either as a growing planktonic cell culture or immobilised in a hydrogel matrix, the performance of the two possible bioreactor systems was investigated. During this comparison R. palustris immobilised in the PVA cryogel beads was operated in the column PBR as a fluidised bed reactor.

The results of this comparison showed that *R. palustris* immobilised in a PVA cryogel (15.74±2.2 mL/g/h) outperformed the planktonic culture (12.6±8.0 mL/g/h) in the column PBR in terms of the maximum specific hydrogen production rate achieved when operating the column PBR at the same conditions. The immobilised cells achieved a substrate conversion efficiency of 43% compared to the planktonic cells that achieved an efficiency of 32%. It can therefore be concluded that immobilisation of *R. palustris* cells lead to improved performance of the column PBR with regards to the specific hydrogen production rate and conversion efficiency.

5. **Compare the performance of the fluidised bed PBR versus the packed bed PBR based on their biological hydrogen production.**

As discussed in section 2.7 two possible reactor configurations standout as promising options to produce hydrogen from immobilised cells, i.e. PBPBR and FBPBR. It was therefore necessary to determine which reactor configuration proves to be the more viable option for operation in the designed PBR in terms of the substrate utilisation and hydrogen production kinetics.

The results of this comparison showed that *R. palustris* immobilised in a PVA cryogel operating as a FBPBR achieved a maximum specific hydrogen production rate of 15.74±2.2 mL/g/h which was significantly higher than the rate of 4.53±0.8 mL/g/h achieved when operating as a PBPBR. These results were achieved operating the column PBR at the same operating conditions with the same immobilised cells. In terms of the substrate conversion efficiency, the FBPBR achieved 43% conversion over the period of constant specific hydrogen production rate. This outperformed the PBPBR, which only achieved a conversion of 26.7% over the period of constant specific hydrogen production. It can therefore be concluded that immobilised *R. palustris* cells show improved performance operating as a FBPBR in the column PBR with regards to the specific hydrogen production rate and conversion efficiency when compared to the PBPBR.

7 RECOMMENDATIONS

The work provided in this dissertation goes some way into answering questions around the design of a process that sees the photofermentation of an organic waste stream, in this case glycerol, by *R. palustris* to produce biological hydrogen. However, the application of photofermentation to produce biohydrogen remains limited to laboratory scale applications, with no industrial implementations to date. Significant work is still required in this field of research to develop a working biological hydrogen production process.

It is believed that the PBRs designed and constructed in this thesis and the corresponding experimental testing done on the performance of the reactors and their different configurations can be used to develop and investigate a working outdoor reactor system to produce biohydrogen. Recommendations to extend the work in this thesis, leading to the development of a working outdoor biological hydrogen production process are provided in this section with the aim to upgrade this project to a PhD. The proposed research scope, key objectives, a brief methodology and the intended contribution of the final body of work is discussed in more detail below.

7.1 Proposal for PhD

7.1.1 Introduction

A biological hydrogen production process is promising. However, key issues with the process still need to be solved, such as its economic viability and whether environmentally sustainable production is possible. The economic viability can be boosted significantly by improvement of the hydrogen production and substrate utilisation through the design and development of an optimal PBR (Adessi and De Philippis, 2014). Comparison between multiple PBR systems has been identified in this study as a potential strategy to enhance the efficiency of the process. Operation of these PBRs in outdoor conditions with sun as the sole source of light energy has also been identified as a scheme for improvement of the economic and environmental sustainability of the process. This is due to solar light energy being the most abundant natural light source available on earth, the fact that it is a free in terms of the available light energy and that it contains the full spectrum of light (Chen et al., 2008). Microbial hydrogen production provides the added benefit of potential waste degradation. This increases the economic viability of the process as unwanted waste material can be used as the feed to the PBR systems.

7.1.2 Research scope

The aim of the PhD is to build onto the objectives achieved in this study by gaining insight into the effects of light-dark cycling on hydrogen production and substrate utilisation and to investigate the operation of the already designed PBR system in outdoor conditions with an industrial waste stream (crude glycerol). Multiple reactor configurations are to be investigated in the above conditions. These include as a free-cell culture, as a membrane PBR (MBPBR) and as a fluidised bed PBR (FBPBR).

Objectives set out to meet the above research aim and to be added to the objectives of this thesis is discussed below.

7.1.2.1 Objectives

1. *Examine the effect of light intensity on the cells and cell growth of R. palustris in a tubular PBR operating with a planktonic cell culture in batch configuration (**Achieved**).*
2. *Model the response of cell growth and average light intensity in the tubular PBR to changing light intensity (**Achieved**).*
3. *Design a PBR that could be a viable option in the culturing of R. palustris in both free-cell and immobilised form, and that performs at a similar or enhanced level in terms of hydrogen production and substrate conversion efficiency when compared to current lab-scale bioreactor systems (**Achieved**).*
4. *Determine whether the hydrogen production of the immobilised bacterium is comparable to that of the free cell bacterial cultures (**Achieved**).*
5. *Compare the performance of the fluidised bed PBR versus the packed bed PBR based on their biological hydrogen production (**Achieved**).*
6. *Examine the effect of light-dark cycling on the growth and hydrogen production of R. palustris in a tubular PBR operating with a planktonic cell culture in batch configuration.*

The biomass growth of a consortium of PNS bacteria (*Rhodopseudomonas*>80%) in a 12 hour light-dark cycle showed identical growth compared to continuous exposure to light (Zhi et al., 2019). This is promising for outdoor culturing with sunlight as the sole light source. However, no major work has been done on the effect of light-dark cycles on the hydrogen production metabolism of *R. palustris*. Specific emphasis will be placed on accurate representation of the light cycle to match that of sunlight which is currently not being done in literature. This objective will therefore aim to fill the gap in literature around the effect of light-dark cycles on the overall performance of a possible outdoor production process.

7. *Design and construct a MBPBR that could be a viable option in the culturing of R. palustris to produce biohydrogen and a clean aqueous product that requires no downstream processing.*

In conventional wastewater treatment the biomass that has consumed the organic waste requires separation from the aqueous phase which is usually done *via* sedimentation. The aqueous phase will typically still require downstream processing to obtain 'clean' water that can either be reused or is safe to dispose of into natural water sources. The membrane bioreactor (MBR) can replace this two-step separation process by filtering the biomass through a membrane, which results in a high-quality water product requiring little or no further downstream processing (Judd, 2008). The biomass can also be recycled for reuse in the system. MBR systems have been used in conjunction with *R. palustris* (Chitapornpan et al., 2013, 2012; González et al., 2017) for the treatment of industrial waste waters, but no work has been done on the development of a MBPBR system for the dual purpose of waste treatment and hydrogen production from *R. palustris*.

8. *Investigate hydrogen production and substrate utilisation by R. palustris in multiple outdoor PBR systems with crude glycerol (CG) as the industrial waste stream.*

The next step from the designed PBR systems is the development of a working outdoor biological hydrogen production process that uses an industrial waste stream as the feedstock. *R. palustris* is able to metabolise a number of compounds which are relatively tough to remove from wastewaters, including aromatic compounds, dyes and phenolics. However CG has been selected as the industrial feedstock because it is a substrate that can facilitate hydrogen production after certain pre-treatment (Pott et al., 2013). The column PBR designed in this thesis will be used in outdoor conditions to investigate the performance of a free-cell culture, a MBPBR operating with planktonic cells and the novel immobilised system in the FBPBR configuration in terms of hydrogen production and treatment of the industrial wastewater.

7.1.3 Methodology

The methodology required for completion of objectives that have not yet been achieved are discussed.

Objective 6:

The PBR system required for this investigation has already be designed and used in this thesis. A design sheet of the tubular PBR is provided in Figure A.1 in Appendix A and the operational procedure of the tubular PBR system is described in 4.4.1.3. Hydrogen production is required in this objective, therefore minimal medium will be used in place of the modified Van Niels medium that was used in the tubular PBR in this thesis.

Currently work into investigating the effect of light-dark cycles on photosynthetic bacteria growth and hydrogen production (Koku et al., 2003; Uyar et al., 2007; Wakayama et al., 2000) have used a simple on/off control to mimic the light-dark cycle that would be experienced when bioreactors are operated outdoors. As illustrated in Figure #, sunlight intensity ramps up and down through the day, following the trend of a sinusoidal curve, and does not merely follow the trend of a step-up and step-down function which is seen in an on/off controller. Therefore, a light controller is to be designed and constructed that will give a more accurate light-dark cycle in terms of mimicking the trend of sunlight. This controller will use an Arduino board to control a dimmer switch, which will allow for adjustment of the light intensity to mimic the trend of sunlight seen through a day.

Objective 7:

Membrane reactors can be used in free cell systems and immobilised systems. Membrane bioreactors (MBR) have a variety of applications and are broadly defined as a flow reactor that is combined with a membrane that is used to separate bacteria from the feed or product stream (Wang and Zhong, 2007).

Figure 7.1 below provides the schematic diagram of the MBPBR system that will be used to achieve the second objective. The column PBR used in this thesis will be adapted to include the membrane system for investigation into the performance of the MBPBR system. The membrane system has already been developed and consists of an Atech single-channel ultrafiltration (UF) ceramic (Al_2O_3) membrane element with an active surface area of 50 cm^2 and selectivity of 100 kD housed in a stainless steel case which will allow for the entire system to be autoclaved This membrane was selected based on preliminary testing already done with a similar membrane (selectivity of 1 kD). Preliminary tests indicate that *R. palustris* growth was not affected by the inclusion of the membrane into the reactor system. Therefore, the membrane described should be well suited for investigation of MBPBR system for the treatment of a synthetic waste stream with the added benefit of hydrogen production.

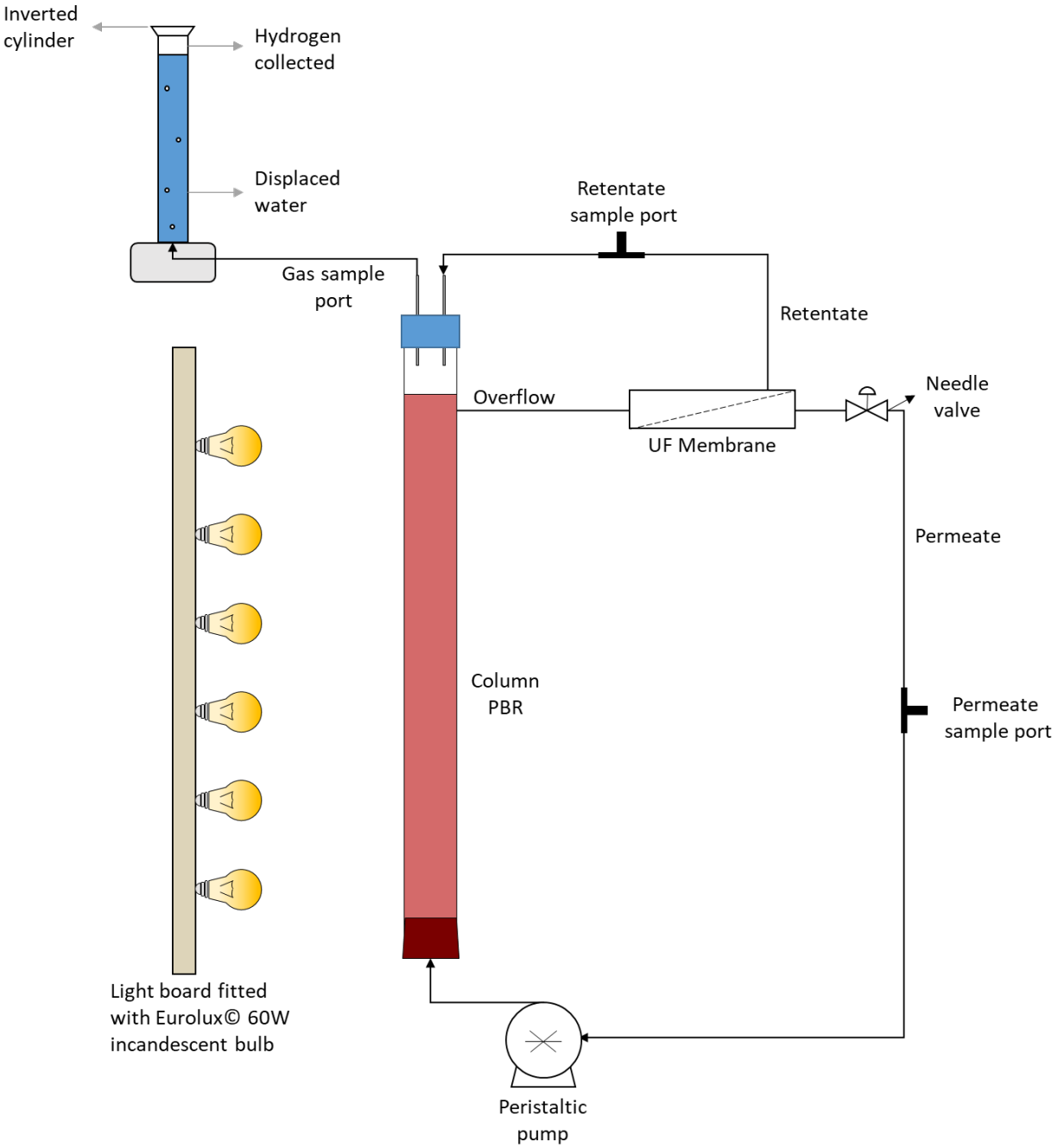

Figure 7.1: *Schematic diagram of the* MB*PBR system operating with a free-cell culture. The above diagram is the side view of the entire setup. The culture was recirculated using a peristaltic pump and the reactor was illuminated by six 60W Eurolux incandescent light bulbs.*

Objective 8:

The three PBR systems that are to be tested in outdoor conditions with CG as the feedstock is the free-cell batch culture, the MBPBR operating with a free-cell culture and the FBPBR operating with immobilised *R. palustris*.

A limiting factor in using CG as a feedstock for biological treatment and conversion to hydrogen is the high impurities present that accrue during the biodiesel production process. The main inhibitory factor present in CG has been identified as saponified fatty acids which can be removed through addition of a calcium chloride solution which promotes formation of calcium salt precipitate that can then be filtered out (Pott et al., 2013). The treated crude glycerol (TCG) has been successfully fermented by *R. palustris* at concentrations as high as 1370 mM (Pott et al., 2013) which is approximately 126 g/L.

The operating procedure of the free-cell batch culture is provided in section 4.4.1.4. The column PBR will be operated in the configuration shown in Figure 4.4 in outdoor conditions with TCG as the feedstock. The outdoor location is on the roof of a four-story building to maximise the duration in which the reactor obtains direct sunlight.

The operating procedure of the FBPBR is provided in section 4.4.3. The column PBR loaded with immobilised *R. palustris* will be operated in the configuration shown in Figure 4.6 in outdoor conditions with TCG as the feedstock.

The operating protocol of the MBPBR is still to be fully developed but will likely follow the procedure set out for the cell-free PBR described in section 4.4.1.4, with alterations in place to include the membrane system described in the methodology for objective 2. The column PBR will be operated in the configuration shown in Figure 7.1 in outdoor conditions with TCG as the feedstock

7.1.4 Intended contribution

A substantial amount of the intended work is drawn from the identified gap in the literature reviewed. Completion of this work and meeting of the stipulated objectives will aim to fill these identified gaps, which will lead to novel designs in the field of PBR design and contribute new science to the field of bioprocess engineering. Some of the expected outcomes and intended contributions of this upgraded PhD is discussed below:

1. Design and development of a novel FBPBR for the production of hydrogen from a synthetic waste stream by *R. palustris* immobilised a PVA cryogel (completed).
2. The effects of light intensity and light-dark cycles on the growth and hydrogen production by *R. palustris* contributes to the further understanding operating PBRs in outdoor conditions which aid

in the development of a working biological hydrogen production process (partially completed with work to be done as part of the upgraded study).

3. Work on the design and development of a MBPBR to produce hydrogen by *R. palustris* has been linked to a potential patent which has meant that a non-disclosure on this work has been established (designed and currently being set up, with experimentation still to be done).
4. The work that has been completed and the work that is still to be done are to be submitted in the form of articles for potential publication in peer reviewed journals. These articles and the possible journals for publication are provided in the table below:

Table 7.1: Proposed articles for submission for peer review in the listed journals.

No.	Article title	Proposed journal	Status
1	Investigating and modelling the effect of light intensity on *Rhodopseudomonas palustris* growth.	Chemical Engineering Journal	WUP
2	Biohydrogen production by *Rhodopseudomonas palustris* immobilised in a PVA cryogel in a novel fluidised bed photobioreactor.	Journal of Cleaner Production	WUP
3	Evaluation of a membrane bioreactor for the production of hydrogen and treatment of crude glycerol by *Rhodopseudomonas palustris.*	Journal of Membrane Science	WSP
4	The effect of light-dark cycles on hydrogen production by the photosynthetic bacteria *Rhodopseudemonas palustris.*	Bioresource Technology	WSP
5	Evaluation of multiple photobioreactor configurations to facilitate photofermentation of crude glycerol and biohydrogen production.	Chemical Engineering Science	WSP

WUP – Write-up in progress

WSP – Written if studies progress

8 REFERENCES

Acar, C., Dincer, I., 2014. Comparative assessment of hydrogen production methods from renewable and non-renewable sources. Int. J. Hydrogen Energy 39, 1–12. https://doi.org/10.1016/j.ijhydene.2013.10.060

Adessi, A., De Philippis, R., 2014. Photobioreactor design and illumination systems for H2production with anoxygenic photosynthetic bacteria: A review. Int. J. Hydrogen Energy 39, 3127–3141. https://doi.org/10.1016/j.ijhydene.2013.12.084

Ahmed, E.M., 2015. Hydrogel: Preparation, characterization, and applications: A review. J. Adv. Res. 6, 105–121. https://doi.org/10.1016/j.jare.2013.07.006

Balat, M., 2008. Potential importance of hydrogen as a future solution to environmental and transportation problems. Int. J. Hydrogen Energy 33, 4013–4029. https://doi.org/10.1016/j.ijhydene.2008.05.047

Barbosa, M.J., Rocha, J.M.S., Tramper, J., Wijffels, R.H., 2001. Acetate as a carbon source for hydrogen production by photosynthetic bacteria. J. Biotechnol. 85, 25–33. https://doi.org/10.1016/S0168-1656(00)00368-0

Basak, N., Jana, A.K., Das, D., 2016. CFD modeling of hydrodynamics and optimization of photofermentative hydrogen production by Rhodopseudomonas palustris DSM 123 in annular photobioreactor. Int. J. Hydrogen Energy 41, 7301–7317. https://doi.org/10.1016/j.ijhydene.2016.02.126

Berberoglu, H., Yin, J., Pilon, L., 2007. Light transfer in bubble sparged photobioreactors for H2 production and CO2 mitigation. Int. J. Hydrogen Energy 32, 2273–2285. https://doi.org/10.1016/j.ijhydene.2007.02.018

Blankenship, R.E., Madigan, M.T., Bauer, C.E. (Eds.), 2006. Anoxygenic photosynthetic bacteria (Vol. 2). Springer Science & Business Media.

Blomen, L.J.M.J., Mugerwa, M.N. (Eds.), 2013. Fuel Cell Systems - Google Books. Springer Science & Business Media.

Brenner, D.J., Krieg, N.R., Staley, J.T., 2005. Bergey's Manual of Systematic Bacteriology (Vol. 2), Second. ed. Springer.

Burris, R., 1991. Nitrogenases. J. Biol. Chem 266, 9339–9342.

Carlozzi, P., 2009. The effect of irradiance growing on hydrogen photoevolution and on the kinetic growth in Rhodopseudomonas palustris, strain 42OL. Int. J. Hydrogen Energy 34, 7949–7958.

https://doi.org/10.1016/j.ijhydene.2009.07.083

Carlozzi, P., Sacchi, A., 2001. Biomass production and studies on Rhodopseudomonas palustris grown in an outdoor, temperature controlled, underwater tubular photobioreactor. J. Biotechnol. 88, 239–249. https://doi.org/10.1016/S0168-1656(01)00280-2

Çengel, Y.A., Boles, M.A., 2006. Thermodynamics : an engineering approach, 5th ed. ed, McGraw-Hill series in mechanical engineering. McGraw-Hill Higher Education, Boston.

Chen, C.Y., Lee, C.M., Chang, J.S., 2006. Hydrogen production by indigenous photosynthetic bacterium Rhodopseudomonas palustris WP3-5 using optical fiber-illuminating photobioreactors. Biochem. Eng. J. 32, 33–42. https://doi.org/10.1016/j.bej.2006.08.015

Chen, C.Y., Saratale, G.D., Lee, C.M., Chen, P.C., Chang, J.S., 2008. Phototrophic hydrogen production in photobioreactors coupled with solar-energy-excited optical fibers. Int. J. Hydrogen Energy 33, 6886–6895. https://doi.org/10.1016/j.ijhydene.2008.09.014

Chitapornpan, S., Chiemchaisri, C., Chiemchaisri, W., Honda, R., Yamamoto, K., 2013. Organic carbon recovery and photosynthetic bacteria population in an anaerobic membrane photo-bioreactor treating food processing wastewater. Bioresour. Technol. 141, 65–74. https://doi.org/10.1016/j.biortech.2013.02.048

Chitapornpan, S., Chiemchaisri, C., Chiemchaisri, W., Honda, R., Yamamoto, K., 2012. Photosynthetic bacteria production from food processing wastewater in sequencing batch and membrane photo-bioreactors. Water Sci. Technol. 65, 504–512. https://doi.org/10.2166/wst.2012.740

Clarke, K.G., 2013. Bioprocess engineering an introductory engineering and life science approach. Woodhead Publishing, Oxford.

Coiffier, A., Coradin, T., Roux, C., Bouvet, O.M. and Livage, J., 2001. Sol–gel encapsulation of bacteria: a comparison between alkoxide and aqueous routes. J. Mater. Chem. 11, 2039–2044.

Cornet, J.F., Dussap, C.G., Gros, J.B., Binois, C., Lasseur, C.A., 1995. A SIMPLIFIED M O N O D I M E N S I O N A L APPROACH FOR M O D E L I N G COUPLING BETWEEN RADIANT LIGHT TRANSFER A N D GROWTH KINETICS IN 50.

Crabtree, G.W., Dresselhaus, M.S., 2008. The hydrogen fuel alternative. MRS Bull. 33, 421–428. https://doi.org/10.1557/mrs2008.84

Crabtree, G.W., Dresselhaus, M.S., Buchanan, M. V, 2004. If the fuel cell is to become the modern steam engine , basic. Phys. Today 39–45.

Dambies, L., Vincent, T., Domard, A., Guibal, E., 2001. Preparation of chitosan gel beads by ionotropic

molybdate gelation. Biomacromolecules 2, 1198–1205. https://doi.org/10.1021/bm010083r

Damjanović, A., Ritz, T., Schulten, K., 1999. Energy transfer between carotenoids and bacteriochlorophylls in light-harvesting complex II of purple bacteria. Phys. Rev. E - Stat. Physics, Plasmas, Fluids, Relat. Interdiscip. Top. 59, 3293–3311. https://doi.org/10.1103/PhysRevE.59.3293

Das, D., Veziroğlu, T.N., 2001. Hydrogen production by biological processes: A survey of literature. Int. J. Hydrogen Energy 26, 13–28. https://doi.org/10.1016/S0360-3199(00)00058-6

Dervakos, G.A., Webb, C., 1991. On the merits of viable-cell immobilisation. Biotechnol. Adv. 9, 559–612. https://doi.org/10.1016/0734-9750(91)90733-C

Dincer, I., Joshi, A.S., 2013. Solar Based Hydrogen Production Systems 7–21. https://doi.org/10.1007/978-1-4614-7431-9

Eroglu, E., Melis, A., 2011. Photobiological hydrogen production: Recent advances and state of the art. Bioresour. Technol. 102, 8403–8413. https://doi.org/10.1016/j.biortech.2011.03.026

Evans, M.B., Hawthornthwaite, A.M., Cogdell, R.J., 1990. Isolation and characterisation of the different B800-850 light-harvesting complexes from low- and high-light grown cells of Rhodopseudomonas palustris, strain 2.1.6. BBA - Bioenerg. 1016, 71–76. https://doi.org/10.1016/0005-2728(90)90008-R

Fiβler, J., Kohring, G.W., Griffhorn, F., 1995. Enhanced hydrogen production from aromatic acids by immobilized cells of Rhodopseudomonas palustris 43–46.

Ghosh, D., Tourigny, A., Hallenbeck, P.C., 2012. Near stoichiometric reforming of biodiesel derived crude glycerol to hydrogen by photofermentation. Int. J. Hydrogen Energy 37, 2273–2277. https://doi.org/10.1016/j.ijhydene.2011.11.011

Godwin, D., Slater, J.H., 1979. The influence of the growth environment on the stability of a drug resistance plasmid in Escherichia coli K12. J. Gen. Microbiol. 111, 201–210. https://doi.org/10.1099/00221287-111-1-201

González, E., Díaz, O., Ruigómez, I., de Vera, C.R., Rodríguez-Gómez, L.E., Rodríguez-Sevilla, J., Vera, L., 2017. Photosynthetic bacteria-based membrane bioreactor as post-treatment of an anaerobic membrane bioreactor effluent. Bioresour. Technol. 239, 528–532. https://doi.org/10.1016/j.biortech.2017.05.042

Guo, C.L., Zhu, X., Liao, Q., Wang, Y.Z., Chen, R., Lee, D.J., 2011. Enhancement of photo-hydrogen production in a biofilm photobioreactor using optical fiber with additional rough surface. Bioresour. Technol. 102, 8507–8513. https://doi.org/10.1016/j.biortech.2011.04.075

Hallenbeck, P.C., 2009. Fermentative hydrogen production: Principles, progress, and prognosis. Int. J. Hydrogen Energy 34, 7379–7389. https://doi.org/10.1016/j.ijhydene.2008.12.080

Hallenbeck, P.C., Ghosh, D., 2009. Advances in fermentative biohydrogen production: the way forward? Trends Biotechnol. 27, 287–297. https://doi.org/10.1016/j.tibtech.2009.02.004

Hay, J.X.W., Wu, T.Y., Juan, J.C., 2013. Biohydrogen production through photo fermentation or dark fermentation using waste as a substrate: Overview, economics, and future prospects of hydrogen usage. Biofuels, Bioprod. Biorefining 6, 246–256. https://doi.org/10.1002/bbb

Höök, M., Tang, X., 2013. Depletion of fossil fuels and anthropogenic climate change-A review. Energy Policy 52, 797–809. https://doi.org/10.1016/j.enpol.2012.10.046

Hu, X., Ritz, T., Damjanović, A., Autenrieth, F., Schulten, K., 2002. Photosynthetic apparatus of purple bacteria, Quarterly Reviews of Biophysics. Stellenbosch University. https://doi.org/10.1017/S0033583501003754

Huang, J., Feng, F., Wan, M., Ying, J., Li, Y., Qu, X., Pan, R., Shen, G., Li, W., 2015. Improving performance of flat-plate photobioreactors by installation of novel internal mixers optimized with computational fluid dynamics. Bioresour. Technol. 182, 151–159. https://doi.org/10.1016/j.biortech.2015.01.067

Hyon, S., Cha, W., Ikada, Y., 1989. Polymer Bulletin 9. Polym. Bull. 29, 119–126. https://doi.org/10.1007/BF00310794

IPCC, 2007. Climate Change 2007 Synthesis Report, Intergovernmental Panel on Climate Change [Core Writing Team IPCC. https://doi.org/10.1256/004316502320517344

Judd, S., 2008. The status of membrane bioreactor technology. Trends Biotechnol. 26, 109–116. https://doi.org/10.1016/j.tibtech.2007.11.005

Kalamaras, C.M., Efstathiou, a. M., 2013. Hydrogen Production Technologies: Current State and Future Developments. Conf. Pap. Energy 2013, 9. https://doi.org/10.1155/2013/690627

Khanal, S.K., Rasmussen, M., Shrestha, Prachand, Van Leeuwen, H.J., Visvanathan, C., Liu, Hong, Shrestha, P, Leeuwen, H. Van, Visvanathan, C., Liu, H, Rausch, K., Belyea, R., Oren, A., Clomburg, JM, Gonzalez, R., Durnin, G., Clomburg, J, Yeates, Z., Alvarez, P., Zygourakis, K., Campbell, P., Gonzalez, R., Gonzalez, R., Murarka, A., Dharmadi, Y., Yazdani, S., Murarka, A., Dharmadi, Y., Yazdani, S., Gonzalez, R., Gonzalez, R., Campbell, P., Wong, M., Nikel, P., Ramirez, M., Pettinari, M., Méndez, B., Galvagno, M., Trinh, C., Srienc, F., Yazdani, S., Gonzalez, R., Hu, H., Wood, T., Zhu, YH, Eiteman, M., Lee, S., Altman, A., Zhang, XL, Shanmugam, K., Ingram, L., Mazumdar, S., Clomburg, JM, Gonzalez, R., Hofvendahl, K., Hahn-Hagerdal, B., Okano, K., Tanaka, T., Ogino, C., Fukuda, H., Kondo, A., Kharas,

G., Sanchez-Riera, F., Severson, D., Vaidya, A., Pandey, R., Mudliar, S., Kumar, M., Chakrabarti, T., Devotta, S., Chang, D., Jung, H., Rhee, J., Pan, J., Dien, B., Nichols, N., Bothast, R., Zhou, S., Shanmugam, K., Ingram, L., Zhu, Y, Eiteman, M., DeWitt, K., Altman, E., Baldoma, L., Aguilar, J., Booth, I., Ferguson, G., Miller, S., Li, C., Gunasekera, B., Kinghorn, S., Booth, I., Totemeyer, S., Booth, N., Nichols, W., Dunbar, B., Booth, I., Schweizer, H., Larson, T., Walz, A., Demel, R., Kruijff, B. de, Mutzel, R., Iuchi, S., Aristarkhov, A., Dong, J., Taylor, J., Lin, E., Yazdani, S., Gonzalez, R., Unden, G., Dünnwald, P., Kashket, E., Jantama, K., Haupt, M., Svoronos, S., Zhang, XL, Moore, J., Shanmugam, K., Ingram, L., Yomano, L., York, S., Zhou, S., Shanmugam, K., Ingram, L., Zhang, X, Jantama, K., Moore, J., Shanmugam, K., Ingram, L., Miller, J., Baba, T., Ara, T., Hasegawa, M., Takai, Y., Okumura, Y., Baba, M., Datsenko, K., Tomita, M., Wanner, B., Mori, H., Metcalf, W., Jiang, W., Daniels, L., Kim, S., Haldimann, A., Wanner, B., Wyckoff, H., Chow, J., Whitehead, T., Cotta, M., Kang, Y., Durfee, T., Glasner, J., Qiu, Y., Frisch, D., Winterberg, K., Blattner, F., Datsenko, K., Wanner, B., Sambrook, J., Fritsch, E., Maniatis, T., Neidhardt, F., Bloch, P., Smith, D., Dharmadi, Y., Gonzalez, R., Dharmadi, Y., Murarka, A., Gonzalez, R., Severn, D., Johnson, M., Olson, N., Tarmy, E., Kaplan, N., 2008. Bioenergy and Biofuel Production from Wastes/Residues of Emerging Biofuel Industries. Water Environ. Res. 80, 1625–1647. https://doi.org/10.2175/106143008X328752

Kim, D.H., Kim, M.S., 2011. Hydrogenases for biological hydrogen production. Bioresour. Technol. 102, 8423–8431. https://doi.org/10.1016/j.biortech.2011.02.113

Koku, H., Eroğlu, I., Gündüz, U., Yücel, M., Türker, L., 2003. Kinetics of biological hydrogen production by the photosynthetic bacterium Rhodobacter sphaeroides O.U. 001. Int. J. Hydrogen Energy 28, 381–388. https://doi.org/10.1016/S0360-3199(02)00080-0

Koku, H., Erolu, I., Gündüz, U., Yücel, M., Türker, L., 2002. Aspects of the metabolism of hydrogen production by Rhodobacter sphaeroides. Int. J. Hydrogen Energy 27, 1315–1329. https://doi.org/10.1016/S0360-3199(02)00127-1

Konieczny, A., Mondal, K., Wiltowski, T., Dydo, P., 2008. Catalyst development for thermocatalytic decomposition of methane to hydrogen. Int. J. Hydrogen Energy 33, 264–272. https://doi.org/10.1016/j.ijhydene.2007.07.054

Kovarova-Kovar, K., Egli, T., 1998. Growth Kinetics of Suspended Microbial Cells: From Single-Substrate-Controlled Growth to Mixed-Substrate Kinetics. Microbiol. Mol. Biol. Rev. 62, 646.

Krujatz, F., Illing, R., Krautwer, T., Liao, J., Helbig, K., Goy, K., Opitz, J., Cuniberti, G., Bley, T., Weber, J., 2015. Light-field-characterization in a continuous hydrogen-producing photobioreactor by optical simulation and computational fluid dynamics. Biotechnol. Bioeng. 112, 2439–2449. https://doi.org/10.1002/bit.25667

Larimer, F.W., Chain, P., Hauser, L., Lamerdin, J., Malfatti, S., Do, L., Land, M.L., Pelletier, D.A., Beatty, J.T., Lang, A.S., Tabita, F.R., Gibson, J.L., Hanson, T.E., Bobst, C., Torres Y Torres, J.L., Peres, C., Harrison, F.H., Gibson, J., Harwood, C.S., 2004. Complete genome sequence of the metabolically versatile photosynthetic bacterium Rhodopseudomonas palustris. Nat. Biotechnol. 22, 55–61. https://doi.org/10.1038/nbt923

Lee, H.S., Vermaas, W.F.J., Rittmann, B.E., 2010. Biological hydrogen production: Prospects and challenges. Trends Biotechnol. 28, 262–271. https://doi.org/10.1016/j.tibtech.2010.01.007

Levin, D.B., Pitt, L., Love, M., 2004. Biohydrogen production: Prospects and limitations to practical application. Int. J. Hydrogen Energy 29, 173–185. https://doi.org/10.1016/S0360-3199(03)00094-6

Liao, Q., Wang, Y.J., Wang, Y.Z., Zhu, X., Tian, X., Li, J., 2010. Formation and hydrogen production of photosynthetic bacterial biofilm under various illumination conditions. Bioresour. Technol. 101, 5315–5324. https://doi.org/10.1016/j.biortech.2010.02.019

Liu, Y., 2007. Overview of some theoretical approaches for derivation of the Monod equation. Appl. Microbiol. Biotechnol. 73, 1241–1250. https://doi.org/10.1007/s00253-006-0717-7

Lozinsky, V.I., Plieva, F.M., 1998. Poly(vinyl alcohol) cryogels employed as matrices for cell immobilization. 3. Overview of recent research and developments. Enzyme Microb. Technol. 23, 227–242. https://doi.org/10.1016/S0141-0229(98)00036-2

Mahanta, D.J., Borah, M., Saikia, P., 2014. A Study on Kinetic Models for Analysing the Bacterial Growth Rate 68–72.

Mcewan, A.G., 1994. Photosynthetic electron transport and anaerobic metabolism in purple non-sulfur phototrophic bacteria 151–152.

McKinlay, J.B., Harwood, C.S., 2010. Carbon dioxide fixation as a central redox cofactor recycling mechanism in bacteria. Proc. Natl. Acad. Sci. U. S. A. 107, 11669–11675. https://doi.org/10.1073/pnas.1006175107

McKinlay, J.B., Oda, Y., Ruhl, M., Posto, A.L., Sauer, U., Harwood, C.S., 2014. Non-growing rhodopseudomonas palustris increases the hydrogen gas yield from acetate by shifting from the glyoxylate shunt to the tricarboxylic acid cycle. J. Biol. Chem. 289, 1960–1970. https://doi.org/10.1074/jbc.M113.527515

McMichael, A.J., 2013. Globalization, Climate Change, and Human Health. N. Engl. J. Med. 368, 1335–1343. https://doi.org/10.1056/NEJMra1109341

Molina Grima, E., Acién Fernández, F.G., García Camacho, F., Chisti, Y., 1999. Photobioreactors: light

regime, mass transfer, and scaleup. Prog. Ind. Microbiol. 35, 231–247. https://doi.org/10.1016/S0079-6352(99)80118-0

Obeid, J., Magnin, J.P., Flaus, J.M., Adrot, O., Willison, J.C., Zlatev, R., 2009. Modelling of hydrogen production in batch cultures of the photosynthetic bacterium Rhodobacter capsulatus. Int. J. Hydrogen Energy 34, 180–185. https://doi.org/10.1016/j.ijhydene.2008.09.081

Palamae, S., Choorit, W., Dechatiwongse, P., Zhang, D., Antonio del Rio-Chanona, E., Chisti, Y., 2018. Production of renewable biohydrogen by Rhodobacter sphaeroides S10: A comparison of photobioreactors. J. Clean. Prod. 181, 318–328. https://doi.org/10.1016/j.jclepro.2018.01.238

Paţachia, S., Florea, C., Friedrich, C., Thomann, Y., 2009. Tailoring of poly(vinyl alcohol) cryogels properties by salts addition. Express Polym. Lett. 3, 320–331. https://doi.org/10.3144/expresspolymlett.2009.40

Paulsen, H., Universität, B. Der, Mainz, D.-, 1999. Chapter 7 Carotenoids and the Assembly of Light-harvesting Complexes. Photochemistry 123–135.

Pott, R.W.M., 2013. The Bioconversion of Waste Glycerol into Hydrogen by Rhodopseudomonas palustris.

Pott, R.W.M., Howe, C.J., Dennis, J.S., 2013. Photofermentation of crude glycerol from biodiesel using Rhodopseudomonas palustris: Comparison with organic acids and the identification of inhibitory compounds. Bioresour. Technol. 130, 725–730. https://doi.org/10.1016/j.biortech.2012.11.126

Pruvost, J., Le Gouic, B., Lepine, O., Legrand, J., Le Borgne, F., 2016. Microalgae culture in building-integrated photobioreactors: Biomass production modelling and energetic analysis. Chem. Eng. J. 284, 850–861. https://doi.org/10.1016/j.cej.2015.08.118

Ren, H.Y., Liu, B.F., Ding, J., Xie, G.J., Zhao, L., Xing, D.F., Guo, W.Q., Ren, N.Q., 2012. Continuous photo-hydrogen production in anaerobic fluidized bed photo-reactor with activated carbon fiber as carrier. RSC Adv. 2, 5531–5535. https://doi.org/10.1039/c2ra20420g

Rhodes, M., 2008. Introduction to Particle Technology, Second. ed. Wiley.

Robinson, J.A., Tiedje, J.M., 1983. Nonlinear estimation of monod growth kinetic parameters from a single substrate depletion curve. Appl. Environ. Microbiol. 45, 1453–1458.

Roszak, A.W., Howard, T.D., Southall, J., Gardiner, A.T., Law, C.J., Isaacs, N.W., Cogdell, R.J., 2003. Crystal Structure of the RC-LH1 Core Complex from Rhodopseudomonas palustris. Science (80-.). 302, 1969–1972. https://doi.org/10.1126/science.1088892

Sabourin-Provost, G., Hallenbeck, P.C., 2009. High yield conversion of a crude glycerol fraction from biodiesel production to hydrogen by photofermentation. Bioresour. Technol. 100, 3513–3517.

https://doi.org/10.1016/j.biortech.2009.03.027

Schuster, A., 1905. RADIATION THROUGH A FOGGY ATMOSPHERE. Astrophys. J.

Shiva Kumar, S., Himabindu, V., 2019. Hydrogen production by PEM water electrolysis – A review. Mater. Sci. Energy Technol. 2, 442–454. https://doi.org/10.1016/j.mset.2019.03.002

Soon, T.K., Al-Azad, S., Ransangan, J., 2014. Isolation and characterization of purple non-sulfur bacteria, Afifella marina, producing large amount of carotenoids from mangrove microhabitats. J. Microbiol. Biotechnol. 24, 1034–1043. https://doi.org/10.4014/jmb.1308.08072

Tandori, J., Hideg, É., Nagy, L., Maróti, P., Vass, I., 2001. Photoinhibition of carotenoidless reaction centers from Rhodobacter sphaeroides by visible light. Effects on protein structure and electron transport. Photosynth. Res. 70, 175–184. https://doi.org/10.1023/A:1017907404325

Tian, X., Liao, Q., Zhu, X., Wang, Y., Zhang, P., Li, J., Wang, H., 2010. Characteristics of a biofilm photobioreactor as applied to photo-hydrogen production. Bioresour. Technol. 101, 977–983. https://doi.org/10.1016/j.biortech.2009.09.007

Uyar, B., Eroglu, I., Yücel, M., Gündüz, U., Türker, L., 2007. Effect of light intensity, wavelength and illumination protocol on hydrogen production in photobioreactors. Int. J. Hydrogen Energy 32, 4670–4677. https://doi.org/10.1016/j.ijhydene.2007.07.002

Vincenzini, M., Materassi, R., Tredici, M.R., Florenzano, G., 1982. Hydrogen production by immobilized cells-II. H2-photoevolution and waste-water treatment by agar-entrapped cells of Rhodopseudomonas palustris and Rhodospirillum molischianum. Int. J. Hydrogen Energy 7, 725–728. https://doi.org/10.1016/0360-3199(82)90021-0

Virtuani, A., Lotter, E., Powalla, M., 2006. Influence of the light source on the low-irradiance performance of Cu(In,Ga)Se2 solar cells. Sol. Energy Mater. Sol. Cells 90, 2141–2149. https://doi.org/10.1016/j.solmat.2005.01.022

Wágner, D.S., Valverde-Pérez, B., Plósz, B.G., 2018. Light attenuation in photobioreactors and algal pigmentation under different growth conditions – Model identification and complexity assessment. Algal Res. 35, 488–499. https://doi.org/10.1016/j.algal.2018.08.019

Wakayama, T., Nakada, E., Asada, Y., Miyake, J., 2000. Effect of light/dark cycle on bacterial hydrogen production by Rhodobacter sphaeroides RV: From hour to second range. Appl. Biochem. Biotechnol. - Part A Enzym. Eng. Biotechnol. 84–86, 431–440. https://doi.org/10.1385/ABAB:84-86:1-9:431

Wall, J.D., 2004. Rain or shine - A phototroph that delivers. Nat. Biotechnol. 22, 40–41. https://doi.org/10.1038/nbt0104-40

Wan, W., Bannerman, a. D., Yang, L., Mak, H., 2014. Polymeric cryogels macroporous gels with remarkable properties, Advances in Polymer Science. https://doi.org/10.1007/978-3-319-05846-7

Wang, S., Zhong, J., 2007. Chapter 6 . Bioreactor Engineering. Science (80-.). 131–161. https://doi.org/http://dx.doi.org/10.1016/B978-044452114-9/50007-4

Wang, Y.Z., Liao, Q., Zhu, X., Chen, R., Guo, C.L., Zhou, J., 2013. Bioconversion characteristics of Rhodopseudomonas palustris CQK 01 entrapped in a photobioreactor for hydrogen production. Bioresour. Technol. 135, 331–338. https://doi.org/10.1016/j.biortech.2012.09.105

Wang, Y.Z., Liao, Q., Zhu, X., Tian, X., Zhang, C., 2010. Characteristics of hydrogen production and substrate consumption of Rhodopseudomonas palustris CQK 01 in an immobilized-cell photobioreactor. Bioresour. Technol. 101, 4034–4041. https://doi.org/10.1016/j.biortech.2010.01.045

Westmacott, D., Primrose, S.B., 1976. Synchronous growth of Rhodopseudomonas palustris from the swarmer phase. J. Gen. Microbiol. 94, 117–125. https://doi.org/10.1099/00221287-94-1-117

Whittenbury, R., McLee, A.G., 1967. Rhodopseudomonas palustris and Rh. viridis-Photosynthetic budding bacteria. Arch. Mikrobiol. 59, 324–334. https://doi.org/10.1007/BF00406346

Wu, X., Wang, X., Yang, H., Guo, L., 2010. A comparison of hydrogen production among three photosynthetic bacterial strains. Int. J. Hydrogen Energy 35, 7194–7199. https://doi.org/10.1016/j.ijhydene.2009.12.141

Xiao, N., 2017. Use a Purple Non-Sulphur Bacterium , Rhodopseudomonas palustris , as a Biocatalyst for Hydrogen Production. https://doi.org/https://doi.org/10.17863/CAM.16680

Xu, Z., 2007. Chapter 21 – Biological Production of Hydrogen from Renewable Resources, Bioprocessing for Value-Added Products from Renewable Resources. Elsevier B.V. https://doi.org/10.1016/B978-044452114-9/50022-0

Yang, Z., Yang, Huijuan, Yang, Hongshun, 2018. Characterisation of rheology and microstructures of κ-carrageenan in ethanol-water mixtures. Food Res. Int. 107, 738–746. https://doi.org/10.1016/j.foodres.2018.03.016

Yen, H.W., Chiang, W.C., 2012. Effects of mutual shading, pressurization and oxygen partial pressure on the autotrophical cultivation of Scenedesmus obliquus. J. Taiwan Inst. Chem. Eng. 43, 820–824. https://doi.org/10.1016/j.jtice.2012.06.002

Zagrodnik, R., Seifert, K., Stodolny, M., Laniecki, M., 2015. Continuous photofermentative production of hydrogen by immobilized Rhodobacter sphaeroides O.U.001. Int. J. Hydrogen Energy 40, 5062–

5073. https://doi.org/10.1016/j.ijhydene.2015.02.079

Zagrodnik, R., Thiel, M., Seifert, K., Włodarczak, M., Łaniecki, M., 2013. Application of immobilized Rhodobacter sphaeroides bacteria in hydrogen generation process under semi-continuous conditions. Int. J. Hydrogen Energy 38, 7632–7639. https://doi.org/10.1016/j.ijhydene.2013.01.023

Zhang, C., Zhu, X., Liao, Q., Wang, Y., Li, J., Ding, Y., Wang, H., 2010. Performance of a groove-type photobioreactor for hydrogen production by immobilized photosynthetic bacteria. Int. J. Hydrogen Energy 35, 5284–5292. https://doi.org/10.1016/j.ijhydene.2010.03.085

Zhang, D., Dechatiwongse, P., del Rio-Chanona, E.A., Maitland, G.C., Hellgardt, K., Vassiliadis, V.S., 2015a. Modelling of light and temperature influences on cyanobacterial growth and biohydrogen production. Algal Res. 9, 263–274. https://doi.org/10.1016/j.algal.2015.03.015

Zhang, D., Xiao, N., Mahbubani, K.T., del Rio-Chanona, E.A., Slater, N.K.H., Vassiliadis, V.S., 2015b. Bioprocess modelling of biohydrogen production by Rhodopseudomonas palustris: Model development and effects of operating conditions on hydrogen yield and glycerol conversion efficiency. Chem. Eng. Sci. 130, 68–78. https://doi.org/10.1016/j.ces.2015.02.045

Zhao, F., Yu, B., Yue, Z., Wang, T., Wen, X., Liu, Z., Zhao, C., 2007. Preparation of porous chitosan gel beads for copper(II) ion adsorption. J. Hazard. Mater. 147, 67–73. https://doi.org/10.1016/j.jhazmat.2006.12.045

Zhi, R., Yang, A., Zhang, G., Zhu, Y., Meng, F., Li, X., 2019. Effects of light-dark cycles on photosynthetic bacteria wastewater treatment and valuable substances production. Bioresour. Technol. 274, 496–501. https://doi.org/10.1016/j.biortech.2018.12.021

Zhu, Y., 2007. Chapter 14 - Immobilized Cell Fermentation for Production of Chemicals and Fuels, Bioprocessing for Value-Added Products from Renewable Resources. Elsevier B.V. https://doi.org/http://dx.doi.org/10.1016/B978-044452114-9/50015-3

APPENDICES

A PHOTOBIOREACTOR DESIGN SHEETS

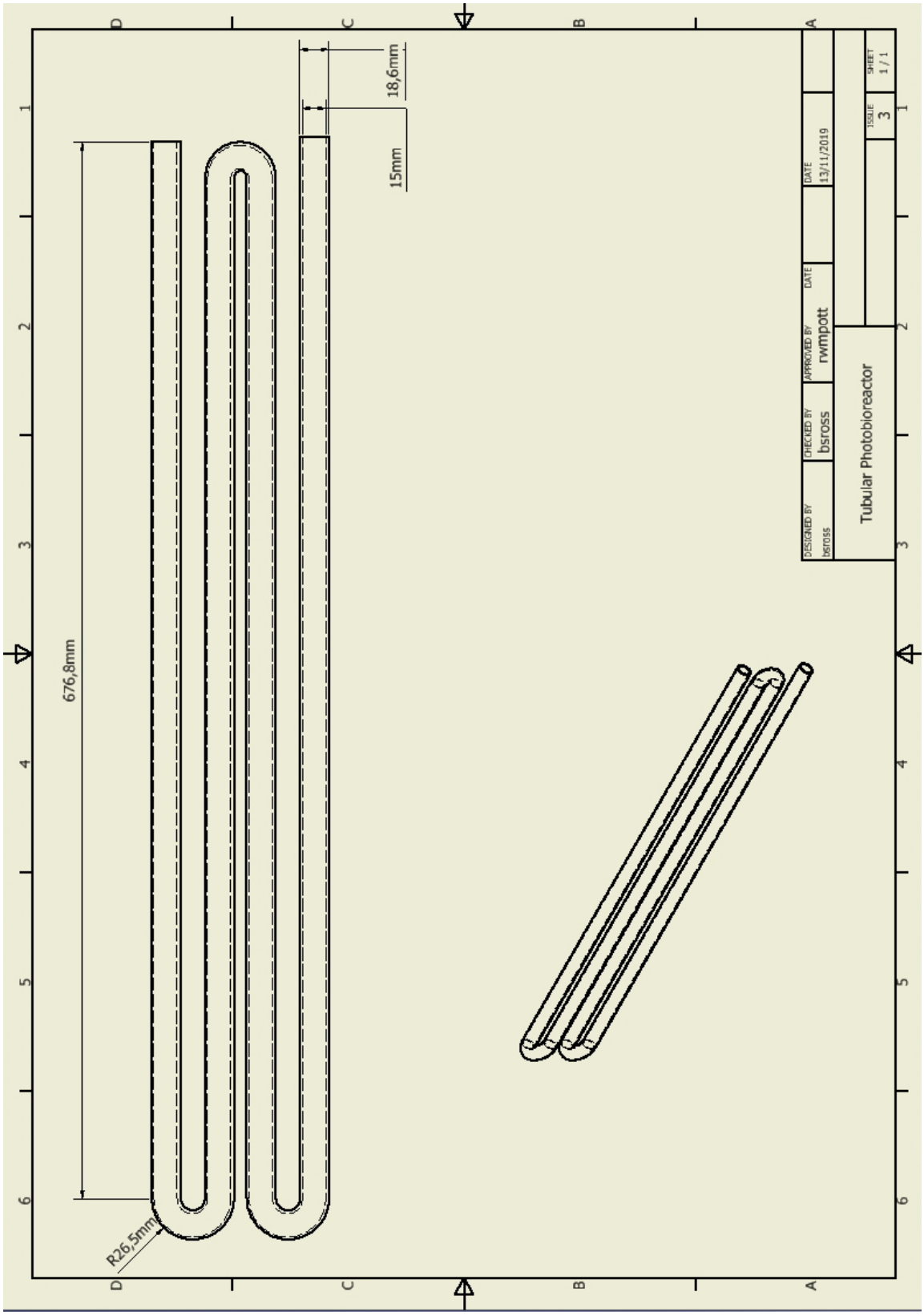

Figure A.1: Tubular PBR design sheet.

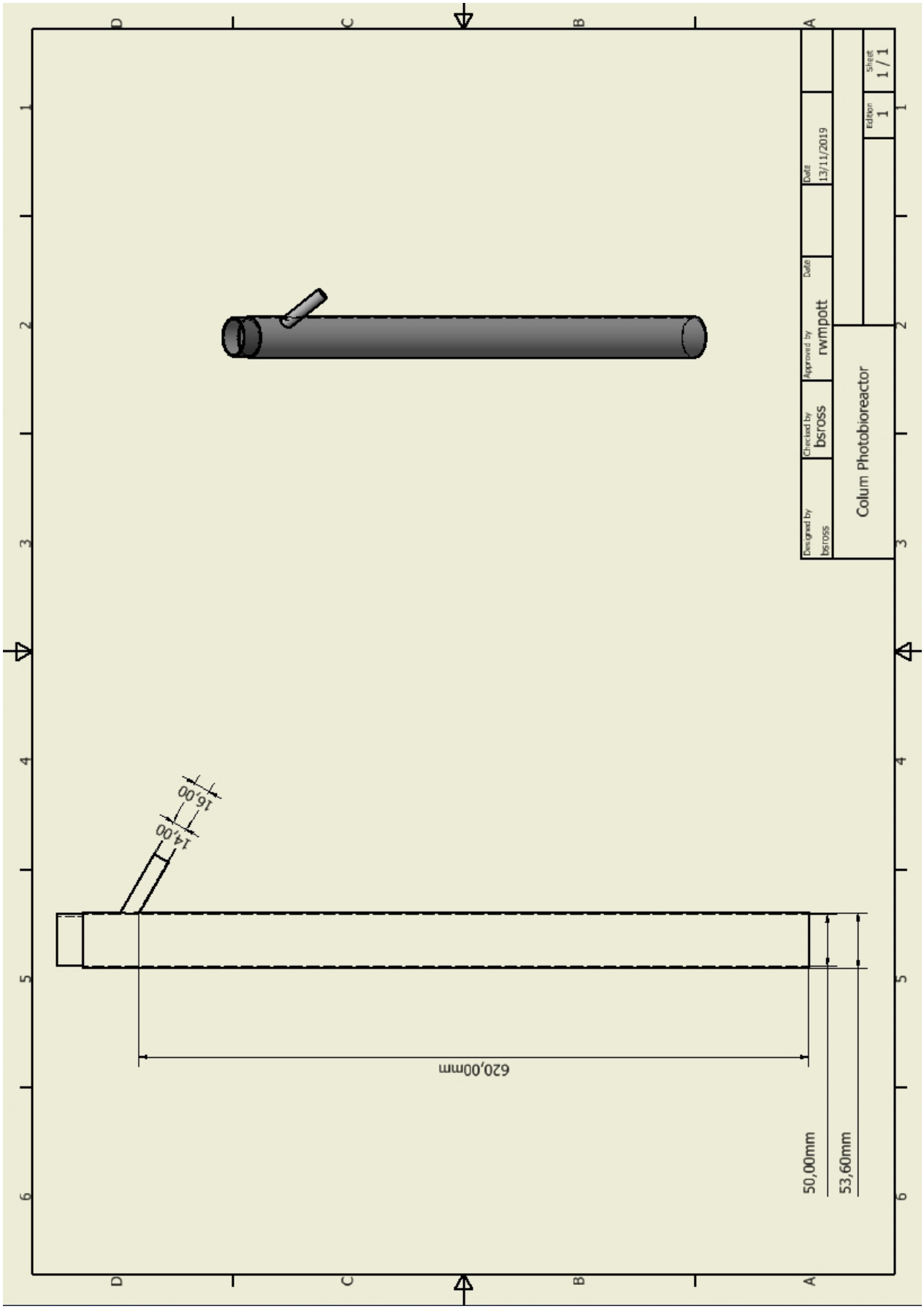

Figure A.2: Column PBR design sheet

B PERISTALTIC PUMP CALIBRATION CURVE

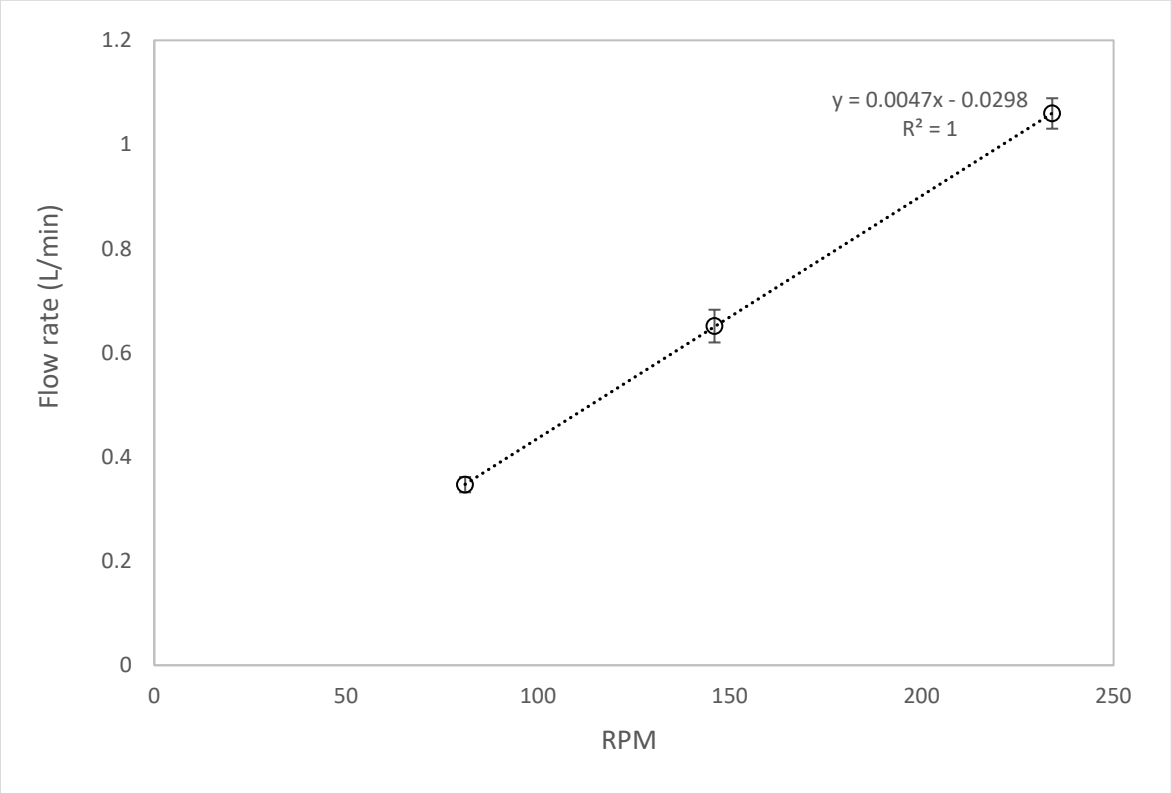

Figure B.1: Peristaltic pump calibration curve. Data points represent the mean of triplicate repeats. The error bars show the uncertainty associated with the flow rate measurements.

C GROWTH AND SUBSTRATE COMPARISON FOR EACH LIGHT INTENSITY

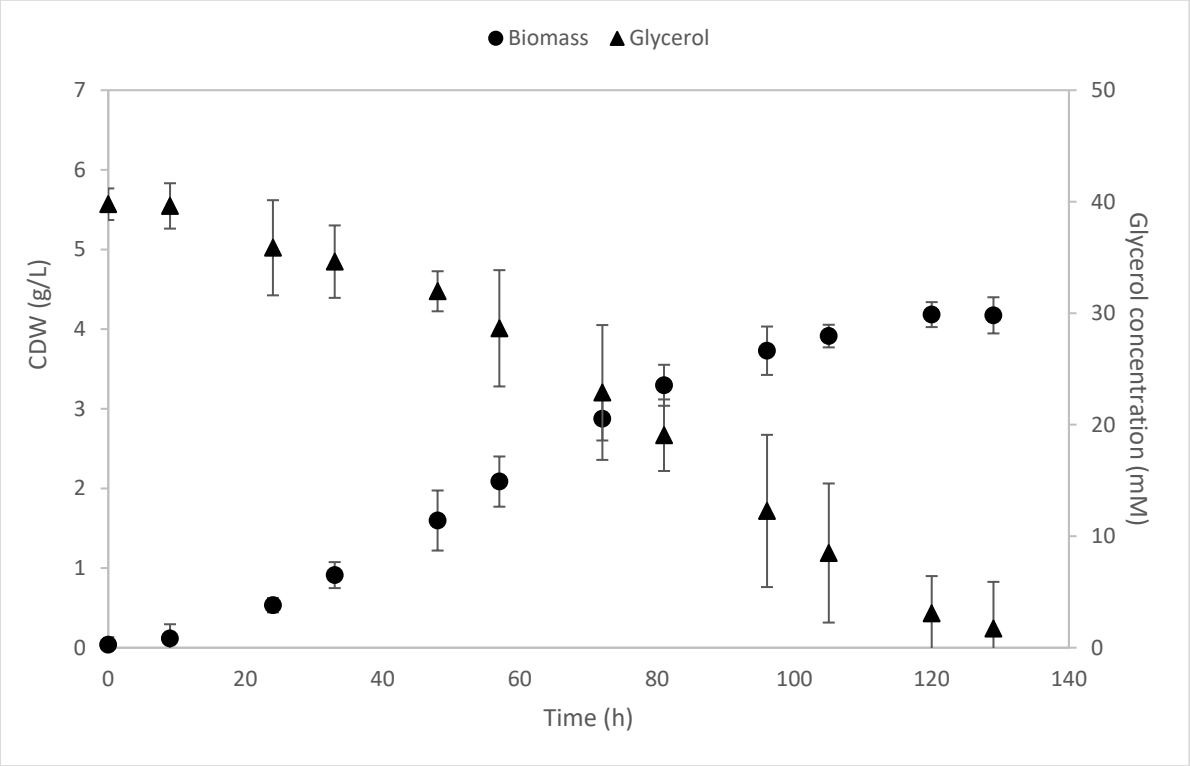

Figure C.1: The growth curve (●) and glycerol utilization (Δ) of R. palustris 11774 with illumination provided by incandescent light bulbs (EUROLUX –100W) at a light intensity of 30 W/m2 is provided in this figure. R. palustris 11774 was cultivated using modified Van Niels medium and sparged with filter sterilised argon to promote anaerobic conditions. All experiments were completed at a constant temperature of 35°C and a volumetric flow rate of 0.651 L/min. Data points represent the mean of quadruple repeats. The error bars show the uncertainty associated with the CDW and glycerol measurements. Biomass concentration corresponds to the left-hand ordinate and the glycerol concentration to the right-hand ordinate.

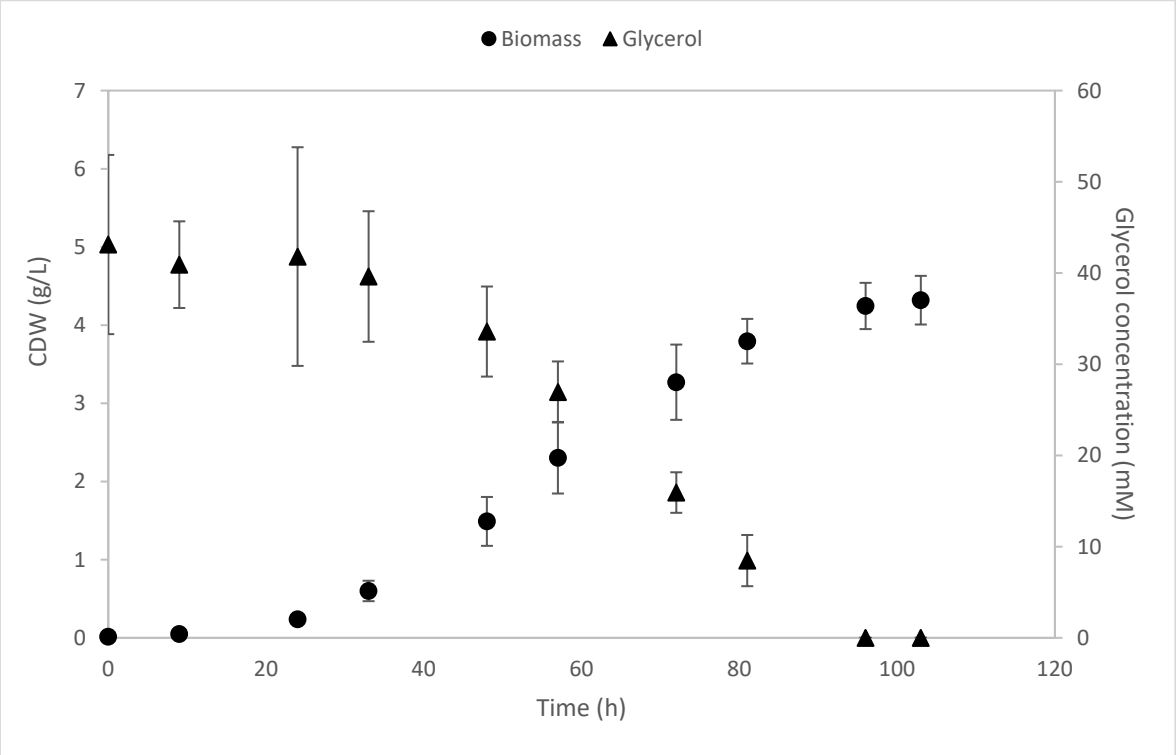

Figure C.2: The growth curve (●) and glycerol utilization (Δ) of R. palustris 11774 with illumination provided by incandescent light bulbs (EUROLUX –100W) at a light intensity of 70 W/m2 is provided in this figure. R. palustris 11774 was cultivated using modified Van Niels medium and sparged with filter sterilised argon to promote anaerobic conditions. All experiments were completed at a constant temperature of 35°C and a volumetric flow rate of 0.651 L/min. Data points represent the mean of quadruple repeats. The error bars show the uncertainty associated with the CDW and glycerol measurements. Biomass concentration corresponds to the left-hand ordinate and the glycerol concentration to the right-hand ordinate.

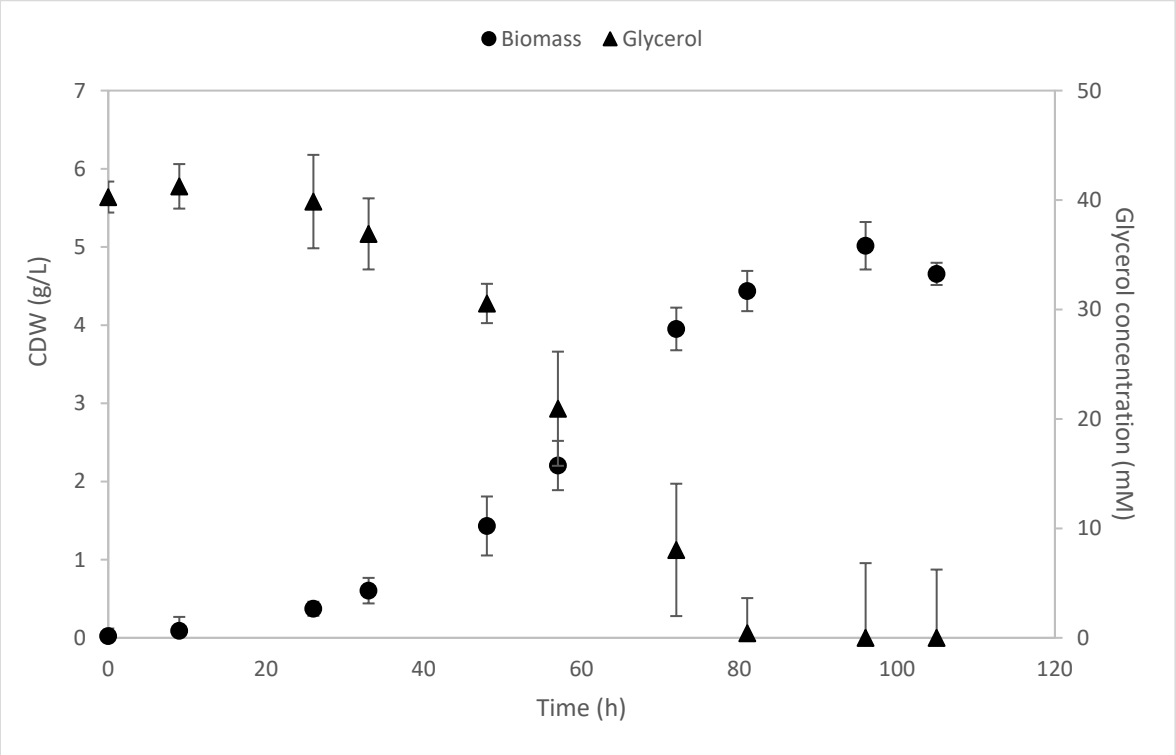

Figure C.3: The growth curve (●) and glycerol utilization (Δ) of R. palustris 11774 with illumination provided by incandescent light bulbs (EUROLUX –100W) at a light intensity of 400 W/m2 is provided in this figure. R. palustris 11774 was cultivated using modified Van Niels medium and sparged with filter sterilised argon to promote anaerobic conditions. All experiments were completed at a constant temperature of 35°C and a volumetric flow rate of 0.651 L/min. Data points represent the mean of quadruple repeats. The error bars show the uncertainty associated with the CDW and glycerol measurements. Biomass concentration corresponds to the left-hand ordinate and the glycerol concentration to the right-hand ordinate.

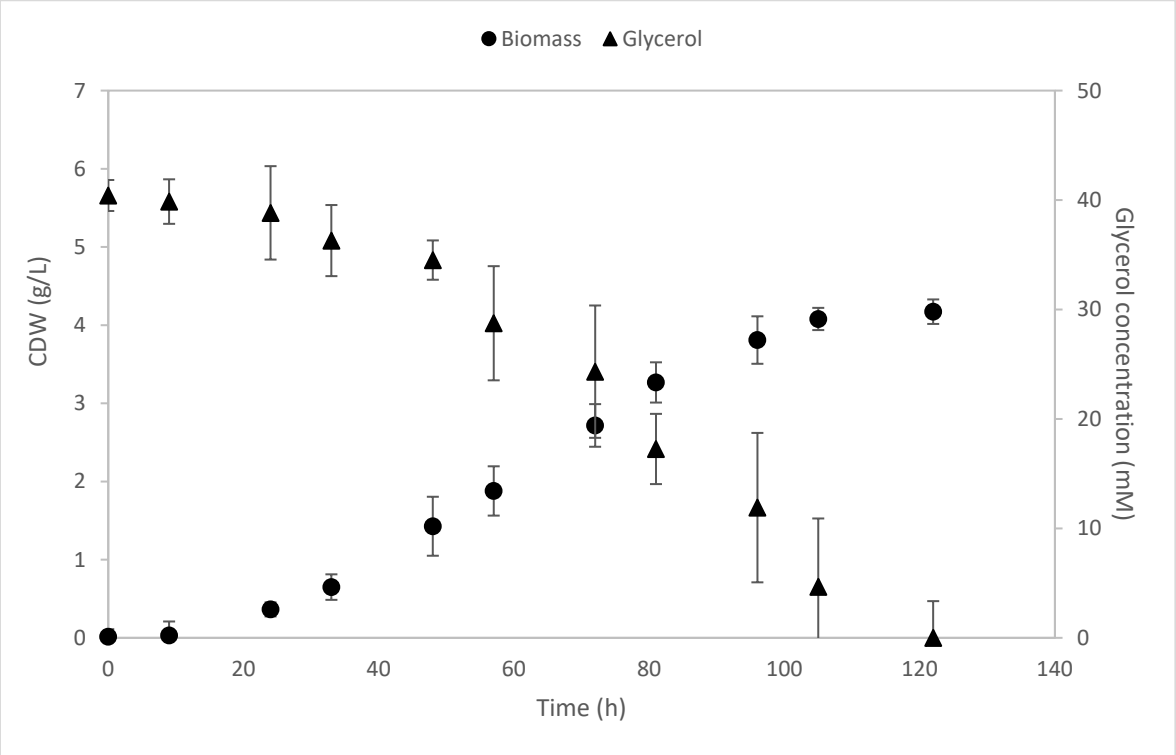

Figure C.4: The growth curve (●) and glycerol utilization (Δ) of R. palustris 11774 with illumination provided by incandescent light bulbs (EUROLUX –100W) at a light intensity of 600 W/m2 is provided in this figure. R. palustris 11774 was cultivated using modified Van Niels medium and sparged with filter sterilised argon to promote anaerobic conditions. All experiments were completed at a constant temperature of 35°C and a volumetric flow rate of 0.651 L/min. Data points represent the mean of quadruple repeats. The error bars show the uncertainty associated with the CDW and glycerol measurements. Biomass concentration corresponds to the left-hand ordinate and the glycerol concentration to the right-hand ordinate.

D GLUTAMATE CONCENTRATION CURVE

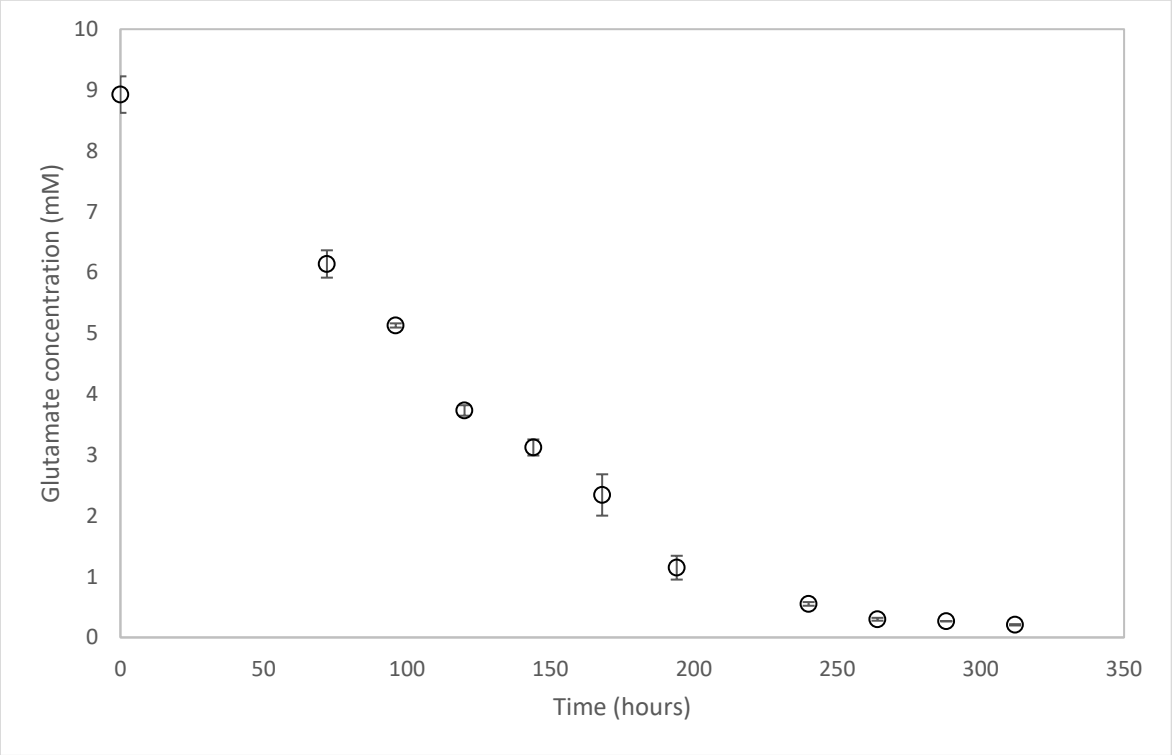

Figure D.1: Glutamate utilization of R. palustris 11774 cultured in a Schott bottle PBR (○). Illumination for both reactor configurations provided by incandescent light bulbs (EUROLUX – 60 W) at an incident light intensity of 100 W/m^2. R. palustris 11774 was cultivated using modified minimal medium with glycerol (50mM) as the carbon source and glutamate (10 mM) as the nitrogen source. Schott bottle experiments were completed at a mixing rate of 300 rpm. Data points for the Schott bottle photobioreactor are the mean of quadruple repeats. The error bars show the uncertainty associated with the glutamate concentrations obtained through a modified ninhydrin analysis.

E GAS COMPOSITION ANALYSIS

Table E.1: Composition of the gas produced by R. palustris determined using GC analysis

	Gas composition diluted with Argon		Normalised gas composition	
Test run No.	H_2 (%)	CO_2 (%)	H_2 (%)	CO_2 (%)
Test run 1	4,0163	0,24	94,36	5,64
Test run 2	12,7239	0,845	93,77	6,23
		Mean composition	94,1	5,9

F PREDICTED GROWTH CURVE IN SCHOTT BOTTLE PBR

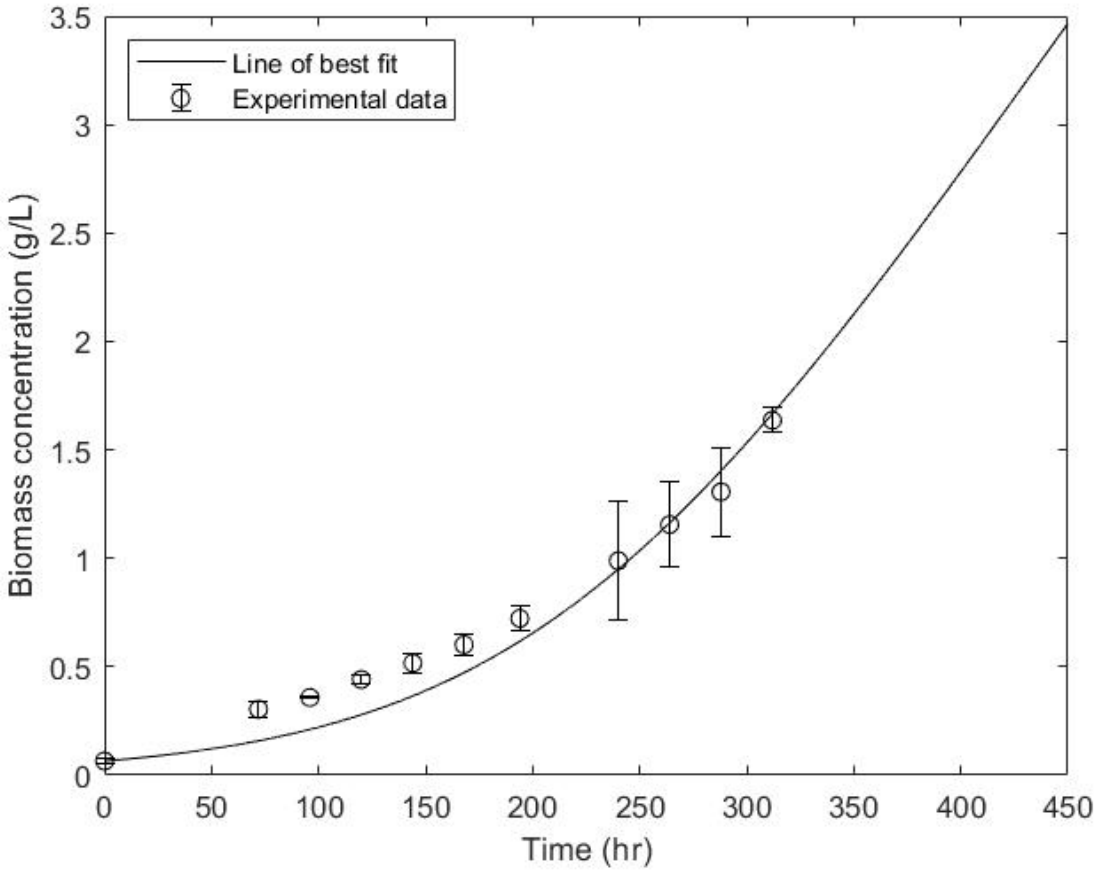

Figure F.1: Experimental data and modelled data of the biomass concentration cultured in the Scott bottle PBR. Experimental data represent the mean of quadruple repeats and the error bars show the uncertainty associated with the measured CDW.

G PREDICTIVE MODEL TEST EXPERIMENT

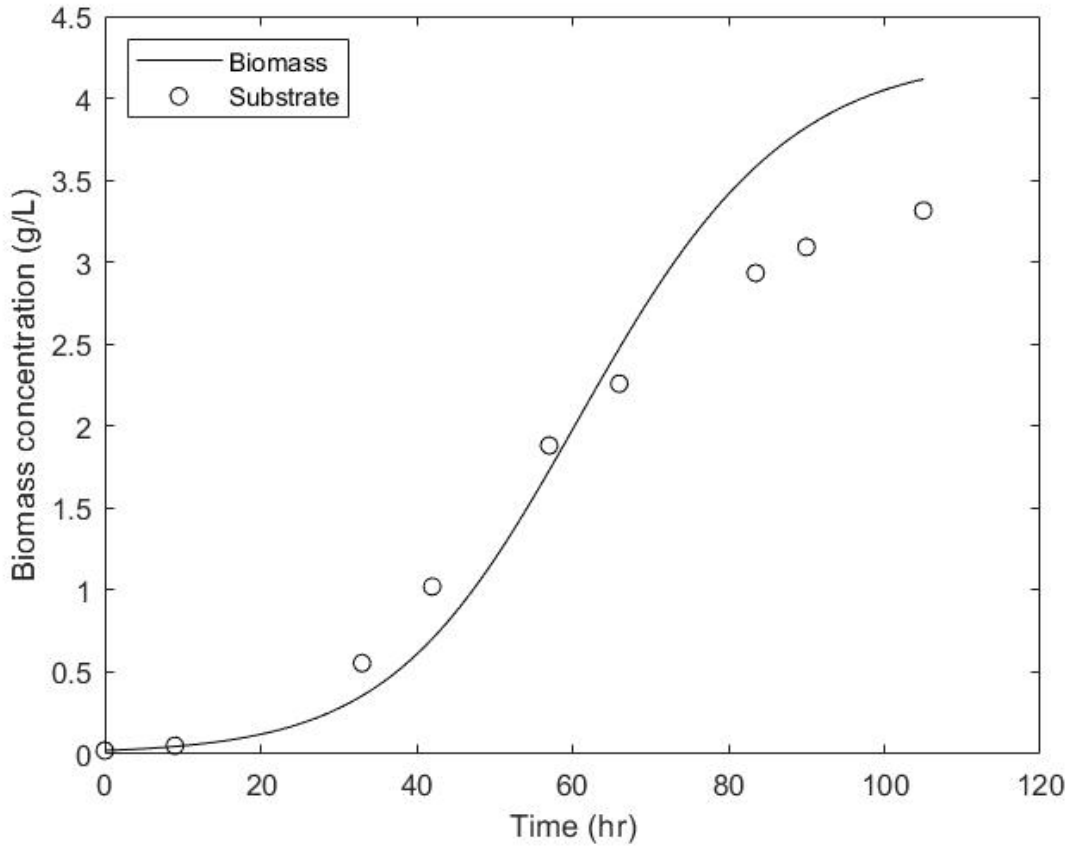

Figure G.1: Prediction of biomass concentration cultured in a 500 mL Schott bottle PBR with illumination provided by 60 W incandescent light bulbs at a constant incident light intensity of 100 W/m^2. Data points are of a single experimental run therefore no statistical analysis has been done.